

Development of Innovative Bioconjugation Strategies for the Generation of Bi-Specific Antibodies Enabling Targeted Protein Degradation



TECHNISCHE
UNIVERSITÄT
DARMSTADT

**vom Fachbereich Chemie
der Technischen Universität Darmstadt**

zur Erlangung des Grades
Doctor rerum naturalium
(Dr. rer. nat.)

**Dissertation
von Tanja Monika Lehmann, M.Sc.**

Erstgutachter: Prof. Dr. Harald Kolmar
Zweitgutachter: Prof. Dr. Dr. Siegfried Neumann

Darmstadt 2024

Tanja Monika Lehmann

Thema: Development of Innovative Bioconjugation Strategies for the Generation of Bi-Specific Antibodies Enabling Targeted Protein Degradation

Darmstadt, Technische Universität Darmstadt

Tag der Einreichung: 15. Mai 2024

Tag der mündlichen Prüfung: 08. Juli 2024

Jahr der Veröffentlichung der Dissertation auf TUpriints: 2024

Lizenz: Veröffentlicht unter CC BY 4.0 International

URN: urn:nbn:de:tuda-tuprints-272688

Die vorliegende Arbeit wurde unter der Leitung von Herrn Prof. Dr. Harald Kolmar am Clemens-Schöpf-Institut für Organische Chemie und Biochemie der Technischen Universität Darmstadt sowie bei der Merck KGaA in Darmstadt von November 2020 bis Mai 2024 angefertigt.

Publication derived from the present work.

Parts of this work have been published.

Lehmann T., Schneider H., Tonillo J., Schanz J., Schwarz D., Schroeter C., Kolmar H., Hecht S., Anderl J., Rasche N., Rieker M. and Dickgiesser S. (2024) Welding PROxAb Shuttles: A modular approach for generating bispecific antibodies via site-specific protein-protein conjugation. *bioRxiv*, 2024-03. (Accepted: May 10th, 2024, Bioconjugate Chemistry)

Contributions to conferences

Lehmann T., Dickgiesser S., Tonillo J., Schwarz D., Hecht S., Anderl J., Kolmar H., Rasche N., Rieker M. (March 20th, 2024) A modular approach to assemble PROxAb shuttles for antibody mediated selective PROTAC delivery. *Poster at Targeted Protein Degradation (TPD) Summit Europe, London, Great Britain*

Table of Contents

Zusammenfassung.....	1
Abstract.....	3
1 Introduction.....	5
1.1 Overview – Cancer and cancer treatment.....	5
1.2 Antibodies as basis for various cancer treatment strategies	6
1.3 Antibody formats and bispecific antibodies	8
1.4 Antibody modification via conjugation.....	11
1.4.1 Antibody-drug conjugates.....	11
1.4.2 Conjugation strategies	12
1.4.2.1 Transglutaminase-mediated conjugation.....	15
1.4.3 Bispecific antibody generation via conjugation	16
1.5 Target proteins and binding antibodies	17
1.5.1 EGFR and HER2	17
1.5.2 PD-L1	19
1.5.3 RNF43.....	20
1.6 Protein degradation	21
1.6.1 Ubiquitin-proteasome pathway of intracellular proteolysis.....	21
1.6.2 Targeted protein degradation inducers as therapeutic modality.....	23
1.6.2.1 PROTAC.....	23
1.6.2.2 Biological targeted protein degradation	26
2 Materials.....	30
2.1 Human cell lines and bacterial strains	30
2.2 Plasmids.....	31
2.3 Proteins and peptides.....	32
2.4 Chemicals.....	39
2.5 Commercially available systems.....	40
2.6 Buffer and Solutions.....	40
2.7 Consumable materials.....	41
2.8 Equipment.....	43
3 Methods.....	45

Molecular Biological Methods	45
3.1 Determination of DNA concentration	45
3.2 Transformation in <i>E. coli</i>	45
3.3 Plasmid preparation	45
Biochemical and Biophysical Methods	46
3.4 Determination of protein concentration	46
3.5 Preparative protein purification	46
3.5.1 Protein A and Amsphere™ A3 Affinity Chromatography	46
3.5.2 Immobilized Metal Affinity Chromatography (IMAC)	47
3.5.3 Preparative Size-Exclusion Chromatography (SEC)	47
3.5.4 Buffer exchange	48
3.6 Sodium dodecyl sulfate polyacrylamide gel electrophoresis (SDS-PAGE)	48
3.7 Protein detection using Coomassie staining	48
3.8 Protein detection using Western blot analysis	48
3.9 Analytical chromatography methods	49
3.9.1 Size Exclusion-HPLC (SE-HPLC)	49
3.9.2 Reversed Phase-HPLC (RP-HPLC)	49
3.9.3 Hydrophobic Interaction HPLC (HI-HPLC)	50
3.10 LC-MS	50
3.11 Bio-layer-Interferometry (BLI)	50
3.11.1 Quantitative BLI	51
3.11.2 Kinetic BLI	51
3.11.2.1 α RNF43 scFv variants	51
3.11.2.2 Simultaneous binding	51
3.11.2.3 VHH-antibody conjugates	51
3.12 Surface plasmon resonance spectroscopy (SPR)	52
3.13 Conjugation methods	52
3.13.1 Random lysine conjugation (pHAb-dye labeling)	52
3.13.2 Enzymatic conjugation	53
3.13.3 Copper-free strain-promoted azide-alkyne cycloaddition (SPAAC)	53
3.14 Complex formation of PROTAC and VHH-antibody conjugate	53
3.15 Determining antibody loading	53

3.15.1	Determination of ligand to antibody ratio – RP-HPLC	53
3.15.2	Determination of VAR (VHH-antibody ratio) – HI-HPLC	54
3.16	Determination of complex formation between antibody and PROTAC.....	54
3.16.1	Determination of DOL.....	54
Cell Biological Methods		55
3.17	Cell cultivation.....	55
3.18	Preparation of cell lysates	55
3.19	Recombinant expression of VHH and scFv variants.....	55
3.20	Cell Binding Assay.....	56
3.21	Immunofluorescence Assay	57
3.22	Internalization Assay.....	57
3.23	Cell Viability Assay.....	58
4	Results.....	59
Chapter 1: Selective cellular delivery of PROTACs using a modular conjugation-based approach.....		59
4.1	Design and generation of VHH for selective PROTAC delivery	59
4.1.1	VHH protein design to enable direct conjugation via MTG	59
4.1.2	Expression, purification, and characterization of PROTAC-binding VHH G ₃ -MIC7	60
4.2	Site-specific conjugation of VHH 'G ₃ -MIC7' to native IgG1-based antibodies	61
4.2.1	Evaluation of MTG-mediated conjugation of G ₃ -MIC7 to Trastuzumab.....	61
4.2.2	Generation of bispecific antibody-VHH conjugates via MTG.....	63
4.2.3	Modularity of MTG-mediated conjugation of G ₃ -MIC7 proven by conjugation to several IgG-based antibodies	64
4.3	Biophysical characterization of antibody-VHH conjugates	65
4.3.1	Soluble antigen binding kinetics.....	65
4.3.2	Kinetics of complex formation between antibody-MIC7 conjugates and PROTACs.....	66
4.3.3	Cellular binding of antibody-MIC7 conjugates and respective controls.....	66
4.3.4	Cellular uptake of antibody-MIC7 conjugates and respective controls.....	68
4.4	Chromatographical analysis of PROTAC loading and evaluation of complex formation.....	69
4.5	Biological evaluation of PROTAC-loaded antibody-VHH conjugates.....	71

4.5.1	Evaluating BRD4 degradation selectivity via targeted delivery of BRD4 PROTACs to HER2-expressing cells.....	71
4.5.2	<i>In vitro</i> cytotoxicity of PROTAC-loaded antibody-VHH conjugates	73
Chapter 2: A modular approach to generate bispecific anti-bodies recruiting cell-surface proteins and a transmembrane E3 ligase		76
4.6	Design and assembly of antibody-scFv conjugates.....	76
4.6.1	scFv design for MTG-mediated conjugation	76
4.6.2	Expression and purification of G ₄ -tagged α RNF43 scFv variant 1	77
4.7	MTG-mediated site-specific direct conjugation of scFv1 to native IgG1-based antibody.....	78
4.8	Design and generation of antibody-based degraders using two-step conjugation strategy.....	78
4.8.1	The scFv protein design for two-step conjugation to IgG-based antibodies.....	78
4.8.2	scFv expression, purification, and characterization.....	80
4.9	Two-step conjugation of scFv variants to native IgG1-based antibodies	81
4.9.1	Evaluation of MTG-mediated conjugation of click derivatives	81
4.9.2	MTG-mediated conjugation of click derivatives in preparative scale.....	83
4.9.3	Click reaction of scFv variants and antibodies using SPAAC mechanism	84
4.9.4	Generation of bispecific IgG-scFv conjugates via SPAAC reaction	85
4.10	Binding analysis of IgG-scFv conjugates.....	87
4.10.1	Binding kinetics and simultaneous binding.....	87
4.10.2	Selective binding of cell surface receptor based on receptor expression levels	89
4.11	Evaluation of targeted protein degradation mediated by generated IgG-scFv conjugates ...	91
5	Discussion.....	92
5.1	Expression of antibody-fragments in mammalian cells.....	92
5.2	Bioconjugation for generation of antibody-MIC7 conjugates as vehicle for PROTAC delivery	94
5.3	Generation of antibody-based protein degraders	96
5.4	Complexation of antibody-MIC7 and PROTAC enables selective target degradation	99
5.5	Addressing membrane-bound E3 ligase for degradation of extracellular targets.....	105
6	Conclusion.....	108
References		110
Appendix		127

A	Supporting information.....	127
B	List of figures.....	143
C	List of tables.....	149
D	Abbreviations.....	150
E	Acknowledgements.....	155
	Affirmation.....	157

Zusammenfassung

Mehr als vierzig Jahre nach der Beschreibung der ersten Technologie zur Herstellung monoklonaler Antikörper haben sich diese zu einer etablierten Arzneimittelklasse für die Behandlung verschiedener Krankheiten entwickelt. Die Entwicklung von Proteinen und die Kombination mit der klassischen medizinischen Chemie haben den Weg für eine Vielzahl von aus Antikörpern abgeleiteten Molekülen geebnet, die heute vor allem in der Krebstherapie eingesetzt werden. Zwei Hauptklassen sind Antikörper-Wirkstoff-Konjugate (ADC), die zytotoxische Nutzlasten an die Zielzellen abgeben sollen, und bispezifische Antikörper (bsAb), die für verschiedene Ansätze verwendet werden, z. B. für eine verbesserte Gewebespezifität oder zur Rekrutierung von Immunzellen an bösartiges Gewebe.

Ziel dieser Arbeit war es, den derzeitigen Werkzeugkasten an Antikörpermodalitäten zu erweitern und modulare Strategien für ihre Erzeugung zu entwickeln. Im ersten Teil der Arbeit wurden Antikörper als Vehikel verwendet, um sogenannte "auf die Proteolyse abzielende duale Moleküle (PROTACs)" in Tumorzellen einzuschleusen. PROTACs sind bivalente kleine Moleküle, die E3-Ligasen an intrazelluläre Proteine von Interesse (POI) rekrutieren und sie dadurch für die Beseitigung durch den endogenen zellulären proteasomalen Abbaumechanismus markieren. Trotz ihres vielversprechenden Potenzials stehen PROTACs vor Herausforderungen wie begrenzte Selektivität, Zellpermeabilität oder schlechte Pharmakokinetik. Eine mögliche Lösung besteht darin, Antikörper mit PROTAC-bindenden Domänen auszustatten, z. B. "camelid single-domain antibody" (VHH), und so bispezifische Antikörper zu schaffen, die PROTACs gezielt und ähnlich wie ADCs verabreichen können. Solche bispezifischen Antikörper können durch genetische Fusion erzeugt werden, was jedoch die individuelle Herstellung jeder Antikörper-VHH-Kombination erfordert. Daher wurde eine modulare Strategie zur raschen Herstellung von bispezifischen Antikörpern entwickelt, die PROTACs freisetzen können. Bei diesem Ansatz werden PROTAC-bindende VHHs enzymatisch mit handelsüblichen Antikörpern gekoppelt. Die resultierenden Konjugate behalten ihre Zielbindungs- und Internalisierungseigenschaften bei. Nach Inkubation mit PROTACs bildeten sich definierte Antikörper-PROTAC-Komplexe. Diese Komplexe induzieren selektiv den POI-Abbau und damit selektiv die Zytotoxizität in Zellen, die das Ziel des Antikörpers exprimieren.

Der zweite Teil der Arbeit zielt auf die Herstellung bispezifischer Antikörper für die Rekrutierung von Transmembran-E3-Ligasen an Zelloberflächenrezeptoren. Durch die gleichzeitige Bindung kann eine räumliche Nähe zwischen den beiden Proteinen hergestellt werden, die letztlich zum Abbau des Rezeptors über den Endosom-Lysosom-Weg führt. Bispezifische Antikörper für diesen Ansatz werden in der Regel durch Antikörper-Engineering und rekombinante Produktion hergestellt. In diesem Projekt wurde ein chemo-enzymatischer Ansatz entwickelt, um solche

Moleküle aus bereits verfügbaren Antikörpern herzustellen. Dazu wurden „einkettige variable Domänen“ (scFv) und Antikörper zunächst durch enzymatische Konjugation mit reaktiven „Handles“ versehen und anschließend durch SPAAC-Klickreaktion miteinander verbunden. Die scFv-Antikörper-Konjugate wurden auf ihre Antigenbindungseigenschaften und auf den Abbau verschiedener Targets untersucht. Die in dieser Arbeit verwendete chemo-enzymatische Konjugation zur Herstellung bispezifischer Antikörper bietet eine flexible und effektive Lösung unter Verwendung handelsüblicher Antikörper. Während die resultierenden Moleküle in erster Linie für den gezielten Proteinabbau eingesetzt wurden, können diese Konjugationsstrategien auch genutzt werden, um Antikörper mit zusätzlichen Bindungseinheiten für verschiedene andere Anwendungen zu erweitern.

Abstract

More than forty years after description of the first technology for generating monoclonal antibodies, they have become a well-established drug class for treating various diseases. Protein engineering efforts and combining forces with classical medicinal chemistry have paved the way to a plethora of antibody-derived molecules that are now being applied, particularly in cancer therapy. Two main classes are antibody-drug conjugates (ADC), meant to deliver cytotoxic payloads to target cells, and bispecific antibodies (bsAb), that are being used for various approaches, e.g. for enhanced tissue specificity or to recruit immune cells to malignant tissue.

This work aimed to expand the current toolbox of antibody modalities and develop modular strategies their generation. In the first part of the work, antibodies were used as vehicles to deliver so-called "proteolysis-targeting chimeras (PROTACs)" into tumor cells. PROTACs are bivalent small-molecules that recruit E3 ligases to intracellular protein of interest (POI) and thereby label them for elimination through the endogenous cellular proteasomal degradation mechanism. Despite their promise, PROTACs face challenges such as limited selectivity, cell permeability or poor pharmacokinetics. A possible solution is to equip antibodies with PROTAC-binding domains, e.g. "camelid single-domain antibody" (VHH), and thereby create bispecific antibodies that can deliver PROTACs in a targeted, ADC-like manner. Such bispecifics can be generated by genetic fusion, which however requires individual production of every antibody-VHH combination. Hence, a modular strategy to promptly produce bispecifics capable of delivering PROTACs was developed. This approach involves enzymatically coupling PROTAC-binding VHHs with commercially available antibodies. The resulting conjugates maintain their target binding and internalization properties. Upon incubation with PROTACs, defined antibody-PROTAC complexes were formed. These complexes selectively induce POI degradation, thereby inducing cytotoxicity selectively in cells expressing the target of the antibody.

The second part of the work aims on generation of bispecific antibodies for the recruitment of transmembrane E3 ligases to cell surface receptors. Simultaneous binding can induce a spatial proximity between both proteins which ultimately results in degradation of the receptor via the endosome-lysosome pathway. Bispecific antibodies for this approach are typically produced by antibody engineering and recombinant production. Herein, a chemo-enzymatic approach to generate such molecules from already available antibodies has been developed. Therefore, single-chain variable domains (scFv) and antibodies were first equipped with reactive handles using enzymatic conjugation and afterwards connected using SPAAC click reaction. The scFv-antibody conjugates were analyzed for their antigen binding properties and regarding the degradation of different targets. The chemo-enzymatic conjugation used in this work for generation of bispecific antibodies offers flexible and effective solution using commercially available antibodies. While the

resulting molecules have been primarily employed for targeted protein degradation, these conjugation strategies can also be harnessed to extend antibodies with additional binder moieties for various other applications.

1 Introduction

1.1 Overview – Cancer and cancer treatment

Cell and tissue growth in the body is strictly controlled, with certain cells needing to grow faster in specific situations such as during childhood or wound healing. This process is governed by various genes and proteins that process and respond to signals. However, in cancer cells, cell division occurs in an uncontrolled manner due to accumulated genetic changes (DNA) that contribute to cancer cell progression. Cancer cells undergo continuous division autonomously, irrespective of external growth signals. They disregard inhibitory growth signals and thereby evade programmed cell death (apoptosis). Eventually, this leads to unrestricted cell division and mass expansion. Combined with the ability to migrate into healthy tissue and potentially spread through the human system via the lymph system or blood vessels they can form metastases in distant areas. Angiogenesis, which is mediated by different growth factors, promotes the formation of blood vessels in order to provide cells with their nutritional requirements. Therefore, tumors often exhibit altered metabolism, such as enhanced glycolysis even in the presence of oxygen, facilitating tumor progression through increased availability of precursors for anabolic pathways.¹ Cancer is a complex and widespread disease that affects people across all countries and regions. It is a leading cause of morbidity and mortality globally. The Global Cancer Observatory (GCO), using data from the World Health Organization (WHO), reported almost 20 million new cases of cancer and 9.7 million premature deaths related to cancer in 2022.² These statistics highlight the significant morbidity and mortality associated with the disease on a global scale. Understanding cellular behavior and cancer biology is crucial for comprehending the mechanisms behind the most commonly used cancer therapies. Another characteristic is the escape from the immune system, which is often achieved through the expression of inhibitory immune checkpoints. Additionally, cancer cells exhibit replicative immortality by expressing telomerases, allowing them to avoid cell cycle arrest.³ Various approaches to cancer therapy have been developed over the last 100 years.⁴ In the past, surgery was the primary option for cancer treatment until the introduction of X-rays for radiotherapy in the late 19th century.⁵ Radiotherapy allowed for localized treatment by damaging DNA in tumor cells while sparing healthy surrounding tissue.⁶ However, the success rates of these therapies are limited as metastasis growth remained difficult to suppress. The advent of chemotherapy in the 1930s allowed for novel treatment approach, and the first reported instance of a cancer patient being cured by chemotherapy occurred in 1958.^{7,8} Initially, monotherapy drugs only provided temporary responses in specific cancer types, but positive outcomes were achieved when chemotherapy was

combined with radiotherapy or surgery, particularly in breast cancer patients in the late 1960s. The understanding of molecular changes in cancer cells led to the introduction of various drugs with different mechanisms of action in the 1980s.⁷ When a tumor has disseminated to multiple distant locations in the body and surgical intervention is no longer viable, systemic treatments such as chemotherapy are commonly employed. These therapies primarily target rapidly dividing cells and utilize various approaches, including DNA-damaging agents, antimetabolites, and microtubule inhibitors. A major drawback is their non-specificity, which leads to side effects to other fast growing cells like hair follicles or blood cells.⁴

In the 1990s, advancements in targeted chemotherapy, focused on specific molecular targets, revolutionized cancer treatment options.⁹ Studies on the genome sequence indicated that protein kinase abnormalities are associated with functional disorders in cancer, leading to the development of kinase inhibitors as a pharmacological trend. Targeted tumor therapy has been expanded to include small proteins and antibodies, such as monoclonal antibodies (mAb), which can intervene in cell signaling and induce immunomodulatory effects.¹⁰ Targeted therapies have shown significant success in cancer treatment by specifically recognizing and differentiating cancer cells based on target expression. The higher selectivity of these therapies results in a higher maximum tolerated dose (MTD) and a lower minimum effective dose (MED) and thus increases the therapeutic window of the drug. The therapeutic window indicates the dosage range where the drug yields beneficial therapeutic effects without inducing toxicity. Thus, targeted therapies and immunotherapies can be delivered at doses that lead to fewer severe side effects in comparison to small-molecule therapy. Recent examples show the relevance of selectivity achieved by targeted therapies, including immune-based therapies like immune checkpoint inhibitors, immune cytokines, or ligand targeted therapeutics.¹¹ The second main approach involves enzyme/small molecule-based therapeutics such as antibody-directed enzyme prodrug therapy,¹² proteolysis targeting chimeras (PROTAC)¹³ or antibody-drug conjugates (ADC).¹⁴ In the scope of this work, antibody-based approaches like ADCs and targeted-protein degradation of PROTACs are of special relevance and will be discussed in more detail in the following sections.

1.2 Antibodies as basis for various cancer treatment strategies

Antibodies, glycoproteins weighing approximately 150 kDa, belong to the immunoglobulin (Ig) family. Their primary function within the immune system is to identify foreign antigens, neutralize them, and initiate an immune response. The basic structure comprises two heavy (HC, ~50 kDa) and two light (LC, ~25 kDa) chains in the form of a Y, which are connected by non-covalent bonds and inter-chain disulfide bridges (Figure 1). At the upper end are the antigen-binding regions (Fab) which recognize the antigens specific to the complementary determining regions (CDRs) and are referred to as variable domains. Here, a differentiation is made between the variable

domain of the heavy chain V_H and the light chain V_L . The basis of the Y is the crystallizable fragment (Fc), which induces interaction with other parts of the immune system.¹⁵ The Fc region is acknowledged by Fc receptor (FcR), which are present in various immune cells. Depending on the type of heavy chain, antibodies can be categorized into five distinct classes: IgA, IgD, IgE, IgG, and IgM. IgG, which was used in this work, as it is the most commonly used form in antibody-based therapy. Because of its binding to the specific Fc receptor, FcγR, expressed on cells that trigger specialized functions such as antibody-dependent cellular cytotoxicity (ADCC) and complement-dependent cytotoxicity (CDC). Notably, IgG antibodies are subdivided into further subclasses that can induce ADCC or CDC, IgG1 and IgG3, or have no effect, like IgG2 and IgG4.¹⁶ ADCC is induced via the recognition of the Fc fragment by CD16 binding of natural killer cells. CDC is triggered by the binding of complement component 1q (C1q) and the associated activation of the complement cascade.¹⁷ The Fc-fragment also ensures the prolonged serum half-life of antibodies through non-specific endosomal uptake via the FcRn receptor. The receptor binds to the Fc portion of IgG at acidic pH (pH 6.0) due to hydrophobic interactions and stabilizing salt-bridges between histidine residues of the IgG and anionic residues on the FcRn. Binding is released at physiological pH (pH 7.4).¹⁸ While the uptake of IgG in an endocytic vesicle, the FcRn binding occurs in the acidified endosome and sorting of FcRn-IgG complex results in endosomal escape and recycling of the IgG, which ensures the extra-long plasma half-life for the IgG class.¹⁸ Typically, soluble proteins are internalized and transported from the endosome to the lysosome, where they are degraded.

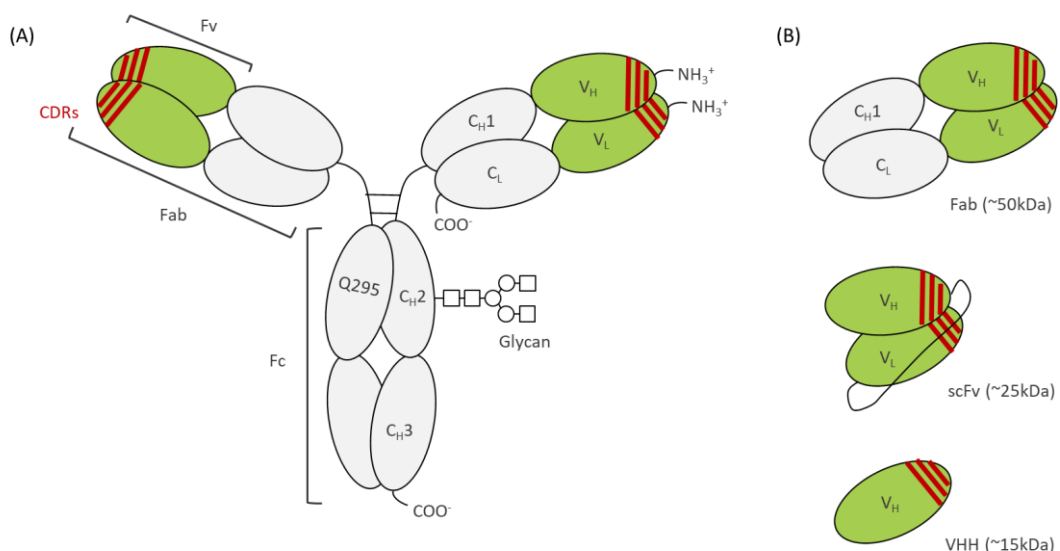


Figure 1 Structure of antibody and fragments. (A) The IgG-based antibody is depicted in a schematic representation, featuring two identical heavy (HC) and light chains (LC). The fragment crystalline (Fc) region is composed of C_{H2} and C_{H3} domains, while the fragment antigen binding (Fab) unit is formed by V_H and C_{H1} of the HC and V_L and C_L of the LC. The antigen binding sites are formed by the Fragment variable (Fv) form with the CDR 1-3 regions. The glycosylation site is in the Fc fragment at position N297. **(B)** Schematic representation of antibody fragments. The monovalent Fab, capable of binding the antigen with the variable region, lacks the Fc part and does not exhibit effector functions. The scFv, comprising the V_H and V_L along with a linker unit, weighs approx. 25 kDa and can bind its antigen through the CDR regions. The smallest antigen-binding unit, the camelid heavy-chain variable domain (VHH), weighs around 15 kDa and binds the antigen with one prolonged CDR region.

The development of "fully human" antibodies through techniques like *in vitro* yeast or phage display or transgenic mice has positioned mAbs as a significant treatment option for cancer. Their capacity to both directly eliminate tumor cells and activate the host immune system, fostering enduring effector responses, renders their mechanism of action distinctive. The combination effect with target specificity is the basis for the ability to elicit strong antitumor responses while minimizing toxicity and side effects. Selective cancer therapy with antibodies was first demonstrated through the concept of generating monoclonal antibodies by hybridoma technology.¹⁶ The presence of an overexpressed or mutated antigen on malignant cells is the most important prerequisite for the development of antibody-based cancer therapy. The antitumor effect can be triggered directly via antigen binding or indirectly via activation of the immune system. Subsequently, this can trigger agonistic or antagonistic functions, for example through the activation of pro-apoptotic signaling pathways.¹⁹ Additionally, the mediation of effector functions can also lead to the selective destruction of tumor cells when they present the antigens on the cell surface.^{20,21} Further approaches use conjugation of toxins to internalize antibodies to kill tumor cells.²² Given their relevance for this work, the subsequent section will discuss the rationale behind the design of different formats, strategies for conjugating toxins and generation of bispecific antibodies.

1.3 Antibody formats and bispecific antibodies

In addition to classical IgG-based antibodies, a plethora of smaller antibody-based formats exists. Often used examples of such smaller derivatives include Fabs, single chain variable domain (scFv), mini bodies, triabodies, diabodies, or single-domain has been developed. Their smaller size, the resulting improved pharmacokinetics for tissue penetration and ease of production make them perfect tools for diagnostic purposes and clinical use.²³ Among the most popular formats that are also used in this work are scFv and camelid heavy-chain variable domains (VHH). The scFv, consisting of V_H and V_L has long been recognized as the smallest antibody fragment possessing the same antigen-binding specificity as the full Ig protein. The scFv are an engineered forms of the variable region of an Ig-molecule in which the two variable domains are not connected by a disulfide bond but by a flexible linker. The length and amino acid composition of the linker are crucial factors influencing the proper folding of the protein. As a rule of thumb, it is approximately 10-25 amino acids long, includes glutamine and lysines to increase solubility, as well as glycine and serine for improved flexibility.²⁴ scFvs comprise a size of about 25 kDa. In each of the two variable domains, there are three hypervariable regions (CDRs) and three framework regions (FRs). These CDRs are responsible for antigen binding. Interestingly, however, they are of varying importance for antigen binding. CDR3 of the heavy chain is most relevant in antigen interaction, accounting for approximately 29% of the interaction.²⁵

However, the identification of VHH from camelids²⁶ and vNAR from sharks²⁷ demonstrated that a single V-like domain can maintain the affinity of a whole antibody molecule. These specific immunoglobulins have a single V-like antigen-binding domain with higher affinity. Due to extensive adaptations in sequence and structure, VHHs exhibit more robust antibody response²⁸ and have higher yield of recombinant expression.²⁹ Similar to V_H , VHHs have nine beta-strands to form the typical IgV fold, the loss of the V_L is reflected in the structural differences, especially in the FR2 and in hypervariable strands.

In the conventional V_H region, four hydrophobic amino acids that are highly conserved facilitate in the joining of V_L . However, these hydrophobic residues are, in VHH, substituted by more hydrophilic amino acids, which induces an modified folding pattern to prevent solvent exposure.³⁰ As a consequence, adjacent residues have rotated their side chains to increase hydrophilicity.³¹ Furthermore, the CDR3 domain of VHH shields amino acids that are otherwise covered by the V_L partner. This enhances the solubility of VHHs relative to single V_H domains and scFv.³² An extension of CDR1 and CDR3 compensates the loss of three V_L CDRs.

Somatic mutation in CDR1 can directly participate in antigen binding, while an extra disulfide bond in some VHHs addresses entropically favored antigen binding caused by an elongated CDR3.^{33,34,35} This leads to the formation of different loop structures that participate in antigen binding. The solubility and stability are improved by a hydrophobic amino acid exchange in the VHHs, which also affects the molecular and thermodynamic stability and makes VHH more resistant to chemical denaturants, proteolytic enzymes, harsh pH conditions or ionic strength.³⁶ Conversely, the two-domain structure of scFvs offers greater flexibility, making them advantageous for certain applications, although it reduces its stability.³⁷ Their small size and the rapid progress in the development of antibody fragments led to a development of a variety of applications. For examples, scFv and VHH are used as neutralizing agents that bind foreign particles and inactive toxins or cancer antigens.³⁸ Alternatively, they can be directly chemically conjugated to therapeutic payloads to minimize non-specific toxicity to normal cells.³⁹

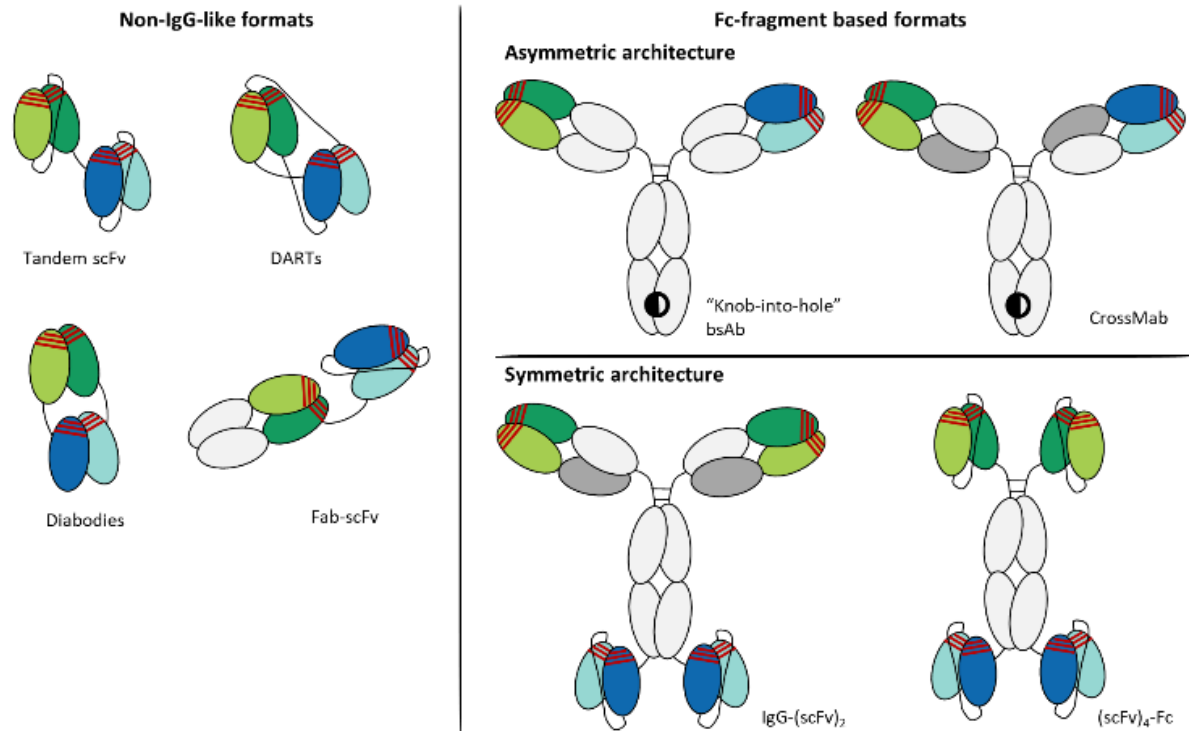


Figure 2 Bispecific antibody formats categorized by non-IgG-like formats without Fc-fragment and Fc-fragment based formats. The Fc-fragment based fragments are further classified in asymmetric and symmetric architecture. Each color represents a variable domain (variable heavy chain specificity 1 - green, variable light chain specificity 1 - light green, variable heavy chain specificity 2 - blue, variable light chain specificity 2 - light blue), the connecting peptide linkers are shown as black line. The dark grey colored C_L shows the light chain switch for. The “knob-into-hole” amino acid exchange for correct heavy chain pairing is shown as black circle within the C_{H3} domain of the antibody.

Bispecific molecules can be generated via chemical conjugation, quadroma and genetic recombination, of which only the most common and relevant for this work are discussed here.^{40,41} In bivalent antibodies, both antigen binding sites are identical, presenting the challenge of deriving a functional bsAb from the pool of ten potential combinations of heavy and light chains. Consequently, correct chain pairing is difficult to achieve for bispecific antibodies. In practice, this can lead to ineffective antibodies or heterodimers. Approaches have been developed to control this problem. Thus, two categories for bsAb, namely *i.)* Ig-like antibody approaches (containing the Fc-fragment) and *ii.)* non-Ig-like (without Fc-fragment) exist. Fc-containing protein depending on their symmetric or asymmetric architecture, can be further divided into two sub-groups. Most often symmetrical structures are used. In these structures, additional binding sites are bound to the termini of the antibody scaffold. When single-domain antibodies or other scaffold proteins are used, a tetravalent molecule is typically generated by expressing two polypeptide chains with a single expression vector. Asymmetric bsAbs maintain the IgG structure and are therefore bispecific monovalent for each antigen. They are produced recombinantly by expression of four peptide chains using two different expression vectors. The heterodimerization of the different chains is mediated by mutations in the Fc fragment and the interface of C_L and C_{H1}.

For instance, the "knob-into-hole" (KIH) technique utilizes an amino acid substitution within the third constant domain of the antibody to facilitate proper pairing.⁴² The CrossMab approach resolves light chain mismatch by substituting the CL domain of the LC with the corresponding C_H1 domain of the HC, promoting proper light chain association.⁴³ The common-light chain approach utilizes common light chains, since the heavy chain is primarily responsible for the antigen interaction. Further, asymmetric formats can be isolated through purification strategies based on differential protein A binding, sequential affinity chromatography, or size differences.^{44,45} Non-Ig-like formats such as tandem scFv, diabodies, DARTs, Fab-scFv, and many more can penetrate tissue better due to their small size, but this also leads to shorter plasma half-lives due to the lack of FcRn binding. Producing non-Ig-like bispecific antibodies lacking an Fc-fragment can be achieved through the utilization of Fab fragments or by linking antibody fragments together. One example are Bispecific T-cell Engager (BiTE®) antibody platforms, in which tandem scFvs are constructed in the form of two scFvs with a repeated glycine-serine linker sequence that allows maximum rotation for antigen binding.^{46,47} The fragments are triggered by combining the V_H and V_L domains of the two scFvs with two peptide chains, within the diabody format.⁴⁸

BsAbs are either produced through synthesis or expression but can also be created via protein-protein fusion. In this context, different conjugation strategies have been described and their characteristic and respective advantages are discussed within the subsequent chapter.

1.4 Antibody modification via conjugation

1.4.1 Antibody-drug conjugates

As early as 1913, Paul Ehrlich envisioned the selective transportation of toxins to tumors,⁴⁹ a concept was realized approximately eighty-seven years later with the first antibody-drug conjugate (ADC) that targeted CD33 (Mylotarg®). The ADC approach involves coupling small toxins to antibodies and utilizes the selectivity of the antibody to transport a drug to the tumor where it can be released under specific conditions. By increasing the MTD and lowering the MED, this concept approach extends the therapeutic window.⁵⁰ ADCs involve the covalent linkage of small cytotoxic drugs to the antibody by a chemical linker. Consequently, a classical ADC typically consists of three components: *i)* the targeting antibody, *ii)* a linker sequence, and *iii)* a cytotoxic warhead. The fundamental mechanism of an ADC therapy involves the selective binding of the antibody to its target on tumor cells. This is followed by receptor-mediated internalization via endocytosis. Once the ADC reaches the tumor environment and following the lysosome, the payload is released via enzymatic cleavage of the linker or the degradation of the antibody. The thereby released payload enters the cytoplasm and can interfere with critical cellular machinery. Ultimately, this leads to cell apoptosis. In the practice, the efficiency of the approach relies on the

kinetics and thermodynamics of antibody-antigen interaction, as well as the rate of internalization.⁵⁰ Generation of ADC products relies on chemical conjugation methods, that can impact the stability and homogeneity of the resulting products.

1.4.2 Conjugation strategies

Traditional conjugation methods, such as lysine⁵¹ and cysteine conjugation,⁵² result in heterogeneous mixtures due to numerous potential coupling sites on the antibody surface. Lysine conjugation involves linkers equipped with N-hydroxysuccinimide esters, which react with the primary amine of lysine residues to form a stable amide bond (Figure 3). However, the high number of accessible lysine residues across the entire antibody surface leads to highly heterogeneous mixtures, that result in a variety number of ADC species with different drug-to-antibody ratios (DAR) and attachment sites. This method allows the generation of ADCs with drug load distribution ranging from 0 to 8 drugs per antibody and can be adjusted to an average of DAR 3-4 under specific manufacturing conditions.⁵¹ Compared to this, conjugation attempts via a cysteine typically result in more homogeneous ADC. This increase in selectivity is due to the reduced number of conjugation sites compared to lysine conjugation. Since the backbone of an IgG1 antibody contain four inter- and twelve intrachain disulfide bonds, reducing agents such as TCEP are used to access the interchain disulfides without affecting the intrachain disulfides. The development of novel conjugation technologies enables the precise placement of linker drugs at selected positions and allow the preparation of more tailored, homogeneous ADCs. One technology introduced cysteines into the mAb by site-directed mutagenesis of light chain residue V205C⁵³ or heavy chain A114C⁵⁴, resulting in THIOMAB™ with additional cysteines.⁵⁴ Different homogenous approaches involve the incorporation of unnatural amino acids, that are not part of the naturally encoded proteinogenic amino acids repertoire. This requires the extension of the genetic code at specific positions of the recombinantly expressed antibodies and is typically achieved using manipulated tRNA incorporated into the antibody sequence by an orthogonal expression system.⁵⁵ Finally, the modification of glycans offers another method for site-specific linker-linker payload conjugation. Modified glycans can be either expressed in the antibody by metabolic engineering or post-translationally modified using glycan-modifying enzymes. Azido anchors are often attached to the mAb-glycan, allowing them to react with reactive alkynes of the linker payloads using copper-free click chemistry.⁵⁶

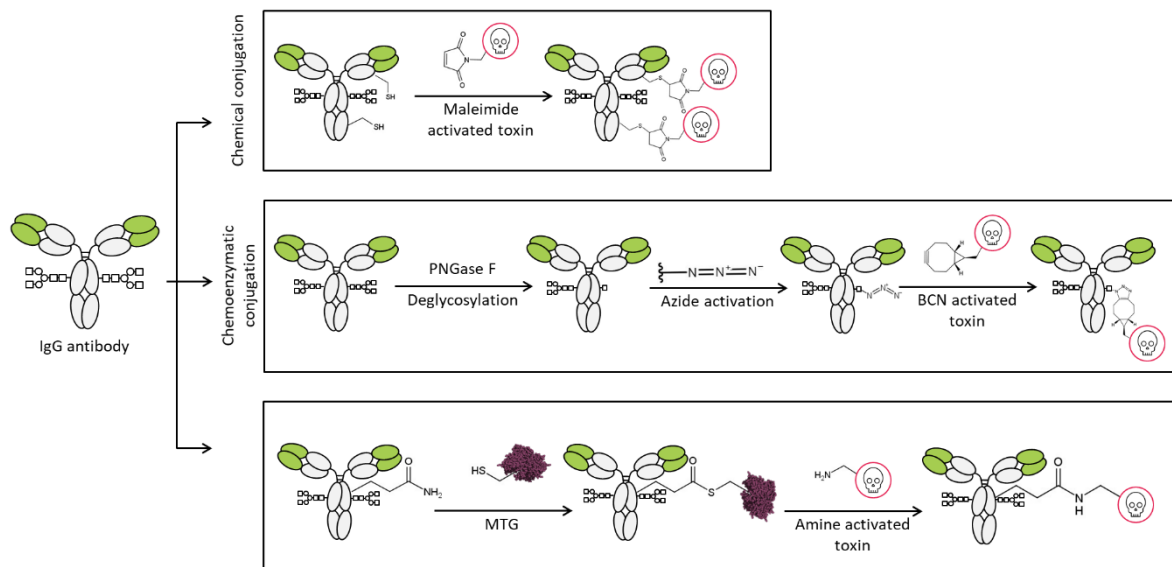


Figure 3 Schematic conjugation strategies for generation of different antibody-drug conjugates (ADC). FDA-approved ADCs are typically conjugated via chemical methods, such as the reaction of cysteines with maleimides in a Michael addition. Newer approaches of chemoenzymatic and enzymatic strategies show promising results in pre-clinical studies. For simplicity, the conjugation to the antibody is only shown on one chain of the protein.

In general, chemoenzymatic methods involve a chemical conjugation step, with most of reactions being grouped under the umbrella term "click chemistry". "Click chemistry" was introduced at the beginning of the millennium and describes original reactions in which the formation of carbon hetero bonds produces products with high yields and selectivity.⁵⁷ The word "click" refers to the modular, energetically favored, specific and versatile chemical transformation to a single reaction product with high yields. The click toolbox has gained prominence, with copper(I)-catalyzed Huisgen azide-alkyne cycloadditions (CuAAC) emerging as the most popular Click reaction.⁵⁸ An activated Cu(I) catalyst can be generated from Cu(I). During the catalytic cycle, σ -bonded copper acetylide with π -coordinated copper coordinates the azide, followed by the formation of an unusual six-membered copper-metal cycle. A second copper atom behaves like a stabilizing donor ligand. The triazole product is formed by the ring constriction to a triazolyl copper compound and the subsequent proteolysis.⁵⁹ In 2004, Bertozzi and coworkers shown that a catalyst is not always necessary to perform a cycloaddition. By using electron deficient alkynes, the reaction can also occur under ambient conditions.^{60,61} Compared to previous methods no metals are required as catalysts, which increases the compatibility of the reaction with biological systems. In the strain-promoted azide-alkyne cycloaddition (SPAAC), the ring stress in the cycloalkane starting material destabilizes the alkyne to such an extent that the reaction proceeds efficiently without a catalyst. Hence, the SPAAC reaction requires an azide group on one molecule and a "strained" alkyne on the other molecule (Figure 4). Clickable alkyne groups are stabilized by ring strain increasing groups such as cyclooctyne and promote the reaction an 1,3-dipolar cycloaddition reaction.

This bioorthogonal reaction results in a triazole⁶¹ and typically, proceeds rapidly ($0.1 \text{ M}^{-1}\text{s}^{-1}$ under physiological conditions) and selectively in aqueous solutions at room temperature or slightly increased temperatures.⁶² Since SPAAC reaction is a second order chemical reaction, the kinetics are not dependent on the concentrations of the chemical structures⁶³ and despite the high reactivity of alkynes with azides both reactants are typically stable under most physiological conditions.⁶² Different ring strained alkynes are available for efficient click reaction, which differ in their structure and charge and thus have different properties in reactivity and lipophilicity.⁶⁴ The hydrophobic nature of aromatic rings is often unsuitable for biochemical conjugation in aqueous solutions, leading to protein aggregation or precipitation. In practice, this decreases the yield and purity of the product.⁶³ However, the hydrophobicity of alkynes can be compensated for by the incorporation of hydrophilic spacers such as polyethylene glycol (PEG).⁶² Due to their low lipophilicity and high reactivity, bicyclononyne (BCN) and dibenzocyclooctyne (DBCO), were selected for the MTG-mediated conjugation to antibody and scFv and subsequent SPAAC of the two proteins.⁶⁵

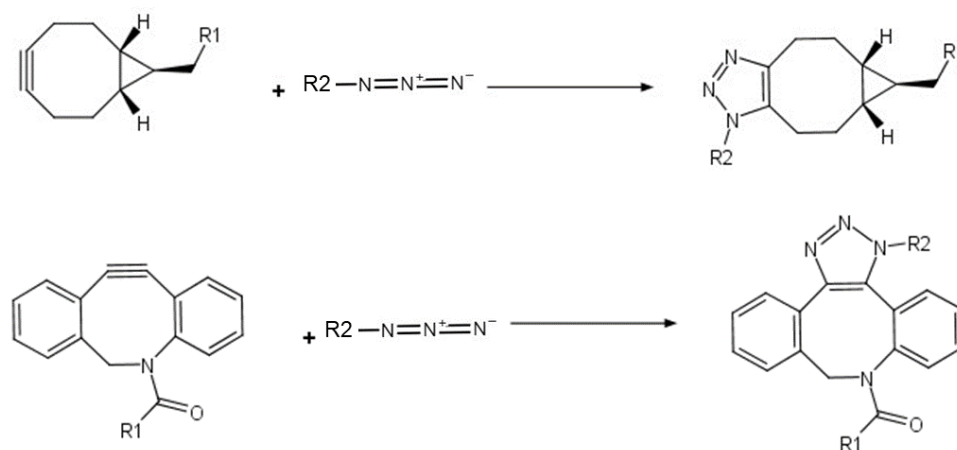


Figure 4 Strain-promoted azide-alkyne cycloaddition (SPAAC). The bicyclononyne- (BCN) or dibenzocyclooctyne- (DBCO) derivative reacts with organic azide and forms a stable 1,2,3-triazole. The R groups represent the rest of the molecule.

In addition to SPAAC, an enzymatic conjugation strategy involving microbial transglutaminase (MTG) was used for installation of click derivatives and the direct conjugation of VHH. MTG is a protein-glutamine amine γ -glutamyl transferase derived from the strain *Streptomyces Mobaraensis* (*S. Mob*). MTG is generated through the expression of the catalytically inactive zymogen in *S. mob*, which is then produced by the proteases TAMP (transglutaminase-activating metalloprotease)⁶⁶ or SM-TAP (*Streptomyces mobaraensis* tripeptidyl aminopeptidase)⁶⁷. Alternatively, MTG can be produced by recombinant expression in *E. coli*, followed by processing with commercial proteases. In nature, ammonia is released when an iso-peptide bond is formed between the acyl donor, usually the γ -carboxamide function of peptide-bound glutamines, and the acyl acceptor, either the ϵ -amino group of lysine residues or other primary amines (Figure 5).⁶⁸

When primary amines are absent, water can serve as an acyl-acceptor which, results in the formation of glutamic acid via deamidation of glutamine.⁶⁹ The activity of MTG is independent of Ca^{2+} or GTP and is most effective at 50 °C and pH 6-7, which was tested in a CBZ- glutaminyglycine assay with hydroxylamine as substrate.⁶⁹ Transamidation by the cysteine protease-like mechanism is enabled by the catalytic triad of Cys64, Asp255 and His274. Cys64 nucleophilic attacks the γ -carboxamide of the acyl-donor and generates a reactive thioester, while Asp255 subtracts a proton of the acyl-acceptor. The nucleophilic attack of the thioester induces the formation of the iso-peptide bond between donor and acceptor with regeneration of Cys64. The impact of the flexibility of the targeted site, the structural arrangement of the target protein, and the polarity of neighboring amino acids has been identified as a major influencing factor on its activity.⁷⁰ In general, MTG transamidates numerous different primary amines and is not selective regarding its acyl-acceptor substrates, in contrast to the corresponding acyl donor. Here, MTG is more stringent. Screening studies attempted peptidic structures based on the antibody environment around Q295 and suggested small amino acid neighbors with polar, hydrophobic or uncharged properties. These were better tolerated by MTG than bulky and aromatic residues, while charged neighbors were found to be highly unfavorable.^{71,67}

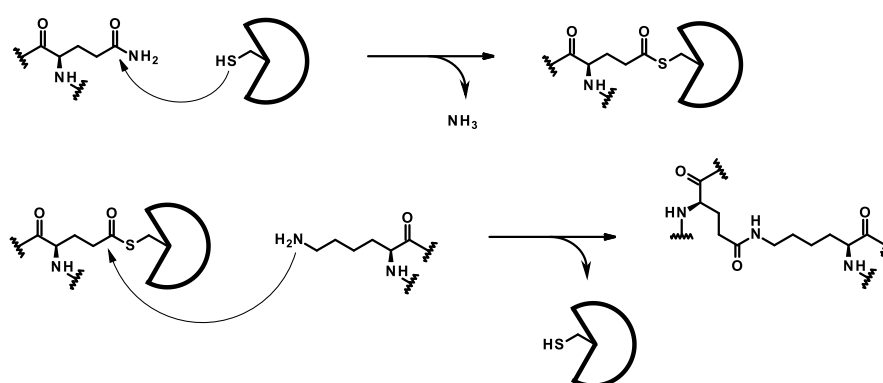


Figure 5 Mechanism of transglutaminase-mediated transamidation. MTG catalyzes the transfer of primary amines to the γ -carboxamide group of the glutamine. The nucleophilic attack of Cys64 on the γ -carboxamide group of the acyl-donor results in the formation of a thioester, accompanied by the release of ammonia. Subsequently, the ϵ -amino group of the acyl-acceptor (in this case, lysine) interacts with the side chain, leading to the formation of an iso-peptide bond between the donor and acceptor, while regenerating Cys64. Figure based on Deweid *et al.*⁷²

1.4.2.1 Transglutaminase-mediated conjugation

Site-specific enzymatic conjugation strategies are gaining popularity as they provide uniform products and thus pharmacological benefits.⁷³ MTG-mediated conjugation to glutamines has been reported in detail for modified antibodies or antibody fragments with glutamine tags. Surprisingly, none of the multiple glutamine residues in an antibody appeared to be an efficient substrate for MTG using the typically applied MTG variant and reactions conditions. A strategy to

use MTG for antibody modification is to genetically fused peptide tags recognized by MTG such as combinations of LLQG to both light chains and heavy chains of antibodies.^{74,75}

Recognition sequences for site-specific conjugation by MTG were rationally designed by Sigmund *et al.*⁷⁴ and the working group around Strop *et al.* used a high-performance screening for identification of LLQG-tag positions with high efficiency, stability and pharmacokinetics of ADCs.⁷⁵ Alternatively, glutamine in native antibodies is accessible to the MTG, Q295 in the heavy chain. Nearby, at N297, the glycosylation site of the antibody is conserved. The removal of the N-glycan increased the accessibility of Q295, resulting in the successful generation of homogeneous ADC.⁷⁶ Benjamin and colleagues facilitated the site-specific conjugation of the payload by deglycosylation and transglutaminase-mediated incorporation of a thiol at the Q295 site, followed by a subsequent click chemical reaction.⁷⁷ These studies enabled the production of uniform ADCs, however required genetical modifications by introducing recognition tags or antibody deglycosylation. As shown in recent studies by Dickgiesser and Rieker *et al.*, efficient conjugation to unmodified native IgG was achieved by mutations of MTG.⁷⁸ A huge advantage is that the ADC antibody remains unmodified. MTG variants were identified which enabled highest conjugation efficiency of two drugs per antibody (DAR 2).⁷⁸

1.4.3 Bispecific antibody generation via conjugation

The early generation of bispecific antibodies is based on the chemical coupling of monospecific variants.⁷⁹ However, at that time, the conjugation technology had not advanced significantly, limited by the expensive and thus non-scalable manufacturing process of Fc-based bsAb's. Initial approaches used thiol-amine chemical linkage of two full-length antibodies, resulting in heterogeneous mixtures due to random-lysine conjugation.^{46,80} Several drawbacks prompted the development of engineering techniques, and today most methods for generating bsAb's are based on protein engineering and expression systems. However, innovations in the linker-drug conjugation of ADCs provided the basis for new chemical approaches to the production of bsAb's.⁸¹ Fab-based bsAb are mostly generated by cysteine bases cross linkage.⁸² Chemical generation of full-length antibodies can be done by disulfide bridging of two native IgG2 antibodies.⁸³ Further, conjugation of two Fabs using unnatural amino acids with orthogonal chemical reactivity,⁸⁴ or by the fusion of Fabs to native antibodies using haloketone derivatives are further methods for generation of bsAb via conjugation.⁸⁵ In this case, the enzymatic installation of reactive groups was reported in the context of sortase A (SrtA), where azide was site-selectively installed on engineered heavy chain SrtA recognition tags without the need of unnatural amino acids. This chemo-enzymatic approach has been utilized to create antibody-protein conjugates by attaching complementary reactive handles to the proteins of interest.⁸⁶ A comparable method employed engineered lipoic acid protein ligase A (LplA) to attach unnatural

lipoic acid analogs to lipoate-acceptor peptide motifs incorporated into recombinant proteins.⁸⁷ The various LpIA contained strained alkynes or alkenes, where BCN was shown to be the most effective dienophile partner with the tetrazines. Besides protein-protein conjugates with EGFP, antibody-protein constructs with trastuzumab were studied.⁸⁷

1.5 Target proteins and binding antibodies

The following chapter briefly summarizes the targets addressed in this study. Specifically, it describes their function, and provides an overview of targeting antibodies.

1.5.1 EGFR and HER2

ERBB receptor tyrosine kinases (RTK) are a protein family that include the epidermal growth factor receptor (EGFR, also known as ERBB1 or HER1) and the human epidermal growth factor receptor 2 (HER2). Both are anchored in the cytoplasmic membrane and comprise a ligand-binding domain on the cell surface, a transmembrane domain and tyrosine kinase domain, which is located intracellular.⁸⁸ Binding of one of the twelve ligands results in autophosphorylation of ERBB receptors. This initiates to downstream signaling pathways that regulate critical cellular functions. These signaling pathways involve adaptors and scaffolding proteins, which commonly contain motifs like Phosphotyrosine-binding (PTB) and Src homology 2 (SH2) domains for binding to Phosphotyrosine, or SH3 domains for binding to proline-rich sequences of target proteins.⁸⁹ The phosphorylated residues function as attachment sites for proteins that influence the expression of multiple tumor-associated genes, that regulate survival, proliferation, migration, invasion, and metastasis.⁹⁰ Despite the crucial importance of receptors for normal cellular processes, a dysregulation of gene amplification, protein overexpression or mutations in key proteins may lead to the development of cancer. For example, HER2 and EGFR are overexpressed in a wide variety of cancers. Therefore, they present interesting targets and various therapies such as tyrosine kinase inhibitors (TKIs) and ectodomain-targeting antibodies have been developed. Upon activating ligand binding with EGF, TGF- α , amphiregulin, or neuregulin, the 170 kDa EGFR protein forms EGFR-EGFR dimers or heterodimers with HER2, HER3 or HER4. Ligand binding leads to activation and phosphorylation of tyrosine residues and subsequent internalization and either degradation or recycling. Heterodimerization with HER2 and neuregulin enhances mitogenic signaling. Activation of the ras- and mitogen-activated protein kinase (MAPK) pathway stimulates proliferation of cells, whereas activation of phosphatidylinositol-3 kinase (PI3K) and protein kinase B (Akt) pathway promotes progression of the cell cycle and survival.⁹⁰ Monoclonal antibodies targeting EGFR, e.g. Cetuximab (Ctx, Erbitux™) bind to its extracellular domain when it's inactive. By interacting with the ligand-binding region, they compete with the

receptor for binding, thus effectively blocking the activation of EGFR tyrosine kinase induced by ligands. Ctx is an IgG1 human-murine chimeric antibody, that binds EGFR in a two orders of magnitude higher affinity as EGF, the natural ligand and thus enables receptor internalization and degradation without activation.⁹¹ Furthermore, Ctx inhibits the production of pro-angiogenic factors which reduced blood vessel formation and metastasis in cancer models.⁹²

First phase I and I/II studies showed the safety of Ctx alone and in combination with chemotherapy when carcinoma of the head and neck, colorectal cancer and non-small-cell lung cancer were investigated.^{93,94} In a phase II trial, the combination of Ctx and irinotecan demonstrated notably higher response rates and disease control rates compared to Ctx alone in patients with EGFR-positive metastatic colon cancer refractory to irinotecan.⁹⁵ As for today, Ctx is approved for use in combination with chemotherapy in squamous cell carcinoma of the head and neck (SCCHN) and *RAS* wild-type metastatic colorectal cancer as well as in SCCHN as combinatory treatment with radiation.^{96,97} The EGFR pathway inhibitory mechanism of Ctx, in combination with avelumab as a blocker of PD-L1 receptor interaction and prevention of T-cell suppression, shows potential complementary effects in clinical trials. In addition to Ctx, panitumumab is another approved anti-EGFR monoclonal antibody but is not relevant in the context of this study.⁹⁸ HER2 exhibits constitutive activity, initiating signaling pathways independent of ligand binding or activation. Furthermore, HER2 can also form homodimers and heterodimers with other family members, subsequently resulting in the activation of signaling pathways and tumor growth. HER2 is upregulated in about 20% of breast and gastric/gastroesophageal junction cancer making it a valid therapeutic target for antitumor therapy.⁹⁹

Trastuzumab (Ttz, Herceptin®) and Pertuzumab (Ptz, Perjeta®) are monoclonal antibodies that bind to different domains of HER2, inhibiting cell proliferation and signaling. While Ttz binds to the extracellular domain 4 (ECD4) and inhibits tumor cell proliferation, suppression of cell signaling and ADCC,¹⁰⁰ Ptz interacts with the ECD2 and inhibits the heterodimer-mediated activation.¹⁰¹ Multiple anti-HER2 drugs have been approved for cancer treatment, such as Ttz, Ptz, neratinib, lapatinib, trastuzumab deruxtecan (Enhertu®) and trastuzumab emtansine (T-DM1). They are applied for HER2-positive breast cancer treatment, and in the case of Ttz and trastuzumab deruxtecan for treating gastric cancer.¹⁰² The conjugation of the proteas-cleavable maleimide linker and DNA topoisomerase I inhibitor payload (DXd, derivate of camptothecin analogue exatecan) and expands trastuzumab's mode of action by making use of its strong internalization rates. The successful internalization of the ADC and the subsequent release of DXd results in an inhibition of DNA replication, which subsequently leads to cell cycle arrest and further apoptosis of the cells.^{103,104}

1.5.2 PD-L1

The programmed cell death ligand-1 (PD-L1) belongs to the immune checkpoint (IC) proteins, a class of immune-modulating proteins with immunosuppressive function. These classes of proteins modulate the self-destruction of cells and thus avoid autoimmunity, ensures that peripheral tolerance is maintained, and inhibit activation of immune responses. IC functions include, for example, the interaction of PD-1 and PD-L1, with PD-L1 being highly expressed on some tumor cells and on antigen-presenting cells (APC) and PD-1 on active T cells. An interaction results in phosphorylation of tyrosine residues in the cytoplasmic region of PD-1 and following recruitment of Src homology 2 domain-containing protein tyrosine phosphatase-2 (SHP-2). This leads to phosphorylation of the tyrosine kinase (Syk) and phospholipid inositol-3-kinase (PI3K) both downstream proteins, and inhibits signaling and biological T cell functions.¹⁰⁵ Interestingly, the microenvironment in nearly all solid tumors exhibits immunosuppressive traits stemming from the secretion of specific molecules like IL-10 and IFN- γ , alongside the modulation of immune cell functions.^{106,107} In many cancers, PD-1 is expressed on tumor-infiltrating lymphocytes, reflecting an immunosuppressive tumor microenvironment. This allows the cancer cells to evade the immune system and its surveillance, leading to cancer progression. The interaction between PD-1 and PD-L1 blocks the antitumor resistance of the host, facilitating tumor immune evasion through a variety of mechanisms. Anti-PD-1/PD-L1 antibodies have shown success in treating tumors, but their effectiveness varies among patients.

Two anti-PD-L1 antibodies atezolizumab (Atz, Tecentriq) and avelumab (Ave, Bavencio) were of interest in this work and therefore their properties are discussed closer. Atz is a phage-derived human IgG1 full-length antibody that blocks PD-L1 and prevents from ADCC and CDC by genetic modification of the Fc fragment (substitution at position 297 Asn to Ala). Different affinities were determined for the binding of Atz to PD-L1 resulting from the different post-translational modification of PD-L1. For example, a K_D of 0.19 nM was reported for the binding of the dimeric form and 0.62 nM for the monomeric form.¹⁰⁸ The binding affinity of Atz to glycosylated PD-L1 showed a K_D of 4.7 nM whereas the non-glycosylated form showed a K_D of 17.8 nM.¹⁰⁹ Apart from PD-L1 binding, the internalization of PD-L1 was observed in different target-positive cell lines. Approximately 40-60% of the PD-L1 protein was internalized in MDA-MB-231 within 2 hours and could be detected in the lysosome after 16 hours of treatment.¹¹⁰ In addition to the treatment of urothelial carcinoma, Atz also showed curative effects in breast cancer, bladder transitional cell carcinoma and kidney cancer.¹¹¹ Ave, also blocked PD-L1 but retained its full Fc-mediated effector function. Therefore, it has the potential to induce ADCC and CDC. The binding affinity of 0.042 nM is significantly higher than that of Atz, with strong binding to glycosylated PD-L1 in particular.¹¹² However, Ave showed a lower endocytosis efficiency with less than 20% in PD-L1 positive cells.¹¹⁰

1.5.3 RNF43

The tumor suppressor, ring finger protein 43 (RNF43) is a stem-cell E3 ligase. It induces endocytosis of Wnt receptors. The *RNF43* and *ZNRF3* gene expression is regulated by the T cell factor 4/ β -catenin complex, which is part of the Wnt/ β -catenin pathway.¹¹³ The RNF43 protein contains an 200-amino acid extracellular protease-associated (PA) domain, which acts as a specific protein recognition site for the target of ubiquitination, as well as an ectodomain, i.e. a single transmembrane region and a cytoplasmic RING domain with a ubiquitin-protein ligase activity.¹¹⁴ Although the precise interaction sites and downstream signaling mechanisms remain unclear, both the extracellular and cytoplasmic domains were previously determined to be crucial for ubiquitination.¹¹⁵ RNF43 was identified as a widely expressed transferase responsible for mediating the ubiquitination of the cytoplasmic loops of the Frizzled (Fzd) receptor, a crucial component of the membrane-associated Wnt receptor complex. During its enzymatic reaction, RNF43 acts as a mediator, transferring S-ubiquitin from an E2 ubiquitin-conjugating enzyme to the cytosolic lysine residues of the targeted acceptor protein.¹¹⁶ RING domain-dependent autoubiquitylation triggers the endocytosis and subsequent lysosomal degradation of Fzd and its associated lipoprotein receptor-related proteins 5 and 6 (LRP5/6).^{117,118} This activity makes RNF43 one of the many negative feedback regulators of the tightly controlled canonical signaling pathway of Wnt.¹¹⁶ Additionally, the non-canonical signaling pathway of Wnt can be downregulated by the C-terminal cytoplasmic region of RNF43, which interacts with targeted acceptor protein and inhibits its phosphorylation, thereby suppressing downstream pathways. Due to its role as a negative Wnt regulator and tumor suppressor, mutations of RNF43 are often associated with the development of various tumor diseases. For example, somatic RNF43 mutations are found in >18% of endometrial carcinomas and colorectal adenocarcinomas.¹¹⁹

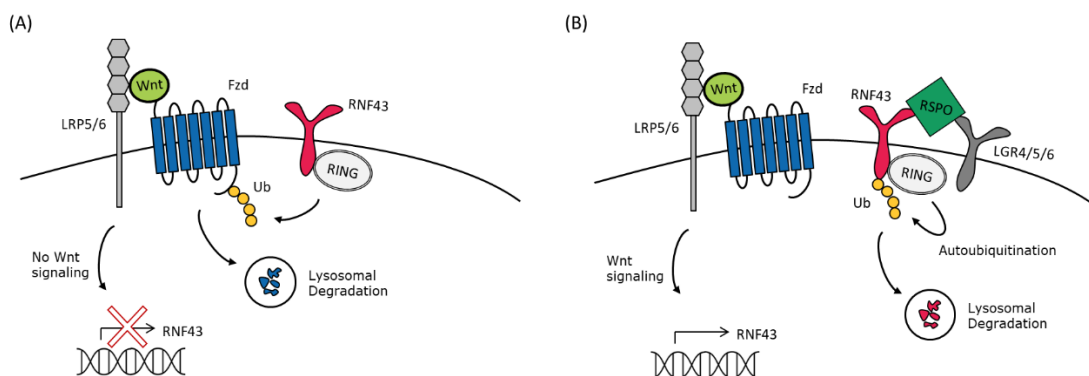


Figure 6 Canonical Wnt-signaling of RNF43 regulating the surface level of Fzd receptor in presence and absence of RSPO. (A) RNF43 inhibits the interaction through intrinsic ubiquitination and subsequent degradation of Fzd, leading to the downregulation of the Wnt signaling pathway. **(B)** Rspodin binds RNF43 and LGR4/5/6 and induces autoubiquitination of RNF43 and following lysosomal degradation of RNF43. Wnt/ β -catenin signaling pathway is activated. Fzd – Frizzled receptor, LRP5/6 - lipoprotein receptor-related proteins 5 and 6, Ub - Ubiquitin, RSPO - Rspodin, LGR4/5/6 - G-protein-coupled receptor 4,5,6. Figure based on Hao *et al.*¹²⁰

Rspondin proteins (RSPO) can negatively regulate RNF43, by simultaneously interacting with leucine-rich repeat containing G-protein-coupled receptor 4,5,6 (LGR4/5/6) and RNF43.^{116,121} This interaction leads to autoubiquitination, endocytosis and degradation of the RSPO-LGR-RNF43 complex. However, the interaction site might correlate with the binding site of Fzd but has not been verified yet.¹²² A second RNF43 membrane clearance proposes the LGR-independent mechanism in which the RSPO binds to heparin sulfate proteoglycans (HSPG). While both mechanisms can downregulate Fzd through RNF43, this can enhance the Wnt-signal pathway.¹²³ Considering the significance of RNF43 in Wnt/ β -catenin signaling, an appropriate understanding of the biology of RNF43 is required. In this context, RNF43 antibodies are used to visualize endogenous RNF43 via immunoblotting or immunofluorescence. Importantly however, the antibodies also have an important role to assess RNF43 protein expression in different tumors.¹²⁴ The therapeutic use of RNF43 antibodies is so far limited to a few, a monoclonal antibodies combined with a yet undisclosed cytotoxic agent that is being investigated as ADC SC-006 in the treatment of advanced colorectal cancer in phase I study. However, this study was terminated due to thrombocytopenia below the predicted efficacy dose.¹²⁵ In 2015, Abbvie Stemcentrx filed a patent application in which various RNF43 antibodies and ADCs were screened for the treatment of cancer. The amino acid sequence of the V_H and V_L of the anti-RNF43 scFv variants used in this thesis also derive from this patent.¹²⁶ Recently, RNF43 has gained considerable interest in the targeted degradation of membrane-bound targets. In various approaches, RNF43 binders have been selected and used in the form of bispecific molecules for protein degradation, which will be discussed in more detail in the next chapters.^{127,128,129}

1.6 Protein degradation

1.6.1 Ubiquitin-proteasome pathway of intracellular proteolysis

Ubiquitin-dependent proteolysis is the basis of targeted protein degradation (TPD). Here, intracellular proteins are degraded as part of normal cellular maintenance processes. The sequence follows a three-stage process with ubiquitin-activating enzyme (E1), ubiquitin-conjugating enzyme (E2) and ubiquitin-protein ligase (E3) as players, and E3 co-determining the transfer of ubiquitin (Ub) to the target protein.¹³⁰ Ub transfer occurs in three steps (Figure 7), with initial E1 using an internal E1-Cys residue to activate the C-terminal glycine of Ub to an energy-rich thiol ester. E2 subsequently transfers the activated Ub via an E2-Ub-thiol ester intermediate to the substrate, and the substrate binds to E3. The transfer can take place directly to the substrate or via another E3-Ub-thiol ester intermediate.

E3 catalyzes the attachment of the Ub to the substrate. Here, the first Ub is coupled to the ϵ -NH₂ group of a lysine residue or to the α -NH₂ group by generation of an iso-peptide bond or linear

peptide bond. Subsequently, a polyubiquitin chain is successively formed by the transfer of further activated Ub residues and serves as a recognition marker for the protease. The most frequently used lysine residues are Lys29, Lys48 or Lys63. In this process, an E1 species is responsible for the activation and transfer of all Ub to different E2 isoforms that can interact with one or more E3 ligases.¹³⁰

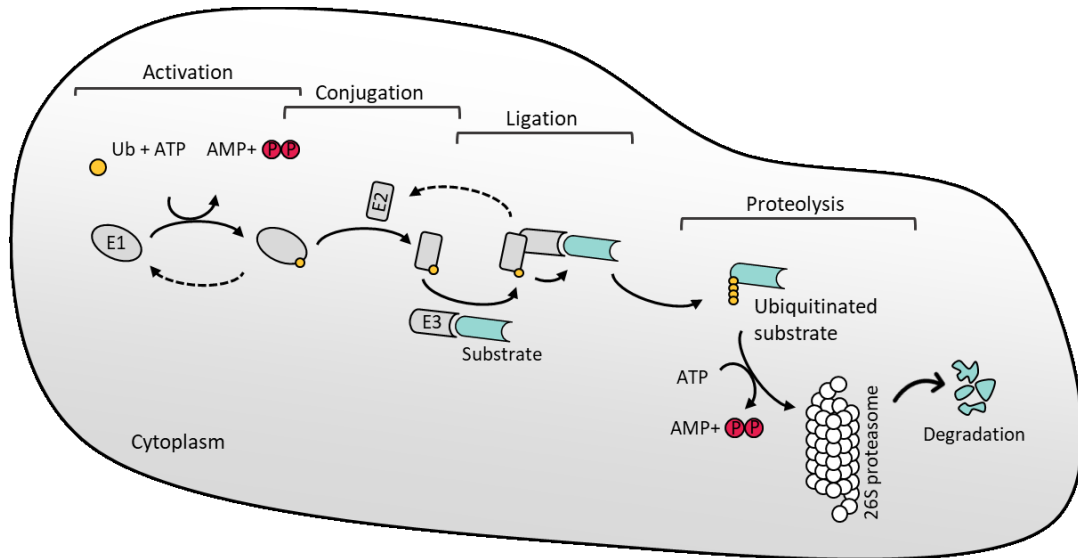


Figure 7 The ubiquitin-proteasome system. Ubiquitin activation by ubiquitin-activating enzyme (E1), then the transmission of activated ubiquitin (Ub) moiety to ubiquitin-conjugating enzymes (E2) and transfer of activated Ub from E2 to a cysteine residue on ubiquitin-protein ligases (E3) or directly to the substrate. The polyubiquitinated substrate is then degraded by the 26S proteasome complex that causes release and reusable Ub and E3 ligase.

Although the components are localized in the cytosol and nucleus, membrane-anchored substrates, and ER luminal proteins are also degraded, which occurs by transport back into the cytosol.¹³¹ The E3 ligase provides the high specificity by recognizing and binding the substrate into the system. Recognition is achieved via specific structural motifs that are either encoded in the substrate itself or recognition elements such as post-translational modifications, for example phosphorylation and association of molecular chaperones. However, the modification of the E3 enzyme or subunits can be essential for activation. The E3 ligase can be divided into at least six subtypes, E3 α recognizes destabilized N-terminal residues,¹³² HECT-domain proteins,¹³³ anaphase promoting complex (APC) or cyclosome,¹³⁴ SCF complexes,¹³⁰ several RING finger proteins (e.g. cereblon)¹³⁵ and von Hippel-Lindau tumor suppressor protein (VHL).¹³⁶ VHL is part of a complex of Elongins B and C, Cullin-2, and Rbx1/Roc1 which induces the polyubiquitination of hypoxia-inducible factors (HIFs) for degradation.¹³⁷

Cereblon (CRBN) is a RING-domain E3 ligase and a conserved regulator of Wnt signaling pathway. This mechanism is not well understood; however, it is suggested that Wnt pathway activation associated with casein kinase 1 α (CK1 α) stimulates CRBN and facilitates ubiquitin dependent CK1 α degradation. CK1 α has been recognized as one of the key negative regulators of Wnt

signaling.¹³⁸ The 26S proteasome comprises two complexes, the 20S core and 19S particle that contain α - and β -rings and is responsible for the degradation of polyubiquitinated proteins into small peptides. The catalytic site is localized in one of the β -subunits of the 20S unit and several ubiquitin recognition sites are located in the 19S unit.¹³⁰ In addition to ubiquitinated proteins, the 19S subunit also recognizes other substrates of the proteasome, which are inserted into the proteolytic chamber via a "gate" in the α -ring. It is hypothesized that the 19S particle unravels the peptide chain to enter into the proteolytic pocket.

1.6.2 Targeted protein degradation inducers as therapeutic modality

The therapeutic potential of utilizing the natural degradation system has been inspired by early studies in viruses and plants using the targeted design of small molecules to hijack E3 ligases and degrade the target. There are dozens of known virus species that hijack the human ubiquitin-proteasome system to enhance their replication and survival.¹³⁹ TPD presents a novel therapeutic approach to degrade pathogenic proteins that have been defying to address using traditional small molecules. More detailed discussions on this topic can be found in the following chapter.

1.6.2.1 PROTAC

The most prominent targeted degraders are hetero-bifunctional molecules known as proteolysis-targeting chimeras (PROTACs), comprising two ligands linked together, one recruiting an E3 ligase and the other binding the protein of interest (POI). The formation of a tertiary "E3-PROTAC-POI" complex leads to the ubiquitination of the POI by the E3 ligase and subsequent proteasomal degradation via the UPS.¹⁴⁰ PROTACs can recruit target molecules through any binding site. This eliminates the need for sustained inhibition. PROTACs are using the UPS pathway to degrade and eliminate targeted proteins. Relative to classical inhibitors, which require access to a cavity or binding pocket, low-affinity PROTAC-protein binding can lead to catalytic target degradation in an event-based driven mechanism of action. Effectively, they merely necessitate a brief interaction to proteolyze the POI and can be recycled to destroy the overall protein target. Unlike traditional inhibitors, PROTACs operate on an event-based mechanism, requiring binding only as long as the E3 ligase and target are recruited for POI degradation. After the target is degraded, PROTACs are released and can be recycled for the degradation of the next target.¹⁴¹ Success is highly concentration-dependent; exceeding a specific range favors the formation of binary complexes between E3-PROTAC or PROTAC-POI over the ternary E3-PROTAC-POI complex. This diminishing effect on activity, also known as the "hook effect," does not require functional activity, unlike classical pharmacology.¹⁴²

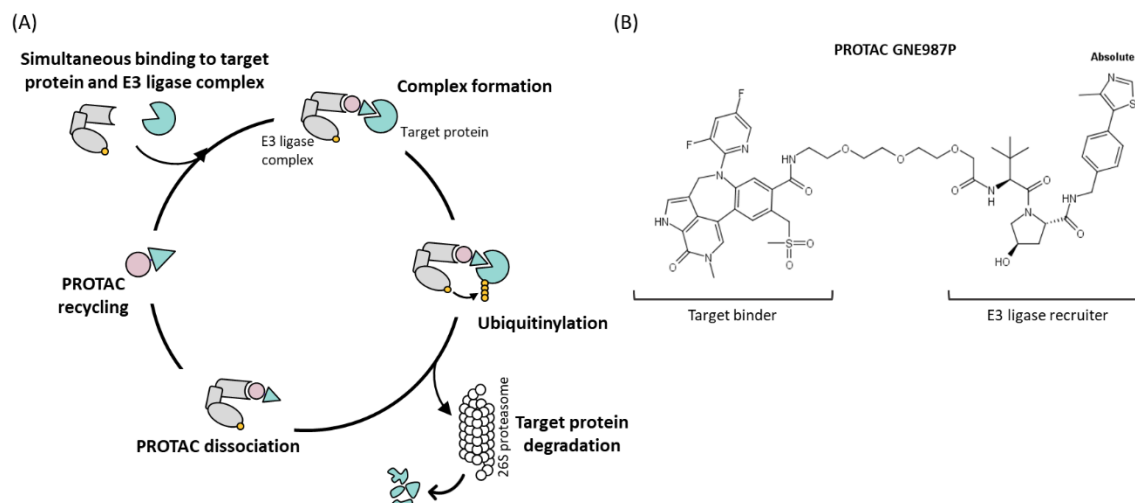


Figure 8 Target protein degradation mediated by PROTACs through the UPS. (A) The PROTAC consists of a ligand for the POI (turquoise) and a E3 ligase ligand (rose) linked by a spacer, enabling the target to be brought into proximity to an E3 ligase complex (gray). Subsequently, the target protein is ubiquitinated (yellow) and degradation is enabled by recognition of the 26S proteasome. Following degradation, the PROTAC can be recycled and bind again. **(B)** VH032-based PROTAC GNE987P targeting BRD4.¹⁴³

Today, over 600 E3 ligases in humans are known. The vast majority of PROTACs recruits either VHL or CRBN.^{144,145} In the first synthetic proof-of-concept PROTAC, methionyl aminopeptidase 2 (METAP2) was targeted, which is bound by the inhibitor ovalicon and brought into close proximity to β -transducin repeat-containing E3 ubiquitin-protein ligase, and consequently METAP2 is ubiquitinated.¹⁴⁰ In this constantly growing field, two PROTACs developed by Arvinas, ARV-110 (NCT0388861) and ARV-471 (NCT04072952) target the androgen and estrogen receptors, respectively. These are the clinically most advanced PROTACs and currently evaluated in clinical phase I/II.¹⁴⁶ Other prominent examples include KT-333 (NCT05225584), a STAT3 degrader, and two IRAK4 degraders, KT-413 (NCT05233033) and KT-474 (NCT04772885), from Kymera Therapeutics, which are tested in clinical phase I and I(a)/I(b).^{147,148} However, small-molecule PROTACs have been discovered to target biological functions especially in cancer, such as BET-bromodomain proteins,¹⁴⁹ estrogen receptor,¹⁵⁰ androgen receptor¹⁵¹ and various kinases.¹⁵² Despite the remarkable properties of PROTACs in tumor therapy, they are mainly limited by their low oral bioavailability due to their large molecular weight (MW, of over 800 Da) and associated with poor solubility in water.

Furthermore, the highly polar surface also hinders permeability and renders physiological barriers like cell membranes unpassable. Another difficulty is the low level of selectivity due to broad expression spectrum of E3 ligases in tumor and healthy tissue, which increases off-target effects.^{153,154} Thus, most PROTACs have so far failed within the preclinical phase of drug development. One of the biggest obstacles, the inability to accurately deliver PROTACs to their targets, has been addressed by the combination with reliable delivery systems. This connection

allows optimization of the physicochemical properties, improvement of targeting accuracy and reduction of off-target side effects.

To improve the therapeutic value of PROTACs, it is important to combine them with reliable delivery systems to optimize its physicochemical properties, improve targeting accuracy and reduce off-target side effects. In this context, the combination of PROTACs and multifunctional delivery systems may offer a novel approach in the field of targeted protein degradation. Currently, various approaches are being investigated using delivery systems to modulate poor water solubility and cell permeability, thus altering PK profiles, and enabling selective delivery to target tissues. These include organic and inorganic nanoparticles, small peptides, or antibody-based carriers.¹⁵⁵ Adapted from the success of ADCs, where the targeted delivery of toxic agents is top priority, few antibody-PROTAC conjugates have already been generated possessing the cellular specificity. Further beneficial pharmacokinetic profile of the antibody along with the protein degrading property of the bound PROTAC.^{156,157,158}

A major limitation in PROTAC conjugation process is the highly challenging synthesis of PROTACs, which complicates the incorporation of a conjugation linker by adding a suitable exit vector into the heterofunctional molecule. In addition, many chimeric degraders lack chemical groups like primary, secondary, or tertiary amines that are used for covalent attachment of cleavable linkers. The selective incorporation of such chemical groups can potentially lead to associated alteration of biological properties, so new ADC linkage approaches are examined that exploit functionalities already present in degraders, such as hydroxyl/phenol groups.¹⁵⁹

The recently described PROxAb technology, a hybrid approach for targeted PROTAC delivery, is thereby applicable to a wide range of cell types.¹⁶⁰ PROxAbs are target-specific antibodies fused to VHH, that bind the E3 ligase-recruiting subunit of PROTACs and thereby enable non-covalent complexation of PROTACs with the antibody.^{161,162} In contrast to covalent binders against small molecules, the PROxAbs approach allows binding of chemically unmodified small molecules by using VHHs which directly interact with the VHL ligand of PROTACs. Schneider *et al.* identified a VHH termed MIC7 which showed high affinity along with the broad specificity towards VH032, a VHL recruiting domain used for PROTACs. After a few hours of incubation, MIC7-based bispecific antibody/antibody-fusion proteins revealed a complex formation between antibody and PROTACs. As such, this strategy provides a modular approach to produce antibody-PROTAC modalities.¹⁶⁰ Schneider and colleagues showed in *in vivo* studies that complexation has positive effects on the half-life of PROTAC, and a prolonged anti-tumor effect was observed upon re-complexation after dosing with free PROTAC. The novel PROxAbs strategy also eliminates the requirement of chemical linker synthesis and conjugation of PROTACs, which facilitates targeted delivery and improves the biological function of the degrader.

There are different approaches to selecting targets for degraders, but for new therapeutic modalities it is important to select known targets for proof of concept. For this purpose, so-called “BioPROTAC” are often used, as they are not complete low-molecular structures but comprise ligands for E3 ligases.¹⁶³ For example, the peptide HIF1 α , an E3 ligase ligand of VHL, served as template of the bromodomain protein inhibitor JQ1. JQ1 is able to recruit VHL and degrade the bromodomain-containing protein 4 (BRD4).¹⁴⁹ BRD4 from the bromo- and extra-terminal (BET) family features two N-terminal bromodomains (BD1 and BD2) and an C-terminal domain (ET), playing a crucial role in transcriptional regulation and making it an attractive target for anticancer drug development.¹⁵⁹ BRD4 is a pan-essential protein. In recent years, chimeric molecules have been developed, forming a ternary E3-ubiquitin-ligase complex between BRD4 and VHL. Three well-characterized BRD4 degraders were used in the underlying work: GNE987, GNE987P (Figure 8 (B)) and ARV771.^{164,143,165} Which share structural features with BET inhibitor JQ1 and VHL-binding moiety. GNE987P and GNE987, structurally similar and based on VH032 a VHL ligand, differ in the replacement of the central PEG moiety with an aliphatic spacer.¹⁴³ This change extends the ternary complex half-life, attributed to the lack of protein interaction of the carbon chain, altering the chimeric molecule's hydrophobicity and associated cell permeability.¹⁶⁰

1.6.2.2 Biological targeted protein degradation

Although the extracellular proteome, consisting of secreted and membrane-bound proteins, accounts about a quarter of the human genome, it remains unaffected by the cytosolic PROTAC approach.¹⁶⁶ In recent years, various methods for targeting the extracellular proteome have been published, particularly in the context of New Biological Entities (NBE)-based TPD. In addition to addressing extracellular targets, NBE-based approaches differ from PROTACs in the degradation pathway, which involves the use of bispecific biologics or small molecules to transport membrane-bound or secreted proteins to the lysosome.¹⁶⁷ Furthermore, proteasomal degradation is much faster, with the full effect unfolding within minutes to hours.¹⁶⁸ Whereas lysosomal degradation is typically initiated within 6-48 hours by vesicular trafficking from the membrane through early and late endosomes, culminating in fusion with the lysosome for protein degradation. Whereas intracellularly mainly E3 ligases CRBN and VHL are addressed, which do not exhibit tissue selectivity, the NBE-based approach uses various degrader systems that enable great flexibility and tissue selectivity.

Additionally, the ability to produce antibodies that bind to protein interfaces and reach extracellular targets is highly advantageous due to their pharmacokinetic (PK) properties of antibodies and associated by prolonged duration and often less frequent dosing. Some approaches are mentioned below and explained in more detail if relevant to the work.

Under the concept of "sweeping antibodies", researchers have ingeniously engineered antibodies to utilize the FcRn to deliver target proteins in a pH-dependent manner to acidic endosomes for lysosomal degradation.¹⁶⁹ The approach was demonstrated using the example of tocilizumab (Tcz), an antibody used in the treatment of rheumatoid arthritis that has been engineered to enable pH-dependent binding of the IL-6 receptor. Tcz is rapidly cleared due to the high IL-6 receptor expression rate, which was addressed in the redesign by increasing the affinity of FcRn binding¹⁷⁰ and reducing antigen binding in a pH-dependent manner by the introduction of histidine residues into the CDR region.¹⁷¹ These modifications result in antibodies capable of transporting the IL-6R to the lysosome while remaining attached to the FcRn, allowing them to be recycled to bind IL-6R once more.¹⁷²

Bertozzi and colleagues made use of the natural degradation mechanism of glycosylated derivatives of specific proteins by the cation-independent mannose 6-phosphate receptor (CI-M6PR) to target proteins for degradation in the lysosome-targeting chimeras (LYTAC) approach.¹⁷³ The CI-M6PR transports endogenous M6P-tagged proteins from the cell membrane or Golgi to the lysosome, serving as a natural pH-switchable receptor that binds cargo at neutral pH and releases it at acidic pH. In LYTAC molecules, M6P-tagging was artificially induced by random conjugation of six to eight mannose 6-phosphonates (M6Pn) to lysine residues of antibodies. These glycan-tagged antibodies bind the target protein for degradation and are internalized into the lysosome through the CI-M6PR and the clathrin-mediated endocytic pathway (Figure 9). When Ctx was used as an antibody to facilitate LYTAC assembly for targeting EGFR, it resulted in the degradation of 70% of the total EGFR level within 24 hours HeLa cell treatment. Furthermore, EGFR downstream protein levels were reduced, while the level of CI-M6PR remained unchanged. In addition to EGFR, glycan-conjugated antibodies targeting CD71 or PD-L1 were evaluated, and their levels decreased to 20% and 30%, respectively, after treatment.¹⁷³

Recently, the mechanism of LYTACs was described in more detail by Ahn *et al.* using genome-wide CRISPER knockdown screens.¹⁷⁴ It was found that in the same target line, the degradation of soluble targets was generally lower than that of membrane-bound targets, which is due to the retromer complex negatively affecting the LYATC-based degradation of EGFR by recycling LYTACs back to the cell surface. Furthermore, it was determined that neddylation of cullin-3 E3 ligase is relevant for trafficking LYTAC-target complex to lysosomes and correlate with degradation efficiency. While the expression of CI-M6PR is universal, there are also tissue-specific lysosomal targeting receptors such as the asialoglycoprotein receptor (ASGPR). This increased selectivity was successfully exploited by the second generation ASGPR-based LYTAC molecules. The site-specific conjugation of ten copies tri-N-acetylgalactosamine (GalNAc) to EGFR-targeting antibodies, Ctx resulted in 70% cell selective EGFR degradation after 24-48 hours of treatment.¹⁷⁵ Additionally, the Ptz antibody could lead to the degradation of as much as 75% of HER2 by binding

eleven tri-GalNAc. In addition to antibody-mediated second generation LYTACs, aptamer-based engagers of ASGPR have recently been reported in which tri-GalNAc was attached to the 5' end of an aptamer and 50% target degradation was induced by treatment of HEPG2.¹⁷⁶

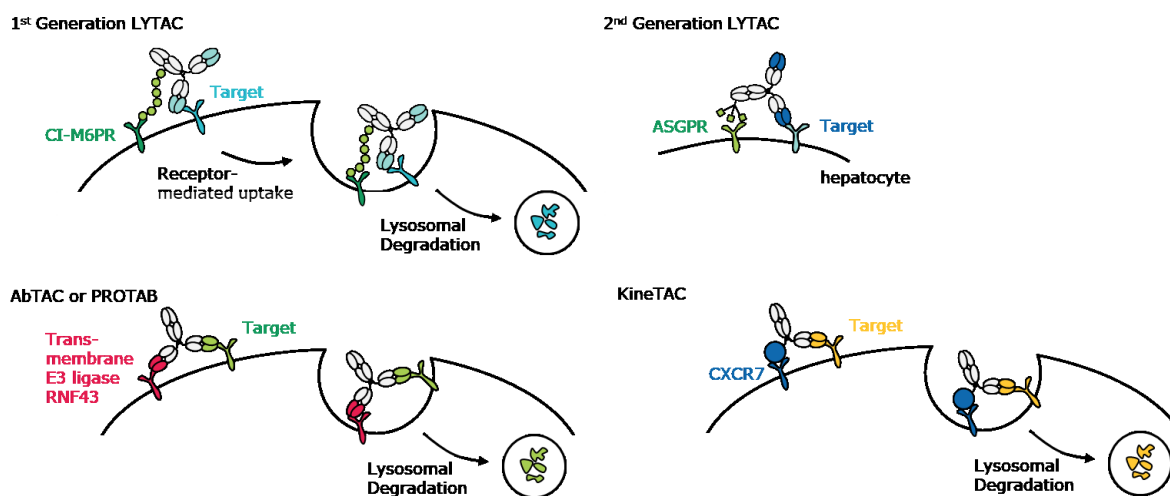


Figure 9 Schematic representation of the mechanisms of NBE-based targeted protein degradation. Glycan-based recycling receptors are addressed by 1st and 2nd generation of LYTAC, which share the same mechanism of action. AbTAC and PROTAB are bispecific antibodies targeting an E3-ligase and the target of interest and cause receptor-mediated uptake and degradation through the endosome-lysosome pathway. KineTACs comprising a target binding arm and a cytokine arm for binding the cytokine receptor.

By using bispecific antibodies, two different research groups demonstrated for the first time the successful use of transmembrane E3 ligases to degrade membrane proteins.^{127,128} In addition to the cytosolic E3 ligases, there are several transmembrane RING-domain-containing E3 ligases with RNF43 being one of the best characterized ligases.¹⁷⁷

The transmembrane E3 ligase-targeting bispecific antibodies, antibody-based PROTAC (AbTAC)¹²⁷ and proteolysis-targeting antibody (PROTAB)¹²⁸ exploit the second antibody binding arm to complex the membrane-bound E3 ligase and POI, and subsequently induce degradation through the endosome-lysosome pathway. Both use classic KIH technology to generate the bsAb. While AbTAC E3-ligase binding arm was selected through Fab-phage display, PROTAB used an immunization campaign to identify high affinity and unique binders. It remains unclear whether the intracellular region of the protein of interest (POI) is ubiquitinated prior to endocytosis or if there are additional interactions when RNF43-based antibodies ubiquitinate the target protein, leading to internalization and degradation. Furthermore, it is not yet known whether recovery and recycling are possible, as is the case with LYTAC technology.

An AbTAC, Ac-1 was designed to degrade PD-L1. The combination with Fab domain arm of Atz led to a decrease in total PD-L1 levels with a DC_{50} (half-degradation concentration) of 3.4 nM and a D_{max} (maximal percent degradation) of 63% after 24 hours of treatment. Several other RNF43 epitopes were analyzed, including an AbTAC that degraded close to 90% of PD-L1 but surprisingly was not among the strongest binders. Moreover, in HCC2935 cells with elevated RNF43

expression levels, AbTACs demonstrated enhanced degradation efficiency with reduced DC_{50} values. Additionally, the structure-activity relationship studies indicated that binder orientation and stoichiometry significantly impacted degradation, with the 1:1 ratio proving most effective, achieving over 95% maximal PD-L1 degradation.

Structure-activity relationship studies using EGFR antibodies with different epitope binding suggested that the epitope is important for EGFR degradation and is even more sensitive than affinity.¹⁷⁸ The impact of the target expression level on the structure-activity relationship of the AbTAC could not be definitively determined.

The results of Marei *et al.* with the PROTAB technology confirmed the approach of using membrane-bound E3 ligases to degrade the POI.¹²⁸ Besides RNF43, the homologous ZNRF3 E3 ligase was targeted to degrade the insulin-like growth factor 1 receptor (IGF1R), that is overexpressed in colorectal cancer (CRC). Depending on the IGF1R antibody, a D_{max} of 30-80% was observed after 48 hours of treatment of CRC cells. The catalytic mechanism of the AbTAC and PROTAB strategy was suggested in prior studies and was validated by screening numerous target cell lines with varying expression levels in the PROTAB approach. Notably, an IGF1R to ZNRF3 ratio of 400:1 was reported in extreme cases. The group confirmed the ubiquitination of the target and observed a reduction in degradation upon the removal of the E3 ligase. Additionally, transient impairment of degradation was noted following treatment with a proteasome inhibitor, leading to the inference that the proteasome might have a secondary role in this process. Contrary to the valence studies on AbTAC, a minimal effect was observed for PROTABs at a 2:1 ratio, but a slight increase for the 1:2 ratio, although with a certain degradation of RNF43.

The cytokine receptor-targeting chimeras (KineTAC) technology is based on recombinant bsAb with a binding arm against the target and a cytokine arm for binding a cytokine receptor.¹⁷⁹ Cytokines and interleukins can be degraded by receptor-mediated transfer in the lysosome, as shown for CXCL12, where its receptor CXCR7 induces internalization by β -arrestin recruitment without downstream signaling.¹⁸⁰ In the KineTAC approach, CXCL12 is complexed as an Fc-fusion protein with an Atz arm using KIH technology to create a bispecific molecule. After 24 hours of treatment with an Atz-KineTAC, an approximately 70% selective reduction in PD-L1 levels was observed in MDA-MB-231 cells co-expressing CXCR7 and PD-L1, and an increase in degradation to 84% after 48 hours. Since KineTACs do not require ubiquitination of the intracellular target domain, a degradation of soluble proteins was also shown using the example of interleukin-2 (IL-2) with D_{max} and 85%.

The receptor Elimination by E3 Ubiquitin Ligase Recruitment (REULR) is a modular VHH-based protein degradation platform that pairs five transmembrane E3 ligases (RNF128, RNF130, RNF167, RNF43, and ZNRF3) with different disease-relevant target receptors.¹²⁹ Furthermore, apart from the established target degradation of EGFR or erythropoietin receptor (EPOR), the self-

elimination of E3 ligase by dual-tandem degraders was also demonstrated. It is already known that E3 ligases can ubiquitinate themselves, and there is a hypothesis that the transmembrane E3 ligase family is capable of this process.

Two projects were performed as part of this work, both using bio-enzymatic conjugation strategies for the production of bispecific antibodies to investigate their biological activity in the field of targeted protein degradation (TPD). The projects aimed to establish protein-protein conjugation strategies to generate a toolbox for improved screening of bispecific antibodies. This aims to enable rapid identification of positive behaving binding partners to accelerate the development process of therapeutic bispecific antibodies for cancer therapy. Antibody-based degrader strategies served as proof-of concept. Therefore, the current strategies for generation of antibodies and their derivatives in cancer therapy as well as the history and technological background of targeted protein degradation and their impact on therapeutic efforts were highlighted in detail.

2 Materials

The following materials were used in this dissertation, whereby the respective manufacturer or supplier is listed. This includes human cell lines, bacterial strains, and plasmid map. Amino acid sequences of proteins and peptides are provided, along with a list of chemicals and commercially available systems. Additionally, recipes for preparing buffers and solutions are included. Consumable materials and equipment round out the materials utilized.

2.1 Human cell lines and bacterial strains

Mammalian cell lines	Supplier
A431	American Type Culture Collection, United States of America
A549	American Type Culture Collection, United States of America
BT474	American Type Culture Collection, United States of America
CaCo2	American Type Culture Collection, United States of America
HCC1954	American Type Culture Collection, United States of America

HCC827	American Type Culture Collection, United States of America
HEK293F Expi293F™ Inducible Cells	Thermo Fisher Scientific, United States of America
HEPG-2	American Type Culture Collection, United States of America
MCF7	American Type Culture Collection, United States of America
MDA-MB-231	American Type Culture Collection, United States of America
MDA-MB-435	American Type Culture Collection, United States of America
MDA-MB-453	Deutsche Sammlung von Mikroorganismen und Zellkulturen, Germany
MDA-MB-468	American Type Culture Collection, United States of America
OE19	European Collection of Authenticated Cell Cultures, United Kingdom
SKBR3	American Type Culture Collection, United States of America
T24	American Type Culture Collection, United States of America
Bacterial strain	
OneShot™ TOP10 Chemically Competent <i>E. Coli</i> cells	Thermo Fisher Scientific, United States of America

2.2 Plasmids

The pTT5 plasmids containing the modified antibodies, scFv or VHH sequence were purchased from GeneArt (Thermo Fisher Scientific, Waltham, USA). These plasmids were specifically designed as human codon-optimized versions for mammalian expression.

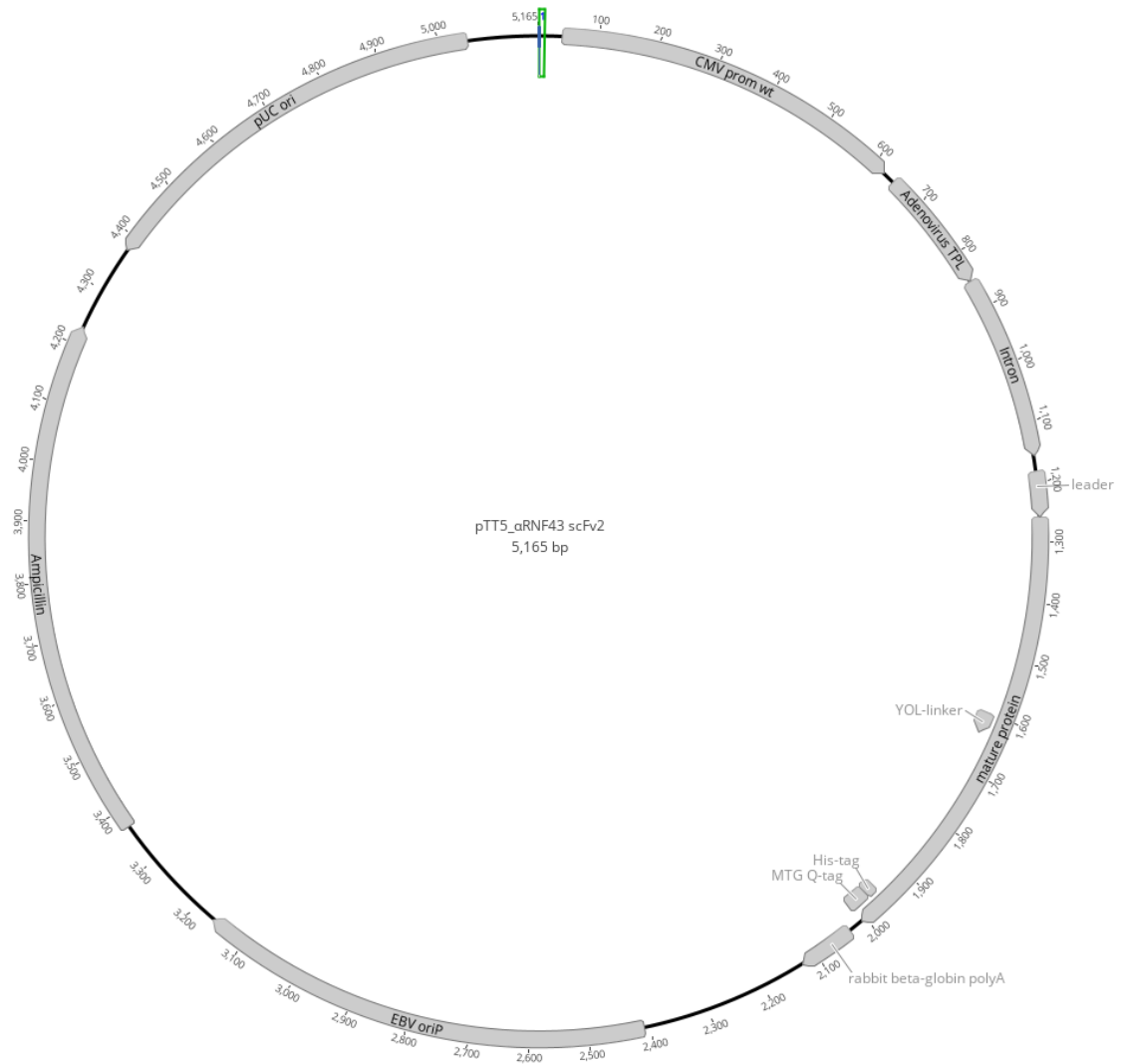


Figure 10 Vector map of pTT5 plasmid. This was used for mammalian expression and contains essential elements, shown using the example of α RNF43 scFv2. It includes an origin of replication (EBV oriP), an ampicillin resistance, a bacterial origin of replication (pUC ori), a cytomegalovirus immediate early promoter (CMV) and the adenovirus tripartite leader (TPL). The TPL is a synthetic intron that includes an enhancer element from the adenovirus major late promoter, which enhances protein expression. Downstream of the protein sequence is the rabbit β -globulin polyadenylation signal, while upstream is the leader sequence. The pTT5 vector was developed by the National Research Council of Canada.

2.3 Proteins and peptides

Proteins

BioRad WB Marker unstained

Gel Filtration Standard

Human HER2 His-tagged

Human RNF43 His-tagged

PD-L1/B7-H1 Protein, Human, Recombinant (ECD, His Tag)

Recombinant Human EGFR Protein

rh HER2 FC Chimera

Manufacturer

BIO-RAD, United States of America

BIO-RAD, United States of America

Sino Biologicals, China

Bio-Techne, United States of America

Sino Biologicals, China

Bio-Techne, United States of America

Bio-Techne, United States of America

rh RNF43 FC Chimera

Bio-Techne, United States of America

Enzymes

Manufacturer

MTG blocker C102

Zedira, Germany

Microbial transglutaminase *S. Ladakanum*

Merck Healthcare KGaA, Germany

FRAPDSDERVTTPAEPLDRMPDPYRPSYGRAETIVNNYIRKWQQVYSHRDGRKQQMTEEQREWLSY
GCVGVTWVNSGQYPTNRLAFAFFDEDEDKYKNELKNGRPRSGETRAEFEGRVAKDSFDEAKGFQRARDV
ASVMNKALENAHDEGAYLDNLKKELANGNDALRNEDARSPFYSALRNTPSFKDRNGGNHDP SKMKA
VIYSKHFWSGQDRSGSSDKRKYGDPEAFRDPDRGTGLVDMSRDRNIPRSPTSPGESFVNFYDYGWFGAQT
EADADKTVWTHGNHYHAPNGSLGMHVYESKFRNWSGDYSDFDGAYVVTVPKSWNTAPDKVTQG
WP

Antibody fragments

G₃-MIC7

Amino acid sequence of G₃-MIC7 VHH. MTG recognition tag, *glycine-serine spacer*

GGGGSGGGSGGGSGGGSGAVQLVESGGGLVQAGGSLRLSCAASGFSFDDYALGWFRQAPGKEPEGLSC
ISSSDGSTWYADSVKGRFTISSDNAKNTVYLQMNSLKPEDTAVYYCSAIYRLSCSVVRPTIRYALDYW
GQGTQVTVSS

αRNF43 scFv1

Amino acid sequence of αRNF43 scFv1. MTG recognition tag, His₆ tag

GGGGGQVQLVQSGAEVKKPGASVKVSCKASGYTFTRYWIEWVRQAPGQRLEWMGEILPGSGSTNYN
EKFKGRVTITADTSASTAYMELSSLRSEDVAVYYCERRGAYWGQGLTVTVSSKLEEGEFSEARVDIQM
TQSPSSLSASVGDRVTITCKASEDIYNRLAWYQQKPKGKAPKLLISGATSLETGVPSRFSGSGSGTDYTL
TISSLQPEDFATYYCQQQWSTPPTFGGGTKVEIKHHHHHH

αRNF43 scFv2

Amino acid sequence of αRNF43 scFv2. MTG recognition tag, His₆ tag, *glycine spacer*

QVQLVQSGAEVKKPGASVKVSCKASGYTFTRYWIEWVRQAPGQRLEWMGEILPGSGSTNYNEKFKG
RVTITADTSASTAYMELSSLRSEDVAVYYCERRGAYWGQGLTVTVSSKLEEGEFSEARVDIQMTQSPS
LSASVGDRVTITCKASEDIYNRLAWYQQKPKGKAPKLLISGATSLETGVPSRFSGSGSGTDYTLTISSLQ
PEDFATYYCQQQWSTPPTFGGGTKVEIKHHHHHHGGGGGGLLQGGGS

αRNF43 scFv3

Amino acid sequence of αRNF43 scFv3. MTG recognition tag, His₆ tag

QVQLVQSGAEVKKPGASVKVSCKASGYTFTRYWIEWVRQAPGQRLEWMGEILPGSGSTNYNEKFKG
RVTITADTSASTAYMELSSLRSEDVAVYYCERRGAYWGQGLTVTVSSGGGGSGGGGSGGGGSDIQMT
QSPSSLSASVGDRVTITCKASEDIYNRLAWYQQKPKGKAPKLLISGATSLETGVPSRFSGSGSGTDYTLTI
SSLQPEDFATYYCQQQWSTPPTFGGGTKVEIKHHHHHHGGLLQGA

αRNF43 scFv4

Amino acid sequence of αRNF43 scFv4. MTG recognition tag, His₆ tag

DIQMTQSPSSLSASVGDRVTITCKASEDIYNRLAWYQQKPKGKAPKLLISGATSLETGVPSRFSGSGSGT
DYTLTISSLQPEDFATYYCQQQWSTPPTFGGGTKVEIKGGGGSGGGGSGGGGSGVQLVQSGAEVKKPG

ASVKVSCASGYTFTRYWIEWVRQAPGQRLEWMGEILPGSGSTNYNEKFKGRVTITADTSASTAYM
ELSSLRSED TAVYYCERRGAYWGQGLTVTVSSHHHHHHGGLLOGA

α RNF43 scFv5

Amino acid sequence of α RNF43 scFv5. MTG recognition tag His₆ tag, *glycine-serine spacer*

QVQLVQSGAEVKKPGASVKVSCASGYTFTRYWIEWVRQAPGQRLEWMGEILPGSGSTNYNEKFKG
RVTITADTSASTAYMELSSLRSED TAVYYCERRGAYWGQGLTVTVSSGGGGSGGGGSGGGGSDIQMT
QSPSSLSASVGDRVTITCKASEDIYNRLAWYQQKPGKAPKLLISGATSLETGVPSRFSGSGSGTDYTLTI
SSLQPEDFATYYCQQQWSTPPTFGGGTKVEIKHHHHHHGGGGSGGLLOGA

α RNF43 scFv6

Amino acid sequence of α RNF43 scFv6. MTG recognition tag His₆ tag, *glycine-serine spacer*

QVQLVQSGAEVKKPGASVKVSCASGYTFTRYWIEWVRQAPGQRLEWMGEILPGSGSTNYNEKFKG
RVTITADTSASTAYMELSSLRSED TAVYYCERRGAYWGQGLTVTVSSGGGGSGGGGSGGGGSDIQMT
QSPSSLSASVGDRVTITCKASEDIYNRLAWYQQKPGKAPKLLISGATSLETGVPSRFSGSGSGTDYTLTI
SSLQPEDFATYYCQQQWSTPPTFGGGTKVEIKHHHHHHGGGGSGGGSGGLLOGA

α RNF43 scFv7

Amino acid sequence of α RNF43 scFv7. MTG recognition tag His₆ tag, *glycine-serine spacer*

QVQLVQSGAEVKKPGASVKVSCASGYTFTRYWIEWVRQAPGQRLEWMGEILPGSGSTNYNEKFKG
RVTITADTSASTAYMELSSLRSED TAVYYCERRGAYWGQGLTVTVSSGGGGSGGGGSGGGGSDIQMT
QSPSSLSASVGDRVTITCKASEDIYNRLAWYQQKPGKAPKLLISGATSLETGVPSRFSGSGSGTDYTLTI
SSLQPEDFATYYCQQQWSTPPTFGGGTKVEIKHHHHHHGGGGSGGGSGGGSGGLLOGA

Antibodies

Herceptin®

F. Hoffmann-La Roche Ltd., Switzerland

Amino acid sequence of Trastuzumab antibody. Genetic modifications are marked in bold.

DIQMTQSPSSLSASVGDRVTITCRASQDVNTAVAWYQQKPGKAPKLLIYSASFLYSGVPSRFSGRSGT
DFTLTISLQPEDFATYYCQQHYTTPPTFGGQTKVEIKRTVAAPSVFIFPPSDEQLKSGTASVCLLN
FYPREAKVQWKVDNALQSGNSQESVTEQDSKDSSTLSKADYEEKHKVYACEVTHQGLSSPV
TKSFNRGECEVQLVESGGGLVQPGGSLRLSCAASGFNIKDTYIHWVRQAPGKGLEWVARIYPTNGYT
RYADSVKGRFTISADTSKNTAYLQMNSLRAEDTAVYYCSRWGDDGFYAMDYWGQGLTVTVSSASTK
GPSVFPLAPSSKSTSGGTAALGCLVKDYFPEPVTVSWNSGALTSKVHTFPAVLQSSGLYSLSSVTVPS
SSLGTQTYICNVNHKPSNTKVDKKVEPKSCDKTHTCPPCPAPELGGPSVFLFPPKPKDTLMISRTPE
VTCVVVDVSHEDPEVKFNWYVDGVEVHNAKTKPREEQYNSTYRVVSVLTVLHQDWLNGKEYKCKV
SNKALPAPIEKTISKAKGQPREPQVYTLPPSREEMTKNQVSLTCLVKGFYPSDIAVEWESNGQPENNY
KTTTPVLDSDGSFFLYSKLTVDKSRWQQGNVFCFSVMHEALHNHYTQKSLSLSPGK

Amino acid sequence of Trastuzumab antibody. Genetic modifications are marked in bold.

DIQMTQSPSSLSASVGDRTITCRASQDVNTAVAWYQQKPGKAPKLLIYSASFLYSGVPSRFSGSRSGT
DFTLTISSLQPEDFATYYCQQHYTTPPTFGQGTKVEIKRTVAAPSVFIFPPSDEQLKSGTASVVCLLNN
FYPREAKVQWKVDNALQSGNSQESVTEQDSKDYSLSTLTLTKADYEKHKVYACEVTHQGLSSPV
TKSFNRGEC**GGLLQGP**PEVQLVESGGGLVQPGGSLRLSCAASGFNIKDTYIHWVRQAPGKGLEWVAR
IYPTNGYTRYADSVKGRFTISADTSKNTAYLQMNSLRAEDTAVYYCSRWGGDGFYAMDYWGQGLV
TVSSASTKGPSVFPLAPSSKSTSGGTAAALGCLVKDYFPEPVTVSWNSGALTSKVHTFPAVLQSSGLYSL
SSVVTVPSSSLGTQTYICNVNHKPSNTKVDKKEPKSCDKTHTCPPCPAPELLGGPSVFLFPPKPKD
TLMISRTPEVTCVVDVSHEDPEVKFNWYVDGVEVHNAKTKPREEQYNSTYRVVSVLTVLHQDWL
NGKEYKCKVSNKALPAPIEKTISKAKGQPREPQVYTLPPSRDELTKNQVSLTCLVKGFYPSDIAVEWE
SNGQPENNYKTTTPVLDSDGSFFLYSKLTVDKSRWQQGNVFCFSVMHEALHNHYTQKLSLSLSPGK

Amino acid sequence of Trastuzumab antibody. Genetic modifications are marked in bold.

DIQMTQSPSSLSASVGDRTITCRASQDVNTAVAWYQQKPGKAPKLLIYSASFLYSGVPSRFSGSRSGTDFTLTIS
LQPEDFATYYCQQHYTTPPTFGQGTKVEIKRTVAAPSVFIFPPSDEQLKSGTASVVCLLNNFYPREAKVQWKVD
NALQSGNSQESVTEQDSKDYSLSTLTLTKADYEKHKVYACEVTHQGLSSPVTKSFNRGECVQLVESGGGLV
QPGGSLRLSCAASGFNIKDTYIHWVRQAPGKGLEWVARIYPTNGYTRYADSVKGRFTISADTSKNTAYLQMNSL
RAEDTAVYYCSRWGGDGFYAMDYWGQGLTVTVSSASTKGPSVFPLAPSSKSTSGGTAAALGCLVKDYFPEPVT
VSWNSGALTSKVHTFPAVLQSSGLYSLSSVVTVPSSSLGTQTYICNVNHKPSNTKVDKKEPKSCDKTHTCPPCP
APPELLGGPSVFLFPPKPKDTLMISRTPEVTCVVDVSHEDPEVKFNWYVDGVEVHNAKTKPREE**A**YNSTYRVVS
VLTVLHQDWLNGKEYKCKVSNKALPAPIEKTISKAKGQPREPQVYTLPPSRDELTKNQVSLTCLVKGFYPSDIAVE
WESNGQPENNYKTTTPVLDSDGSFFLYSKLTVDKSRWQQGNVFCFSVMHEALHNHYTQKLSLSLSPGK

MabThera®

F. Hoffmann-La Roche Ltd., Switzerland

Amino acid sequence of Rituximab antibody. Genetic modifications are marked in bold.

QIVLSQSPAILSASPGEKVTMTCRASSSVSYIHWVFQQKPGSSPKWIYATSNLASGVPVRFSGSGSGTS
YSLTISRVEAEDAATYYCQQWTSNPPTFGGGTKLEIKRTVAAPSVFIFPPSDEQLKSGTASVVCLLNNF
YPREAKVQWKVDNALQSGNSQESVTEQDSKDYSLSTLTLTKADYEKHKVYACEVTHQGLSSPV
KSFNRGECQVQLQPGAEVLPKASVMSCKASGYTFTSYNMHWVKQTPGRGLEWIGAIYPGNGDT
SYNQKFKGKATLTADKSSSTAYMQLSSLTSEDSAVYYCARSTYYGGDWFYFNVWGAGTTVTVSAAST
KGPSVFPLAPSSKSTSGGTAAALGCLVKDYFPEPVTVSWNSGALTSKVHTFPAVLQSSGLYSLSSVVTVP
SSSLGTQTYICNVNHKPSNTKVDKKAEPKSCDKTHTCPPCPAPELLGGPSVFLFPPKPKDTLMISRT
PEVTCVVDVSHEDPEVKFNWYVDGVEVHNAKTKPREEQYNSTYRVVSVLTVLHQDWLNGKEYKCK
VSNKALPAPIEKTISKAKGQPREPQVYTLPPSRDELTKNQVSLTCLVKGFYPSDIAVEWESNGQPEN
NYKTTTPVLDSDGSFFLYSKLTVDKSRWQQGNVFCFSVMHEALHNHYTQKLSLSLSPGK

Matuzumab

Merck KGaA, Germany

Amino acid sequence of Matuzumab antibody. Genetic modifications are marked in bold.

QIVLSQSPAILSASPGEKVTMTCRASSSVSYIHWVFQQKPGSSPKWIYATSNLASGVPVRFSGSGSGTS
YSLTISRVEAEDAATYYCQQWTSNPPTFGGGTKLEIKRTVAAPSVFIFPPSDEQLKSGTASVVCLLNNF
YPREAKVQWKVDNALQSGNSQESVTEQDSKDYSLSTLTLTKADYEKHKVYACEVTHQGLSSPV
KSFNRGECQVQLQPGAEVLPKASVMSCKASGYTFTSYNMHWVKQTPGRGLEWIGAIYPGNGDT
SYNQKFKGKATLTADKSSSTAYMQLSSLTSEDSAVYYCARSTYYGGDWFYFNVWGAGTTVTVSAAST
KGPSVFPLAPSSKSTSGGTAAALGCLVKDYFPEPVTVSWNSGALTSKVHTFPAVLQSSGLYSLSSVVTVP
SSSLGTQTYICNVNHKPSNTKVDKKAEPKSCDKTHTCPPCPAPELLGGPSVFLFPPKPKDTLMISRT
PEVTCVVDVSHEDPEVKFNWYVDGVEVHNAKTKPREEQYNSTYRVVSVLTVLHQDWLNGKEYKCK
VSNKALPAPIEKTISKAKGQPREPQVYTLPPSRDELTKNQVSLTCLVKGFYPSDIAVEWESNGQPEN
NYKTTTPVLDSDGSFFLYSKLTVDKSRWQQGNVFCFSVMHEALHNHYTQKLSLSLSPGK

Erbitux®

Merck KGaA, Germany

Amino acid sequence of Cetuximab antibody. Genetic modifications are marked in bold.

DILLTQSPVILSVSPGERVSFSCRASQSIGTNIHWYQQRNNGSPRLLIKYASESISGIPSRFSGSGSGTDFT
LSINSVESEDIADYYCQNNNWPTTFGAGTKLELKRVAAPSVEFIFPPSDEQLKSGTASVCLLNDFY
PREAKVQWKVDNALQSGNSQESVTEQDSKDYSLSTLTLKADYEKHKVYACEVTHQGLSSPVTK
SFNRGECQVQLKQSGPGLVQPSQSLITCTVSGFSLTNYGVHWVRQSPGKGLEWLGVIWSSGNTDYN
TPFTSRLSINKDNSKQVFFKMNSLQSNDAIYYCARALTYDYEFAYWGQGLVTVSAASTKGPSVF
PLAPSSKSTSGGTAALGCLVKDYFPEPVTVSWNSGALTSVHTFPAVLQSSGLYSLSSVTVPSSSLGT
QTYICNVNHKPSNTKVDKRVKPKCDKHTCPPCPAPELGGPSVFLFPPKPKDTLMISRTPEVTCV
VDVSHEDPEVKFNWYVDGVEVHNAKTKPREEQYNSTYRVVSVLTVLHQDWLNGKEYKCKVSNKAL
PAPIEKTISKAKGQPREPQVYTLPPSREEMTKNQVSLTCLVKGFYPSDIAVEWESNGQPENNYKTTP
VLDSGDSFFLYSKLTVDKSRWQQGNVFCFSVMHEALHNHYTQKSLSLSPGK

Amino acid sequence of Cetuximab antibody. Genetic modifications are marked in bold.

DILLTQSPVILSVSPGERVSFSCRASQSIGTNIHWYQQRNNGSPRLLIKYASESISGIPSRFSGSGSGTDFT
LSINSVESEDIADYYCQNNNWPTTFGAGTKLELKRVAAPSVEFIFPPSDEQLKSGTASVCLLNDFY
PREAKVQWKVDNALQSGNSQESVTEQDSKDYSLSTLTLKADYEKHKVYACEVTHQGLSSPVTK
SFNRGECQVQLKQSGPGLVQPSQSLITCTVSGFSLTNYGVHWVRQSPGKGLEWLGVIWSSGNTDYN
TPFTSRLSINKDNSKQVFFKMNSLQSNDAIYYCARALTYDYEFAYWGQGLVTVSAASTKGPSVF
PLAPSSKSTSGGTAALGCLVKDYFPEPVTVSWNSGALTSVHTFPAVLQSSGLYSLSSVTVPSSSLGT
QTYICNVNHKPSNTKVDKRVKPKCDKHTCPPCPAPEA**AG**GPSVFLFPPKPKDTLMISRTPEVTCV
VVDVSHEDPEVKFNWYVDGVEVHNAKTKPREEQYNSTYRVVSVLTVLHQDWLNGKEYKCKVSNKA
L**G**APIEKTISKAKGQPREPQVYTLPPSREEMTKNQVSLTCLVKGFYPSDIAVEWESNGQPENNYKTTP
PVLDSGDSFFLYSKLTVDKSRWQQGNVFCFSVMHEALHNHYTQKSLSLSPGK

Tecentriq®

Genentech Inc., United States of America

Amino acid sequence of Atezolizumab antibody. Genetic modifications are marked in bold.

DIQMTQSPSSLSASVGRVTITCRASQDVSTAVAWYQKPKGKAPKLLIYSASFLYSGVPSRFSGSGSGT
DFTLTISLQPEDFATYYCQQYLYHPATFGQGTKEIKRTVAAPSVEFIFPPSDEQLKSGTASVCLLN
FYFPREAKVQWKVDNALQSGNSQESVTEQDSKDYSLSTLTLKADYEKHKVYACEVTHQGLSSPV
TKSFNRGECEVQLVESGGGLVQPGGSLRLSCAASGFTFSDSWIHWVRQAPGKGLEWVAWISPYGGST
YYADSVKGRFTISADTSKNTAYLQMNSLRAEDTAVYYCARRHWPGGFYWGQGLVTVSSASTKGP
SVFPLAPSSKSTSGGTAALGCLVKDYFPEPVTVSWNSGALTSVHTFPAVLQSSGLYSLSSVTVPSSS
LGTQTYICNVNHKPSNTKVDKRVKPKCDKHTCPPCPAPELGGPSVFLFPPKPKDTLMISRTPEVT
CVVVDVSHEDPEVKFNWYVDGVEVHNAKTKPREEQYASTYRVVSVLTVLHQDWLNGKEYKCKVSN
KALPAPIEKTISKAKGQPREPQVYTLPPSREEMTKNQVSLTCLVKGFYPSDIAVEWESNGQPENNYKT
TPPVLDSGDSFFLYSKLTVDKSRWQQGNVFCFSVMHEALHNHYTQKSLSLSPGK

Bavencio®

Merck KGaA, Germany

Amino acid sequence of Avelumab antibody. Genetic modifications are marked in bold.

QSALTQPASVSGSPGQSITISCTGTSSDVGNYVSWYQHPGKAPKLMYDVSNRPSGVSNRFSGSKS
GNTASLTISGLQAEDEADYYCSSYSSSTRVFGTGKVTVLGQPKANPTVTLFPPSSEELQANKATLVC
LISDFYPGAVTVAWKADGSPVKAGVETTKPSKQSNKYAASSYLSLTPEQWKSHRSYSCQVTHEGST
VEKTVAPTECSEVQLLESGLLVQPGGSLRLSCAASGFTFSSYIMMWVRQAPGKGLEWVSSIYPSGGI
TFYADTVKGRFTISRDNKNTLYLQMNSLRAEDTAVYYCARIKLGTVTTVDYWGQGLVTVSSASTK
GPSVFPLAPSSKSTSGGTAALGCLVKDYFPEPVTVSWNSGALTSVHTFPAVLQSSGLYSLSSVTVPS
SSLGTQTYICNVNHKPSNTKVDKRVKPKCDKHTCPPCPAPELGGPSVFLFPPKPKDTLMISRTPE

VTCVVVDVSHEDPEVKFNWYVDGVEVHNAKTKPREEQYNSTYRVVSVLTVLHQDWLNGKEYKCKV
SNKALPAPIEKTISKAKGQPREPQVYTLPPSRDELTKNQVSLTCLVKGFYPSDIAVEWESNGQPENNY
KTPPVLDSDGSFFLYSKLTVDKSRWQQGNVFCSCVMHEALHNHYTQKSLSLSPGK

Perjeta®

F. Hoffmann-La Roche Ltd., Switzerland

Amino acid sequence of Pertuzumab antibody. Genetic modifications are marked in bold.

DIQMTQSPSSLSASVGDRVTITCKASQDVSIGVAWYQQKPGKAPKLLIYSASYRYTGVPSRFSGSGSGT
DFTLTISLQPEDFATYYCQQYYIYPYTFGGGTKVEIKRTVAAPSVFIFPPSDEQLKSGTASVCLLNNF
YPREAKVQWKVDNALQSGNSQESVTEQDSKSTYLSSTLTLSKADYEKHKVYACEVTHQGLSSPVT
KSFNRGECQVQLVESGGLVQPGGSLRLSCAASGFTFTDYTMDWVRQAPGKGLEWVADVNPNSGGS
IYNQRFKGRFTLSVDRSKNTLYLQMNSLRAEDTAVYYCARNLGPSTFYFDYWGQGTLLVTVSSASTKGP
SVFPLAPSSKSTSGGTAALGCLVKDYFPEPVTVSWNSGALTSKVHTFPAVLQSSGLYSLSSVTVPSST
LGTQTYICNVNHKPSNTKVDKVEPKSCDKTHTCPPCPAPELGGPSVFLFPPKPKDTCSVMHEALH
NHYTQKSLSLSPGLMISRTPEVTCVVVDVSHEDPEVKFNWYVDGVEVHNAKTKPREEQYNSTYRVV
SVLTVLHQDWLNGKEYKCKVSNKALPAPIEKTISKAKGQPREPQVYTLPPSREEMTKNQVSLTCLVK
GFYPSDIAVEWESNGQPENNYKTPPVLDSDGSFFLYSKLTVDKSRWQQGNVFS

αDIG antibody

F. Hoffmann-La Roche Ltd., Switzerland

Amino acid sequence of αDIG antibody. Genetic modifications are marked in bold.

DIQMTQSPSSLSASVGDRVTITCRASQDIKYNLNWYQQKPGKAPKLLIYSSSTLLSGVPSRFSGSGSGT
DFTLTISLQPEDFATYYCQQSITLPPFTFGGGTKVEIKRTVAAPSVFIFPPSDEQLKSGTASVCLLNNF
YPREAKVQWKVDNALQSGNSQESVTEQDSKSTYLSSTLTLSKADYEKHKVYACEVTHQGLSSPVT
KSFNRGECQVQLVESGGLVKPGGSLRLSCAASGFTFSDYAMSWIRQAPGKGLEWVASINIGATYAYY
PDSVKGRFTISRDNKNSLYLQMNSLRAEDTAVYYCARPGSPYEYDKAYYSMAYWGQGTLLVTVSSAS
TKGSPVFLAPSSKSTSGGTAALGCLVKDYFPEPVTVSWNSGALTSKVHTFPAVLQSSGLYSLSSVTV
PSSSLGTQTYICNVNHKPSNTKVDKRVPEPKSCDKTHTCPPCPAPELGGPSVFLFPPKPKDTLMISRT
PEVTCVVVDVSHEDPEVKFNWYVDGVEVHNAKTKPREEQYNSTYRVVSVLTVLHQDWLNGKEYKC
KVSNAKALPAPIEKTISKAKGQPREPQVYTLPPSREEMTKNQVSLTCLVKGFYPSDIAVEWESNGQPE
NYKTPPVLDSDGSFFLYSKLTVDKSRWQQGNVFCSCVMHEALHNHYTQKSLSLSPGK

Anti-human RNF43 antibody

Creative Biolabs, United States of
America

Amino acid sequence of anti-human RNF43 antibody. Genetic modifications are marked in bold.

DIQMTQSPSSLSASVGDRVTITKASEDIYNRLAWYQQKPGKAPKLLISGATSLETGVPSRFSGSGSGT
DYTLTISLQPEDFATYYCQQWSTPPTFGGGTKVEIKRTVAAPSVFIFPPSDEQLKSGTASVCLLNN
FYPREAKVQWKVDNALQSGNSQESVTEQDSKSTYLSSTLTLSKADYEKHKVYACEVTHQGLSSPV
TKSFNRGECQVQLVQSGAEVKKPGASVKVSCKASGYTFTRYWIEWVRQAPGQRLEWMGEILPGSGS
TNYNEKFKGRVTITADTSASTAYMELSSLRSEDTAVYYCERRGAYWGQGTLLVTVSSASTKGPVFLA
PSSKSTSGGTAALGCLVKDYFPEPVTVSWNSGALTLVKDYFPEPVTVSWNSGALTSKVHTFPAVLQSS
GLYSLSSVTVPSSTLGTQTYICNVNHKPSNTKVDKRVPEPKSCDKTHTCPPCPAPELGGPSVFLFPPK
PKDTLMISRTPEVTCVVVDVSHEDPEVKFNWYVDGVEVHNAKTKPREEQYNSTYRVVSVLTVLHQD
WLNGKEYKCKVSNKALPAPIEKTISKAKGQPREPQVYTLPPSREEMTKNQVSLTCLVKGFYPSDIAVE
WESNGQPENNYKTPPVLDSDGSFFLYSKLTVDKSRWQQGNVFCSCVMHEALHNHYTQKSLSLSPG

Alexa Fluor® 488 AffiniPure™ F(ab')₂ Fragment
Goat Anti-Human IgG, Fcy fragment specific
Alexa Fluor® 488 AffiniPure™ Fab Fragment
Goat Anti-Human IgG (H+L)

Jackson ImmunoResearch,
United States of America
Jackson ImmunoResearch,
United States of America

Anti- β -Actin mouse Monoclonal Ab, Clone AC-74, A2228

Sigma-Aldrich,
United States of America
Bio-Techne,
United States of America

GAPDH (D4C6R) Mouse mAb

Goat anti-Rabbit IgG (H+L) Highly Cross-Adsorbed Secondary Antibody, Alexa Fluor™ 488

Invitrogen™,
United States of America

Mouse IgG (H&L) Antibody DyLight™ 680 Conjugated Pre-Adsorbed

Rockland Immunochemicals, Inc.,
United States of America
Cell Signaling Technologies,
United States of America

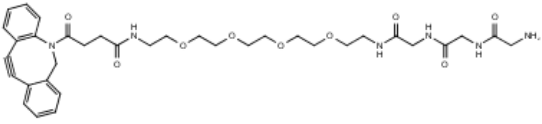
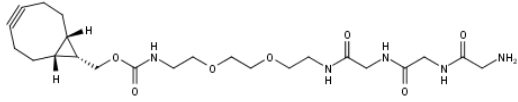
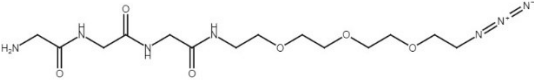
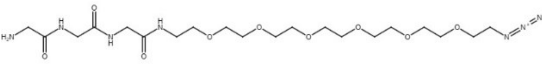
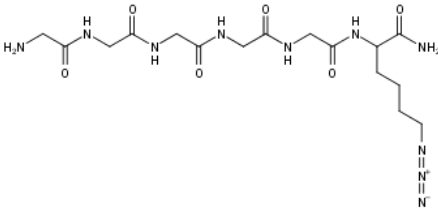
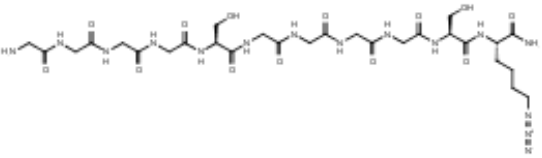
PD-L1 (E1L3N®) XP® Rabbit mAb

Rabbit IgG (H&L) Antibody DyLight™ 800 Conjugated Pre-Adsorbed

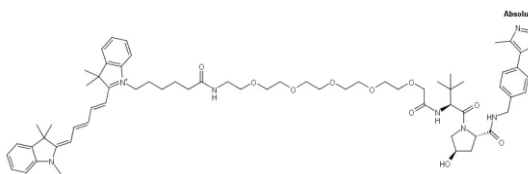
Rockland Immunochemicals, Inc.,
United States of America
Abcam, Great Britain

Recombinant Anti-Brd4 antibody [EPR5150(2)]

Peptides

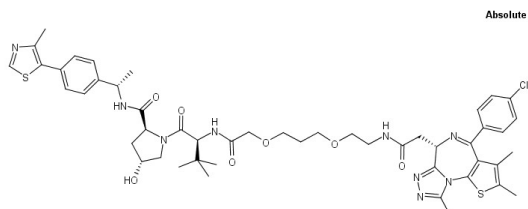
Name	Derivate number	Structure	Manufacturer
G ₃ -PEG ₄ -DBCO	1		SV Chembiotech, Inc., Canada
G ₃ -PEG ₂ -BCN	2		BroadPharm, United States of America
G ₃ -PEG ₃ -N ₃	3		Biosynton, Germany
G ₃ -PEG ₆ -N ₃	4		Biosynton, Germany
G ₅ -Lys-N ₃	5		Merck KGaA, Germany
(G ₄ S) ₂ -Lys-N ₃	6		Merck KGaA, Germany

VHL-Cy5



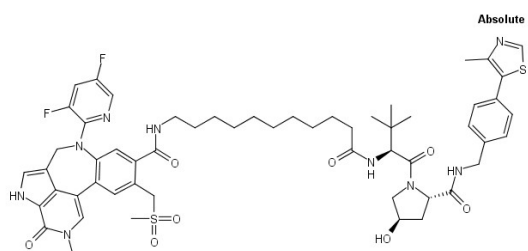
WuXi Biologics,
China

ARV-771



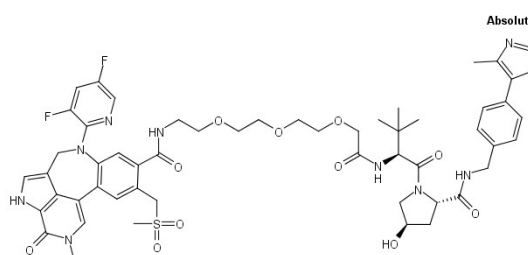
MedChemExpress,
United States of
America

GNE987



MedChemExpress,
United States of
America

GNE987P



MedChemExpress,
United States of
America

2.4 Chemicals

Calbiochem:

Tris(hydroxymethyl)-aminomethane-hydrochloride

Merck Millipore, Merck KGaA:

Acetonitrile, ampicillin, ammonium sulfate, 1,4-Dithiothreitol, bicinechonic acid, ethanol, formic acid, HCl, HEPES, N-Acetylcysteine, Milli Q-water, imidazole, sodium chloride, sodium phosphate monobasic solution, sodium azide, sodium phosphate dibasic solution, di-sodium hydrogen phosphate, sodium dihydrogen phosphate monohydrate, sodium perchlorate, Triton X-100, Trifluoroacetic acid, Tween® 20, water for chromatography, 2-propanol, hydrochloric acid,

Thermo Fisher Scientific Inc.:

Accutase®, Formaldehyde, Gibco™ Phosphate-Buffered saline, Gibco™ 2-Mercaptoethanol, Gibco™ DMEM GlutaMax, Gibco™ RPMI-1640 GlutaMax,

Honeywell International:

Dimethyl sulfoxide

2.5 Commercially available systems

CellTiter-Glo® Luminescent Cell Viability Assay	Promega, Germany
ExpiFectamine™ 293 Transfection Kit	Thermo Fisher Scientific, United States of America
GenElute™ HP Plasmid Midiprep Kit	Sigma-Aldrich, United States of America
pHAb Amine Reactive Dye	Promega, Germany
Vi-CELL® Reagent Kit	Beckmann Coulter, United States of America

2.6 Buffer and Solutions

Analytical HIC buffer	A: 2.0 M ammonium sulfate, 25 mM Tris-HCl, pH 7.5 B: 25 mM Tris-HCl, pH 7.5 C: 100% isopropanol
Analytical SEC buffer	0.05 M sodium phosphate, 0.4 M sodium perchlorate, pH 6.3
DNA storage buffer	0.01 M Tris-HCl, pH 8.5
Kinetics buffer (KB) for BLI	0.1% (w/v) BSA, 0.02% (v/v) Tween-20, PBS, pH 7.4
LB agar	1.5% (w/v) agar in LB medium
LB medium	10 g/L peptone, 5 g/L yeast extract, 10 g/L NaCl
LB-ampicillin medium	LB medium, 50 µg/mL (w/v) ampicillin
MES buffer	0.05 M MES, 0.05 Tris-Base, 0.1% SDS, 0.001 M EDTA, pH 7.3
MTG conjugation buffer	0.024 M HEPES, pH 7.0
Nickel sulfate solution	0.5 M Ni ₂ SO ₄
PBS buffer	0.15 M NaCl, 0.0084 M Na ₂ HPO ₄ ·2H ₂ O, 0.0016 M KH ₂ PO ₄ , pH 7.4
pHAb amine reactive dye conjugation buffer	0.01 M NaHCO ₃ , pH 8.5
Pierce™ IP Lysis Buffer	0.025 M Tris-HCl, 0.15 M NaCl, 0.001 M EDTA, 1% NP-40, 5% (v/v) glycerol, pH 7.4
Preparative Amsphere™ A3 chromatography elution buffer	0.05 M sodium acetate, pH 3.0

Preparative IMAC buffer	A: 0.05 M sodium phosphate, 0.5 M NaCl, pH 7.4 B: 0.05 M sodium phosphate, 0.5 M NaCl, 0.5 M imidazole, pH 7.4
Preparative Protein A chromatography elution buffer	0.05 M acetic acid, pH 3.2

2.7 Consumable materials

All materials not listed are standard laboratory material.

µClear bottom 384-well plate	Greiner Bio-One, Austria
10x PBS	Thermo Fisher Scientific, United States of America
125 µl GRIPTIP, sterile	INTEGRA Biosciences KK, Japan
15 mL, 50 mL falcon tubes	Becton Dickinson GmbH, Germany
Albumin fraction V (from bovine serum)	Merck KGaA, Germany
Attune focusing fluid	Invitrogen™, United States of America
Attune Performance Tracking Beads	Invitrogen™, United States of America
Attune shutdown solution	Invitrogen™, United States of America
Attune wash solution	Invitrogen™, United States of America
Bottle top vacuum filtration system, 0.2µm	VWR International, United States of America
Buffer solution pH 4.01	Merck KGaA, Germany
Buffer solution pH 7.00	Merck KGaA, Germany
Buffer solution pH 9.00	Merck KGaA, Germany
Cell culture flask T75	Greiner Bio-One, Austria
Cell culture microplate, 96- and 384- wells	Greiner Bio-One, Austria
D4+ dispensehead cassettes	Tecan Trading AG, Switzerland
Der blaue Jonas	German Research Products, Germany
Expi293™ Expression Medium	Thermo Fisher Scientific, United States of America
Fetal bovine serum (FBS)	Sigma-Aldrich, United States of America
HEPES acid	Merck KGaA, Germany
Hoechst 33342 Dye	Invitrogen™, United States of America
HTRF 96-well low volume white plate	Cisbio, United States of America
Imidazole	Merck Millipore, Germany

InfinityLab Well Plates and Sealing Mats	Agilent Technologies, United States of America
L-Glutamine 200mM	Sigma-Aldrich, United States of America
MABPac™ HIC-Butyl 4.6 mm ID x 100 mm, 5 µm HPLC column	Thermo Fisher Scientific, United States of America
Micro-insert, clear glass	VWR International, United States of America
NuPAGE LDS Sample buffer (4x)	Invitrogen™, United States of America
NuPAGE MES SDS Running buffer (20x)	Invitrogen™, United States of America
NuPAGE Reducing Agent (10x)	Invitrogen™, United States of America
NuPAGE® 4-12% Bis-Tris Gels	Life Technologies Corp., Germany
Octet® Anti-human IgG Fc capture (AHC) Biosensors	Sartorius, United States of America
Octet® Anti-Penta-HIS (HIS1K) Biosensors	Sartorius, United States of America
Opti-MEM™ I cell culture medium	Thermo Fisher Scientific, United States of America
Pierce™ IP lysis buffer	Thermo Fisher Scientific, United States of America
PLRP-S 4000Å, 2.1 x 50 mm, 5 µm HPLC column	Agilent Technologies, United States of America
Protease Inhibitor Cocktail cOmplete™	F. Hoffmann-La Roche Ltd., Switzerland
RIPA lysis buffer	Thermo Fisher Scientific, United States of America
S.O.C. medium	Invitrogen™, United States of America
Safe Lock Tubes 0.2, 1.5, 2.0, 5.0 mL	Eppendorf AG, Germany
Short thread vials	VWR International, United States of America
Sodium pyruvate 100mM	Sigma-Aldrich, United States of America
Steriflip® Sterile filter 50 ml 0.22 and 0.45 µm	Merck Millipore, Merck KGaA, Germany
Sytox Green™	Invitrogen™, United States of America
Sytox Red™	Invitrogen™, United States of America
T8+ dispensehead cassettes	Tecan Trading AG, Switzerland
TSKgel® SuperSW3000 HPLC Column phase diol	Merck KGaA, Germany
Ultrafree-CL, 0.22µm	Merck KGaA, Germany

ViaFlo II Pipette 8-Ch.; 5-125 µl	INTEGRA Biosciences KK, Japan
Vi-CELL BLU QuadPack	Beckmann Coulter, United States of America
Zeba™ Spin Desalting column	Thermo Fisher Scientific, United States of America
ZORBAX RR Bonus-RP, 80Å, 4.6 x 150 mm, 3.5 µm	Agilent Technologies, United States of America

2.8 Equipment

All equipment not listed are standard laboratory equipment.

16-channel Viaflow II pipets	INTEGRA Biosciences AG, Switzerland
Agilent 1100 Series	Agilent Technologies, United States of America
Agilent 1260 Infinity	Agilent Technologies, United States of America
Agilent 1260 Infinity II	Agilent Technologies, United States of America
ÄKTAAvant	GE Healthcare, United States of America
ÄKTAPure	GE Healthcare, United States of America
ÄKTExpress	GE Healthcare, United States of America
Amicon® Ultra centrifugal units	Merck KGaA, Germany
Amsphere™ A3 column	JSR Life Sciences, United States of America
Attune™ NxT flow cytometer	Invitrogen™, United States of America
Bio Resolve SEC mAb column	Waters, Germany
Centrifuge 5427R, 5415R and 5415D	Eppendorf AG, Germany
Centrifuge, Megafuge 1.0R	Heraeus Holding, Germany
Centrifuge, Megafuge 16R	Heraeus Holding, Germany
Centrifuge, Megafuge 40R	Heraeus Holding, Germany
Cytation 5	BioTek, Agilent Technologies, United States of America
Dispenser D300e	Tecan Group Ltd., Switzerland
Electronic multichannel pipette E4 XLS	Mettler-Toledo, United States of America
Evos FL Auto 2	Invitrogen™, United States of America
Fastblot B44	Biometra, Germany
High performance liquid chromatography, 1260	Agilent Technologies, United States of America

HiLoad™ Superdex 200 pg 26/60	Cytiva, United States of America
HiPrep™ 26/10 desalting column	Cytiva, United States of America
HisTrap™ HP column	Cytiva, United States of America
HiTrap™ Mab Select SuRe	Cytiva, United States of America
Incubator (37°C, 8% CO ₂ , ≥80% relative humidity)	Thermo Scientific GmbH, Germany
LaminarAir Flow	Merck Millipore, Merck KGaA, Germany
Magnetic stirrer, RCT basic	IKA®-Werke GmbH & CO. KG, Germany
NanoDrop ND-1000 spectrophotometer	Thermo Scientific GmbH, Germany
Octet® RED96 system	Sartorius, United States of America
Odyssey® DLx Imaging system	Li-COR Biosciences, United States of America
Orbital Shaker Certomat SII	Sartorius, United States of America
pH meter SevenExcellence™	Mettler-Toledo, United States of America
Plate reader, Envision 2104 multiplate reader	Perkin Elmer Inc., United States of America
Plate reader, Synergy 4	Heraeus Holding, Germany
PLRP-S	Agilent Technologies, United States of America
Polyvinylidene difluoride membrane	Merck KGaA, Germany
PowerPac™ Basic Power Supply	Biorad laboratories, Inc., United States of America
QIAxpert®	Qiagen, Germany
Sierra SPR®-32 Pro	Brucker, United States of America
Single channel electronic pipette E4 XLS	Mettler-Toledo, United States of America
Single channel pipets	Eppendorf AG, Germany
ThermoMixer comfort	Eppendorf AG, Germany
ThermoMixer F1.5	Eppendorf AG, Germany
TSKgel® Butyl-NPR column	Tosoh bioscience, Japan
Vi-CELL™ BLU	Beckmann Coulter, United States of America
Vortex mixer	VWR International, United States of America

3 Methods

The methods used are described in the following section. The methods are organized according to molecular biological methods, biochemical and biophysical methods as well as cell biological methods.

Molecular Biological Methods

3.1 Determination of DNA concentration

To determine the concentration of nucleic acids in aqueous solutions, spectrometric measurements using NanoDrop ND 1000 were performed. Equal volume of 2 μL was used for sample or blank measurement with milli-Q water. The Lambert-Beer law serves as the foundational physical principle governing the absorption of aromatic nucleobases in DNA at 260 nm. The A_{260}/A_{280} and A_{260}/A_{230} absorbance ratios serve as quality benchmarks for DNA purity, with optimal ranges being 1.8 and 2.0-2.2, respectively. Values below these ranges suggest contamination with unwanted substances, usually proteins or aromatic compounds.

3.2 Transformation in *E. coli*

Expression plasmids were amplified using heat shock bacterial transformation of OneShot™ TOP10 Chemically Competent *E. Coli* cells. Briefly, 50 μL of ice thawed chemically competent *E. Coli* cells were added to 1 μL plasmid DNA (approx. 500 ng/mL) and incubated on ice for 30 minutes followed by a heat shock in water bath at 42 °C for 45 seconds. Incubation of the transformed cells was performed on ice for 2 minutes. Subsequently, 250 μL of preheated S.O.C. medium was added. The cells were incubated at 37 °C, 450 rpm for 1 hour. Afterward 50 μL of the cell suspension was plated on each selective agar plate containing LB-ampicillin. The plates were incubated at 37 °C overnight.

3.3 Plasmid preparation

Single *E. Coli* colonies were selected from the agar plates and transferred into 100 mL LB-ampicillin medium. The cultures were then incubated at 37 °C, 250 rpm for 18 h. To determine the cell titer, the optical density (OD) of the cell culture grown overnight was measured at 600 nm using UV/Vis spectrophotometer. Plasmid purification was executed utilizing the GenElute™ HP Plasmid Midiprep Kit, following the manufacturer's protocol. Elution of plasmid DNA was accomplished with 1 mL of 10 mM Tris-HCl, pH 8.5, and quantification was performed using NanoDrop ND 1000. The purified plasmid DNA was stored at -20°C until transfection.

Biochemical and Biophysical Methods

3.4 Determination of protein concentration

Protein concentration was determined either by spectrophotometer NanoDrop ND 1000 or by bicinchoninic acid (BCA) assay. For UV spectrophotometric measurement, equal volume of 2 μL was used for blank measurement, with the corresponding sample solvent, and of the sample resolution. Instrumental setting of A_{280} was used to determine the antibody concentration (in mg/mL), and protein concentration was calculated according to the Lambert-Beer law, taking the molar extinction coefficient of the protein and the path lengths of the device into account. The BCA assay was used to determine the protein concentration of lysates. Bivalent copper ions are reduced to monovalent copper ions by the peptide bonds of proteins in alkaline environment. This reaction is proportional to the number of peptide bonds and thus to protein concentration. A violet complex of monovalent copper with two molecules BCA is detectable. A serial dilution of BSA (0.06-2.0 mg/mL) served as protein standard curve. 10 μL of each sample or standard dilution and 200 μL freshly prepared BCA reagent were transferred to 96-well microtiter plate. BCA reagent A and B (4% copper sulphate) were mixed in a 1:50 ratio. After shaking for 30 s and incubation for 30 min at 37°C in the dark, adsorption at 562 nm was measured. The protein concentration of each sample was determined using linear regression analysis of the calibration curve.

3.5 Preparative protein purification

3.5.1 Protein A and Amsphere™ A3 Affinity Chromatography

Antibodies and VHHs from cell free Expi293F™ supernatants were sterile filtered through 0.22 μm PES filter before purification. Purification was performed with affinity chromatography using ÄKTExpress systems equipped with 5 mL HiTrap™ Mab Select SuRe (for antibodies) or 1 mL Amsphere™ A3 affinity column (for VHHs) followed by a HiPrep™ 26/10 desalting column. Affinity chromatography columns were equilibrated with 5 column volumes (CV) PBS, pH 7.4 at a flow rate of 2.5 mL/min and desalting columns were equilibrated with 3 CV 24 mM HEPES pH 7.0 at 7.5 mL/min. Then, supernatant was loaded on affinity chromatography column followed by a washing step of 5 CV. 3 CV of isocratic elution using 50 mM acetic acid, pH 3.2 (Protein A) and 50 mM sodium acetate, pH 3.0 (Amsphere™ A3) was used for sample elution. Eluate was directly buffered exchanged through desalting column with 24 mM HEPES, pH 7.0. Fractions of 1 mL were collected in 96-deep well plates. Fractions containing target protein were pooled and analyzed for purity using SDS-PAGE and SE-HPLC. Proteins were concentrated using Amicon® Ultra

centrifugal units (VHH: 3K MWCO, IgG: 50k MWCO) and sterile filtered using Ultrafree-CL filter units (0.22 μm). Protein concentration was determined by UV-Vis spectroscopy at 280 nm. The protein identity was determined via intact mass analysis. After purification, all proteins were snap frozen in liquid nitrogen and stored at $-80\text{ }^{\circ}\text{C}$ until needed for subsequent experiments.

3.5.2 Immobilized Metal Affinity Chromatography (IMAC)

The scFv fragments from Expi297F™ supernatants comprising a His₆-tag were purified by IMAC using ÄKTA pure system. A 1 mL HisTrap™ HP column was used. After harvesting Expi297F™ supernatant and sterile filtration through 0.22 μm PES filter, 1 mM nickel sulfate final was added to the supernatant. HisTrap™ HP column was equilibrated with 50 mM sodium phosphate, 0.5 M NaCl, pH 7.4 (5 CV) at 5 mL/min. Subsequently, an automatic sample application and column wash at 2.5 mg/mL was performed on ÄKTA system. Complexed His₆-tagged scFv protein was stepwise eluted with a six-step gradient (5 mL/min, 10 CV each step) of 20 mM, 50 mM, 100 mM, 200 mM, 300 mM and 500 mM imidazole in 50 mM sodium phosphate, 0.5 M NaCl. Samples of 1 mL were gathered in 96-deep well plates. Fractions containing the desired protein were combined and assessed for purity using SDS-PAGE and SE-HPLC. Proteins were concentrated using Amicon® Ultra centrifugal units (scFv: 10K MWCO) and sterile filtered using Ultrafree-CL filter units (0.22 μm). Protein was subjected to preparative SEC, if the SE-HPLC monomeric content was less than 96%. Protein concentration was determined by UV-Vis spectroscopy at 280 nm. The protein identity was determined via intact mass analysis. After purification, all proteins were snap frozen in liquid nitrogen and stored at $-80\text{ }^{\circ}\text{C}$ until needed for subsequent experiments.

3.5.3 Preparative Size-Exclusion Chromatography (SEC)

Impure protein solutions i.g. antibodies, scFv, VHH and small-scale conjugates were purified by preparative SEC to separate low and high molecular weight species, like aggregates. The process involved using an ÄKTA pure or ÄKTA avant system. A HiLoad™ Superdex 200 pg 26/60 column was used. The column was initially equilibrated with a 3 CV formulation buffer at 10.0 mL/min. Subsequently, a protein solution concentrated to $\leq 1\text{ mL}$ was loaded onto the column at a flow rate of 1.0 mL/min via a sample loop. Fractions of 0.5 mL were collected for 1.5 CV in 96-deep well plates. Fractions containing the desired protein were combined and assessed for purity using SE-HPLC. Proteins were concentrated using Amicon® Ultra centrifugal units (VHH: 3K MWCO, scFv: 10K MWCO, IgG and conjugates: 50k MWCO) and sterile filtered using Ultrafree-CL filter units (0.22 μm). After purification, all proteins were snap frozen in liquid nitrogen and stored at $-80\text{ }^{\circ}\text{C}$ until needed for subsequent experiments.

3.5.4 Buffer exchange

Desalting is a simple and fast method for rapidly removing of low molecular weight contaminations while transitioning the sample into the desired buffer, all in one step. Therefore, Zeba™ Spin Desalting Columns for transglutaminase, and PD-10 Desalting Columns for antibody samples were used. The fundamental system here is size exclusion chromatography which separated the sample mixture based on their molecular size. Firstly, larger molecules were eluted followed by smaller molecules like salts or other impurities. The molecular weight cut offs (MWCO) for Zeba™ Spin Desalting Columns was 7 K, and 5 kDa for PD-10 columns. All steps were performed as prescribed by the manufacturer, first the column equilibration was performed by application of three column volumes storage buffer, followed by adding the sample on top of the column bed. Elution was performed using the desired buffer.

3.6 Sodium dodecyl sulfate polyacrylamide gel electrophoresis (SDS-PAGE)

SDS-PAGE is used to evaluate the protein purity or analyze the cell lysates under reduced or non-reduced conditions. It separates proteins primarily according to their MW as they move towards the anode under an electric field. To achieve this, protein samples were mixed with either 4x LDS sample buffer for non-reduced samples, or 4x LDS sample buffer supplemented with a 10x sample reducing agent for reduced samples, with the intention of breaking disulfide bonds. The samples were denatured at 70 °C for 10 minutes in a heating block while shaking (550 rpm). Subsequently, samples containing 2 µg of protein per lane, along with a molecular weight marker, were loaded onto NuPage Bis-Tris gel (4 - 12%). The gel was installed in an electrophoresis chamber filled with 1x MES SDS running buffer. The running time was set to 40 minutes and 200 V constant with 125 mA/gel were set.

3.7 Protein detection using Coomassie staining

To visualize proteins directly after gel electrophoresis, the gels were washed with deionized water, and protein bands were revealed by Coomassie staining. To achieve this, the gels were immersed in “Der Blaue Jonas” Protein Stain on an orbital shaker for 1 hour, followed by destaining with deionized water until background was reduced.

3.8 Protein detection using Western blot analysis

For Western blot analysis of cell lysates, adherent cells were seeded in 12-well tissue culture (TC) plates and incubated overnight in the respective medium of the cell line. One million cells were treated with analytes at standard cultivation conditions for 12 to 48 hours depending on the experiment requirements. Cell lysis was performed, and lysates were subjected to SDS-PAGE.

Western blotting mediated by fluorescent dyes was carried out either by dry blotting system iBlot according to manufacturer's instructions or by semi-dry blotting using Fastblot B44. The proteins separated by SDS-PAGE analysis were transferred onto polyvinylidene difluoride (PVDF) membranes and probed with target specific antibodies as outlined in chapter 2.3. Therefore, PVDF membranes were blocked in 5% BSA in DPBS for 1 h at RT. Afterwards, membranes were incubated with primary antibodies in 1% BSA, 0.1% Tween®20 in DPBS overnight at 4 °C. After three washing steps with 0.1% Tween®20 in DPBS, detection, antibodies were added and it was incubated at RT for 60 min. After additional three washing steps with 0.1% Tween®20 in DPBS, fluorescent bands were visualized using fluorescent reader Odyssey® DLx Imaging system and Image Studio™ software.

3.9 Analytical chromatography methods

3.9.1 Size Exclusion-HPLC (SE-HPLC)

Analytical size exclusion chromatography (SE-HPLC) was employed to assess protein purity and detect high molecular weight protein aggregates using a Bio Resolve SEC mAb column (4.6 x 150 mm, 2.5 µm, 200 Å). The SEC parental buffer was 0.05 M sodium phosphate, 0.4 M sodium perchlorate, pH 6.3. First, the equilibration of the column was performed with SEC parental buffer. Flow rate of 0.35 ml/min was used until stable baseline was reached. Generally, sample amount of 10 µg was injected, and 214 nm or 280 nm signal was detected. Furthermore, gel filtration standard was prepared according to manufacturer's instructions and used as molecular weight standard reference. The elution was performed isocratic at a flow rate of 0.35 mL/min and a total run time of 7 minutes were used. Data acquisition and processing was performed by using ChemStation of LC 3D system (Agilent Technologies). Data were analyzed using ChemStation software by integration of peaks.

3.9.2 Reversed Phase-HPLC (RP-HPLC)

Investigation of ligand to antibody ratio (DAR) and VHH-to-antibody ratio (VAR) of conjugated proteins was carried out on Agilent 1260 infinity HPLC system equipped with a PLRPS column (2.1 x 50 mm, 5 µm, 4000 Å). A gradient of 30 to 45% over 7.5 min at 1 mL/min of solvent B was used. Generally, sample amount of 10 µg was injected, and 214 nm signal was detected. (Solvent A: water supplemented with 0.1% (v/v) TFA, solvent B: acetonitrile supplemented with 0.1% (v/v) TFA). All measurements were performed at 55 °C together with the flow rate of 1 mL/min. Data acquisition and processing was performed by using ChemStation of LC 3D system. Data were analyzed using ChemStation software by integration of peaks. Subsequently, labeling ratio was calculated from peak area of individual species using unconjugated parent antibody as reference.

3.9.3 Hydrophobic Interaction HPLC (HI-HPLC)

To measure the DAR and loading efficiency of PROTACs, conjugates and antibody-PROTAC complexes were analyzed using HI-HPLC. Therefore, samples were adjusted to 0.5 M ammonium sulfate and 42.5 µg sample were injected into Agilent 1260 infinity HPLC system equipped with a TSKgel® Butyl-NPR (4.6 x 100 mm, 2.5 µm) column heated to 35 °C. Sample were separated by applying a gradient of 40 to 80% over 40 minutes at 0.45 ml/min from 0.025 M Tris HCl pH 7.5 to 20% isopropanol, 0.025 M Tris HCl, 2 M ammonium sulfate pH 7.5. Signal recording was performed at the wavelength of 280 nm. Data acquisition and processing was performed by using ChemStation of LC 3D system (Agilent Technologies). Data were analyzed using ChemStation software by integration of peaks.

3.10 LC-MS

To determine the DAR and VAR using LC-MS, the conjugates were diluted with 0.1% formic acid. A final concentration of 0.05 mg/ml was set. Next, 100 µL of this solution was reduced with 1 µL TCEP (500 mM) for 5 min at RT. The LC-MS analysis was conducted via an Exion HPLC system (Buffer A: water containing 0.1% formic acid, Buffer B: acetonitrile containing 0.1% formic acid) connected to a Sciex 6600+ mass spectrometer by a Turbo V ESI source. Protein solution was loaded onto a bioZEN 3.6 µm Intact C4, 2.1 x 50 mm column (Phenomenex). Elution was performed with a linear gradient from 15% to 95% buffer B with a flow rate of 0.25 ml/min for 3 min. Instrument settings were set to source voltage 5.5kV, declustering potential 180 V, source temperature 350 °C, accumulation time 1 s, gas1 50 l/h, gas2 25 l/h, and curtain gas 10 l/h. The mass spectrometer was calibrated with ESI positive calibration solution for the SCIEX X500B. Data was processed with Genedata Expressionist 16.5. Spectra were deconvoluted with the maximum entropy method. For protein mapping the following modifications were chosen with tolerance of 10 Da, glutamine to pyroglutamate conversion and C-terminal lysine loss. The mass spectrometric analysis was executed by laboratory Roland Kellner, department of ADCs and Targeted NBE Therapeutics, Merck Healthcare KGaA.

3.11 Bio-layer-Interferometry (BLI)

Bio-layer-Interferometry was performed to determine kinetics and affinity of molecular interactions. Therefore, Octet® RED96 system (ForteBio, Pall Life Science) at 25 °C and Octet® software for data acquisition and analysis was used.

3.11.1 Quantitative BLI

For quantitative BLI of Expi293F™ supernatant containing His₆-tagged scFv molecules Octet® HIS1K biosensors were used for immobilization. Four dilutions of the supernatant were performed to calculate the concentration in the detection range. An eight-step dilution series from 50 µg/mL to 0.35 µg/mL of purified His₆-tagged scFv was used as standard curve. The concentration was calculated based on the binding rate and using linear regression of the standard curve.

3.11.2 Kinetic BLI

3.11.2.1 αRNF43 scFv variants

For RNF43 binding analysis of scFv, anti-human IgG Fc capture (AHC) biosensors were loaded with recombinant human Fc-RNF43 fusion protein (5 µg/mL in PBS) for 180 s. The biosensors were subsequently moved into kinetic buffer (KB) and allowed to incubate for 45 seconds, followed by a 300-second association step. The analyte for association was diluted in a concentration range varying from 20 nM to 0.8 nM. The following dissociation step was performed in KB for 600 s to determine k_{on} and k_{off} values (KB: PBS + 0.1% Tween-20 + 1% bovine serum albumin (BSA)). For reference measurement and negative control analytes were replaced by KB. Non-binding recombinant human HER2-Fc fusion protein and a His₆-tagged anti-EGFR scFv were used as negative control. Data were fitted using ForteBio data analysis software 8.0. The KB reference served as control curve and was subtracted from sample measurement before data fitting. The Savitzky-Golay filter and a 1:1 global full-fit binding model were utilized.

3.11.2.2 Simultaneous binding

For simultaneous binding analysis, 63 nM of scFv-antibody conjugate was loaded onto AHC biosensors for 180 s. Following biosensors were incubated in KB buffer for 45 s. The first association step was performed in 125 nM His₆-tagged RNF43 for 300 s and for the second association step 125 nM respective antigen was used for 600 s. Respective controls and reference measurements were included and data analysis was performed as mentioned before.

3.11.2.3 VHH-antibody conjugates

For kinetic binding analysis, a concentration of 12.5 µg/mL of parental antibodies and VHH-antibody conjugate samples in PBS were loaded on AHC biosensor for 180 s. Then rinsed in KB for 45 s and associated with the corresponding antigen for 300 s. An antigen concentration range of 15.6 nM to 500 nM was used for rhHER2 and rhEGFR. Association was monitored for 180 s and subsequent dissociation was performed in KB for 600 s. The association in KB was used as

reference value. Non-binding antigens were used for negative control. The buffer reference served as control curve and was subtracted from sample measurement before data fitting. The Savitzky-Golay filter and a 1:1 global full-fit binding model were utilized.

3.12 Surface plasmon resonance spectroscopy (SPR)

Binding kinetics between VHH-antibody conjugate and VHL-based PROTACs were assessed by SPR. Therefore, antibody-VHH conjugates were immobilized onto a high-capacity amine sensor chip (Bruker Daltonics) using the standard amine coupling method at 25 °C. Prior to immobilization, the carboxymethylated surface of the chip was activated with 200 mM 1-ethyl-3-(3-dimethylaminopropyl)-carbodiimide and 25 mM N-hydroxy succinimide for 10 min. The VHH-conjugate variants were diluted to 10 µg/mL in 10 mM BisTris at pH 6.0. The immobilization was performed on the activated surface chip for 3 to 7 minutes, achieving 3,000 to 9,000 response units (RU). The remaining activated carboxymethylated groups were blocked with 1 M ethanolamine pH 8.0 in a 7 minute injection step. HBS-N, comprising 10 mM HEPES pH 7.4 and 150 mM NaCl, served as the background buffer during immobilization. PROTACs were pre-diluted in DMSO, further diluted 1:50 in running buffer (12 mM phosphate, pH 7.4, 137 mM NaCl, 2.7 mM KCl, 0.05% Tween-20®, 2% DMSO), and injected at 10 different concentrations using a two-fold dilution series, ranging from 0.5 µM to 0.001 µM. A DMSO solvent correction (1% - 3%) was applied to adjust for bulk signal variations and ensure data quality. Interaction analysis cycles comprised a 300 s sample injection (30 µL/min; association phase) followed by 1800 s of buffer flow (dissociation phase). All sensorgrams were processed by subtracting the binding response recorded from the control surface (reference flow-channel), followed by subtraction of the buffer blank injection from the active flow-channel (target protein immobilized). All datasets were fitted to a simple 1:1 Langmuir interaction model to determine the kinetic rate constants. The experiments were conducted using an SPR-32 PRO instrument at 25 °C, and data analysis was performed using the provided Sierra Analyser Software (version 3.4.5).

3.13 Conjugation methods

3.13.1 Random lysine conjugation (pHAb-dye labeling)

For pHAb-dye labeling, the Promega labeling kit was used. The conjugation of amine reactive dye containing a succinimidyl ester group was performed according to manufacturer's protocol. Therefore, antibodies were prepared in 10 mM sodium bicarbonate buffer pH 8.5 using Zeba™ Spin Column and pHAb amine reactive dye was added with 20 molar excess. Afterward, the mixture was incubated in darkness at 25 °C, 500 rpm for 1 h. Subsequently, free excess of dye was removed by Zeba™ Spin Columns equilibrated with DPBS. Concentration of dye labeled conjugate

and the degree of labeling were calculated as recommended by the manufacturer using UV-Vis spectroscopy and LC-MS method.

3.13.2 Enzymatic conjugation

For site-specific enzyme conjugation, microbial transglutaminase (MTG) in 24 mM HEPES pH 7.0 formulation buffer was used. The concentration of the final antibody or scFv in the reaction mixture was 5 mg/ml or 10 mg/ml. The linker peptide or VHH concentration used ranged from 5 to 10 molar equivalents per conjugation site. Additionally, the final MTG concentration was within the range of 1 U/mL to 75 U/mL. Reaction mixes were incubated with 550 rpm either at 37 °C for 18 h or 30°C for 24 h and chilled to 10 °C. After incubation the reaction was stopped with 0.1 mM final MTG blocker (Zedira) or directly purified by preparative SE-HPLC. The MTG was produced inhouse and the enzyme activity determined via photometric assay ZediXclusive (Zedira) and according to manufacturer's instruction.

3.13.3 Copper-free strain-promoted azide-alkyne cycloaddition (SPAAC)

SPAAC was performed for modification of enzymatically modified antibodies and scFv variants. Therefore, site-specifically conjugated alkyne-carrying antibodies and scFv variants equipped with azide were mixed in the following ratio: 3 mg/mL to 5 mg/mL antibody with 1.5 molar equivalents of scFv per conjugation site. Incubation was performed for 3 h or 24 h at 37 °C and 550 rpm and afterwards purified by preparative SE-HPLC.

3.14 Complex formation of PROTAC and VHH-antibody conjugate

Reaction to generate the complex of PROTAC and VHH-antibody conjugate was performed at 25 °C, 650 rpm for 3 hours. Therefore, 10 µM final VHH-antibody conjugate was mixed with different equivalent VHL-based PROTAC in PBS pH 7.4 + 5% DMSO. In cellular experiments, 0.3% Tween-20® final was added to enable sample application to cells by Tecan D300e dispenser. Sample preparation for HI-HPLC, SPR, BLI and flow cytometric analysis were performed without addition of aqueous Tween-20®.

3.15 Determining antibody loading

3.15.1 Determination of ligand to antibody ratio – RP-HPLC

The level of ligand to antibody ratio was investigated using intact RP-HPLC. The populations of unconjugated, one ligand, and two ligand per antibody were separated chromatographically. The respective percentage area under the curve (AUC) from the results of the UV absorption spectrum was used to calculate the ratio of ligand to antibody (DAR). The equation (1) sums the individual

calculations consisting of the percentage AUC of the ligand per antibody divided by the total area of all peaks multiplied by the respective VHH loading.

$$DAR = 1 * \frac{\% AUC \text{ DAR 1 species}}{\% AUC \text{ total Ab species}} + 2 * \frac{\% AUC \text{ DAR 2 species}}{\% AUC \text{ total Ab species}} \quad (1)$$

3.15.2 Determination of VAR (VHH-antibody ratio) – HI-HPLC

For determination of VHH-to-antibody ratio (VAR), antibody species with individual VHH loading were separated by HI-HPLC and analyzed using UV/VIS spectrometry. The VAR is calculated from the sum of the weighted ratio of percental AUC multiplied by the degree of VHH represented by that peak. The equation for VAR calculation is shown in equation (2).

$$VAR = \sum_{n=0}^2 \frac{\% AUC * n_{VHH}}{\text{sum of the \% AUC}} \quad (2)$$

3.16 Determination of complex formation between antibody and PROTAC

The complexation of VHH-conjugated antibody with PROTACs was determined using HI-HPLC. Calculation of complexation was performed as described before. Equation (2) was modified by replacing the degree of VHH with the degree of PROTAC (equation (3)).

$$\text{Complexation ratio} = \frac{Area_{R0} * 0 + Area_{R1} * 1 + Area_{R2} * 2}{VAR * Area_{total}} \quad (3)$$

3.16.1 Determination of DOL

The degree of labeling (DOL) value was determined using the absorption spectrum of the labeled antibody. For this, free excess of dye was removed by gel filtration and the absorbance of the pHAb-dye conjugated antibody was measured at 280 nm and 532 nm using NanoDrop ND 1000. The molarity of the antibody was calculated according to equation (4) with the correction factor (CF) for pHAb reactive dye of 0.256 and molar extinction coefficient of the antibody (ϵ).

$$\text{Antibody concentration} = \frac{A_{280} - (A_{532} \times CF)}{\epsilon} \quad (4)$$

The DOL was calculated with equation (5) using molecular weight (MW) of the antibody and the extinction coefficient for pHAb reactive dye (ϵ') of 75000.

$$DOL = \frac{(A_{532} \times MW \text{ of antibody})}{\text{Antibody concentration} \times \epsilon'} \quad (5)$$

Cell Biological Methods

3.17 Cell cultivation

Cell suspensions were thawed rapidly in a water bath at 37 °C and mixed with 9 mL of pre-warmed cell culture media. Following, the cell suspension was centrifuged for 5 min, 500 x g at room temperature (RT). The supernatant was discarded, and the cell pellet was gently re-suspended in 10 mL of pre-warmed medium. Adherent cancer cells were treated according to standard culture conditions (37 °C, 5% CO₂, 95% humidity) in tissue culture flasks of 25 cm² or 75 cm². Cells were subcultured every three to four days. Prior passaging, a visual control of the cell lines was performed using Evos FL microscope to exclude contamination, monitor the phenotype such as shape, size, etc. and determine the confluence of the cells. Briefly, confluent cell lines were washed using 13 mL DPBS and detached using 1 mL pre-warmed Accutase™ containing proteolytic and collagenolytic enzymes. After incubation of 5-10 min at 37 °C, the detachment was blocked by addition of 9 mL fresh medium. The viable cell number and cell viability were determined using Vi-CELL™ BLU. For further cultivation, a suitable number of cells were seeded in a new cultivation flask with fresh medium and placed in the incubator. Suspension cells Expi293F™ were cultured in Erlenmeyer shake flasks congruent with the manufactures protocol.

3.18 Preparation of cell lysates

To analyze expression level of cellular target proteins within western blot analysis, adherent cells were lysed, and protein concentration determined. The complete procedure was performed on ice. Therefore, medium was removed, cells were washed with ice-cold DPBS, and lysis buffer was added. Cells for western blot analysis of membrane bound targets were lysed with ice-cold radioimmunoprecipitation assay (RIPA) lysis buffer supplemented with cOmplete™ protease inhibitor cocktail. After the incubation of 100 µL buffer per well for 20 min on ice, cells were scraped using cell scraper and transferred to Eppendorf cups. Centrifugation for 30 min at 4 °C and 12700 rpm was performed, and supernatant was snap frozen in liquid nitrogen. Cell lysates were stored at -80 °C for further use.

3.19 Recombinant expression of VHH and scFv variants

The antibody fragments, scFv, and VHH were produced through transient transfection in the Expi293F™ expression system, following the manufacturer's instructions and utilizing the corresponding transfection kit. Cells were cultured in Expi293™ expression media from Life Technologies, with the plasmids used in the transfection at a ratio of 1 µg per 1 ml cell culture volume. The expression volumes varied between 50 mL and 200 mL approaches. Six days post-

transfection, the supernatant was collected by centrifugation at 2000 rpm, 4 °C for 25 min and sterile filtered before chromatographic purification.

3.20 Cell Binding Assay

The cellular binding experiments were performed using parental antibodies and antibody conjugates on antigen expressing tumor cells using a flow cytometry-based assay. Cellular binding was analyzed on two target-positive and one target-negative cancer cell lines. In general, in this method, all steps were performed on ice, the centrifugation steps were done at 4 °C, 2000 rpm for 5 minutes using microcentrifuge and for the washing steps, 100 µL cold DPBS + 1% (w/v) BSA per well was used.

More precisely, cells were detached, and cell count of respective cancer cell lines was measured. Following, cells were seeded in 96-well round-bottom microplate with 10000 cells/well. After centrifugation, supernatant was removed, and cells were washed twice. Analytes were then added in 1:2 dilution series, with a starting concentration approximately 100-fold higher than the obtained K_D values. The incubation step was for 1 h on ice to prevent internalization. The plate was then centrifuged and washed twice. The second labeling step was performed with AF488-labeled antibodies targeting the analyte (IgG-scFv conjugates: #109-546-008, antibody-VHH conjugates: #109-547-003, Jackson ImmunoResearch). The concentration ranged between 300 nM and 500 nM, with triple molar excess based on the molar concentration of the analyte. Cells were incubated for 30 min on ice in absence of light, washed twice, centrifuged and the resulting cell pellets resuspended in 200 µL DPBS + 1% (w/v) BSA containing Sytox Red™ (1:000). After a further incubation of 15 min the plate was transferred to Attune™ NxT flow cytometer and fluorescence of cells was analyzed (30000 counts/well). The fluorescence signal was analyzed with emission filter 670/14 nm for Sytox Red™ (Exc. 638 nm) and emission filter 530/30 nm for AlexaFluor® (Exc. 488 nm). In the direct staining experiment, VHL-Cy5 was complexed with antibody-VHH conjugates. Therefore, the antibody samples were mixed with VHL-Cy5 in molar equivalent ratio and incubated for 2 hours at 25 °C and 650 rpm in PBS + 5% DMSO. Samples were protected from light. Subsequently, samples were desalted via Zeba™ Spin Desalting Column 7K MWCO. Further, procedure was as described before: cells were seeded in 96-well plates, washed twice and incubated with 100 nM analyte for 60 min on ice and protected from light. After two washing steps, cells were taken up in 200 µL DPBS + 1% (w/v) BSA containing Sytox Green™ (1:000). Fluorescence signal was analyzed with emission filter 670/14 nm for Cy5 (Exc. 651 nm) plus emission filter 530/30 nm and Sytox Green™ (Exc. 504 nm).

3.21 Immunofluorescence Assay

The protein degradation experiments were performed with antibody-VHH conjugates and controls on SKBR3 cells using an immunofluorescence (IF) assay. Cells were seeded in 96-well plates and treated at 70-90% cell confluency. Protein level were generally analyzed 24 hours after treatment on target positive cells treated with antibody-VHH conjugates, isotype control and respective negative controls. After incubation, three washing steps with DPBS were performed. Binding reagents were diluted in 3% (w/v) BSA in DPBS pH 7.4, with final concentrations of 15.3 nM primary antibody, 32.9 nM secondary antibody and 8.12 μ M Hoechst 33342 dye. Triton X-100, formaldehyde and sodium azide were diluted in DPBS.

The IF assay was performed according to the following procedure. The media was removed, and cells were washed with DPBS. Fixation was performed by incubation with 2% (v/v) formaldehyde solution for 15 minutes, after washing cells were permeabilized with 0.2% Triton X-100 for 10 minutes. The cells were blocked at RT for 60 minutes with 3% (w/v) BSA in DPBS and incubated overnight at 4°C with the respective primary antibody. Following the staining with secondary antibody was performed for 120 minutes and Hoechst 33342 staining for 90 minutes, both in the dark and at room temperature. For long-term storage, 0.1% (v/v) sodium azide in DPBS was added. Analysis was performed using the Cell Imaging Multimode Reader Cytation 5 (BioTek/Agilent) with 10x objective, GFP channel with Exc. 469 nm and Em. 525 nm, integration time of 42 msec, camera gain 24 and led intensity 10. The DAPI settings included a 10x objective, a DAPI channel with Exc. 377 nm and Em. 447 nm, integration time of 5 msec, camera gain 17 and led intensity 10. Image processing was performed using BioTek gen5 software. Data analysis was performed by normalizing the fluorescence intensity of each image to the final cell count obtained by DAPI staining. GFP fluorescence intensity was subtracted using the fluorescence signal of the media control samples. The BRD4 level was observed after 24 hour treatment of PROATC, PROTAC-loaded conjugates or the respective negative controls. Further, as reference untreated cells were used. Staining with secondary antibody only was used to exclude unspecific binding.

3.22 Internalization Assay

Internalization of parental antibodies and VHH-antibody conjugates was studied via live-cell imaging. The cells were centrifuged at 2000 rpm for 5 min, supernatant was discarded, and cells resuspended in respective medium. Cell suspension (10000 cells/well) were seeded in black 384-well plate with μ Clear bottom (Greiner) and cultivated overnight under standard conditions (see section 3.17). The antibodies labeled with pHAb-dye were mixed with a final concentration of 0.3% Tween-20, diluted to 3 μ M and applied to the cells at a final concentration of 100 nM using the Tecan D300e digital dispenser. Analysis was performed using Cell Imaging Multimode Reader

Cytation 5 (BioTek/Agilent) including 10x objective, RPF channel with Exc. 531 nm and Em. 593 nm, integration time of 14 msec, camera gain 24 and led intensity 10. For brightfield images, the following settings were used: 10x objective, integration time 9 msec, camera gain 24 and led intensity 5. Images were acquired every 30 min for 24 h, cell cultivation during the experiment was conducted in BioSpa 8 device. After the final set of images, 1 $\mu\text{g}/\text{mL}$ Hoechst 33342 dye was added using Tecan D300e dispenser to obtain an additional endpoint image for determination of cell count by nuclear staining. The DAPI settings included a 10x objective, DAPI channel with Exc. 377 nm and Em. 447 nm, integration time of 5 msec, camera gain 18 and led intensity 5. Image processing was performed using BioTek gen5 software. Data analysis was performed by normalizing the fluorescence intensity of each image to the final cell count obtained by DAPI staining. The background signal was subtracted from the fluorescence signal of the zero hour sample. Normalized intensities were then divided by DOL of the pHAb-dye of each construct and plotted against the time. Internalization rates were obtained by linear regression of the data using GraphPad Prism (GraphPad Software, Inc.).

3.23 Cell Viability Assay

Cytotoxicity assay was performed to evaluate cell viability after treatment with PROTAC-complexed antibody-VHH conjugates and corresponding controls. Therefore, cancer cells were seeded in the respective medium in white 384-well plates (2000 viable cells/well), followed by incubation overnight at 37 °C and 5% CO₂. Complexation of antibody-VHH conjugates with different PROTACs was performed the next day and as described in section 3.14. Analytes were added to the cells in 1:2 or 1:10 dilution series, starting at 100 nM using Tecan D300e dispenser. Final concentrations of 0.003% Tween-20 and 0.05% DMSO were adjusted with 0.3% Tween-20 in PBS pH 7.4 and DMSO stock solution. Normalization of the application volume was performed for each well. After addition of analyte, the cells were incubated at 37 °C and 5% CO₂. Analysis using CellTiter Glo® reagent was performed after three or six days as described in the manufacturer's protocol. The luminescence signal was measured with Envision reader (Perkin Elmer). Luminescence values were normalized to the luminescence of untreated cells, and a slope sigmoidal response fit model was used for data analysis. The calculation and displayed dose-response curves were plotted using GraphPad Prism (GraphPad Software, Inc.).

4 Results

The following results section is subdivided into two chapters. The first chapter describes the selective cellular delivery of PROTACs through a modular conjugation-based approach, which was partially published in "Welding PROxAb Shuttles: A modular approach for generating bispecific antibodies via site-specific protein-protein conjugation".¹⁸¹ The second chapter describes the results of the modular approach for the generation of bispecific antibodies for the recruitment of cell surface proteins and a transmembrane E3 ligase.

Chapter 1: Selective cellular delivery of PROTACs using a modular conjugation-based approach.

4.1 Design and generation of VHH for selective PROTAC delivery

The subsequent chapter focuses on the structural composition and properties of the VHH used for the direct conjugation, and details its generation, purification and analytical characterization.

4.1.1 VHH protein design to enable direct conjugation via MTG

Non-covalent PROTAC-antibody complex formation enables selective delivery of PROTACs into tumor cells, as demonstrated in the PROxAb shuttle approach and previously fully described in 1.6.2.1.¹⁶⁰ IgG antibodies are employed to target tumor-associated antigens which were fused with VHHs. The VHHs were selectively able to bind to the E3 ligase-recruiting subunit of PROTACs, thus enabling non-covalent drug delivery. The PROTAC-binding VHH is called 'MIC7', and it binds with high affinity to the E3 ligase VHL recruiting domain of PROTACs, VH032.¹⁶⁰ The PROTAC and MIC7-based antibody-fusion protein incubation enables complex formation within hours and induced degradation of the PROTAC target protein in cells expressing the antibody target on the surface. While the most prevalent method for generating bispecific antibodies involves different engineering technologies, it has limitations in terms of modularity, as each bsAb must be manufactured individually.¹⁸² However, the recent advancement of various chemical conjugation strategies in the ADC field has introduced new prospects for the chemical production of bispecific antibodies, offering modular platforms for screening. Therefore, biochemical conjugation of PROTAC-binding VHH to commercially available antibodies was envisioned to expand the modularity and flexibility of this strategy. This converts non-engineered antibodies into bispecific antibody-based PROTAC shuttles, enabling the rapid screening of antibody-PROTAC combinations. Out of the available technologies for site-specific conjugation of native antibodies, we opted for enzymatic coupling using microbial transglutaminase (MTG).

While MTG is known to catalyze iso-peptide bond formation between glutamines and acyl acceptor substrates, it was previously demonstrated that specific MTGs can address Q295 in the HC of native IgG-based antibodies.⁷⁸ To apply the modular MTG-mediated conjugation approach for antibody VHH coupling, MIC7 was modified with an N-terminal triple-glycine (G₃) motif and termed 'G₃-MIC7'. The introduction of the spacer sequence and conjugation tag (for detailed sequence information reader is referred to chapter 2.3) increased the molecular weight to 15.32 kDa and the pI value shifted from 7.11 to 5.24. The resulting conjugates exhibited equivalent binding and internalization characteristics compared to the parental antibodies. Exposure to PROTACs resulted in the formation of stable complexes that facilitated targeted protein degradation and cell cytotoxicity selectively in target cells exclusively.

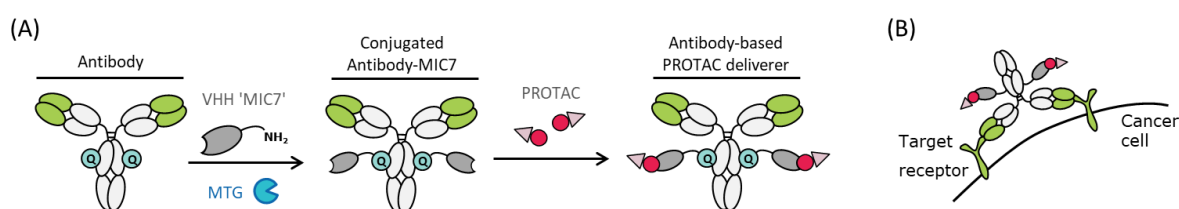


Figure 11 Modular approach to generate bispecific PROTAC-binding antibodies using bioconjugation. (A) Process for generating an antibody-MIC7 conjugate loaded with PROTAC to enable (B) target receptor-mediated binding and internalization of complexed PROTACs. Figure adapted from Lehmann *et al.*¹⁸¹.

4.1.2 Expression, purification, and characterization of PROTAC-binding VHH G₃-MIC7

The VHH 'G₃-MIC7' was produced in mammalian Expi297F cells and purified using protein A affinity chromatography with an Amsphere™ A3 column followed by a desalting step. During purification, protein elution from the Amsphere™ A3 column was initiated by isocratic sodium acetate pH 3.0 gradient (chromatogram shown in Figure S 1 (A)) and eluted fractions were directly buffer exchanged using a desalting column. The final protein was collected in 1.5 mL fractions, and the purity was determined using non-reducing SDS-PAGE. Additionally, samples from each purification step were loaded (Figure S 1 (B)). Protein concentration was measured using UV spectroscopy with NanoDrop. The protein yield was 16.4 mg per liter culture volume. Analytical SE-HPLC was used to determine the final purity of the protein, which was 98% at a concentration of 13.95 mg/mL (Figure S 1 (C)) and remained unchanged after freeze-thaw cycle. To assess the binding capability of the expressed VHH to PROTAC, G₃-MIC7 and GNE987 were mixed, and complex formation was analyzed by Hydrophobic Interaction Chromatography (HI-HPLC). The G₃-MIC7 was complexed with one molar equivalent GNE987 for three hours at room temperature. GNE987, a highly hydrophobic molecule with a log*K* of 2.08¹⁶⁵, caused a shift in retention time of loaded VHH. This shift indicated the formation of 90% G₃-MIC7+GNE987 complex (Figure 12).

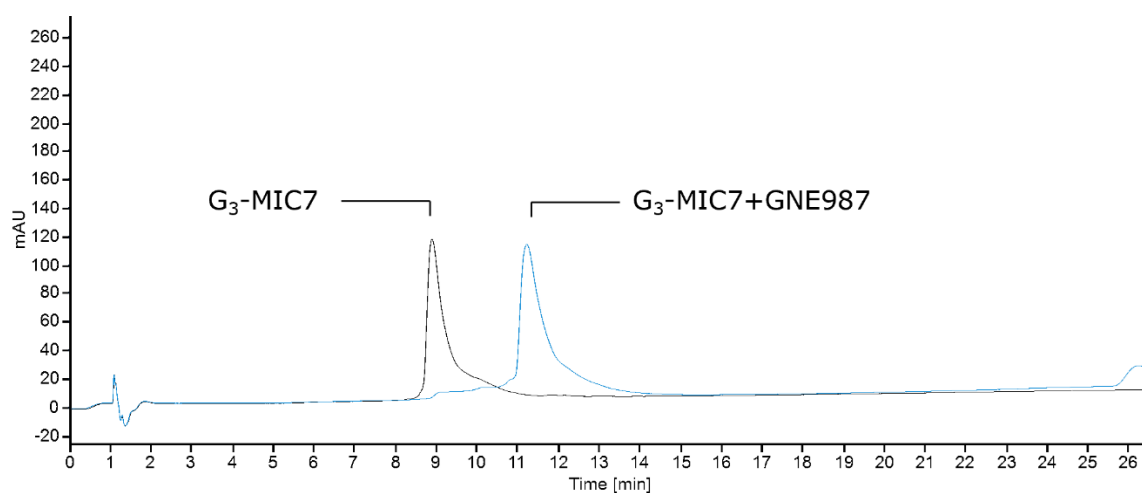


Figure 12 Chromatogram of analytical HI-HPLC. Overlay of the UV-absorption signals of G₃-MIC7 (black) and PROTAC-loaded G₃-MIC7 (blue). 10.9% unloaded G₃-MIC7 at retention time 8.89 min and 89.1% of G₃-MIC7+GNE987 at retention time 11.21 min were detected.

4.2 Site-specific conjugation of VHH 'G₃-MIC7' to native IgG1-based antibodies

In this chapter, the enzyme-mediated conjugation of monospecific antibodies with VHVs to produce bispecific antibody scaffolds is examined.

4.2.1 Evaluation of MTG-mediated conjugation of G₃-MIC7 to Trastuzumab

Site-specific homogenous conjugation through enzymatic transamination between the primary amine of the N-terminal linker attached to G₃-MIC7 and the side chain of glutamine 295 of Trastuzumab (Ttz) was catalyzed by MTG. Ttz was used as tool antibody in the course of this work to evaluate and optimize MTG-mediated conjugation of VHH to antibodies. In general, a reaction mixture with final concentrations of 5 mg/mL Ttz, buffer and 10 molar equivalents G₃-MIC7 was prepared. The reaction was initiated by adding 10 U/mL MTG and after 24 hours of shaking at 30 °C, the reaction was stopped using enzyme inhibitor C102 (Zedira) 0.1 mM final. The MTG activity was previously determined using the Zedira activity kit.

To assess side reactions such as crosslinking of reactants, separate control reactions were performed with either 5 mg/mL Ttz or G₃-MIC7 mixed with 10 U/mL MTG. The reactions were semi-quantitatively analyzed using reduced SDS-PAGE. The analysis revealed the presence of one VHH per heavy chain (65 kDa) in the reaction mixture (Figure 13, lane 7). Notably, no cross-linking was observed in the control reactions, here lanes showed bands of the individual components under reduced conditions, including antibody light chain at 25 kDa and heavy chain at 50 kDa, the VHH at 15 kDa and MTG at 38 kDa. To provide reference samples, individual components and MTG-incubated parent molecules were analyzed separately. In addition, a conjugation reaction with G₃-tag-free MIC7 was performed under the same reaction conditions to verify the MTG recognition side, the data are shown in the appendix in Figure S 8.

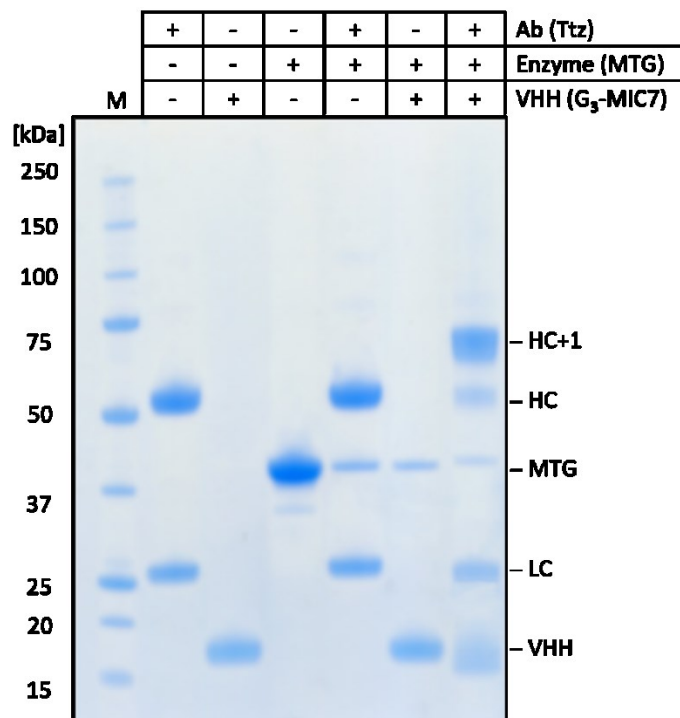


Figure 13 Semi-quantitative analysis of MTG-mediated conjugation. 4-12% Bis-Tris SDS-PAGE gel showing reduced reaction mixes and respective controls. As expected, bands of parental antibody appear at 25 kDa (LC) and 50 kDa (HC) and free excess of G₃-MIC7 appears at approx. 15 kDa and MTG at 38 kDa. No cross-linking was observed between Ttz and MTG or G₃-MIC7 and MTG. Within the reaction mixture (lane 7), a shift of the heavy chain band towards 65 kDa is visible. The Precision Plus Protein™ Unstained Standard was used as the marker for size estimation. Figure adapted from Lehmann *et al.*¹⁸¹.

Further, the conjugation of VHH, antibody and MTG were varied to establish a relationship between concentration and conjugation result in order to optimize the yield. To evaluate the conjugation efficiency, the VHH-to-antibody ratio (VAR) was determined using LC-MS analysis. A clear correlation was found. With increasing concentration of enzyme MTG, a higher conjugation efficiency was obtained (Table 1). Similar results were obtained with increasing antibody concentration, the VAR value increased. Highest VAR values were obtained with increasing molar equivalents (molar eq.) up to 10 VHH per antibody.

Table 1 Evaluation of different reaction conditions for increasing conjugation efficiency. Studies were performed by keeping two concentrations of the reaction components constant and varying one. The VHH-to-antibody ratio (VAR) represents the conjugation efficiency determined by LC-MS.

Antibody conc.	VHH [molar eq.]	Enzyme amount [U/mL]	VAR
3	2	3	0.85
3	2	5	0.94
3	2	10	1.03
3	2	10	0.86
5	2	10	1.01
5	6	10	1.75
5	10	10	1.88

4.2.2 Generation of bispecific antibody-VHH conjugates via MTG

In this study, antibody-VHH conjugates were generated in preparative scale based on antibodies targeting human epidermal growth factor 2 (HER2), human epidermal growth factor receptor (EGFR) and digoxigenin (DIG). The VHH used for coupling with these antibodies was G₃-MIC7, as described previously. The resulting conjugates were named based on the connection of the respective antibody with G₃-MIC7, such as Ttz-MIC7 for Trastuzumab-MIC7, Ctx-MIC7 for Cetuximab-MIC7, and α DIG-MIC7 for anti-digoxigenin antibody-MIC7.

The conjugation reactions between G₃-MIC7 and the respective antibodies were performed following the conditions identified in section 4.2.1. Subsequently, the reaction mixes were purified and characterized. Purification was done using preparative SEC with PBS buffer pH 7.4, at a flow rate of 0.35 mL/min, and peak collection in 0.5 mL fractions. An exemplary chromatogram illustrating the purification process is shown in Figure 14. Figure S 2 shows the chromatogram of preparative SEC purification of Ctx-MIC7 and α DIG-MIC7.

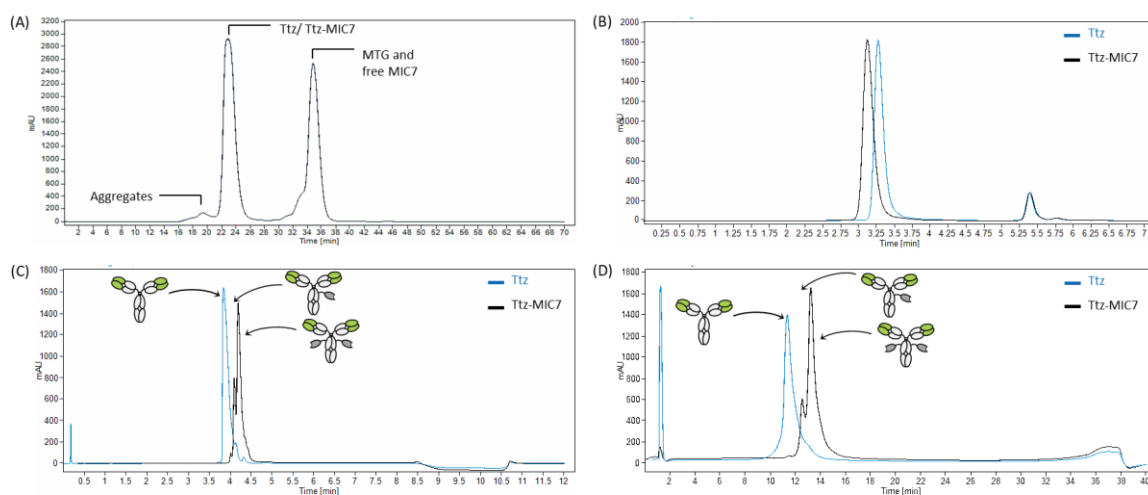


Figure 14 Chromatograms of Ttz-MIC7 preparation and analysis. (A) Chromatogram of preparative SEC. The probe was injected onto a SEC column. Sample was separated by an isocratic gradient in target peak (Ttz/ Ttz-MIC7), HMW, excess G₃-MIC7 and MTG. (B) Chromatogram of analytical SE-HPLC. Overlay of the UV-absorption signals of blue, the Ttz and black, the purified Ttz-MIC7. The shift towards higher molecular weight is in the expected range but does not indicate formation of further multimeric species. (C) RP-HPLC chromatogram of purified Ttz-MIC7. Overlay of the UV-absorption signals of the Ttz and the purified Ttz-MIC7. No unconjugated mAb at retention time 3.85 min, 16.1% of VAR 1 species at retention time 4.10 min and VAR 2 species at retention time 4.19 min were detected. This reaction had an overall VAR of 1.80 (D) Chromatogram of HI-HPLC analysis. Overlay of the UV-absorption signals of Ttz and the purified Ttz-MIC7. Purified Ttz-MIC7 analysis revealed final VAR of 1.72. Figure adapted from Lehmann *et al.*¹⁸¹.

After concentration and sterile filtration, the resulting purified Ttz-MIC7 conjugate was analyzed by analytical chromatography (Figure 14). Characterization included the determination of monomeric content by SE-HPLC, and VAR determination using RP-HPLC and HI-HPLC. For VAR determination, the obtained chromatogram was used to separate species with different numbers of VHH conjugated from unreacted antibody. The VAR was calculated by assigning weighted area-under-the-curve values to each species and using the equation (2) (as described in section 3.15.2).

Additionally, LC-MS analysis confirmed VAR values (Figure S 2). Homogeneous Ttz-MIC7 conjugates with VAR > 1.72 were generated with a monomer content of 99% and a yield of 87.3%. In addition to that, G₃-MIC7 was conjugated to EGFR targeting antibody Ctx and digoxigenin targeting antibody α DIG. The resulting conjugates were prepared in good yields of 72.8% and 79.5% respectively. While VAR of 1.84 was achieved in the preparation of Ctx-MIC7, the preparation α DIG-MIC7 yielded VAR of 1.76. The monomeric content was high with values of >99%. The characterization results are summarized in Table 2.

Table 2 Upscaling conjugation of G₃-MIC7 to different antibodies using MTG. Chromatographic analysis, including SE-HPLC, allowed determination of the highest final purity and VAR determination was performed using RP-HPLC, HI-HPLC and LC-MS. Percent yield was calculated by $m(\text{conjugate})/m(\text{parental mAb}) \times 100$.

Antibody	Yield [%]	Purity [%]	VAR _{RPC}	VAR _{HIC}	VAR _{MS-ESI}	VAR _{Mean}
Ttz-MIC7	87.3	99.6	1.80	1.72	1.72	1.74
Ctx-MIC7	72.8	99.5	1.82	1.84	1.90	1.84
α DIG-MIC7	79.5	99.7	1.81	1.73	1.76	1.76

4.2.3 Modularity of MTG-mediated conjugation of G₃-MIC7 proven by conjugation to several IgG-based antibodies

This chapter focuses on the applicability of the modular approach of conjugating VHH to antibodies with MTG. Several VHH-coupled conjugates were generated based on commercially available IgG1 antibodies with glutamine 295 located in the Fc region. The antibodies for generation of conjugated antibody-MIC7 were summarized in Table 3.

Table 3 Conjugation MIC7 VHH to several native mAbs to verify modular approach and confirm of conjugation site. G₃-MIC7 was conjugated using MTG and reaction mixes were analyzed using LC-MS and SE-HPLC. Efficient conjugation with VHH-to-antibody ratios (VAR) close to 2 and high purity was revealed. The glutamine to alanine substitution at position 295 showed no conjugation, confirming Q295 position as selective antibody conjugation site.

Antibody	VAR	Monomeric content [%]
Trastuzumab	1.88	97.8
Trastuzumab Q295A LC-Qtag	1.86	93.1
Trastuzumab Q295A	0.0	98.5
Cetuximab PG-LALA	1.98	97.6
Cetuximab	1.97	97.2
Matuzumab	1.91	96.7
Atezolizumab	1.62	98.0
Avelumab	1.96	97.4
Pertuzumab	1.93	97.4
Rituximab	1.95	96.4
α DIG IgG1	1.84	97.4

The conjugation of G₃-MIC7 to IgG1-based antibodies was performed according to the conditions described in section 4.2.1, involving an analytical scale reaction mediated by MTG and stopped by addition of 0.1 mM final concentration C102. The reaction mixes were analyzed by gel electrophoresis (Figure S 5), SE-HPLC and ESI-MS (Figure S 6 and Figure S 7). Successful conjugation of G₃-MIC7 with Q295-bearing antibodies was observed, with the lowest VAR value of 1.62 among the tested antibodies for Atezolizumab (Table 3). Variants of Cetuximab, including the native form and the PG-LALA mutated form, exhibited VAR of 1.97 and 1.98, respectively. Moreover, the antibodies Matuzumab, Avelumab, Pertuzumab, and Rituximab had VAR values greater than 1.91, accompanied by a monomeric content of at least 96%.

4.3 Biophysical characterization of antibody-VHH conjugates

After successful conjugation, the antibody-VHH conjugates were evaluated for the antibody-antigen binding and interaction between anti-PROTAC antibody MIC7 and PROTACs. Additionally, the investigation included evaluation of the cell receptor binding and the observation of antibody-mediated internalization.

4.3.1 Soluble antigen binding kinetics

The equilibrium dissociation constant (K_D) based on the association (k_{on}) and dissociation rate (k_{off}) were determined for antibody-VHH conjugates and parental antibodies by biolayer interferometry (BLI) on the Octet RED96 system. Briefly, anti-human Fc (AHC) biosensor tips were loaded with parental antibodies and conjugates at approximately 12.5 $\mu\text{g/mL}$. As isotype control, a $\alpha\text{DIG-MIC7}$ was used. Kinetic data sets were fitted using 1:1 Langmuir binding model using Octet data analysis software with Savitzky-Golay filtering. Association and dissociation of recombinant human (rh) HER2 or rhEGFR were monitored. The fitted curves of conjugates and antibodies were shown in Figure S 9, while the kinetic parameters are summarized in Table 4.

Table 4 Binding kinetics of conjugates and parental antibodies against respective soluble antigen.

Antibody	Antigen	K_D [M]	k_{on} [$\text{M}^{-1}\text{s}^{-1}$]	k_{off} [s^{-1}]
Ttz-MIC7	rhHER2	2.2×10^{-9}	8.0×10^4	1.7×10^{-4}
Ttz	rhHER2	2.5×10^{-9}	7.8×10^4	1.9×10^{-4}
Ctx-MIC7	rhEGFR	7.2×10^{-9}	1.8×10^5	1.3×10^{-3}
Ctx	rhEGFR	6.2×10^{-9}	1.9×10^5	1.2×10^{-3}

BLI measurements revealed binding affinities in the single-digit nanomolar range, with minimal differences in binding affinities between Ttz and Ttz-MIC7 towards rhHER2, as well as between Ctx and Ctx-MIC7 towards rhEGFR. The data confirmed that conjugation of Ttz and Ctx with MIC7

did not alter the kinetic soluble receptor binding profiles. Respective controls showed no unspecific antigen binding or biosensor loading.

4.3.2 Kinetics of complex formation between antibody-MIC7 conjugates and PROTACs

To study the binding kinetic between conjugated G₃-MIC7 and PROTAC, surface plasmon resonance (SPR) analysis was performed. SPR is a label-free optical technique to investigate molecular interactions between proteins and small molecules. Briefly, Ttz-MIC7 and Ctx-MIC7 conjugates and parent antibodies were immobilized and serial dilutions of different VH032-based PROTACs were injected and flowed along the surface. SPR measurements revealed that conjugated VHH interacted with each tested PROTAC in single-digit to sub-nanomolar range independent of the coupled antibody backbone (Ttz-MIC7 or Ctx-MIC7). Moreover, the measurements showed similar K_D to previously published binding affinities of MIC7 and PROTAC, suggesting that conjugation of MIC7 to native antibodies did not alter PROTAC binding behavior (Table 5 and Figure S 10). The parental antibodies Ttz and Ctx showed no unspecific binding up to a concentration of 0.5 μM.

Table 5 Binding affinities of conjugated VHH G₃-MIC7 to PROTACs GNE987, GNE987P and ARV771. *no binding detected up to a tested concentration of 0.5 μM. #determined off-rates are outside of instrument specifications and were therefore reported as k_{off} < 0.0001 1/s; reported KD values are estimated by an assumption of k_{on} > 1.0 x 10⁵ [1/(M*s)]. \$n.d. – not determined as k_{off} is not measured unambiguously.

Antibody	PROTAC	K _D [M]	k _{on} [1/(M*s)]	k _{off} [1/s]
Ttz-MIC7	GNE987	< 1.0 x 10 ^{-9#}	n.d. \$	< 1.0 x 10 ^{-4#}
	GNE987P	3.82 x 10 ⁻¹⁰	7.09 x 10 ⁵	1.59 x 10 ⁻⁴
	ARV771	2.19 x 10 ⁻⁹	1.83 x 10 ⁵	4.19 x 10 ⁻⁴
Ctx-MIC7	GNE987	< 1.0 x 10 ^{-9#}	n.d. \$	< 1.0 x 10 ^{-4#}
	GNE987P	3.83 x 10 ⁻¹⁰	4.97 x 10 ⁵	1.91 x 10 ⁻⁴
	ARV771	2.35 x 10 ⁻⁹	2.29 x 10 ⁵	5.04 x 10 ⁻⁴
Trastuzumab	GNE987, GNE987P, ARV771		no binding *	
Cetuximab	GNE987, GNE987P, ARV771		no binding *	

4.3.3 Cellular binding of antibody-MIC7 conjugates and respective controls

As previously described, the Ttz-MIC7 conjugate exhibited desirable binding characteristics, with high affinities for its specific targets HER2 and PROTAC. Hence, the subsequent step involved analyzing whether the binding of soluble protein could be translated into functional binding of the

target receptor on cancer cells. Selective binding of cell surface receptor was assessed by flow cytometry. Cell lines were selected based on varying levels of HER2 receptor expression (HER2_{high}: SKBR3 > BT474 > MDA-MB-435).¹⁸³ HER2-binding variants Ttz-MIC7 and Ttz, were tested at concentration of 100 nM on two HER2_{high} expression cell lines (SKBR3 and BT474) and one HER2_{low} (MDA-MB-435). Controls were included, such as an isotype control antibody (α DIG-MIC7), unstained cells, and cells treated only with AF488-labeled detection antibody, to account for cellular autofluorescence. Histograms for relative cell surface HER2 labeling intensities are depicted in Figure 15.

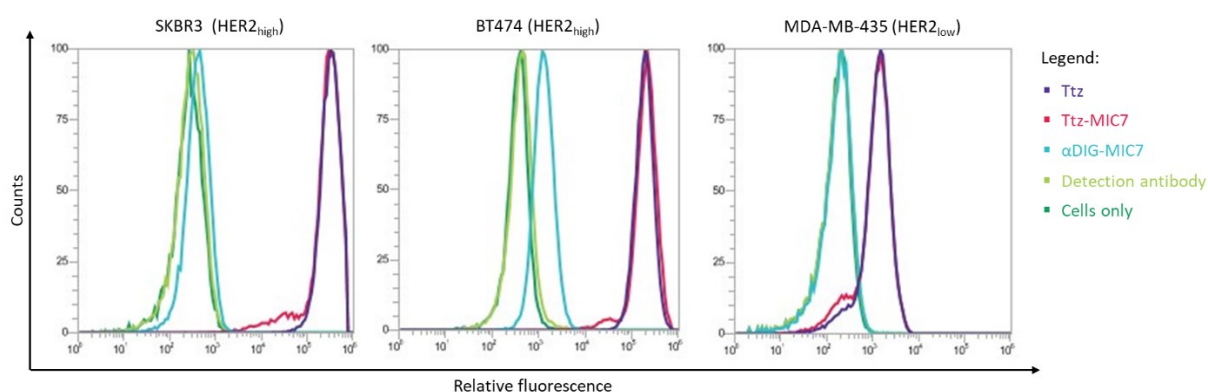


Figure 15 Cellular binding of Ttz-MIC7, Ttz and reference molecules to different HER2 expressing cell lines. The HER2-targeting antibodies and references selectively bind to HER2 overexpressing cell lines, SKBR3 and BT474. A slight binding was observed to HER2_{low} cells MDA-MB-435. The experimental procedure included incubation of cells at a concentration of 100 nM for each treatment condition for 60 min at 4 °C. After incubation, cells were washed twice with DPBS + 1% (w/v) BSA and then incubated for 30 min in the dark at 4 °C with 500 nM AF488-labeled detection antibody. After two further washes with DPBS + 1% (w/v) BSA, the fluorescence intensity was measured by flow cytometry. Figure adapted from Lehmann *et al.*¹⁸³.

Ttz-MIC7 exhibited strong cellular binding to HER2 overexpressing cell lines BT474 and SKBR3, comparable to the unconjugated Ttz variant. However, reduced binding was observed for HER2_{low} MDA-MB-435 cells with both Ttz-MIC7 and Ttz. This binding behavior generally correlated with higher expression of the target on the cell surface. Importantly, reduced cellular binding of the isotype control α DIG-MIC7 was detected, indicating the absence of non-specific binding effects. To further investigate the binding behavior, an additional experiment was performed that studied the binding in relation to MIC7 loading. Therefore, cancer cells were treated with pre-complexed Ttz-MIC7 and α DIG-MIC7 loaded with the fluorogenic probe VHL-Cy5, consisting of the VHL ligand VH032 and the fluorophore Cy5. Unbound ligands were removed from the complex mixtures via Zeba™ Spin Column prior the flow cytometry analysis. Flow cytometric analysis confirmed binding of VHL-Cy5-complexed Ttz-MIC7 to the cells in a receptor expression-dependent manner. This further supports that VHH conjugation and VHH loading with VHL-ligand containing small molecules does not impact antibody receptor binding (Figure S 11).

4.3.4 Cellular uptake of antibody-MIC7 conjugates and respective controls

Besides selective binding, internalization and intracellular release of the drug are further important factors for antibody based PROTAC delivery. To explore whether VHH conjugation impacts antibody-mediated internalization, cellular uptake was investigated. Therefore, all HER2 binding variants and the isotype control were labeled with pH-sensitive fluorescent dye (pHAb-dye). Under neutral pH conditions, the pHAb-dye exhibits minimal fluorescence. However, in the acidic pH environment typically found in endosomal and lysosomal vesicles, the fluorescence intensity significantly increases. This property enables detection of molecules that have specifically accumulated intracellularly in the endosomal and lysosomal compartments. The pHAb-dye structure contains a succinimidyl ester group that enabled coupling to lysine residues of antibodies (Figure S 12). To investigate cellular uptake, Ttz, Ttz-MIC7, and α DIG-MIC7 were labeled using random lysine coupling with a pHAb dye, following the manufacturer's protocol. To compare the fluorescence signals between constructs labeled with pHAb dye, it is necessary to normalize the signals by considering the different number of attached pHAb dye molecules. Therefore, the labeling ratio was determined by LC-MS and UV spectroscopy and the degree of pHAb-dye labeling (DOL) was determined based on the specific pHAb absorbance at 535 nm (Figure S 12). A detailed experimental procedure for measuring and calculating the DOL can be found in the method section 3.13.1.

Table 6 pHAb-dye labeled constructs generated for internalization studies. The labeling of the constructs was achieved through random lysine conjugation. The DOL values, determined via LC-MS, correspond to the quantity of pHAb-dyes conjugated to each antibody.

Antibody	Degree-of-labeling (DOL)
Ttz-MIC7	6.7
α DIG-MIC7	9.3
Ttz	6.5

Table 6 summarizes the generated pHAb-dye labeled conjugates. Comparable DOL were achieved for Ttz and Ttz-MIC7, the isotype control α DIG-MIC7 showed higher dye content. This was considered in the final calculation to ensure appropriate normalization.

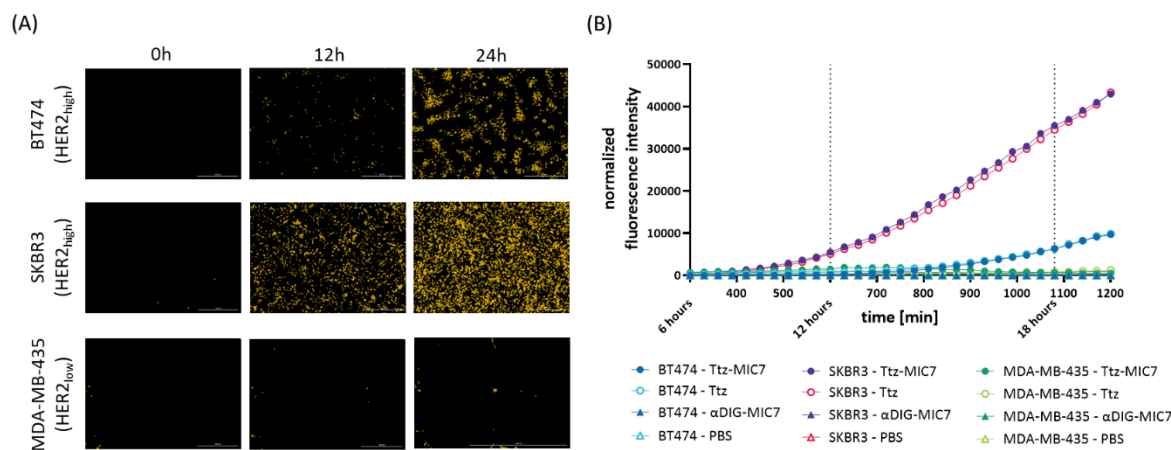


Figure 16 Receptor-mediated internalization of pHAb-dye labeled constructs in HER2 expressing cell lines. (A) Intracellular accumulation of Ttz-MIC7 in BT474, SKBR3 and MDA-MB-435 cancer cells were presented as an example for selected time points. The cells were incubated at 37 °C, 80% humidity and 5% CO₂ with 100 nM pHAb-dye labeled Ttz-MIC7. Images of the cells in the RFP channel (Exc. 531 nm, Em. 593 nm) were recorded every 30 min for 24 h using a cell imaging reader. **(B)** The time series images demonstrated an increase in cellular uptake for HER2-binding constructs. The fluorescence intensity was normalized based on both the cell number and the pHAb-dye DOL value of each construct.

To evaluate the selective uptake of antibody-based PROTAC shuttle, pHAb-dye labeled conjugates, Ttz, Ttz-MIC7 and α DIG-MIC7 were tested on HER2_{pos} (SKBR3, BT474) and HER2_{low} (MDA-MB-435) cell lines. The parental antibody Ttz served as reference, while α DIG-MIC7 was used as isotype control. The pHAb-dye labeled constructs were incubated on adherently grown cells, that reached 70-80% confluency, and the pHAb-dye related fluorescence was continuously monitored over a 24-hour incubation period. Subsequently, the cell nuclei were stained, and cell counts were conducted using software assistance. The fluorescence intensity of the images obtained from pHAb-labeled constructs was normalized to the pHAb-dye DOL and the cell count. The kinetics of cellular uptake were determined by plotting the normalized fluorescence signal of the pHAb-dye against time (Figure 16(B)). The HER2-targeting conjugates, Ttz and Ttz-MIC7, showed selective intracellular accumulation, indicating intact receptor-mediated uptake and intracellular trafficking to the endosomal and lysosomal compartments (Figure 16 (A)). The fluorescence signal was detected in SKBR3 cells after approximately seven hours and in BT474 cells after around 12 hours (Figure 16 (B)). Importantly, no difference was observed in the internalization kinetics between unconjugated and VHH-coupled antibodies, Ttz and Ttz-MIC7, respectively. No cellular uptake was observed in HER2_{low} MDA-MB-435 cells. Additionally, no fluorescence signal was detected for isotype control α DIG-MIC7 treated cells (Figure 16 (B), data set: filled triangle).

4.4 Chromatographical analysis of PROTAC loading and evaluation of complex formation

The binding of VH032-based PROTACs, namely GNE987 and GNE987P, by MIC7 VHH is required for selective delivery of the PROTAC to receptor-expressing cells and subsequent degradation of

the target. Detailed confirmation of the binding affinity between MIC7 and VH032-based PROTACs can be found in section 4.3.2. To analyze the formation of complexes between PROTAC and antibody-MIC7 conjugate prior to cell treatment, HI-HPLC was used. Therefore, GNE987 and GNE987P were complexed with Ttz-MIC7, Ctx-MIC7 and α DIG-MIC7. The complex formation was achieved by incubating 3.5 mg/mL of antibody-VHH conjugate with 0.5, 1 or 2 molar equivalents PROTAC per binding site in PBS pH 7.4. The incubation was performed at room temperature with continuous shaking for 3 hours. To determine the PROTAC-to-VHH ratio after complexation, HI-HPLC analysis was performed.

$$\text{Loading efficiency} = \frac{\text{Area}_{R0} * 1 + \text{Area}_{R1} * 1 + \text{Area}_{R2} * 2}{\text{VAR} * \text{Area}_{\text{total}}} \quad (6)$$

Equation (6) was utilized to calculate the loading percentage, considering the VAR (VHH-to-antibody ratio). While Area_{R0} is the range referred to Ttz-MIC7 without any bound PROTAC, Area_{R1} the area of the range referred to Ttz-MIC7 with 1 PROTAC molecule and Area_{R2} to the area of the range referred to Ttz-MIC7 with 2 PROTAC molecules. VAR is the VHH-to-antibody ratio, and $\text{area}_{\text{total}}$ the total area of all peaks in the chromatogram.

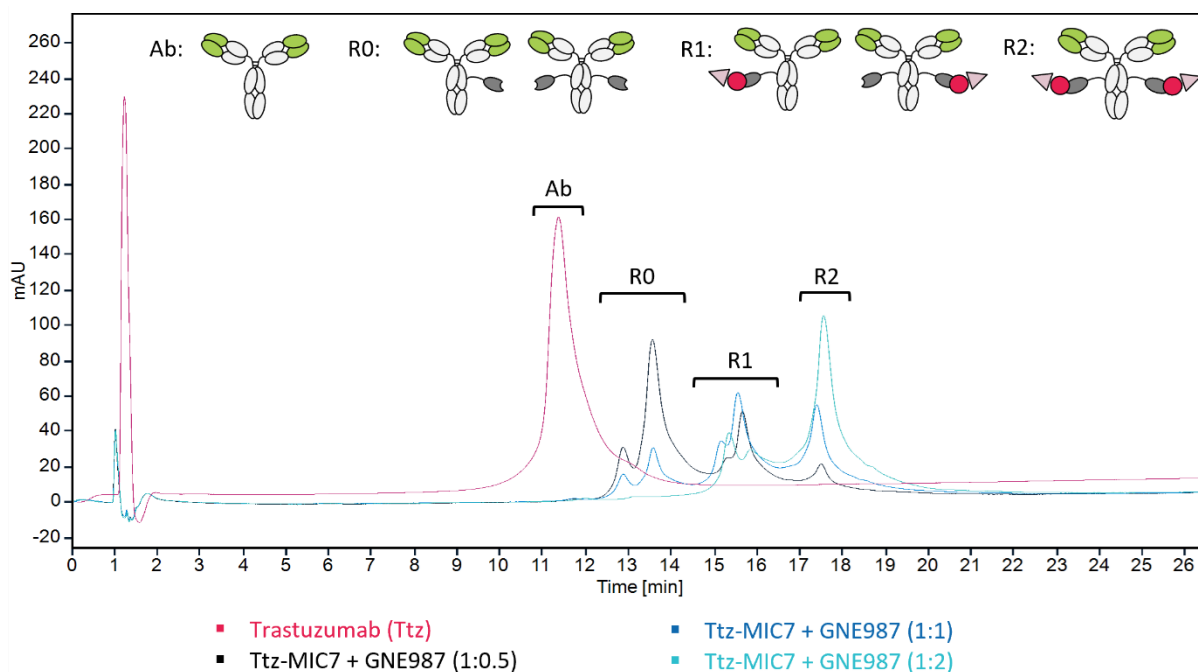


Figure 17 Generation of Ttz-MIC7 PROTAC complexes. Incubation of Ttz-MIC7 with GNE987 at molar ratios of 1:0.5, 1:1 to 1:2 followed by monitoring of complex formation via HI-HPLC. R0, R1 and R2 indicate the ratio elution range corresponding to conjugates loaded with 0, 1, or 2 PROTACs, respectively. Figure adapted from Lehmann *et al.*¹⁸¹

Figure 17 presents an overlay of HI-HPLC chromatograms, showcasing GNE987-loaded Ttz-MIC7 and the corresponding unloaded and parental control samples. The HI-HPLC analysis was employed to visualize the outcome of the complexation reaction of GNE987 at molar ratios of 1:0.5, 1:1 and 1:2. As the loading of GNE987 increased, there was a noticeable elevation in overall

hydrophobicity, reflected by an increase in retention time. The chromatograms provided evidence of successful complex formation between GNE987 and Ttz-MIC7, with clear distinctions observed between the loaded and unloaded variants.

Table 7 Complexation results of different PROTACs with Ttz-MIC7, Ctx-MIC7 and α DIG-MIC7. Loading efficiency was determined for molar complexation ratios of 1:2 Ttz-MIC7 to PROTAC. n.d.: not determined.

Parental mAb-MIC7		GNE987	GNE987P
Construct	VAR (VHH/mAb)	Loading efficiency [%]	Loading efficiency [%]
Ttz-MIC7	1.72	93.6	90.2
Ctx-MIC7	1.90	72.8	n.d.
α DIG-MIC7	1.76	98.1	93.2

The results demonstrate the complexation of different PROTACs with Ttz-MIC7, Ctx-MIC7 and α DIG-MIC7 at a 1:2 molar ratio (Table 7). When two GNE987 molecules were mixed with Ttz-MIC7 (VAR 1.72), a high loading of 96% PROTAC-to-VHH was achieved. Similarly, at the same loading ratio, GNE987P was loaded onto Ttz-MIC7 at 90%. The complexation of GNE987P with Ctx-MIC7 (VAR 1.90) resulted in 80% PROTAC loading. Additionally, the α DIG-MIC7 conjugate (VAR 1.76) showed nearly complete loading of GNE987 at 98% and 93% with GNE987P. Supplementary chromatographic overlays can be found in Figure S 13, providing further evidence of successful complex formation between the different PROTACs and the respective antibody-VHH conjugates.

4.5 Biological evaluation of PROTAC-loaded antibody-VHH conjugates

The Ttz-MIC7 conjugate, with its confirmed binding to the target receptor and receptor-mediated internalization, has the required properties to be considered as an antibody-based PROTAC delivery vehicle. The antibody-VHH conjugates generated in the study have the potential to deliver VH032-based PROTACs, improving their selectivity while maintaining their efficacy in degrading the target protein BRD4.

4.5.1 Evaluating BRD4 degradation selectivity via targeted delivery of BRD4 PROTACs to HER2-expressing cells

To evaluate the biological activity of the generated HER2-binding conjugate, Ttz-MIC7, serial dilution of PROTAC-loaded Ttz-MIC7 or α DIG-MIC7 were incubated on HER2_{high} cancer cells (SKBR3) for 24 hours. Similar treatments were performed with PROTAC or Ttz-MIC7 only as control. Prior to treatment, Ttz-MIC7 and α DIG-MIC7 were complexed with GNE987 and GNE987P at a molar ratio of 1:1.

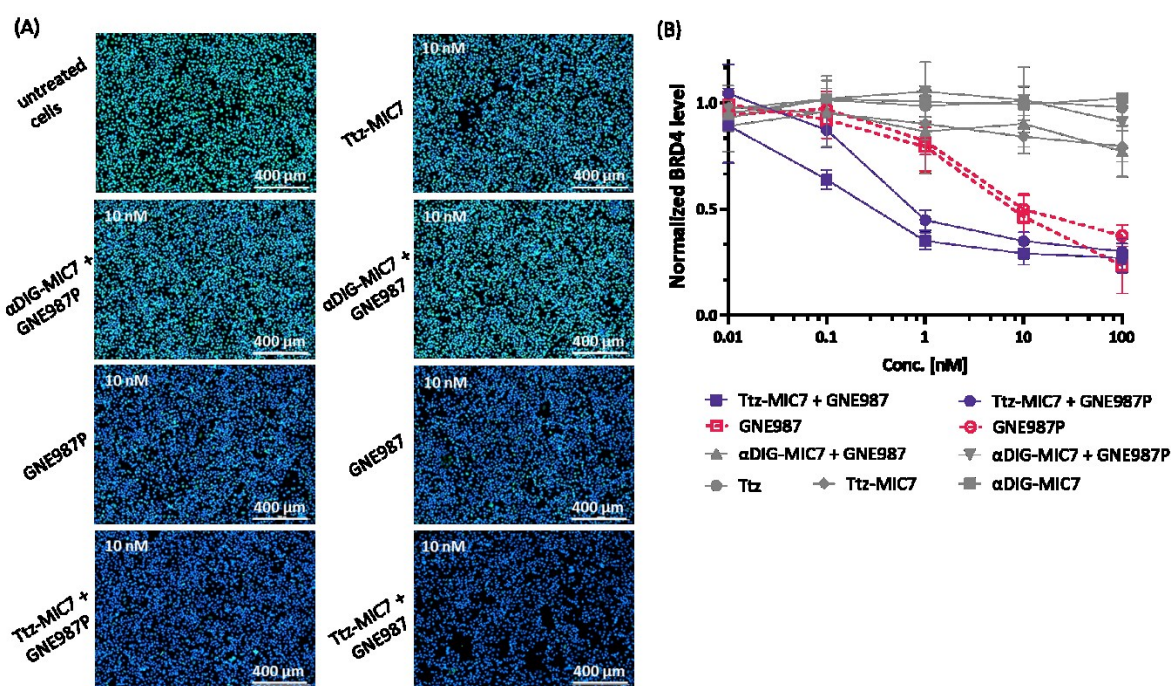


Figure 18 Targeted BRD4 degradation mediated by antibody delivery of PROTAC. (A) Degradation of BRD4 evaluated in SKBR3 (HER2_{pos}) cancer cells using immunofluorescence microscopy analysis. Cells were treated with 10 nM Ttz-MIC7 or αDIG-MIC7 complexed with GNE987P at molar ratio 1:1, along with respective controls, for 24 h. Following the treatment, cells were fixed, permeabilized and stained using primary anti-BRD4 antibody. For staining with secondary antibody an Alexa Fluor™ 488-labeled antibody was used (green). Cell nuclei are counterstained with Hoechst 33342 dye (blue). **(B)** Relation between normalized BRD4 level and different treatment concentrations. The BRD4 level was normalized to cell count and untreated cells. Serial dilution of treatment concentrations between 0.01 and 100 nM treatment were selected and plotted, which were performed in technical triplicates. The solid line connects the data points for the BRD4 level at respective concentration for the antibody-based treatment, while the dotted line connects free GNE987 and GNE987P data points.

The level of BRD4, the target protein, was assessed using immunofluorescence microscopy. Therefore, after 24-hour incubation, the cells were washed, fixed and permeabilized. Subsequently, samples were blocked with BSA in PBS and incubated overnight with anti-BRD4 antibody. The following day, Alexa Fluor™ 488-labeled detection antibody was added, and the cell nuclei were stained with Hoechst 33342 dye. The cell count and fluorescence intensity were quantified using Cell Imaging Multimode Reader Cytation 5.

The signal intensities obtained from BRD4 immunofluorescence images were normalized to the cell count. To confirm the specificity of the detection antibody, direct staining with detection antibody alone was performed (Figure S 14). This step ensured that the observed signal was a result of target protein binding and not due to nonspecific interactions. Experiments were performed in technical triplicates and biological duplicates. Treatment with Ttz-MIC7 complexed with GNE987 and GNE987P, as well as GNE987 and GNE987P alone, showed BRD4 degradation, indicating effective receptor-mediated delivery and degradation efficiency of the PROTAC (Figure 18 (A)). In SKBR3 cells, a notable decrease in normalized BRD4 levels was observed upon treatment with 1, 10, and 100 nM concentrations of Ttz-MIC7 + GNE987 and Ttz-MIC7 + GNE987P (Figure 18 (B)). Similarly, treatment with GNE987 and GNE987P alone at concentrations of 10 nM

and 100 nM resulted in a reduction in BRD4 levels. In contrast, PROTAC-loaded isotype control α DIG-MIC7 did not induce BRD4 degradation. Furthermore, treatment with unloaded Ttz-MIC7 and Ttz alone did not show significant BRD4 degradation (Figure 18 and Figure S 14).

4.5.2 *In vitro* cytotoxicity of PROTAC-loaded antibody-VHH conjugates

BRD4 is a pan-essential protein, and its degradation typically leads to cell death.¹⁸⁴ Therefore, it was studied if the loaded antibody-VHH conjugates can induce pharmacological effects in *in vitro* cell viability assays. Hence, an orthogonal readout was used to demonstrate selective PROTAC delivery. HER2-targeting conjugate Ttz-MIC7 and isotype control α DIG-MIC7 were loaded with PROTACs GNE987 and GNE987P in a molar ratio 1:1 and incubated on HER2_{high} cells (SKBR3 and BT474) and HER2_{low} cells (MDA-MB-435) together with unloaded controls and PROTACs only. Cell viability was evaluated six days after compound addition using the ATP-based luminescent assay CellTiter-Glo®. The resulting luminescence signal was utilized to generate a dose-response curve, enabling the determination of the half-maximal inhibitory concentration (IC₅₀) and quantification of the potency.

In BT474 and SKBR3, a reduction of viability about 70% was observed for PROTAC-loaded Ttz-MIC7 with IC₅₀ values in the sub-nanomolar range. In MDA-MB-435 (HER2_{low}) in contrast, no or only low cytotoxic effects was observed in the tested concentration range up to 100 nM. At the highest GNE987P concentration, a reduction of cell viability of 80-90% was observed for all cell lines irrespective of HER2 expression with IC₅₀ values in single digit nanomolar range. In the control treatment with Ttz-MIC7 and Ttz, a reduction in viability of approximately 40% was observed for HER2_{high} cell lines. Further, treatment with free GNE987 resulted in a maximal reduction in cell viability of 95% in all cell lines and to IC₅₀ values in the sub-nanomolar range (Figure 19 and supplement Table S 1). Notably, isotype control α DIG-MIC7 loaded with GNE987P and GNE987 did not show significant reduction in cell viability in all experiments.

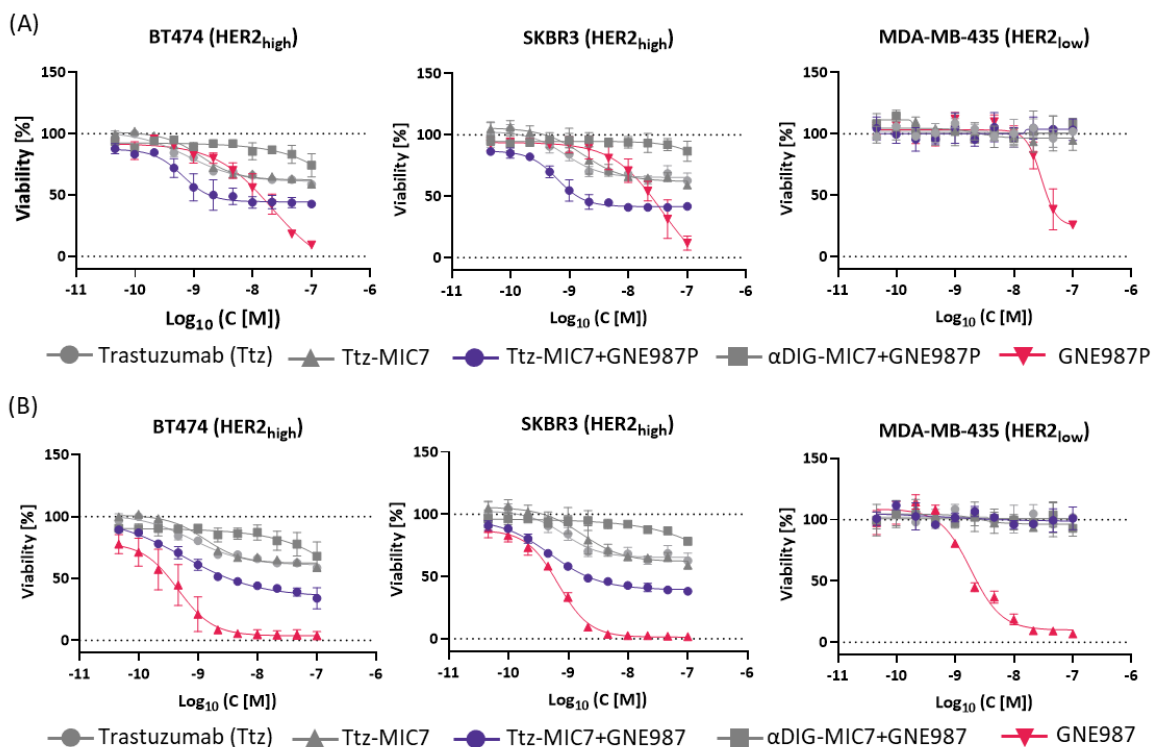


Figure 19 Dose-response curves of PROTAC-loaded Ttz-MIC7 and respective controls. HER2_{high} and HER2_{low} cells were treated with Ttz-MIC7 and α Dig-MIC7 complexed with (A) GNE987P (molar ratio 1:1) and (B) GNE987 and control molecules. Cells were treated for six days with serial dilution. Each curve represents the mean of technical duplicates, standard deviation shown as error bars. Figure adapted from Lehmann *et al.*¹⁸¹.

Furthermore, EGFR-targeting Ctx-MIC7 was loaded with GNE987P in a molar ratio 1:1 and incubated on EGFR_{high} (A431 and MDA-MB-468) and EGFR_{low} (HEPG2) cells together with GNE987P-loaded α DIG-MIC7, unloaded Ctx-MIC7 and GNE987P only. The cell viability was evaluated three days after initiation of treatment by quantification of ATP with CellTiter-Glo®. As shown in Figure 20, the viability of A431 and MDA-MB-468 cells (EGFR_{high}) was reduced by approximately 90% upon treatment with GNE987P-loaded Ctx-MIC7, with IC₅₀ values in the sub-nanomolar range. In contrast, minimal to no cytotoxic effects were observed in HEPG2 cells within the investigated concentration range of up to 100 nM. At the highest concentration of GNE987P, a 75-80% decrease in cell viability was observed, accompanied by IC₅₀ values in the nanomolar range. Notably, the isotype control α DIG-MIC7+GNE987P did not exhibit a significant reduction in cell viability in any of the cell lines irrespective of EGFR expression.

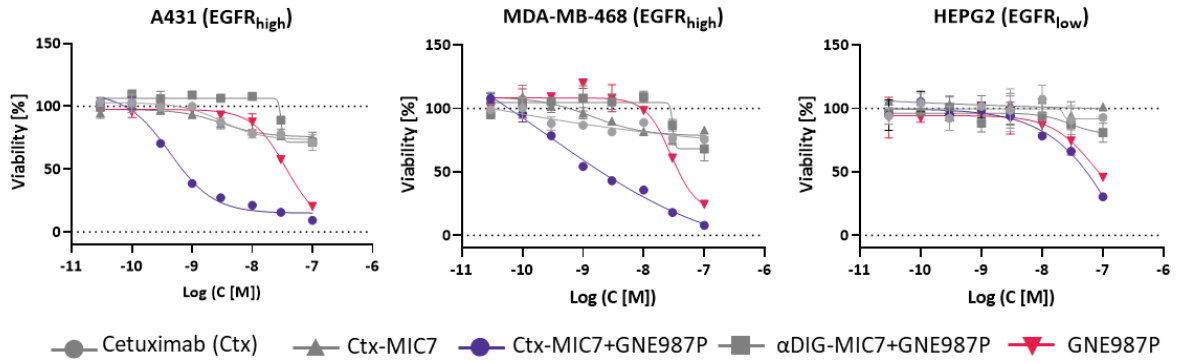


Figure 20 Dose-response curves of GNE987P-loaded Ctx-MIC7 and respective controls. EGFR_{high} and EGFR_{low} cells were treated with Ctx-MIC7 and αDig-MIC7 complexed with GNE987P (molar ratio 1:1) and control molecules. Cells were treated for three days with serial dilution. Each curve represents the mean of biological triplicates, standard deviation shown as error bars.

To further investigate the antibody-mediated selectivity, the toxic effect of GNE987P loaded to unconjugated G₃-MIC7 were examined. G₃-MIC7 was loaded with GNE987P in a 1:1 molar ratio and incubated on A431, MDA-MB-468 and HEPG2 cell lines, together with unloaded G₃-MIC7 and GNE987P only (Figure 21). Following three days of compound incubation, cell viability was evaluated using the CellTiter-Glo®. Treatment with GNE987P induced a substantial reduction in cell viability, with 80-90% decreases observed across all cell lines. In contrast, no cytotoxic effects were observed for GNE987-loaded G₃-MIC7 and G₃-MIC7 alone up to 100 nM.

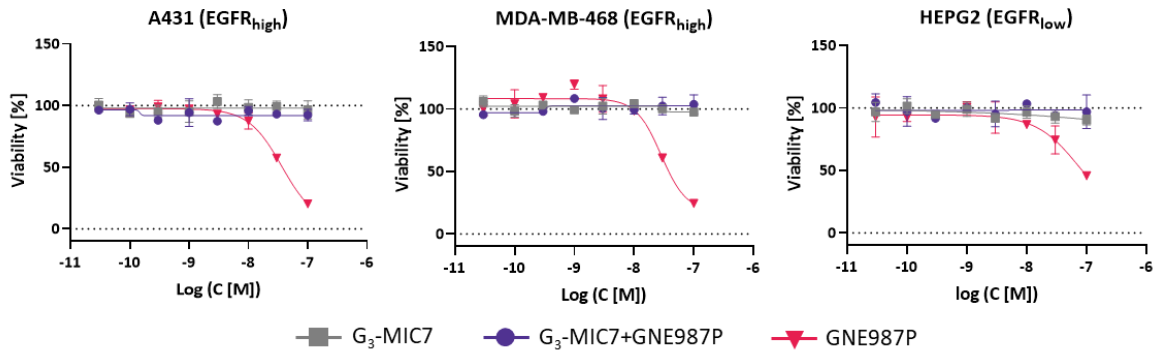


Figure 21 Dose-response curves of GNE987P-loaded G₃-MIC7 and respective controls. Cells were treated for three days with G₃-MIC7 complexed with GNE987P (molar ratio 1:1) and control molecules in serial dilution. Each curve represents the mean of biological triplicates, standard deviation shown as error bars.

Chapter 2: A modular approach to generate bispecific antibodies recruiting cell-surface proteins and a transmembrane E3 ligase

4.6 Design and assembly of antibody-scFv conjugates

The subsequent chapter focuses on the structural composition and properties of the scFv variants used for MTG-mediated conjugation. Furthermore, the generation, purification and analytical characterization of scFv variant 1 is described.

4.6.1 scFv design for MTG-mediated conjugation

In the following chapter the focus is on binding transmembrane E3 ligase RNF43 and a cell surface receptor. The two binding units were the native IgG-based mAb for binding the cell surface receptor of interest and a single-chain variable fragment (scFv) for recruiting the E3 ligase RNF43. The antibody and scFv were covalently linked through chemical conjugation. The simultaneous binding induces close proximity between RNF43 and target receptor and subsequently initiates degradation via endosome-lysosome pathway (Figure 22 (C)). The induced degradation is caused by the protein-protein interaction between E3 ligase and cell surface receptor which would not occur naturally.

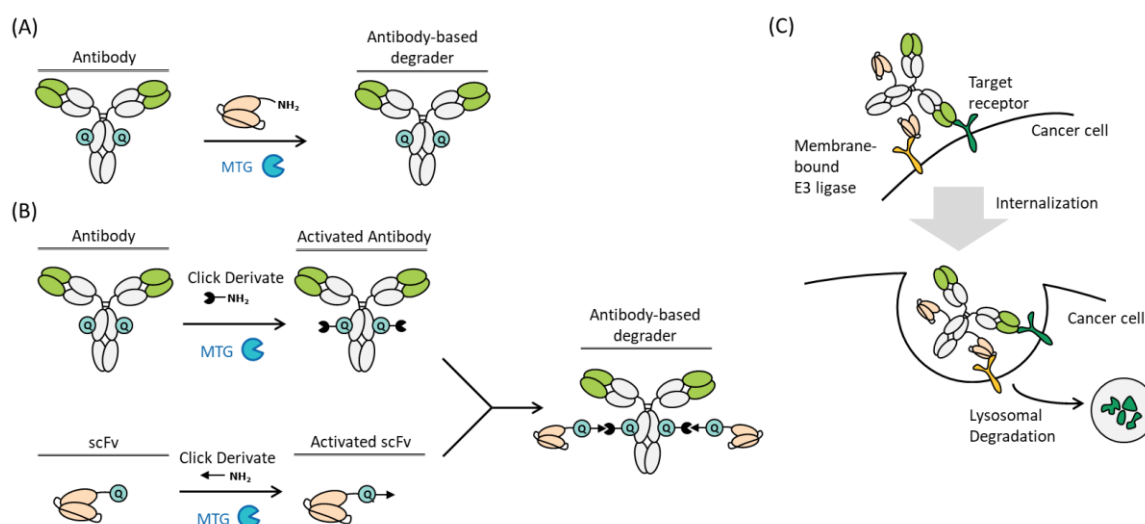


Figure 22 Schematic representation of chemoenzymatic conjugation steps to generate an antibody-based degrader and the mediated target receptor degradation mode. (A) MTG-mediated direct conjugation strategy for generation of bispecific anti-body-scFv conjugates was not successful. **(B)** Native IgG1-based antibodies are site-selectively coupled with click derivate using microbial transglutaminase (MTG). A SPAAC reaction was performed to covalently bind scFv and antibody. **(C)** Mode of action of transmembrane E3 ligase mediated internalization and lysosomal degradation.

MTG has previously been used to conjugate VHs to various antibodies (Chapter 4.2) and resulted in stable conjugates with high VAR values and good yields. Therefore, the conjugation strategy has

been extended to the conjugation of scFv and mAb. MTG-mediated conjugation was performed using mAb, Ttz and α RNF43 scFv, scFv1. The assembly of scFv1 from N- to C-terminus as follows: conjugation-tag, penta-glycine; V_H-YOL-linker-V_L; purification-tag, His₆-tag (Table 8). The amino acid sequence of the RNF43-binding V_H and V_L is from the patent of Boontanrart *et al.*¹⁸⁵, covalently linked via a YOL-linker (sequence: KLEEGEFSEARV).¹⁸⁶ The N-terminal penta-glycine sequence serves as recognition site of the MTG, for direct conjugation to the mAb.¹⁸⁷ A His₆-tag for purification of the scFv protein from the cell culture supernatant.

Table 8 Modified scFv variant used in this study. SeqID refers to each scFv variant. Protein orientation shows the V_H to V_L sequence alignment in N- to C-terminal direction, connected by either YOL (sequence: KLEEGEFSEARV) or glycine-serine linker. A His₆-tag for purification and the terminal tag for MTG-mediated conjugation were installed. The N- and C-terminal tag represent the terminal attachment site of the scFv. N/A: not available.

SeqID	N-terminal tag	Protein orientation	Linker	Purification tag	C-terminal tag	MW [DA]	Conjugation strategy
scFv1	GGGGG	V _H /V _L	YOL	His ₆	N/A	26485.5	direct
scFv2	N/A	V _H /V _L	YOL	His ₆	G ₆ LLQGGGGS	27155.2	2-step
scFv3	N/A	V _H /V _L	(G ₄ S) ₃	His ₆	GGLLQGA	26367.2	2-step
scFv4	N/A	V _L /V _H	(G ₄ S) ₃	His ₆	GGLLQGA	26367.2	2-step
scFv5	N/A	V _H /V _L	(G ₄ S) ₃	His ₆	(G ₄ S) ₃ -GGLLQGA	26682.5	2-step
scFv6	N/A	V _H /V _L	(G ₄ S) ₃	His ₆	((G ₄ S) ₃) ₂ -GGLLQGA	26997.8	2-step
scFv7	N/A	V _H /V _L	(G ₄ S) ₃	His ₆	((G ₄ S) ₃) ₃ -GGLLQGA	27313.1	2-step

4.6.2 Expression and purification of G₄-tagged α RNF43 scFv variant 1

The scFv1 variant was produced using mammalian Expi293F cells and subsequently purified by metal chelate affinity chromatography (IMAC), equilibrated in PBS pH 7.4. Protein elution was achieved through a stepwise imidazole gradient, ranging from 0% to 100% of 0.5 M imidazole (Figure S 15 (A)). The target protein fraction was eluted at imidazole concentrations between 200 mM to 500 mM imidazole. The scFv1 has an estimated molecular mass of approximately 26.5 kDa, which is consistent with the migration pattern observed during gel electrophoresis (Figure S 15 (C)). Purification was further refined by removing aggregates using gel filtration on Superdex 75 pg 16/40, equilibrated in 25 mM Histidine, 100 mM NaCl, pH 7.4. The peak corresponding to the monomeric scFv1 was collected and concentrated using Amicon® Ultra-15

centrifugal devices. The quality of the protein was assessed through SE-HPLC, indicating highly purified scFv1 (Purity: 100%, Figure S 15 (D)).

4.7 MTG-mediated site-specific direct conjugation of scFv1 to native IgG1-based antibody

The MTG-mediated direct conjugation of glycine-tagged scFv variants and native IgG-based mAb was investigated for chemo-enzymatic generation of bispecific antibodies. In a reaction with 10 U/mL MTG, 10 molar equivalents scFv1 and 3 mg/mL Ttz were used. The reaction conditions were 30°C and 24 hours and were based on the studies on antibody-VHH conjugation from chapter 4.2. The first evaluation was performed semi-quantitatively using gel electrophoresis. Sample preparation for SDS-PAGE was performed using reducing conditions. Band with the molecular weight of 26,5 kDa for scFv1, 38,3 kDa for MTG and 49,3 kDa of reduced HC and 23,4 kDa reduced LC were detected (Figure S 16 (A)). No band was observed with the mass of conjugated scFv to the heavy chain (approximately 75 kDa), indicating the absence of conjugation between scFv1 and the heavy chain of Ttz. Additionally, no conjugation to the antibody was observed in the chromatographic analysis by RP-HPLC. Furthermore, high molecular weight species were observed in SDS-PAGE as well as analytical SE-HPLC and were approximately 25% (Figure S 16 (B)).

4.8 Design and generation of antibody-based degraders using two-step conjugation strategy

In the upcoming chapter, the structural composition and properties of the scFv variants employed for MTG-mediated direct conjugation are described. Additionally, it covers the generation, purification, and analytical characterization of various scFv variants.

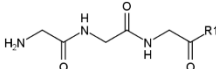
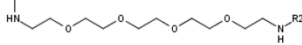
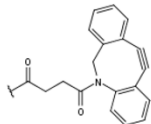
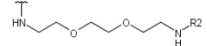
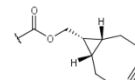
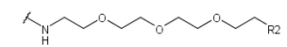
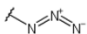
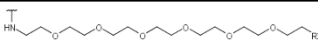
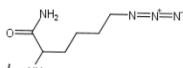
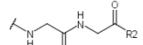
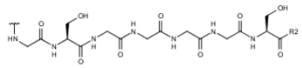
4.8.1 The scFv protein design for two-step conjugation to IgG-based antibodies

A chemo-enzymatic two-step conjugation approach with MTG-mediated conjugation of click derivatives to antibody and scFv, and following SPAAC reaction was next used to generate bispecific antibodies (Figure 22 (B)). The combination of two key steps, the site-specific conjugation of click-reactive handles to antibody and scFv via MTG, and the reaction of both reactive components in the strain-promoted alkyne-azide cycloaddition (SPAAC), were analyzed and optimized. The optimization process commenced with the development of various scFv variants, each varying in linker length, conjugation site, and protein orientation. A total of six different scFv variants with distinct structural properties were designed (Table 8). Each scFv variant contained the V_H and V_L amino acid sequence of hSC37.67 reported in a previous patent application.¹²⁶ The scFv variants were connected either via a glycine-serine or YOL-inker.¹⁸⁶

A His₆-tag was introduced to harvest the scFv proteins from the cell culture supernatant. For chemo-enzymatic conjugation, different MTG recognition tags were introduced at the N-terminus of the α RNF43 scFv and are discussed subsequently. Additionally, the MTG recognition tags are available as C-terminal tags in Table 8. The MTG recognition site of scFv2 contains the LLQG peptide sequence evaluated in detail by Strop *et al.* in the MTG-mediated conjugation of linker-drugs⁷⁵ and is buried in glycine residues for tag elongation. Further, scFv2 consists of the N-terminal V_H domain, followed by a YOL linker, V_L domain and the His₆-tag. The calculated molecular weight (MW) of scFv2 is 27155.2 Da. The peptide sequence LLQGA has also been successfully used as an engineered recognition site on the antibody for MTG-mediated conjugation of linker-drugs and was translated to the scFv3 to scFv7 variants.¹⁸⁸ The scFv3 was generated with the N-terminal V_H domain, a glycine-serine (G₄S)₃ linker, followed by the V_L domain and His₆-tag, along with the MTG recognition tag. scFv3 along with scFv4, shared an identical sequence composition, but varied in the orientation of the V_H and V_L domains. Furthermore, scFv5, scFv6 and scFv7 consisted of the V_H domain, a (G₄S)₃ linker, V_L domain, His₆-tag, a prolonged (G₄S)₃ linker, and the MTG recognition tag. The MW increased accordingly from 26682.5 Da up to 27313.1 Da.

Furthermore, the choice of click derivative is an important parameter for the success of both the MTG-mediated conjugation and the subsequent SPAAC reaction. For this purpose, nine different derivatives were designed to evaluate the MTG-mediated conjugation efficiency, the impact on antibody and scFv stability and the click reactivity. The derivatives were grouped based on their structural features in dibenzocyclooctyne (DBCO), bicyclononyne (BCN) and azide (N₃) (Table 9). Each derivate carried the N-terminal G₃ sequence, functioning as acyl-acceptor in the MTG conjugation reactions. The DBCO and BCN derivatives featured of PEG₄ **1** and PEG₂ **2** chains, respectively. The azide-series included two derivatives: PEG₃ **3** and PEG₆ **4**, which incorporated azido PEG molecules of different lengths to serve as counterparts to the cyclooctyne within the SPAAC reaction. Additionally, two further variants, azido-peptides **5** and **6**, introduced the N₃ moiety to the side chain of lysine (Lys(N₃)), with **5** featuring Gly-Gly spacer and **6** having a Gly-Ser spacer unit.

Table 9 Chemical structure of click derivatives used in this study. Derivate number and structure of each peptide are listed and related to the click reactive side (R2).

Derivate number	N-terminus	R1	R2
1			
2			
3			
4			
5			
6			

4.8.2 scFv expression, purification, and characterization

The scFv variants were produced in mammalian Expi293F cells and purified using IMAC affinity chromatography. In general, the yield of purified scFv protein varied with overall good expression with mean yields per culture volume between 57.8 mg/L and 82.7 mg/L. Protein yield for scFv4 was reduced changing the protein orientation of V_L -to- V_H . Highest monomeric purity (100%) of all scFv variants was confirmed through SE-HPLC and gel electrophoresis. Additionally, the sequence identity of the scFv variants was confirmed through LC-MS peptide mapping (Figure 23 and Figure S 17). Selective binding to the target antigen is a fundamental requisite of antibody-based degraders. Kinetic parameters, such as the equilibrium dissociation constant (K_D) were assessed via BLI using anti-human Fc biosensors (AHC). The antigen-binding ability of scFv variants was studied towards rhRNF43. Dissociation constants were derived from concentration-dependent antigen-binding. High binding affinities within sub-nanomolar range among the different scFv variants were observed (Figure 23). The strong binding and thus low K_D values were mainly driven by the low antigen dissociation (Figure S 18).

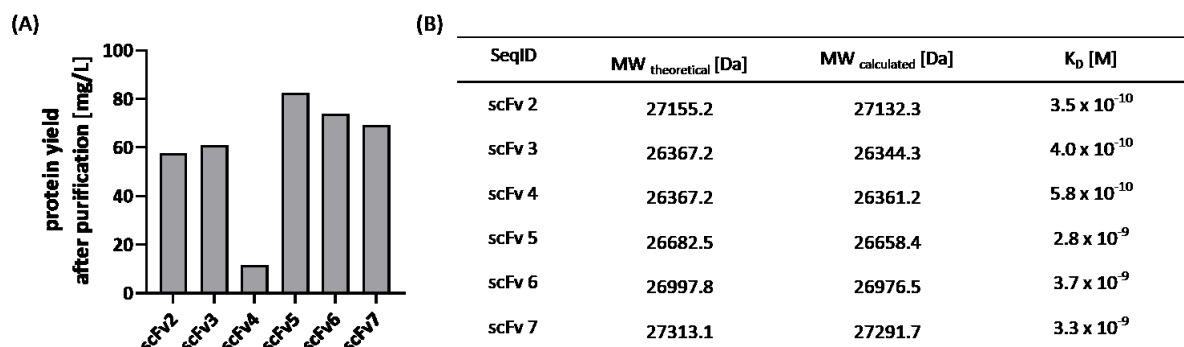


Figure 23 (A) Protein yields after purification. (B) Confirmed sequence identity by peptide mapping and determination of molecular weight. The binding affinity is expressed as K_D value and were derived by a 1:1 global full-fit binding model.

4.9 Two-step conjugation of scFv variants to native IgG1-based antibodies

This chapter focuses on the investigation of a chemoenzymatic two-step conjugation process. This was partly conducted within the scope of Laura Basset master's thesis under my supervision, with the topic being provided by me. The workflow involves the installation of click derivatives mediated by MTG, followed by SPAAC. Monospecific antibodies will be combined with α RNF43 scFv variants to generate bispecific antibodies.

4.9.1 Evaluation of MTG-mediated conjugation of click derivatives

In the first step of the chemo enzymatic generation of bispecific antibodies, the MTG-mediated conjugation of the click-derivatives to mAb and scFv variants was performed.

For the conjugation of scFv variants, reaction mixtures containing 5 mg/mL scFv variant, 5 molar equivalents click derivate and conjugation buffer were prepared. The reaction was started by adding of 1 U/mL MTG. After 16 hours of shaking at 37 °C, the reaction was stopped using enzyme inhibitor C102 and conjugation outcome was evaluated by determining the DAR using RP-HPLC and LC-MS (Figure 24 and

Table S 2). Different click derivatives were analyzed for their conjugation efficiency based on the DAR and impact on protein stability based on the monomeric content. A maximum DAR of 1 was anticipated since the scFv variants contain one MTG recognition tag only. Monomeric content of final monomer click derivate conjugate was analyzed by SE-HPLC.

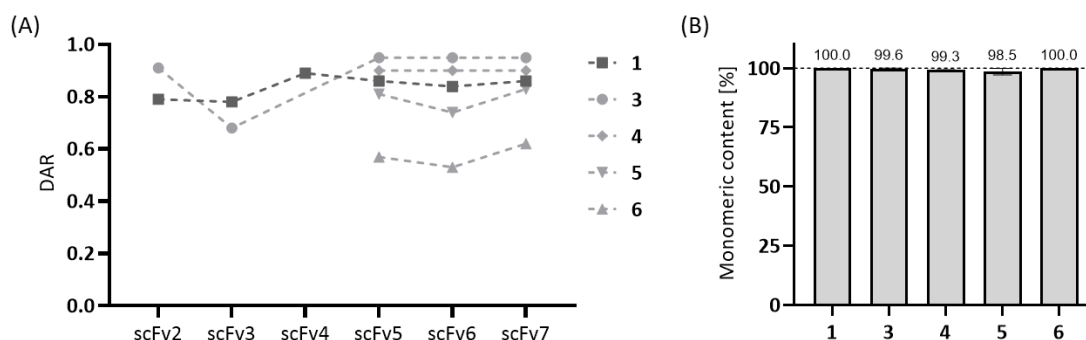


Figure 24 Results of click derivate conjugation to scFv variants. (A) Conjugation efficiency of different click derivatives to scFv variants shown as DAR. **(B)** Mean and \pm SD of protein stabilities based on the monomeric content upon conjugation with different click derivatives (1, 3-6). Data set obtained by SE-HPLC analysis.

The scFv conjugates based on DBCO derivate **1** showed comparable DAR values between 0.79 and 0.86 and high purities of 100%. The scFv conjugates with azido-PEG derivatives **3** and **4** reached DAR values >0.9 , while an increase in PEG length led to a decrease in DAR. The conjugates had high purities of more than 99%. Azido-peptide **5** based scFv conjugates had DAR values between 0.74 and 0.83 and purities of $>97.4\%$. The lowest DAR values with high purity were observed for the scFv conjugates based on azido peptides **6**, which contain serine residues in the spacer sequence. Among the azide-scFv conjugates, azido-PEG derivate **3** showed the highest monomeric purity and highest DAR value, thus being selected for the subsequent upscaling process.

Once the optimal combination of reaction conditions and click derivate was established, the focus was now on the optimization of the attachment of the corresponding click derivatives to the antibodies. Since the azide derivate **3** was selected for conjugation with the scFv variants, the ring-strained alkyne derivatives were analyzed for antibody conjugation. Antibodies were conjugated using 5 mg/mL mAb, 5 molar equivalents click derivate **1** or **2** and 10 to 75 U/mL MTG. Ttz was used as reference antibody to evaluate the conjugation reaction. DAR values were evaluated by RP-HPLC and LC-MS and monomeric content using SE-HPLC. A maximum DAR of 2 can be reached since the native, homodimeric antibody contains two heavy chain Q295 residues and thus two possible MTG conjugation sites. Both click derivatives **1** and **2** were successfully conjugated with a DAR of 2 even at reduced MTG amounts and high purities $>99\%$ were obtained (Table S 3).

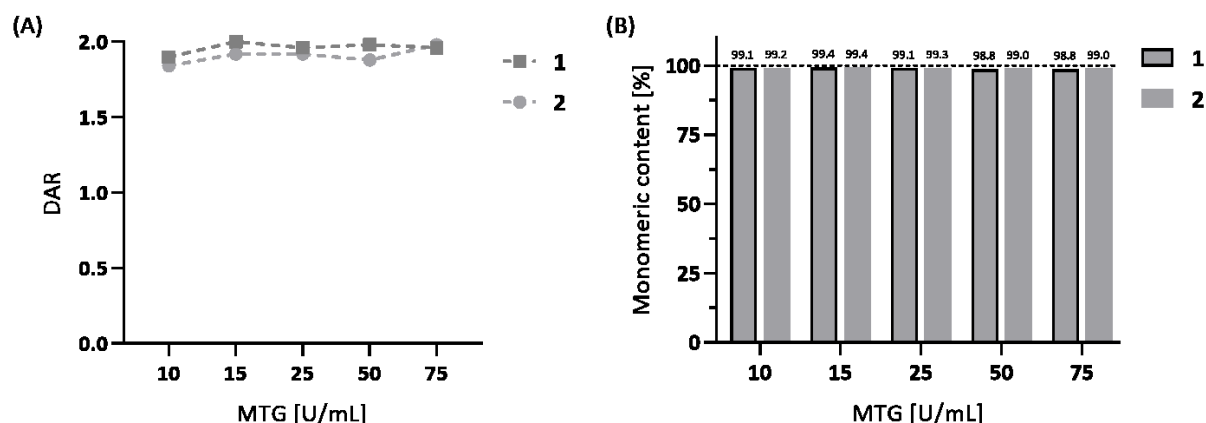


Figure 25 Results of click derivate conjugation to Ttz. (A) Conjugation efficiency of click derivatives 1 and 2 to Ttz shown as DAR. (B) Mean and \pm SD of protein stabilities based on the monomeric content upon conjugation with different click derivatives. Data set obtained by SE-HPLC analysis.

4.9.2 MTG-mediated conjugation of click derivatives in preparative scale

For preparative-scale conjugation, scFv variants were conjugated to azide derivate, while different antibodies targeting programmed death-ligand 1 (PD-L1), HER2 and EGFR as well as anti-digoxigenin antibody (α DIG) were conjugated to ring-strained alkyne derivatives. After optimizing conjugation conditions, click derivate 3 was conjugated to scFv variants and the click derivatives 1 and 2 were used for conjugation to mAbs. For scFv conjugation reaction the optimized conditions with 5 mg/mL scFv, 5 molar equivalents click derivate 3 and 1 U/mL MTG were used. After incubation, conjugates were purified by preparative SEC using Superdex® 200 Increase 10/300 GL column equilibrated with PBS buffer pH 7.4. The collected fractions were pooled based on product peak elution as obtained in the preparative SEC chromatogram. Following, pooled samples were concentrated using Amicon® (MWCO: 10K) and chromatographically characterized.

Table 10 Azide-based scFv conjugates. All scFv variants were conjugated with click derivate 3 by MTG-mediated transamination. DAR values are given as mean of RP-HPLC and LC-MS analysis. Monomer content of conjugates was derived from SE-HPLC analysis.

SeqID	Click	DAR	Purified protein yield [%]	Monomeric content [%]
scFv2.3	3	0.91	57.3	100
scFv3.3	3	0.68	65.3	99.8
scFv5.3	3	0.77	73.9	100
scFv6.3	3	0.74	70.2	100
scFv7.3	3	0.82	61.3	100

High monomeric purity of all scFv conjugates was confirmed by analytical SE-HPLC. Table 10 displays DAR values assessed by RP-HPLC and LC-MS analysis (Figure S 19), ranging from 0.77 to

0.91. The final yields, ranging between 57% and 74% whereby protein loss might primarily be due to interactions with the column or membrane during the concentration process.

Table 11 Ring-strained alkyne-based antibody conjugates. Click derivate **1** was conjugated to Ttz, Ptz and Atz while **2** was installed at Atz, Mtz, α DIG and Ctx. DAR is given by LC-MS analysis. Monomeric content was derived from SE-HPLC analysis.

SeqID	Click derivate	DAR	Purified protein yield	Monomeric content [%]
Ttz.1	1	1.94	65	100
Ptz.1	1	1.84	61	100
Atz.1	1	2.00	62	100
Atz.2	2	1.96	49	100
Mtz.2	2	1.96	67	99.9
α DIG.2	2	1.92	73	100
Ctx.2	2	2.00	74	100

The monospecific antibodies, including Trastuzumab (Ttz), Pertuzumab (Ptz), Matuzumab (Mtz), Cetuximab (Ctx), Atezulizumab (Atz), and α DIG (isotype control), were enzymatically conjugated to ring-strained alkynes **1** and **2** on a preparative scale. The conjugation reaction was performed using 5 mg/mL antibody, 10 molar equivalents of click derivative, and 50 U/mL of MTG. Reactions were purified by SEC using a HiLoad® 16/600 Superdex®200 pg column equilibrated with PBS, pH 7.4. Collected product fractions were pooled, concentrated using Amicon® (MWCO: 100K) and characterized by SE-HPLC and LC-MS. High monomeric purity of all mAb conjugates was confirmed by analytical SE-HPLC (Figure S 20). DAR values were determined by reduced RP-HPLC and LC-MS analysis and ranged between 1.84 and 2.00 shown in Table 11. The final yields were between 49% and 76%, with protein loss mainly due to aggregation during the conjugation reaction.

4.9.3 Click reaction of scFv variants and antibodies using SPAAC mechanism

The final step to generate bispecific antibody scaffolds with scFv variants, was done by copper-free SPAAC making use of the click reactive handles installed in the previous steps. Therefore, in an initial reaction 3 mg/mL Ttz.1 was incubated with 3 molar equivalents scFv5.3 and analyzed after 3 hours at 30 °C by SDS-PAGE. Semi-quantitative evaluation of non-reduced SDS-PAGE showed characteristic pattern of antibody scaffolds with an increase in MW corresponding to the amount of clicked scFv (Figure 26 (A)). This included MW values of 147 kDa, 174 kDa and 201 kDa representing zero, one and two scFv conjugated to the antibody (scFv-to-antibody ratio, SAR) and since no purification was performed free excess scFv5.3 was detected. Additionally, control scFv5.3 and Ttz.1 were added separately in lane 2 and lane 3.

After this initial proof-of-concept reaction, the SPAAC reaction was further investigated regarding reaction time, temperature, and protein concentration. Reaction efficiency was evaluated using SE-HPLC analysis by determining the percent click efficiency represented by scFv clicked per antibody site. By extending the reaction time at constant antibody concentration of 3 mg/mL Ttz.1 and 3 molar equivalents scFv5.3 at 25°C, the click efficiency increased from 65% after 3 hours to 79% after 24 h. Upon increasing the reaction temperature within a 3-hour reaction, the percentage of clicked scFv per antibody increased from 65% at 25 °C to 76% at 37 °C. Next, the effect of antibody concentration on click efficiency was studied using 3 mg/mL and 5 mg/mL Ttz.1, resulting in click reactivities of 65% to 73%, respectively, at 25 °C and 3 hours. In summary, by employing the conditions of 37 °C, 3 mg/mL, and a reaction time of 3 hours, the click reactivity was enhanced by approximately 15%, resulting in a yield of 79%.

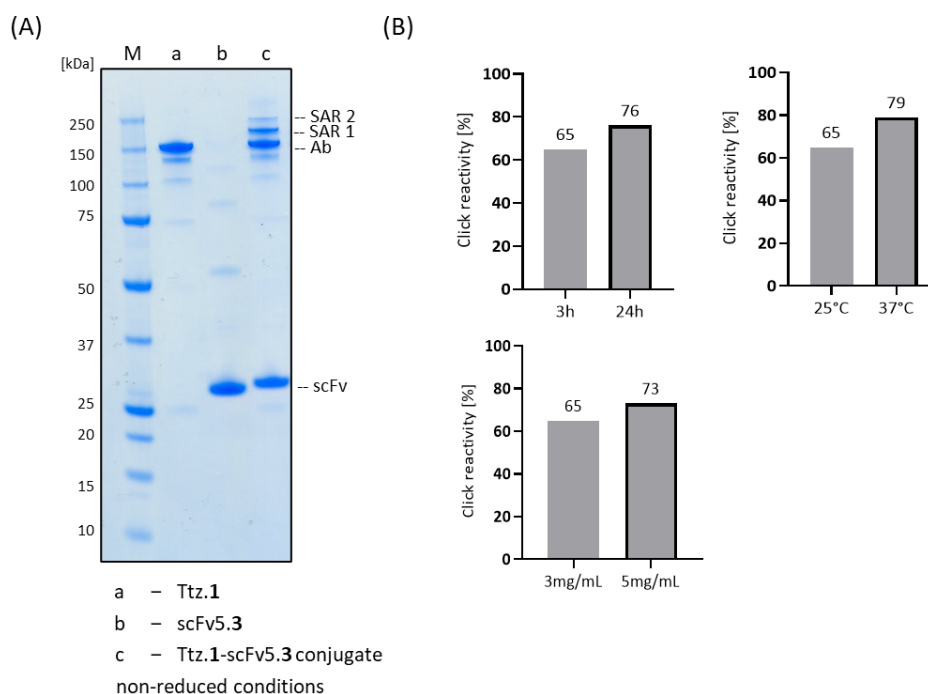


Figure 26 Optimization of SPAAC reaction. (A) Semi-quantitative gel electrophoresis of Ttz.1-scFv5.3 after 3 hours and 30°C SPAAC click reaction and controls. Samples were prepared under non-reduced conditions. **(B)** Ttz.1 was clicked with scFv5.3 using different reaction conditions. Reaction time (h), temperature (°C) and Ttz.1 protein concentration (mg/mL) was studied. Reactivity was evaluated using SE-HPLC with respective chromatograms in Figure S 21 (B) and gel electrophoresis. The percentage reactivity is determined by the proportion of 100% free, non-clicked antibody in the reaction mixture.

4.9.4 Generation of bispecific IgG-scFv conjugates via SPAAC reaction

In the final generation of bispecific antibodies using a two-step chemoenzymatic approach, activated azido-scFv variants were coupled to ring-strained alkyne-conjugated antibodies in preparative scale. The SPAAC reaction between the azido-scFv variants and their respective antibodies was conducted by incubating 24 hours at 37 °C using 3 mg/mL activated antibody and 3 molar equivalents activated scFv. Following the reaction, the mixtures underwent

purification and characterization processes. Purification was achieved through preparative SEC using PBS buffer pH 7.4 with a flow rate of 0.35 mL/min, and the eluted fractions were collected in 0.5 mL fractions and pooled. Characterization involved determining the molecular mass and distribution via SDS-PAGE, monomeric content, and click reactivity through SE-HPLC analysis and LC-MS.

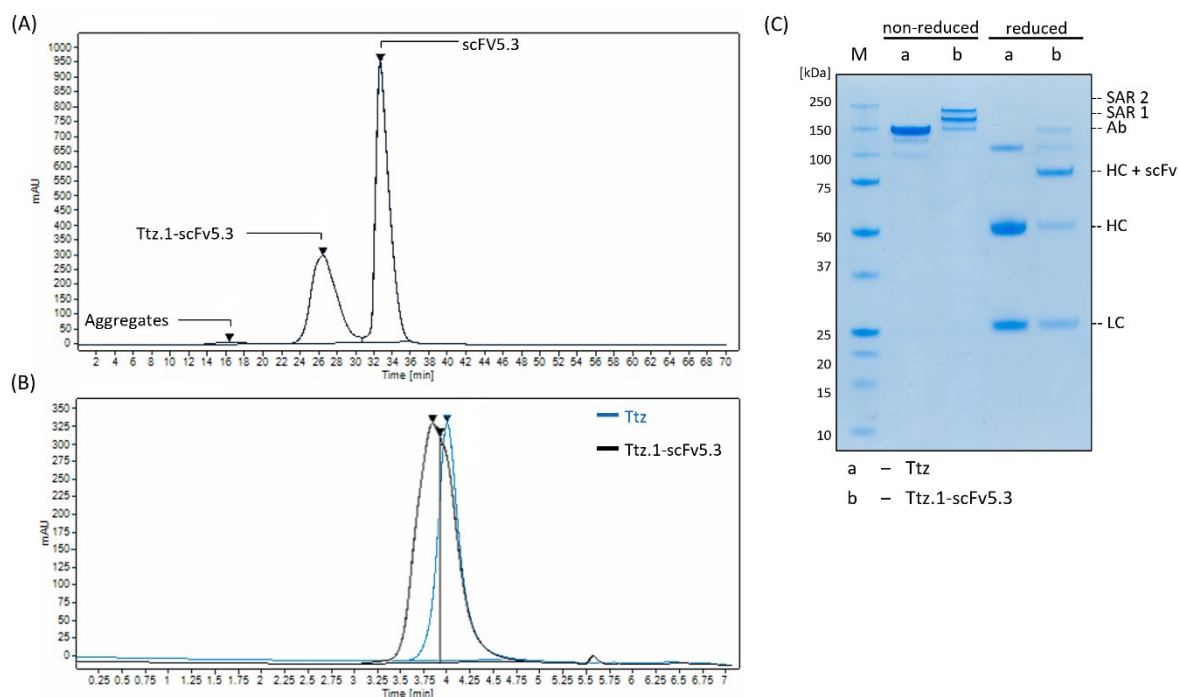


Figure 27 Antibody-based degrader production and analysis. (A) Chromatogram of preparative SEC analysis. The probe was injected to a PBS pH 7.4 equilibrated column. Linear gradient was used for elution and fractions were collected and pooled. The UV-signal is shown in black. (B) Chromatographical analysis of analytical SE-HPLC. The blue signal is the UV absorption of Ttz and the black signal corresponds to Ttz.1-scFv5.3. (C) Semi-quantitative analysis of final purified Ttz.1-scFv5.3 and Ttz. Non-reduced and reduced sample preparation was performed.

Table 12 summarizes the generated bispecific antibodies and Figure 27 details an exemplary purification chromatogram and analysis results. The preparative SEC successfully removed excess scFv and aggregates. Analytical SE-HPLC analysis confirmed high monomeric content of 98.3% to 100% for all purified bispecific conjugates (Figure 27 (B), Table 12 and supplement Figure S 22). The SAR values were determined by SE-HPLC and LC-MS analysis and is given as a mean. To assess click reactivity, the DAR was divided by SAR and expressed as a percentage of loading. Effective click reactions were confirmed for Ttz.1 and Ptz.1 variants, with click reactivity ranging from 82.4% to 93.3% for scFv5.3, scFv6.3, and scFv7.3. In contrast, when the Atezolizumab-based Atz was coupled with the DBCO derivative 4, a click reactivity of 60% was observed for scFv2.3. However, when coupled with the BCN derivative 2, a higher click reactivity of 80.2% was determined. For the additional Atz coupled to derivative 2, click reactivities around 86% were observed when clicked with scFv1.3. The scFv2.3 reacted in the SPAAC with Mtz.2, α DIG.2 and Ctx.2 with a click reactivity of 86.5, 86.7 and 88.0, respectively. The yield for the clicked bispecific

antibody scaffolds was greater than 50% for most of the constructs, except for Atz.1, which had a yield of only 21.2%.

Table 12 Overview of generated antibody-based degraders using two-step chemoenzymatic conjugation.

SeqID (bsAb)	SeqID + click derivate (Ab)	DAR	SeqID + click derivate (scFv)	SAR (scFv/antibody)	Click reactivity [%]	Yield [%]	Monomeric content [%]
Ttz.1+ scFv5.3	Ttz.1	1.94	scFv5.3	1.60	82.4	71.5	100
Ttz.1+ scFv6.3	Ttz.1	1.94	scFv6.3	1.62	83.5	68.5	100
Ttz.1+ scFv7.3	Ttz.1	1.94	scFv7.3	1.60	82.4	66.5	100
Ptz.1+ scFv5.3	Ptz.1	1.84	scFv5+3	1.68	91.3	62.5	100
Ptz.1+ scFv6.3	Ptz.1	1.84	scFv6.3	1.68	91.3	64.8	100
Ptz.1+ scFv7.3	Ptz.1	1.84	scFv7.3	1.66	90.2	60.0	100
Atz.1+ scFv3.3	Atz.1	1.67	scFv3.3	1.34	80.2	21.2	100
Atz.2+ scFv3.3	Atz.2	1.96	scFv3.3	1.16	59.2	47.9	100
Mtz.2+ scFv2.3	Mtz.2	1.92	scFv2.3	1.66	86.5	85.8	98.3
α DIG.2+ scFv2.3	α DIG.2	1.96	scFv2.3	1.70	86.7	89.8	100
Ctx.2+ scFv2.3	Ctx.2	2.00	scFv2.3	1.76	88.0	81.2	100

4.10 Binding analysis of IgG-scFv conjugates

After successful conjugation, the antibody-scFv conjugates were evaluated for the antibody-antigen binding. Additionally, the investigation included simultaneous binding and the observation of selective cell surface binding.

4.10.1 Binding kinetics and simultaneous binding

BLI analysis was performed to evaluate the effects of conjugation with the Q295 heavy chain on the target binding properties of the bispecific antibodies as well as the monospecific controls. The results of this chapter were partly developed in collaboration with Laura Basset as part of her master's thesis under my supervision. For this analysis, the antibodies were immobilized onto AHC biosensor tips, and the association and dissociation of rhHER2 and rhRNF43 were monitored. The resulting kinetic parameters are summarized in Table 13, confirming that conjugation of scFv variants to Q295 did not alter the kinetic binding profiles to the respective soluble receptors RNF43 and HER2.

Table 13 Binding of rhHER2 an rhRNF43 by conjugates and controls. Both affinities (K_D) and rates of association and dissociates (K_{on} and K_{dis}) were determined.

Antibody	Analyte	K_D [M]	k_{on} [$M^{-1}s^{-1}$]	k_{dis} [s^{-1}]
Ttz	rhHER2	3.8×10^{-9}	1.05×10^5	4.01×10^{-4}
Ttz.1+scFv5.3	rhHER2	1.5×10^{-9}	9.68×10^4	1.45×10^{-4}
Ttz.1+scFv5.3	rhRNF43	1.2×10^{-8}	7.51×10^5	8.65×10^{-3}
Anti-RNF43 mAb	rhRNF43	3.5×10^{-9}	6.61×10^5	2.33×10^{-3}

To ensure that simultaneous binding of both antigens to bispecific conjugates is not hindered by steric effects, a bridging experimental setup using BLI was performed. AHC biosensor tips were first loaded with antibodies, followed by association of rhRNF43 and subsequently with rhHER2.

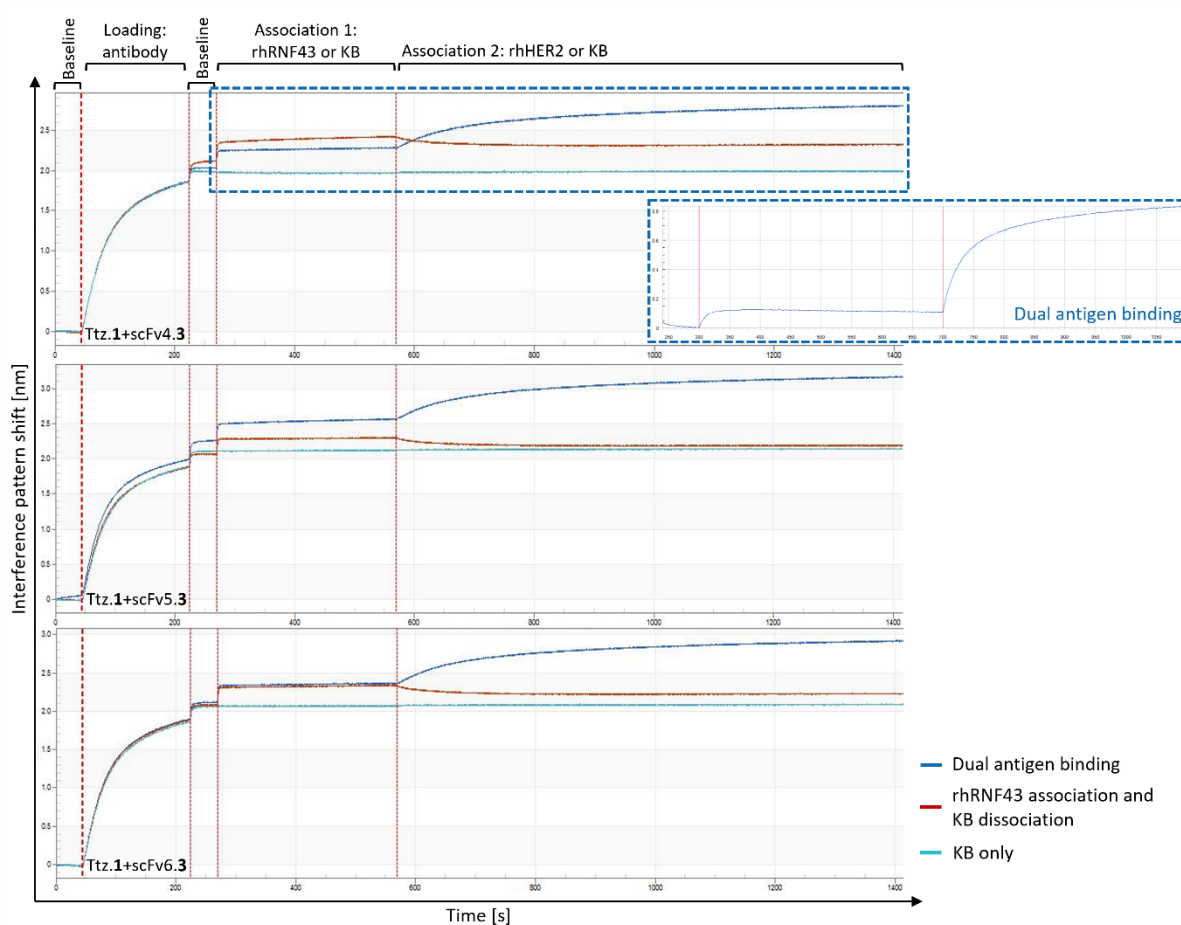


Figure 28 Simultaneous binding analysis of RNF43 and HER2 by IgG-scFv conjugate via BLI. The conjugates were immobilized on AHC biosensors. Then, association of rhRNF43 followed by HER2 was monitored. For both association steps a shift could be observed indicating simultaneous binding of both antigens. Buffer controls indicated no unspecific binding to AHC biosensors.

Exemplary graphs depicting the association steps can be found in Figure 28. Since rhRNF43 (20.5 kDa) is smaller in size compared to rhHER2 (71 kDa), the shift in the association varies depending on the antigen loading. In Figure 28, the addition of rhRNF43 resulted in a shift of 0.15 nm, followed by an additional shift of 0.65 nm upon the subsequent addition of rhHER2. This indicates

that an equimolar amount of RNF43 and HER2 is associated. The second shift revealed in the interface pattern exclusively indicates the association of RNF43, as the buffer control did not show any association with the biosensor tips.

4.10.2 Selective binding of cell surface receptor based on receptor expression levels

The IgG-scFv conjugates demonstrated favorable kinetic characteristics, exhibiting affinities in single to double-digit nanomolar range to their respective targets. Following this, an evaluation was carried out to ascertain whether the binding of soluble protein could be translated into the functional binding of target proteins presented on cells. Hence, the binding of 100 nM bispecific conjugate to various cancer cell lines was assessed using flow cytometry. The cancer cell lines were selected based on varying levels of receptor expression for HER2 and RNF43 which were chosen based on theoretical RNA expression stated in DepMap portal from Broad Institute (Figure 29 (A)).¹⁸⁹ The cell lines were grouped using transcript per million (TPM) introduced by Lia *et al.*,¹⁹⁰ which is calculated based on the number of reads assigned to each gene sequence. Three groups were defined, cell lines with low expression TPM less than 20 (\log_2 TPM: 4.32), medium expression TPM between 20 and 1000 (\log_2 TPM: 4.32-9.96) and high expression with TPM \log_2 greater than 1000 (\log_2 TPM: 4.32, Figure 29 (B)). The criteria to classify gene expression was on the basis of open-source Expression Atlas from European Bioinformatics Institute (EMBL-EBI).¹⁹¹

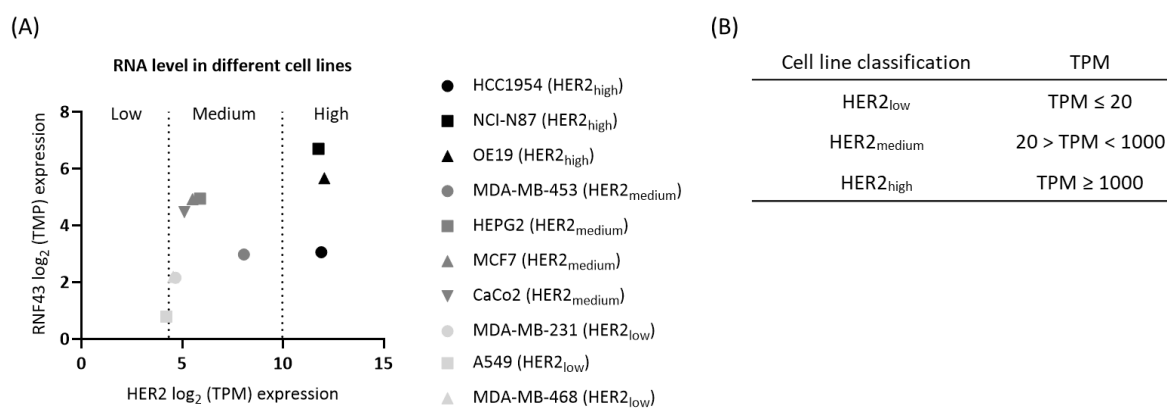


Figure 29 Theoretical RNA expression levels of HER2 and RNF43 in different cancer cell lines. (A) Expression level is stated as \log_2 of transcripts per million (TPM) stated in DepMap portal from Broad Institute.¹⁸⁹ The \log_2 TPM represents the expression level of the gene at one million transcripts in one sample. **(B)** The cell lines were grouped into low (light grey), medium (grey) and high (black) HER2 expressing cell lines depending on their TPM value.

The isotype control mAb (α DIG), unstained cells or cells only treated with detection antibody served as control to quantify the level of cellular self-fluorescence. Furthermore, RNF43 binding was examined using a full-length anti-RNF43 mAb with the same CDR region as the investigated scFv variants.

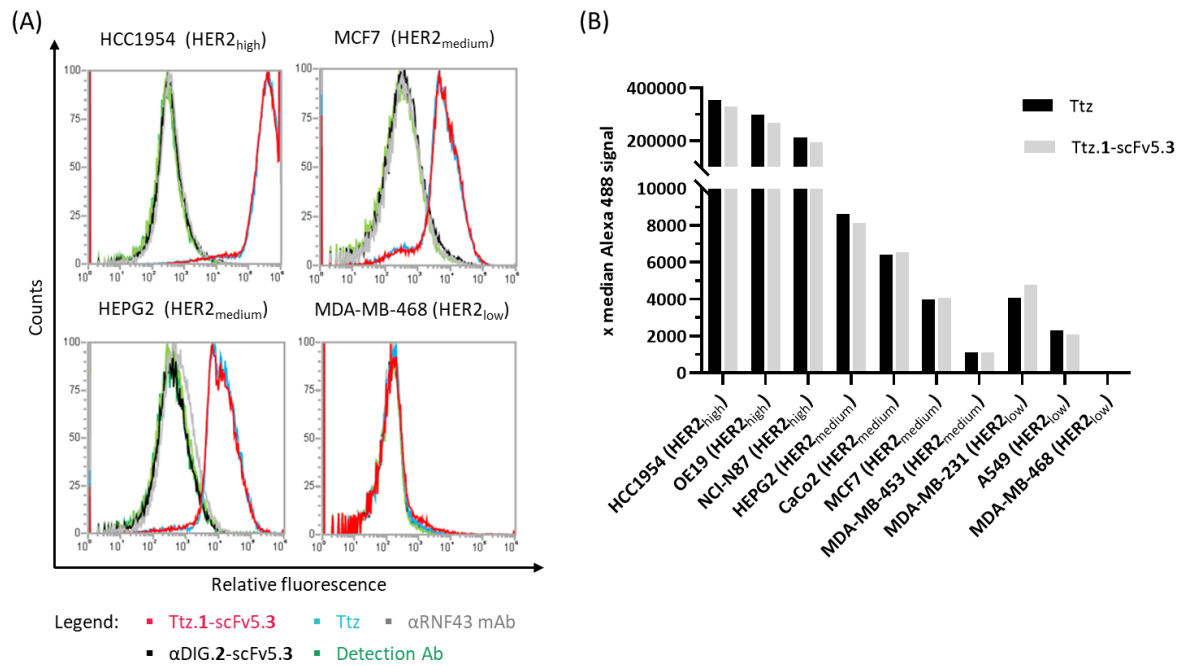


Figure 30 Cellular binding of IgG-scFv conjugates and references to several cell lines. Cell lines were incubated with 100 nM antibody and binding was revealed with AF488-labeled detection antibody. **(A)** HER2 expressing cells incubated with Ttz.1-scFv5.3 (red) and Ttz (blue) and a fluorescent detection antibody show equal MFI compared to controls (α DIG.2-scFv5.3 (black), α RNF43 mAb (grey), and AF488-labeled anti-human detection antibody (green) in flow cytometry analysis. **(B)** MFI values obtained for Ttz.1-scFv5.3 and Ttz on HER2 cell lines expressing different levels of HER2.

The relative fluorescence intensities are illustrated as exemplary histograms in Figure 30, demonstrating a correlation between theoretical HER2 mRNA expression levels and the observed signal intensities. The IgG-scFv conjugates displayed strong cellular binding to HER2 overexpressing cell lines (HCC1954, OE19, NCI-N87), comparable to respective monospecific reference antibody. In cell lines with medium HER2 expression levels (HEPG2, CaCo2, MDA-MB-453, MCF7), the IgG-scFv conjugates exhibited minimal stronger binding compared to the corresponding parental antibody. Notably, no HER2 and RNF43 binding was observed for the MDA-MB-468 cell line, serving as negative control. Furthermore, no RNF43 signal was detected using the present molecules, including the scFv variants and commercial mAb (Figure 30 and Figure S 23 (A)). These values align with the theoretical RNA levels provided in the Broad Institute's DepMap portal, where TPM is below 20 (Figure 29). The extremely low RNF43 expression level was confirmed through native mass spectrometry analysis of several cell line lysates. Notably, RNF43 was not detected among the first 6000 proteins analyzed in these cells (data not shown). A noticeable increase in RNF43 binding was observed with an extended incubation time (Figure S 23 (B)). However, in contrast, the signal for HER2 decreased with longer incubation periods, potentially due to the trastuzumab-induced degradation of HER2 (Figure S 24). Hence, it is important to exercise caution and carefully interpret the results obtained from

flow cytometry experiments. The procedure used in this study may not be suitable for investigating RNF43 binding, as later discussed.

4.11 Evaluation of targeted protein degradation mediated by generated IgG-scFv conjugates

The results of this chapter were partly developed in collaboration with Laura Basset as part of her master's thesis under my supervision.

Although binding of RNF43 epitope was not detected in cellular flow cytometry assays, the biological activity of generated IgG-scFv conjugates was studied. Given recent findings indicating a substantial difference in abundance between E3 ligase and target protein, the current study aimed to explore whether HER2 or PD-L1 could be degraded by targeting the transmembrane E3 ligase RNF43 using the IgG-scFv conjugates.¹²⁸ Western blot experiments and flow cytometry analysis were conducted in receptor positive cell lines to analyze IgG-scFv conjugates binding RNF43 for receptor degradation (detailed description see section 3.8). Briefly, cells were exposed to 10 nM analyte for 24 hours, and after cell preparation, detection was conducted using antibodies against the receptor of interest (HER2 or PD-L1), along with GAPDH or actin serving as loading controls. IgG-scFv conjugates based on Ttz and Ptz effectively reduced the HER2 level in HEPG2 (HER2_{medium}) cells, although parental antibodies also exhibited a significant reduction. Treatment with the scFv5 variant did not show any observable decrease in HER2 levels (Figure 31). Furthermore, β -actin, used as the loading control, did not show any changes, and in negative MDA-MB-468 cells, no HER2 signal was detected (Figure S 25). These results were consistent across two assays, Western blot analysis, and flow cytometry, with two to three technical replicates performed for each method.

In addition to targeting HER2 degradation, the study also addressed PD-L1 for TPD. Experimental settings were used as previous, but no reduction in PD-L1 was observed in the PD-L1-positive cells (T24, HCC827, MDA-MB-231) using Western blot analysis (Figure 31). Due to glycosylation heterogeneity, PD-L1 appeared as a doublet in Western blot analysis.¹⁹² No changes of GAPDH levels were detected. Flow cytometry analysis revealed a modest decrease in PD-L1 levels in samples treated with Atz.2-scFv3.3. However, the extent of this reduction varied among the tested cell lines and technical replicates. Despite conducting optimization studies on treatment duration or concentration, and assay development, the data did not exhibit conclusive evidence of improved target degradation induced by Atz.2-scFv3.3 (data not shown).

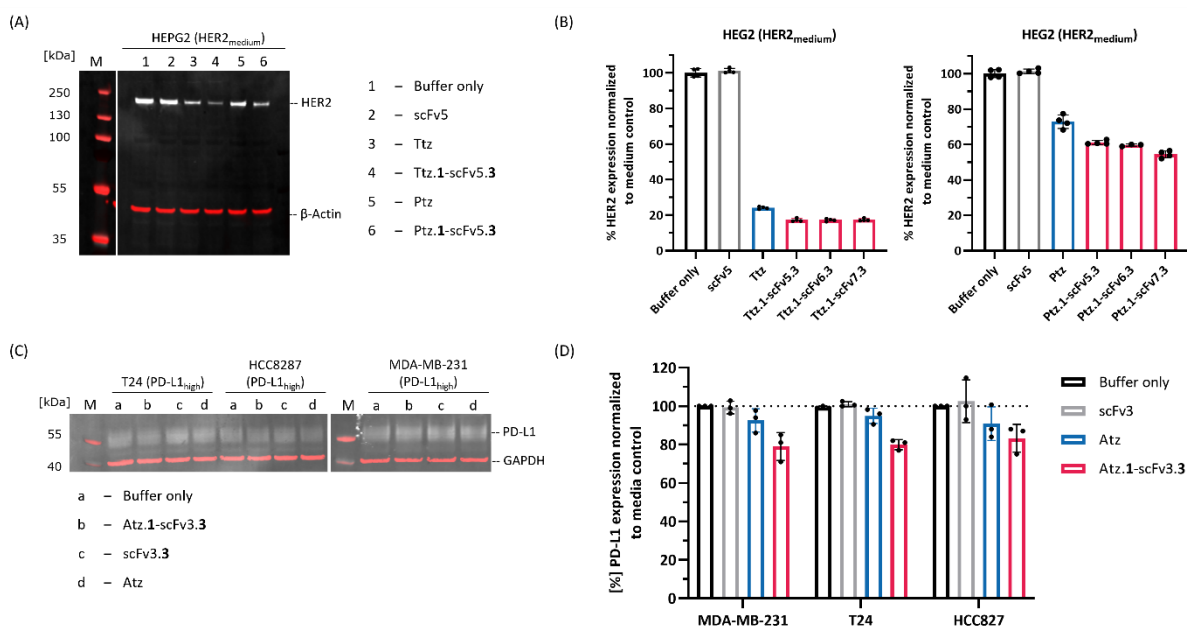


Figure 31 Target cell receptor degradation. (A) Western Blot analysis of HER2 level in HEPG2 cells after treatment with 10 nM Ttz.1-scFv5.3 and Ptz.1-scFv5.3 for 24 hours. For reference monospecific molecules, including scFv5, Ttz and Ptz along with buffer treatment were used. After treatment cells were lysed and 150 μ M protein was used for analysis. β -actin served as housekeeping control and was detected with fluorophore-labeled secondary antibody. **(B)** Flow cytometric analysis of HER2 level on HEPG2 cell surface. Cells were treated with 10 nM Ttz.1-scFv5.3 and Ptz.1-scFv5.3 for 24 hours and after harvest and staining FACS analysis was performed. Treatment results are normalized to buffer only treatment. The values represent the mean of technical triplicates with SD as error bar. **(C)** Western Blot analysis of PD-L1 level in different cancer cell lines (MDA-MB-231, T24, HCC827) after treatment with 10 nM Atz.1-scFv3.3 for 24 hours. GAPDH was used as housekeeping protein. **(D)** Flow cytometric analysis of PD-L1 level on surface of different cell lines (MDA-MB-231, T24, HCC827) after treatment with Atz.1-scFv3.3 and controls. Treatment results are normalized to buffer only treatment. The values represent the mean of technical triplicates with SD as error bar.

5 Discussion

5.1 Expression of antibody-fragments in mammalian cells

As part of this work, different antibody fragments, including VHH and scFv, were expressed in mammalian cells and purified by affinity chromatography. The chosen mammalian expression platform was anticipated advanced protein folding, post-translational modifications, and ensured stable and robust expression. The decision to not use bacterial or yeast expression systems, despite their fast growth rates and efficient protein expression, was based on reports of solubility or stability problems and incorrect protein folding.¹⁹³ For the synthesis of DNA vectors encoding the fragments, the VHH amino acid sequence from the patent PROxAb shuttle¹⁸⁵, as well as the V_H and V_L domains of the scFv variants from the patent application of Boontanrart *et al.*¹²⁶, were chosen. Overall, comparable protein yields were achieved, with the highest monomeric purity exceeding 98%. Firstly, the non-covalent VH032-based PROTAC binder G₃-MIC7 was investigated, a VHH from the patent application of Rieker *et al.*¹⁸⁵, which was successfully modified by an N-terminal G₃-tag.

Following Amsphere™ A3 chromatography, a protein yield of 16.7 mg/L was obtained with a high purity of 98%. Subsequently, the functionality of MIC7 was investigated by complex formation between G₃-MIC7 and VHL-engaging PROTAC GNE987 which was confirmed through HI-HPLC analysis. Additionally, different RNF43-binding scFv variants with variations in their molecular design were evaluated regarding their antibody-based TPD efficiency. These scFv variants were assembled in two orientations: V_H-linker-V_L and V_L-linker-V_H. The rationale for testing both orientations arose from previous studies by Luo *et al.*¹⁹⁴, who demonstrated that the expression of scFv in *Pichia pastoris* system is dependent on V_L-linker-V_H orientation. Ahmad *et al.*³⁸ published findings supporting the importance of V_H-linker-V_L orientation for successful expression.

Observation of the expression rate showed differences in the sequence arrangements of the V_L and V_H subunits. The occupation of the N-terminal position by the V_L subunit resulted in an expression rate of only 11.7 mg/L for scFv4. Consequently, there was a decrease in yield of approximately 20% compared to the V_H-linker-V_L orientation. An important parameter of stable expression is the correct folding of scFv molecules. Here, linker design plays a crucial role. As a rule of thumb, the linkers should be around 10-25 amino acids long and contain glutamine and lysine to increase solubility and glycine and serine for better flexibility.²⁴ Apart from considering the length and orientation of the linker, the specific composition of amino acids also significantly affects the success. Studies have shown that a distance of 3.5 nm (35 Å) between the carboxy and amino termini, corresponding to approximately twelve amino acid residues, is necessary for ensuring stable folding and proper linkage.¹⁹³ One extensively studied and commonly used linker structure is the (G₄S)₃ combination consisting of 15 amino acids with short side chains to promote high flexibility and hydrophilic amino acids to minimize interactions between the linker and variable domains, thus enhancing solubility. Additionally, we conducted an investigation on a twelve amino acid long YOL linker, which possesses similar properties as mentioned above.¹⁸⁶ Notably, no difference in the expression yield of the scFv variants was observed between the two linkers. Furthermore, the effects of employing three, six, or nine (G₄S₁) motifs as spacers between the scFv backbone and the MTG conjugation site was examined. These designs aimed to evaluate stability, flexibility, and any potential interference with antigen binding sites across all valences. However, elongation of the spacer was primarily designed to examine steric hindrances in the two-step bioconjugation process of scFv variants to mAbs. It is worth noting that scientific literature supports the inclusion of three (G₄S₁) motif sequences as an effective means to achieve satisfactory levels of both stability and flexibility in genetic IgG-scFv fusion proteins.¹⁹⁵ The observed decrease in expression levels with the elongation of spacer sequences could potentially be attributed to interactions with cellular compartments, reduced solubility, or decreased stability in the supernatant influenced by the increased spacer length.¹⁹³

Lastly, the incorporation of His₆ peptide proved to be a reliable sequence for protein recovery from the supernatant through the specific interaction between His₆ peptide and immobilized charged metal ion resin of the IMAC column. Evaluation of antigen binding for the produced scFv variants demonstrated a high affinity in BLI. These scFv variants exhibited nanomolar affinity towards rhRNF43, placing them within the range of the monospecific anti-RNF43 antibody control and other molecules mentioned in the AbTAC paper for comparison.¹²⁷ The observed high affine binding was driven by the absence of dissociation, while the association constant was in the range of 6×10^5 M/s. Concluding, binding kinetics revealed that all scFv variants as well as VHH, were capable of binding to their respective antigens and thus neither the V_H/V_L orientation nor the spacer length had an effect on antigen binding.

5.2 Bioconjugation for generation of antibody-MIC7 conjugates as vehicle for PROTAC delivery

The importance of the enzymatic conjugation strategy for site-specific coupling has already been highlighted in various studies in the ADC field. Enzymatic conjugation is rapidly gaining popularity as it provides homogeneous products and thus pharmacokinetic advantages.⁷³ For example, modification of antibodies or antibody fragments with glutamine tags has enabled MTG-mediated conjugation.^{74,75} Surprisingly, none of the numerous glutamines naturally occurring in the antibody proved to be an efficient substrate for MTG when the usual MTG variant and reaction conditions were used. However, one glutamine, Q295 in the heavy chain of the antibody is addressable by MTG when the neighboring glycosylation site was removed.⁷⁶ Further studies optimized the enzyme via mutations, to use Q295 as a conjugation site for site-specific coupling of linker payloads even without de-glycosylation.⁷⁸ MTG, shows high flexibility in its choice of acyl-acceptor substrates, however, the N-terminal primary amine of the triple glycine (G₃) has been shown to be among the most efficient recognition sequences. Previous protein-protein coupling studies have shown G₃ to be an MTG recognition peptide, as demonstrated by Tanaka *et al.*¹⁹⁶, who linked two proteins (EGFP and DHFR) using MTG as catalyst, and Bourmans and colleagues, successfully coupled G₃ as an acyl-acceptor substrate for MTG in their patent application.¹⁹⁷

In the present work, the conjugation of VHH to the Fc heavy chain on Q295 was achieved via enzymatic conjugation. By using G₃ as an acyl acceptor substrate in the MTG-mediated transamination reaction, conjugation of G₃-MIC7 to antibody was evaluated.

The VHH G₃-MIC7 was successfully conjugated to Ttz using MTG at a ratio of 1.88 VHH per antibody (VAR) when position Q295 was present. Reactivity studies revealed a correlation between higher VAR values and increasing antibody concentration, as well as larger amounts of MTG, resulting in enhanced conjugation efficiency. Moreover, a greater molar equivalent of VHH in the reaction mixture resulted in further enhancement of conjugation efficiency. Following the

establishment of the final conditions, further extension of VHH conjugation was carried out with ten additional IgG1 antibodies, all possessing Q295 in the Fc region. The conjugation efficiency for all these antibodies exceeded 93% of the available conjugation sites. This resulted in antibodies with two conjugation sites carrying at least 1.86 VHHs in the conjugated variant. However, an exception was observed with atezolizumab, which showed a VAR of 1.62. This difference can be attributed to the N297A (Amino acids position according to the EU nomenclature) mutation in the Fc region of atezolizumab, resulting in absence of N-glycosylation pattern. This has not yet been observed in the conjugation of linker-drugs; in fact, an increased conjugation efficiency of antibody was observed when conjugating with MTG.¹⁹⁸ However, the literature reports reduced thermal stability of C_H2 and higher aggregation rates were observed for deglycosylated antibodies, which could be a reason for lower VAR.¹⁹⁹

Overall, the VHH-antibody conjugates had a high purity of >97%. Conjugation of Ttz with C-terminal light chain (LC) glutamine tag (LLQGA) and Q295A mutation was used to evaluate conjugation sites alternative to Q295. The glutamine tag at the light chain was found to have improved accessibility and flexibility in MTG-mediated conjugation of linker peptides, which was investigated in various studies.⁷⁸ Although the conjugation efficiency was identical when comparing the conjugation of G₃-MIC7 to LLQGA-tagged Ttz with Ttz Q295 conjugation, a higher level of HMW species, approximately 6.9%, was observed for LLQGA-tagged Ttz. Additionally, MTG-mediated conjugation with MIC7 lacking the G₃-tag required for conjugation was performed to confirm the MTG recognition motif and excluded an additional MTG recognition site, specifically accessible lysine residues in the CDR region or lysines on the protein surface (Figure S 8).

Additionally, successful conjugation of G₃-MIC7 to Ttz, Ctx, and α DIG was achieved using MTG in a 5 mg batch. The reaction led to a heterogeneous mixture of species with different VHH load and high molecular weight species. Preparative SEC separated the product from HMW, excess VHH and MTG resulting in VAR values of greater 1.74. Neither the purification method nor the antibody variant had any effect on conjugation efficiency or final yield, indicating that efficient conjugation with high purity was achieved. Targeted delivery of PROTACs offers the advantage of minimizing side effects, thereby enabling the use of higher doses. The conjugation method employed in this study enables the coupling of two VHHs per antibody, facilitating the delivery of two PROTACs. Modifying antibodies with MTG-tags provides a platform to achieve higher VAR values, thereby increasing the PROTAC loading per antibody. This approach is a common strategy in ADC drug delivery to enhance cell killing.²⁰⁰

Nevertheless, the successful site-specific conjugation of VHH demonstrated the potential of the strategy to produce bispecific molecules in a modular approach. This strategy is not necessarily limited to the generation of conjugates for selective, non-covalent PROTAC delivery.

By combining VHHs with unique target specificities and antibodies possessing additional specificities, a combinatorial library of bispecific antibodies can be rapidly generated, allowing for efficient screening of optimal target combinations, offering considerable potential for various therapeutic applications. The interest and necessity for scalable and robust methods to screen bispecific antibody constructs have been effectively addressed in the "AJICAP second generation" strategy.⁸⁵ This approach involves the use of affinity peptides to pre-orient reactive amino groups, enabling the binding of Fab fragments to antibodies.

However, it is important to note that this strategy involves a two-step synthesis process in which excess reaction compounds must be removed between steps. Alternative approaches for generating dual binding constructs include intein-based conjugation,²⁰¹ the SypTag/SypCatcher approach,²⁰² or the controlled exchange of Fab arms.²⁰³ However, these technologies have limitations, as they rely on specific functionalities present in antibodies or Fc fragments and cannot be applied to commercially available and native antibodies but require genetic introduction of tags prior to expression.

5.3 Generation of antibody-based protein degraders

Following the successful conjugation of G₃-MIC7, the feasibility of direct conjugation was explored with a RNF43-binding scFv. The N-terminal G₃ peptide sequence served as a suitable acyl-acceptor substrate for MTG-mediated transamination in VHH conjugation. Therefore, a glycine sequence (G₅) was positioned ahead of the V_H-linker-V_L sequence in the scFv construct (scFv1), and identical conjugation conditions were employed. However, in the semi-quantitative gel electrophoresis, no evidence of selective conjugation, represented by a clear and distinct shift to higher masses indicating the presence of one or two scFv per antibody, was observed. Instead, aggregates were visible, as indicated by smeary bands primarily located within the gel pockets, visible under both non-reduced and reduced conditions. This visual observation was confirmed by analytical SE-HPLC, in which 23% of high molecular weight species was detected. The reduced stability of scFv in the salt-free conjugation buffer or the occurrence of cross-linking between scFv molecules may be factors contributing to the low conjugation efficiency and formation of HMWS. In buffer solutions with higher salt concentrations, protein stability can be enhanced due to the binding of salt ions to charged residues on the protein surface, resulting in increased hydration.²⁰⁴

When comparing the structural composition of a VHH and scFv, differences in size result in varying proportions of surface-exposed amino acids. This increases the probability of the 25 kDa scFv to containing an additional recognition site for MTG cross-linking. The ϵ -amino group of lysine, for example, serves in nature as the primary amine for the stable γ -glutamyl- ϵ -lysine linkage of MTG, which can result in the non-desired cross-linking of scFv.

Overall, the structural flexibility of the specific amino acid, the structural arrangement of the target protein, and the polarity of neighboring amino acids are key factors for successful MTG-mediated conjugation.⁷⁰ Generally, MTG shows quite promiscuous behavior towards options of acyl-acceptor substrate and different primary amines.²⁰⁵ In the absence of primary amines, side reactions occur, such as the deamidation of glutamines to glutamic acid, with water acting as an acyl acceptor.²⁰⁶ Despite the challenges encountered, exploring a modular system for screening antibody-based degraders would be an intriguing avenue of investigation. A strategy was developed in which the target specificities of native antibodies were combined with scFv variants that possessed specificity against membrane-bound E3 ligase, enabling the rapid generation of a combinatorial library for targeted protein degradation (TPD).

Next, an intermediate step was introduced, whereby the parental molecules were first equipped with a small molecule click derivative and subsequently assembled in a strain-promoted azide-alkyne cycloaddition (SPAAC) reaction. In initial proof-of-concept studies, different click derivatives were conjugated to the scFv variants via MTG conjugation and evaluated based on purity and DAR. Subsequently, the conjugation efficiency of the click derivatives to the antibodies was analyzed. The selection of click derivatives was based on published data. Cyclooctyne and azide, the two components of SPAAC, have already been described as components for covalent linkage in various molecules.²⁰⁷ For MTG-mediated conjugation, the click derivatives contained N-terminal G₃ peptide sequences which was well established for linker-peptide conjugation.⁷⁸

Overall, the scFv variants and native antibodies were successfully conjugated by MTG using the peptide click derivatives: DBCO, BCN and Azide. At first, the different click derivatives were conjugated to the different scFv variants, and the results are now being discussed individually. The ring-strained alkynes and scFv proved to be good partners for high conjugation efficiency, reflected in >86% occupied conjugation position and high DAR values. However, the alkyne had negative impact on the stability of scFv. In contrast to the results with ring-strained alkyne, the conjugation of different scFv variants with PEG azide derivatives **3** and **4** yielded highly pure products with a purity level greater than 99%. The DAR values achieved with these conjugates were greater than 0.9. Furthermore, when directly comparing the conjugation efficiency of **3** and **4**, a decrease was observed with increasing length of the PEG linker. Interestingly, these findings contradict the results reported in the literature regarding MTG-mediated conjugation of amino-PEG to C-terminal tags at mAbs, but are consistent with previous unpublished in-house experiments.²⁰⁸ Despite previous indications of the positive influence of extended peptide chains in the MTG reaction, this effect was not observed in the MTG conjugation of derivatives **5** and **6** to the scFv.¹⁹⁶ Additionally, the incorporation of serine residues in **6** to enhance solubility in aqueous solutions, a strategy previously employed in scFv linkers, did not yield any improvements in conjugation efficiency.

In summary, these results indicate that large hydrophobic click derivatives, such as derivative **1**, and long glycine peptide chains within **5** and **6** are not suitable for conjugation to RNF43-binding scFv variants due to steric hindrances or excessive linker flexibility. These obstacles can impede the enzymatic reaction, as supported by both the elongation of linkers in the study and previous literature findings.¹⁹⁷ Consequently, click derivative **3** was identified as a suitable option for efficient and high-yield conjugation of scFv.

Following these optimization studies, the scFv variants were conjugated with click derivative **3** using MTG on a 20-mg scale and subsequently purified through preparative SEC. DAR values ranging from 0.77 to 0.91 were attained with the highest purity. Notably, the highest purity was obtained with each activated scFv molecule. As reported in the literature, stability of scFv molecules was demonstrated when coupled with azide moieties, where the scFv proteins were activated with G₃-N₃ peptides using SrtA and catalase was equipped with DBCO via NHS ester coupling.²⁰⁹ As discussed in section 5.3, transglutaminase shows minimal restriction in its selection of acyl-acceptor substrates and can also link water molecules to glutamines in the absence of primary amines. The substrate specificity likely played a role in facilitating cross-linking during the direct conjugation of scFv to the antibody. Conversely, in the conjugation of click derivatives to scFv variants, an excess of preferred primary amines was present during the reaction process, avoiding side reactions.

Since the azide moiety for the SPAAC reaction was conjugated to the scFv variants, the ring-strained alkyne derivatives had to be conjugated to the antibodies. Fortunately, the hydrophobicity of the alkynes had no impact on the solubility and stability of the DAR 2 Ttz conjugates, which was achieved even at lower MTG levels of 30 U/mL. Finally, the two ring-strained alkyne structures, **1** and **2**, were conjugated with antibodies in a larger scale to test the performance in SPAAC reaction. The antibodies Ttz, Ptz and Atz were successfully equipped with DBCO derivative **1** with DAR values greater 1.84 using MTG. In addition, the BCN-based click derivative **2** was successfully conjugated to Ttz, Mtz, α DIG and Ctx (DAR >1.92). In all MTG-mediated conjugations, a final highest purity was achieved, with yields of purified conjugates ranging between 50% and 70%. It should be noted that the increased hydrophobicity resulting from scFv conjugation may lead to stronger interactions with column resin and membranes during processes such as concentration or sterile filtration, possibly resulting in increased protein loss. The copper-free SPPAC reaction, which was awarded the Nobel prize, has proven to be extremely versatile in both *in vitro* and *in vivo* applications. The Bertozzi group effectively used click derivatives, specifically DBCO and azide, for conjugating glycoproteins to antibodies.¹⁷³ Additionally, in the second-generation AJICAP approach, Fab fragments were successfully attached to DBCO-modified antibodies using click chemistry.⁸⁵

Within the present work, semi-quantitative gel electrophoresis demonstrated a successful click reaction of ring-strained alkynes attached to Ttz and scFv5+3 after just 3 hours at 30 °C. Gradual modifications of the reaction conditions, including reaction duration, temperature, and antibody concentration, increased the click reactivity from 65% to a maximum of 79%, with temperature elevation having the greatest impact. By extending the reaction time at elevated temperature, the click reactivity reached a maximum of 91.3%. However, a consistent amount of approximately 6% HMW species was observed at both 25 °C and 37 °C. While Ahn *et al.*¹⁷⁵ described a complete click reaction performed over three days at room temperature, Fuji *et al.*⁸⁵ did not provide specific percentage values for the click efficiency of Fabs onto the antibody, indicating missing analytical methods. This was also a difficulty in the present study, where only LC-MS was used to assess conjugation efficiency and validation of the conjugation was based solely on semi-quantitative gel electrophoresis. Comparison of solubility, stability, and click efficiency among the scFv variants with varying spacer lengths in scFv5, scFv6, and scFv7 revealed negligible differences. The shortest spacer length in scFv5 provided sufficient flexibility to avoid steric hindrance during bispecific conjugate generation. Furthermore, the solubility and stability of the final constructs were not influenced by the length of the scFv spacer. The reactivity of the two ring-strained alkynes in the click reactions was consistently efficient, ranging from 82% to 90%, regardless of the specific antibodies involved or the clicked scFv variants. These results align closely with the theoretical reactivity of alkynes towards benzyl azide, as reported in Debets *et al.* publication.⁶⁵ However, a difference in click efficiency of 20% was observed when comparing conjugation to Atz and click reaction with scFv3+6. This difference is reflected in SAR values, which range from 1.16 to 1.34. Additionally, the yield of these two molecules, Atz.5-scFv3.6 and Mtz.5-scFv3.6, was below 50%, indicating potential antibody-dependent stability issues for Atz, which is A-glycosylated, leading to reduced reactivity. As already discussed before, literature reported higher aggregation rates for deglycosylated antibodies.¹⁹⁹ The glycosylation of the antibody significantly contributes to its stability and solubility.²¹⁰ For instance, enhancing the solubility of IgG1 was accomplished by adding an extra glycosylation site in either the Fab domain²¹¹ or on Q179N²¹² in the heavy chain.

5.4 Complexation of antibody-MIC7 and PROTAC enables selective target degradation

PROTACs have revolutionized the field of targeted protein degradation. They possess the ability to induce proteolysis by binding to E3 ligases and recruiting target proteins. However, the broad expression of E3 ligases in both healthy and tumor tissues limit the selectivity of PROTACs, leading to potential off-target effects. In order to fully target the range of TPD-eligible targets, the development of solutions for delivery of PROTACs are advisable. The first wave of degraders based on small-molecule designs are under optimization for oral delivery.²¹³ These strategies

focus on short, rigid linkers to minimize rotatable binding properties and a minimal number of hydrogen bond donors.²¹⁴ Furthermore, various parameters such as lipophilicity and water solubility, polar surfaces or chemical stability are considered in the design of the chemical molecules.^{215,216} The development of PROTACs, which are mainly based on ligand systems, has been primarily focused on the E3 ligases CRBN and VHL. However, the large diversity of E3 ligases in humans allows an extension of the approach to other disease- or tissue-specific degraders.²¹⁷ For example, E3 ligands have been identified against DDB1-CUL4-associated factor (DCAF1)²¹⁸ and mouse double minute 2 homologue (MDM2).^{219,220,221} DCAF1 is an E3 ligase required in the cancer cell cycle and thus less likely to be downregulated as a resistance mechanism against PROTAC treatment, while MDM2 negatively regulates the tumor suppressor p53.^{222,223}

Aside from optimizing the comprehensive chemical structure of TPD molecules, the use of drug delivery systems allows to improve the generally low permeability and cancer cell selectivity. Nanoparticles, which have seen substantial growth in recent years, offer a suitable solution for this purpose.²²⁴ They facilitate the delivery of PROTACs through nanoscale drug-delivery systems, enhancing stability, distribution, and specific accumulation and release in tissue.²²⁵

Additional approaches for enhancing selectivity involve small-molecule drug conjugates (SMDCs)²²⁶ or degrader ADCs (DACs).²²⁷ SMDCs and DACs share the strategy of conjugating therapeutic agents with specific ligands that bind tumor cells. SMDC combined with PROTACs showed a significant increase in tumor tissue penetration due to the combinatorial improvement of water solubility and tumor antigenic capacity.²²⁸ The first reported DAC targeted CLL1, an overexpressed surface target in acute myeloid leukemia (AML), along with BRD4, which has transcriptional and epigenetic regulatory functions. GNE987, a potent BRD4 degrader, was linked to an anti-CLL1 mAb using cysteine conjugation to engineered cysteines.¹⁴³ This demonstration revealed that antibody conjugation can improve unfavorable pharmacokinetic properties of the degrader. Further DACs have been developed in recent years to target BRD4 in STEAP1-expressing prostate cancer cells¹⁶⁵ or HER2-overexpressing breast cancer cells.¹⁵⁷ Beginning this year, two cereblon (CRBN)-engaging DACs were published, while Nakazawa *et al.* generated a CEACAM6-targeting DAC to inhibit pancreatic cancer growth,²²⁹ the group by Zhang *et al.* developed a CD79b DAC linked with a CRBN Binding Bruton's Tyrosine Kinase (BTK) Degrader.²³⁰ In addition to BRD4-targeting DACs, ER α -targeted degraders¹⁵⁶, TGF β R2-targeted degraders²³¹ and GSPT1-targeting DACs²³² were developed in recent years.²²⁷ The recently described PROxAb Shuttle approach enables the targeted delivery of PROTACs in a DAC-like manner, but without the chemical modification of the PROTACs.¹⁶⁰

The PROxAb Shuttle technology is a non-covalent platform designed for the rapid generation of tumor-addressing antibody-PROTAC chimeras. As part of this work, the flexibility and modularity of the strategy was further enhanced.

In this study a modular approach for selective PROTAC delivery was developed using enzymatic bioconjugation. Following the successful MTG-mediated conjugation of G₃-MIC7 to Ttz and Ctx and subsequent purification the physicochemical properties of the parental antibodies and their conjugates were investigated, including antigen binding, cell receptor binding, internalization, and biological activity. The binding kinetics of protein-protein interactions were assessed using the well-established BLI technique, which revealed no differences in antigen binding kinetics between the parental antibodies and VHH conjugates. Both Ttz-MIC7 and Ctx-MIC7 exhibited sub-nanomolar K_D values, consistent with the binding affinities of the parental antibodies and reports in literature.²³³ Negative controls indicated the absence of non-specific antigen binding or biosensor loading, highlighting that conjugation of 14.5 kDa VHHs to the C_H2 domain of antibodies did not interfere with antibody-antigen binding.

Subsequently, the binding affinities of VHHs to three VH032-based PROTACs were evaluated using SPR. While no differences in MIC7 binding affinity were observed when conjugated to different antibodies, the MIC7 conjugates showed varying binding affinities with different PROTACs. High binding affinity in the sub-nanomolar range was calculated for GNE987P binding, while MIC7 showed nanomolar binding affinities for GNE987 and ARV771. These findings are in line with previous studies involving the genetic fusion of MIC7 to the C-terminus of Ctx.¹⁶⁰ The lower binding affinity of MIC7 to ARV771 compared to GNE987 might be related to the presence of an additional methyl group in the VH032 subunit. The differences in MIC7's affinity to GNE987 and GNE987P could be due to the interaction of the PEG chain with neighboring amino acids during the binding process. The binding of MIC7 to PROTACs was confirmed by the absence of binding with the parental antibodies, up to a tested concentration of 0.5 μM.

Flow cytometry was used to confirm the selective receptor binding of Ttz-MIC7 and Ttz to cancer cells with varying HER2 expression levels, including SKBR3, BT474, and MD-MB-435. Ttz-MIC7 and Ttz demonstrated comparable binding to cancer cells expressing HER2 receptor, while non-specific binding was not observed with the isotype control. Moreover, significantly reduced binding was observed in the HER2_{low} cell lines, indicating the specificity of the binding interaction. To validate the effective delivery of PROTACs, it is essential for the antibody-based PROTAC shuttles to undergo internalization within the target cells. Internalization relies on various processes including phagocytosis, macro- and micropinocytosis, or clathrin-dependent receptor-mediated endocytosis.²³⁴ With the last as the best characterized and predominant mechanism for cell receptor internalization and the uptake of bound antibodies. Receptor-mediated internalization was observed for antibody-VHH conjugates and parental molecules to study potential effects related to VHH conjugation. Selective internalization was confirmed using pHAb dye-labeled Ttz-MIC7, along with references. The pH-sensitive dye exhibited high fluorescence in the acidic environment of lysosomes, enabling the detection of successful internalization.²³⁵

The conjugates were labeled through random lysine conjugation, resulting in different degrees of labeling, which were considered when calculating the normalized fluorescence signals. Live-cell imaging conducted over a period of 24 hours revealed a selective increase in fluorescence signals upon treatment with Ttz-MIC7 and Ttz in receptor-expressing cells. Receptor-mediated internalization was confirmed by the absence of fluorescence signals in HER2_{low} cell lines and when treating HER2_{high} cell lines with the isotype control α DIG-MIC7. Additionally, previous reports by Jäger *et al.*,²³⁶ have indicated a correlation between receptor-dependent internalization rate and lower mean fluorescence intensity (MFI) values in BT474 cells with lower HER2 levels compared to SKBR3 cells with higher HER2 levels.²³⁷ Such variations might be influenced by target density and cell cycle status. For instance, the doubling time of SKBR3 cells is approximately 30 hours, whereas for BT474 cells, it ranges from 60 to 80 hours, potentially affecting internalization based on the cell cycle phase of both cell lines.^{238, 239} Mitosis during the G2/M checkpoint has been shown to strongly inhibit endocytosis.²⁴⁰ Overall, the presented data indicates that the strategy of direct MTG-mediated G₃-MIC7 conjugation to native antibodies did not alter the physicochemical and receptor-binding properties of the final molecule.

Next, the biological activity of the MIC7 conjugates was evaluated by complex formation with BRD4-degrading PROTACs, namely GNE987 and GNE987P. BRD4, a transcription regulator protein present in healthy and tumor cells, is an attractive target in cancer and an interesting target of PROTAC-induced degradation due to its role in transcription dysregulation.²⁴¹ BRD4 is a member of the bromodomain and extra-terminal (BET) protein family. Interestingly, the regulation of the expression and function of the proto-oncogene MYC is closely linked to BRD4.¹⁸⁴ They both have overlapping effects and directly regulate each other, thus BRD4 contributes to the maintenance of homeostatic MYC levels and MYC regulates functions of BRD4 by inhibiting its histone acetyl transferase (HAT) activity.²⁴² This has implications for the transcriptional regulation and stability of the MYC oncoprotein. Several BET inhibitors have demonstrated promising results in cancer treatment, yet they still face certain challenges in intrinsic acquired drug resistance.²⁴³ First selectively designed BRD4 inhibitors were mostly pan-BET inhibitors, which led to toxic side effects such as nausea or vomiting.²⁴⁴

However, the inhibitor studies highlighted the close association between BET proteins and cancer. This promotes a detailed investigation of BET-targeted PROTACs.^{245, 244} GNE987 and GNE987P are PROTACs designed to target the bromodomain-containing protein (BRD4) and the von Hippel-Lindau tumor suppressor (VHL).¹⁴³ VHL is a key component of an E3 ligase complex. VHL-engaging PROTACs are currently undergoing clinical development for cancer therapy.^{246, 247} Although they offer unique advantages, the BET-targeted PROTACs have limitations such as metabolic instability, poor cell permeability, reduced *in vivo* pharmacokinetics and efficacy, and off-target toxicity. The unique benefits of BET-targeted PROTACs promotes the development of

alternative strategies for targeted delivery to address their limitations.^{248,247} The complexation of PROTAC and MIC7 conjugates enabled targeted receptor-mediated uptake through the binding antibody. Consequently, the release of PROTACs occurred in receptor-expressing cells, extending the selectivity while minimizing off-target effects.

The successful loading of PROTACs was confirmed by HI-HPLC analysis and the percentage of PROTAC loading was calculated based on the average number of MIC7 conjugated per antibody molecule (VAR). Concentration-dependent complexation of GNE987 and GNE987P with all MIC7 conjugates (Ttz-MIC7, Ctx-MIC7, and α DIG-MIC7) was observed, achieving nearly complete loading with a twofold excess of PROTAC. Loading Ttz-MIC7 and Ctx-MIC7 with a GNE987 ratio of 1:2 resulted in loading efficiencies of 94% and 98%, respectively, while loading with GNE987P achieved efficiencies of 90% and 93%. SPR analysis confirmed the complexation of GNE987 and GNE987P with both Ttz-MIC7 and Ctx-MIC7. However, quantitative determination of PROTAC loading for all PROTAC-antibody combinations was challenging due to limitations in achieving sufficient chromatographic peak separability within the HI-HPLC chromatogram. A loading difference of 20% was observed between Ttz-MIC7 and Ctx-MIC7 when loaded with GNE987, with lower loading efficiency calculated for Ctx-MIC7. These discrepancies may arise from the high salt concentration during sample preparation and chromatographic analysis, which can compromise complex stability and diminish PROTAC binding. An attempt to adjust the salt gradient was not applicable as it resulted in reduced peak resolution. Given the challenges in analytical resolution and the minimal variation observed in VAR values among the conjugates, a 50% PROTAC complexation approach was adopted for subsequent biological evaluations to ensure identical PROTAC loading for direct comparisons.

The biological activity of BRD4 degrading PROTACs was observed in HER2 expressing SKBR3 cells. Complexed GNE987P and free GNE987P effectively induced BRD4 degradation, whereas unloaded Ttz-MIC7 and the isotype control α DIG-MIC7 loaded with GNE987P had no impact on BRD4 levels. Thus, indicating antibody-dependent selective delivery of PROTACs in target cells and their subsequent lysosomal escape. Together with the unaffected BRD4 levels observed in cancer cells treated with the PROTAC-loaded isotype control, this suggests that PROTACs are captured by the conjugated MIC7. This not only highlights the selectivity achieved through antibody-mediated delivery, but also indicates the high complex stability under cell culture conditions. Degradation results obtained for GNE987 and Ttz-MIC7 + GNE987 showed similar results to related GNE987P treatments. In the work of Dragovich *et al.* several DACs were generated, including conjugates with anti-STEAP1 mAb and GNE987 or GNE987P.¹⁶⁵ Higher aggregation behaviour was observed for the GNE987P conjugates, which attributed to the aliphatic linker connecting BRD4 binder and VHL ligand, and the resulting higher lipophilicity compared to the PEGylated spacer unit in GNE987P.¹⁶⁵

Additionally, the use of an anti-CLL1 antibody alongside the increased stability and improved pharmacokinetic properties of the conjugate using GNE987 was reported.¹⁴³ The observed BRD4 degradation, when treated with the complexed PROTAC even at a low concentration of 1 nM, demonstrated the influence of receptor-mediated uptake. This enabled efficient delivery of the PROTAC molecules with low solubility, bypassing their limitation of passive transmembrane diffusion. Particularly, treatment of complexed, less hydrophobic GNE987P showed increased BRD4 degradation efficiency compared to the free molecule, likely due to more efficient cellular uptake of GNE987P through receptor-mediated internalization mechanisms. In comparison, the receptor-mediated uptake of GNE987, which is already a membrane-permeable molecule, showed a less pronounced boosting effect. Consistent with our findings, previous studies by Maneiro *et al.*¹⁵⁷ demonstrated enhanced BRD4 degradation in immunofluorescence assays following targeted delivery of GNE987.

In cell viability assay, complexed PROTACs demonstrated similar increased toxicity compared to free PROTACs, targeting two distinct receptors: EGFR and HER2, across various receptor-expressing cell lines. GNE987 showed a strong ability to kill tumor cells, but it also showed cytotoxicity towards non-target cells, resulting in increased side effects, and higher systemic exposure. On the other hand, complexed GNE987 and GNE987P exhibited comparable cell killing to their free counterparts but selectively affected target receptor-expressing cells. This is advantageous, since the control molecule α DIG-MIC7, when complexed, did not affect cell viability. Furthermore, the complexation of GNE987 with Ttz-MIC7 demonstrated sub-nanomolar IC₅₀ values in SKBR3 and BT474 cells, consistent with previous results on BRD4 degradation, and further described in the PROxAb shuttle approach.¹⁸⁵ As expected, no toxic effects were observed in cell lines with low or absent target receptor expression. However, a difference in toxicity was observed between GNE987P and GNE987.

While both PROTACs, when complexed with Ttz-MIC7, exhibited sub-nanomolar IC₅₀ values, the free PEGylated linker variant GNE987P showed reduced efficacy compared to GNE987, consistent with its lower cell permeability. Nonetheless, when GNE987P was complexed with a receptor-binding antibody and selectively internalized by tumor cells via receptor-mediated uptake, the toxic effect of complexed GNE987P was similar to that of complexed GNE987. This observation in different target receptor-expressing cell lines suggests the potential applicability of this approach to other antibody formats, as exemplified by the selective toxicity observed with Ctx-MIC7 against EGFR. Additionally, the treatment control GNE987-complexed with unconjugated G₃-MIC7 did not exhibit cytotoxicity in any of the cancer cell lines, confirming the expected antibody-mediated selectivity.

Overall, it is important to consider that the *in vitro* experiments were performed in closed systems, which limits their direct translation to the *in vivo* system. *In vitro*, the PROTAC can be re-

bound by the MIC7 antibody, leading to an equilibrium between free and bound PROTAC. In the *in vivo* system, if the complex stability is low, the PROTAC can dissociate and may not re-bind but rather be cleared, thereby altering the equilibrium based on the kinetics. However, the SPR analysis indicated slow dissociation rates and a prolongation of PROTAC half-life from hours to days using the antibody-VHH complex.¹⁸¹

Numerous PROTACs show strong target binding properties and high degradation efficiencies, yet they possess characteristics that complicate administration. For instance, free GNE987P demonstrated BRD4 degradation but was further improved through complexation with the antibody and the targeted delivery of GNE987P. The improvement was reflected in a reduction in the minimum effective concentration when GNE987P was complexed. Therefore, this strategy provides an example for non-covalent drug delivery and might be of interest for further applications.¹⁶⁵ Examples of such non-covalent drug delivery have been reported by Ocean *et al.*²⁴⁹ or Schmieid *et al.*²⁵⁰, who successfully used non-covalently linked drugs for effective transfer across the blood-brain barrier.

5.5 Addressing membrane-bound E3 ligase for degradation of extracellular targets

Membrane proteins, which comprise 23% of encoded genes, pose challenges for PROTAC-based targeting due to the requirement of cytosolic binding domains for small molecule ligands.¹⁶⁶ However, advancements in large molecule-based degradation technologies such as LYTACs,¹⁷³ AbTACs,¹²⁷ and PROTABs¹²⁸ have demonstrated the potential of large molecules in targeted protein degradation. Of particular interest are the E3 ubiquitin ligase targeting approaches of AbTACs and PROTABs, which utilize bispecific antibodies targeting both the receptor of interest and the RNF43 receptor to facilitate degradation of the protein of interest (POI). In this study, a modular approach based on enzymatic conjugation was used for the modular generation of antibody-based degraders. Following the successful two-step conjugation and subsequent purification, the physicochemical properties of the parental antibodies and their conjugates were investigated, including antigen binding, cell receptor binding, and biological activity.

The ability of antibodies to bind antigens was confirmed through binding kinetics measured using BLI. The conjugate Ttz.1-scFv5+3 and the control molecules Ttz and RNF43 binding full-length antibody were evaluated for their affinity towards soluble recombinant antigens. The affinity of the scFv-antibody conjugate Ttz.1-scFv5+3 for soluble recombinant antigens was measured in the nanomolar range, with single-digit nanomolar affinity observed for rhHER2 binding and double-digit nanomolar affinity for rhRNF43 binding. Conjugation did not significantly impact the binding to soluble antigens, as the control molecules Ttz and RNF43-binding full-length antibody also showed nanomolar-range binding affinities. Although a reduction in binding affinity in the single

digit nanomolar range was observed for rhRNF43 binding by the conjugate compared to free scFv variants, this discrepancy could be attributed to the experimental setup in which the antigen was loaded onto biosensor tips and scFv was subsequently added. Existing studies have characterized the antigen binding of the scFv from Boontanrart *et al.* with an affinity of 4.2 nM,¹²⁶ while the binding constant of AbTAC, enabling successful PD-L1 degradation, was reported as 12.5 nM against RNF43.¹²⁷

Bispecific antibodies possess the capability to simultaneously bind multiple antigens. BLI experiments confirmed the association of RNF43 with immobilized bispecific scFv antibody conjugates and subsequent binding of HER2, indicating that both soluble antigens can be sterically accommodated. A recently published study critically examined the antibody-based detection of mainly endogenous RNF43.¹²⁴ The study discredited the absence of evaluation of the antibodies used in prior studies and revealed missing and false-positive signals of the antibodies tested in their experiments. This may have also impacted the underlying experiments.

Next, the binding of the bispecific scFv-antibody conjugates to cell lines with varying receptor surface expression levels was investigated. The binding to HER2 exhibited an expression-dependent pattern, correlating with the theoretical RNA levels. Conversely, there were minimal binding intensities observed with the tested RNF43-binding full-length antibodies, and the binding of the bispecific scFv-antibody conjugates was solely mediated by HER2 binding. These findings differ from previous studies where binding of the RNF43-binding antibody to specific epitopes in MDA-MB-231 cells was detected. Notably, the MDA-MB-231 cells examined in this study showed no detectable RNF43 receptor expression. It should be noted that a subsequent study reported a low frequency of RNF43 RNA transcripts in these cells, which nevertheless resulted in target degradation. Furthermore, the studies demonstrated that high affinities of RNF43 binders are not mandatory for successful targeted protein degradation and that degradation strongly depends on binding to the correct epitope and antibody formatting.¹⁷⁸

The final TPD efficiency studies in Western blot and flow cytometry showed degradation of the targets upon treatment with the bispecific scFv-antibody conjugates. Despite the absence of binding of the investigated RNF43 moiety in HEPG2 cells in flow cytometry assays, a maximum degradation of 89% was observed for Ttz.1-scFv5.3 to Ptz.1-scFv7.3 in Western blot. The experimental design was based on studies by Ahn *et al.* investigating HER2 degradation using Ptz and corresponding LYTACs in HEPG2 cells.¹⁷⁵ Notably, despite the different approaches between LYTACs and our approach, treatment with Ptz alone and Ptz.1-scFv7.3 showed similar degradation rates under the same treatment conditions. While Ahn *et al.* reported degradation rates of 76% and 38% for LYTAC and Ptz, respectively, this work observed HER2 degradation rates of 75% and 43% for Ptz.1-scFv7.3 and Ptz (Figure 31 (A) and (C)).

This demonstrates that the conjugates generated through two-step conjugation are capable of inducing lysosomal TPD. However, to make more precise statements, the extension of the data set with controls such as paired treatment of monospecific variants and isotype controls is necessary. Additionally, a comparison of the two HER2 epitopes targeted by Ttz and Ptz revealed that degradation levels can increase by up to 15% when Ttz is used instead of Ptz as antibody-based degrader. The conformational changes induced by the binding of Ttz could promote the interaction with RNF43 or enhance the process of internalization and subsequent degradation. The induction of protein degradation by Ttz itself is explained by the cross-linking of the HER2 receptor after mAb binding.¹⁰¹ The importance of the targeted epitope of the POI was also highlighted by Gramespacher *et al.*, who investigated various EGFR-binding antibodies targeting different epitopes of the receptor.¹⁷⁸

To compare the bispecific “knob-into-hole” molecules of the AbTAC and PROTAB approaches, the RNF43-binding scFv3 was conjugated to PD-L1-binding antibody Atz. The assay criteria were adapted based on the conditions described in the AbTAC publication.¹²⁷ Across three different PD-L1 overexpressing cell lines, Western blot analysis did not show a decrease in PD-L1 levels, and only a reduction of around 20% was observed in flow cytometry. This contrasts with the degradation efficiency reported by Cotton *et al.* for their AbTAC constructs, where a maximum PD-L1 degradation of 63% was observed after 24 hours of treatment.¹²⁷ The variability in degradation efficiency can be attributed to several factors, including the binding properties of the antibodies, the cell surface expression levels of the receptors, the stoichiometry of the E3 ligase, the kinetics of endocytosis upon antibody binding, the turnover rate of the POIs, or the specific E3 ligase being targeted.^{127, 128} The RNF43-binding scFv used in this study showed reduced PD-L1 degradation compared to the KIH approach described for AbTAC generation. Besides the binding of different epitopes, the conjugation of scFv to the C_H2 region of the heavy chain might lead to a greater distance between the two binders and thus inhibit degradation. This elongation of distance may allow targeting of receptors that are not directly neighboring and thus blocking degradation. The geometric limitation of antibody binding arms to membrane-anchored targets is approximately 9 nm,^{251, 252} restricting their interaction to the immediate vicinity and lateral diffusion of antigens within the membrane.²⁵³

Consequently, the successful degradation of the POI relies significantly on the interaction between RNF43 and the POI on the cell surface. The antibody format plays a central role in enabling efficient degradation.¹²⁸ This was observed in protein engineering studies where the influence of the distance between the bound antigen on the kinetics of ubiquitin transfer and degradation of the target was investigated using one-armed Fv-IgG formats.¹²⁸ Another strategy showed successful degradation of EGFR, PD-1 and erythropoietin receptor (EPOR) through the development of Receptor Elimination by E3 Ubiquitin Ligase Recruitment (REULR) molecules as

a VHH-based platform.¹²⁹ Based on the results of these studies and the conjugation strategy of the underlying work, expanding the conjugation platform to antibody fragments e.g. scFv-VHH or VHH-VHH conjugates is relatively straightforward and potentially enhances the target degradation. Furthermore, Gramespacher *et al.* studied the impact of orientation and valency on the degradation of PD-L1 using various antibody scaffolds.¹⁷⁸ They fused scFv molecules against PD-L1 with monospecific anti-RNF43 antibodies, either at the terminal ends of the mAb heavy chains or at the C-terminus of the light chain. The findings indicate that antibody formatting can affect degradation efficiency, and that bivalent IgG constructs with dual binding are effective for achieving higher efficacies.¹⁷⁸ Considering this, the careful selection of the conjugation site may enhance the degradation of the target.

In summary, the findings indicate that the conjugates generated through the two-step conjugation approach can induce lysosomal targeted protein degradation. However, additional controls, such as paired treatments with monospecific variants and isotype controls, are necessary to provide more precise and reliable evaluation. Furthermore, the choice of the targeted epitope plays a crucial role in the degradation efficiency, as certain epitopes may result in higher degradation rates due to their specific interaction with the receptor.

6 Conclusion

This study presents modular approaches to create bispecific antibody-protein conjugates for targeted delivery of PROTACs to specific cells and to act as antibody-based degraders. It demonstrates the successful assembly of bispecific antibodies through MTG-based direct conjugation of VHHs to antibodies. This approach enabled the selective delivery of PROTACs to cells. After successful conjugation of two G₃-MIC7 VHHs at two available sites in different commercially available antibodies, the remaining binding properties and PROTAC loading were demonstrated. In cellular assays, enhanced biological activity of the complexed antibody-shuttled PROTACs was observed, both in target degradation and cytotoxic activity on target receptor-expressing cell lines.

However, the transfer of the direct conjugation strategy of G₃-MIC7 VHH to a glycine-tagged RNF43-binding scFv variant was unsuccessful. This led to the introduction of a two-step conjugation approach to produce antibody-based degraders. The installation of azide and strained alkynes on scFv and antibody enabled successful SPAAC reaction, generating conjugates capable of inducing lysosomal targeted protein degradation. However, it also points out the necessity of including additional controls, such as paired treatments with monospecific variants and isotype controls, to ensure more accurate evaluation of the results.

Furthermore, the target epitope is important for the efficiency of degradation, as certain epitopes can lead to higher degradation rates due to their specific interaction with the receptor. In addition, the binding properties of the antibodies, the expression levels of the receptors on the cell surface and the stoichiometry of the E3 ligase, among other factors, are enormously important for the efficiency of degradation.¹²⁸ The potential influence of the distance between the binding sites due to the conjugation of scFv with the CH2 region of the antibody heavy chain is also a factor that can affect the degradation results.

Overall, the study has made progress in the development of antibody-based degraders and emphasizes the need for further research, consideration of various factors and controls, and precise and reliable evaluation process to fully assess the potential of antibody-based degraders. The work has demonstrated the generation of modular approaches to successfully create bispecific antibodies using chemoenzymatic strategies, offering potential applications beyond coupling two binders, such as coupling cytotoxic proteins. The coupling of cytotoxic proteins enables the separate expression of the antibody in mammalian cells and the toxin in bacteria or plant cells and the subsequent fusion. The non-covalent binding of PROTACs also extends the possibilities, which has already been shown in some approaches by non-covalent delivery of drugs.^{254,255}

References

- (1) Bertram, J. S. The Molecular Biology of Cancer. *Mol. Aspects Med.* **2001**, *21* (1), 167–223. [https://doi.org/10.1016/S0098-2997\(00\)00007-8](https://doi.org/10.1016/S0098-2997(00)00007-8).
- (2) Wild, C. P.; Weiderpass, E.; Stewart, B. W. *World Cancer Report: Cancer Research for Cancer Prevention*; 2020. <https://doi.org/10.1016/j.cma.2010.02.010>.
- (3) Dunn, G. P.; Old, L. J.; Schreiber, R. D. The Three Es of Cancer Immunoediting. *Annu. Rev. Immunol.* **2004**, *22* (1), 329–360. <https://doi.org/10.1146/annurev.immunol.22.012703.104803>.
- (4) Anand, U.; Dey, A.; Chandel, A. K. S.; Sanyal, R.; Mishra, A.; Pandey, D. K.; De Falco, V.; Upadhyay, A.; Kandimalla, R.; Chaudhary, A.; et al. Cancer Chemotherapy and beyond: Current Status, Drug Candidates, Associated Risks and Progress in Targeted Therapeutics. *Genes Dis.* **2023**, *10* (4), 1367–1401. <https://doi.org/10.1016/j.gendis.2022.02.007>.
- (5) Faguet, G. B. A Brief History of Cancer: Age-Old Milestones Underlying Our Current Knowledge Database. *Int. J. Cancer* **2015**, *136* (9), 2022–2036. <https://doi.org/10.1002/ijc.29134>.
- (6) Baskar, R.; Lee, K. A.; Yeo, R.; Yeoh, K. W. Cancer and Radiation Therapy: Current Advances and Future Directions. *Int. J. Med. Sci.* **2012**, *9* (3), 193–199. <https://doi.org/10.7150/ijms.3635>.
- (7) Arruebo, M.; Vilaboa, N.; Sáez-Gutierrez, B.; Lambea, J.; Tres, A.; Valladares, M.; González-Fernández, Á. Assessment of the Evolution of Cancer Treatment Therapies. *Cancers*. September 2011, pp 3279–3330. <https://doi.org/10.3390/cancers3033279>.
- (8) LI, M. C.; HERTZ, R.; BERGENSTAL, D. M. Therapy of Choriocarcinoma and Related Trophoblastic Tumors with Folic Acid and Purine Antagonists. *N. Engl. J. Med.* **1958**. <https://doi.org/10.1056/NEJM195807102590204>.
- (9) Shah, M. A.; Schwartz, G. K. Cyclin-Dependent Kinases as Targets for Cancer Therapy. *Cancer Chemother. Biol. Response Modif.* **2005**, *22*, 135–162. [https://doi.org/10.1016/s0921-4410\(04\)22007-5](https://doi.org/10.1016/s0921-4410(04)22007-5).
- (10) Chari, R. V. J.; Miller, M. L.; Widdison, W. C. Antibody-Drug Conjugates: An Emerging Concept in Cancer Therapy. *Angewandte Chemie - International Edition*. Wiley-VCH Verlag April 7, 2014, pp 3796–3827. <https://doi.org/10.1002/anie.201307628>.
- (11) Bashraheel, S. S.; Domling, A.; Goda, S. K. Update on Targeted Cancer Therapies, Single or in Combination, and Their Fine Tuning for Precision Medicine. *Biomed. Pharmacother.* **2020**, *125* (September 2019), 110009. <https://doi.org/10.1016/j.biopha.2020.110009>.
- (12) Sharma, S. K.; Bagshawe, K. D. Translating Antibody Directed Enzyme Prodrug Therapy (ADEPT) and Prospects for Combination. *Expert Opin. Biol. Ther.* **2017**, *17* (1), 1–13. <https://doi.org/10.1080/14712598.2017.1247802>.
- (13) Li, K.; Crews, C. M. PROTACs: Past, Present and Future. *Chem. Soc. Rev.* **2022**. <https://doi.org/10.1039/d2cs00193d>.
- (14) Aggarwal, D.; Yang, J.; Salam, M. A.; Sengupta, S.; Al-Amin, M. Y.; Mustafa, S.; Khan, M. A.; Huang, X.; Pawar, J. S. Antibody-Drug Conjugates: The Paradigm Shifts in the Targeted Cancer Therapy. *Front. Immunol.* **2023**, *14* (August), 1–13. <https://doi.org/10.3389/fimmu.2023.1203073>.
- (15) Murphy, K. T.; TRAVERS, P. P. & Walport, M.(2008) Janeway's Immunobiology, 7th Edn. Garland Science. Taylor & Francis Group LLC, New York, NY, USA.
- (16) Weiner, L. M.; Surana, R.; Wang, S. Monoclonal Antibodies: Versatile Platforms for Cancer Immunotherapy. *Nat. Rev. Immunol.* **2010**, *10* (5), 317–327. <https://doi.org/10.1038/nri2744>.
- (17) Natsume, A.; Niwa, R.; Satoh, M. Improving Effector Functions of Antibodies for Cancer Treatment: Enhancing ADCC and CDC. *Drug Des. Devel. Ther.* **2009**, No. 3, 7–16. <https://doi.org/10.2147/DDDT.S4378>.
- (18) Roopenian, D. C.; Akilesh, S. FcRn: The Neonatal Fc Receptor Comes of Age. *Nat. Rev.*

- Immunol.* **2007**, 7 (9), 715–725. <https://doi.org/10.1038/nri2155>.
- (19) Sanders, J.; Núñez Miguel, R.; Furmaniak, J.; Rees Smith, B. TSH Receptor Monoclonal Antibodies with Agonist, Antagonist, and Inverse Agonist Activities. *Methods Enzymol.* **2010**, 485 (C), 393–420. <https://doi.org/10.1016/B978-0-12-381296-4.00022-1>.
- (20) Goldstein, N. I.; Prewett, M.; Zuklys, K.; Rockwell, P.; Mendelsohn, J. Biological Efficacy of a Chimeric Antibody to the Epidermal Growth Factor Receptor in a Human Tumor Xenograft Model. *Clin. Cancer Res.* **1995**, 1 (11), 1311–1318.
- (21) Belyanskaya, L. L.; Marti, T. M.; Hopkins-Donaldson, S.; Kurtz, S.; Felley-Bosco, E.; Stahel, R. A. Human Agonistic TRAIL Receptor Antibodies Mapatumumab and Lexatumumab Induce Apoptosis in Malignant Mesothelioma and Act Synergistically with Cisplatin. *Mol. Cancer* **2007**, 6, 1–13. <https://doi.org/10.1186/1476-4598-6-66>.
- (22) Fu, Z.; Li, S.; Han, S.; Shi, C.; Zhang, Y. Antibody Drug Conjugate: The “Biological Missile” for Targeted Cancer Therapy. *Signal Transduction and Targeted Therapy*. Springer US 2022. <https://doi.org/10.1038/s41392-022-00947-7>.
- (23) Holliger, P.; Hudson, P. J. Engineered Antibody Fragments and the Rise of Single Domains. *Nat. Biotechnol.* **2005**, 23 (9), 1126–1136. <https://doi.org/10.1038/nbt1142>.
- (24) Whitlow, M.; Bell, B. A.; Feng, S. L.; Filpula, D.; Hardman, K. D.; Hubert, S. L.; Rollence, M. L.; Wood, J. F.; Schott, M. E.; Milenic, D. E.; et al. An Improved Linker for Single-Chain Fv with Reduced Aggregation and Enhanced Proteolytic Stability. *Protein Eng. Des. Sel.* **1993**, 6 (8), 989–995. <https://doi.org/10.1093/protein/6.8.989>.
- (25) Wilson, I. A.; Stanfield, R. L. Antibody-Antigen Interactions: New Structures and New Conformational Changes. *Curr. Opin. Struct. Biol.* **1994**, 4 (6), 857–867. [https://doi.org/10.1016/0959-440X\(94\)90267-4](https://doi.org/10.1016/0959-440X(94)90267-4).
- (26) Hamers-Casterman, Atarchouch, T.; Muyldermans, S.; Robinson, G.; Hamers, C.; Bajjana, E.; Bendahman, N.; Hamilton, R. Naturally Occurring Antibodies Devoid of Light Chains. *Nature* **1993**, 363 (June), 446–448. <https://doi.org/10.1038/363446a0>.
- (27) Streltsov, V. A.; Carmichael, J. A.; Nuttall, S. D. Structure of a Shark IgNAR Antibody Variable Domain and Modeling of an Early-developmental Isotype. *Protein Sci.* **2005**, 14 (11), 2901–2909. <https://doi.org/10.1110/ps.051709505>.
- (28) Dooley, H.; Flajnik, M. F. Shark Immunity Bites Back: Affinity Maturation and Memory Response in the Nurse Shark, *Ginglymostoma Cirratum*. *Eur. J. Immunol.* **2005**, 35 (3), 936–945. <https://doi.org/10.1002/eji.200425760>.
- (29) Zielonka, S.; Weber, N.; Becker, S.; Doerner, A.; Christmann, A.; Christmann, C.; Uth, C.; Fritz, J.; Schäfer, E.; Steinmann, B.; et al. Shark Attack: High Affinity Binding Proteins Derived from Shark VNAR Domains by Stepwise in Vitro Affinity Maturation. *J. Biotechnol.* **2014**, 191, 236–245. <https://doi.org/10.1016/j.jbiotec.2014.04.023>.
- (30) Vu, K. B.; Ghahroudi, M. A.; Wyns, L.; Muyldermans, S. Comparison of Llama V(H) Sequences from Conventional and Heavy Chain Antibodies. *Mol. Immunol.* **1997**, 34 (16–17), 1121–1131. [https://doi.org/10.1016/S0161-5890\(97\)00146-6](https://doi.org/10.1016/S0161-5890(97)00146-6).
- (31) Muyldermans, S.; Cambillau, C.; Wyns, L. Recognition of Antigens by Single-Domain Antibody Fragments: The Superfluous Luxury of Paired Domains. *Trends Biochem. Sci.* **2001**, 26 (4), 230–235. [https://doi.org/10.1016/S0968-0004\(01\)01790-X](https://doi.org/10.1016/S0968-0004(01)01790-X).
- (32) Davies, J.; Riechmann, L. “Camelising” Human Antibody Fragments: NMR Studies on VH Domains. *FEBS Lett.* **1994**, 339 (3), 285–290. [https://doi.org/10.1016/0014-5793\(94\)80432-X](https://doi.org/10.1016/0014-5793(94)80432-X).
- (33) Fernandes, C. F. C.; Pereira, S. dos S.; Luiz, M. B.; Zuiliani, J. P.; Furtado, G. P.; Stabeli, R. G. Camelid Single-Domain Antibodies as an Alternative to Overcome Challenges Related to the Prevention, Detection, and Control of Neglected Tropical Diseases. *Front. Immunol.* **2017**, 8 (JUN), 1–8. <https://doi.org/10.3389/fimmu.2017.00653>.
- (34) Kunz, P.; Ortale, A.; Mücke, N.; Zinner, K.; Hoheisel, J. D. Nanobody Stability Engineering by Employing the Δ tm Shift; A Comparison with Apparent Rate Constants of Heat-Induced Aggregation. *Protein Eng. Des. Sel.* **2019**, 32 (5), 241–249. <https://doi.org/10.1093/protein/gzz017>.

- (35) Kunz, P.; Zinner, K.; Mücke, N.; Bartoschik, T.; Muyldermans, S.; Hoheisel, J. D. The Structural Basis of Nanobody Unfolding Reversibility and Thermoresistance. *Sci. Rep.* **2018**, *8* (1), 1–10. <https://doi.org/10.1038/s41598-018-26338-z>.
- (36) Govaert, J.; Pellis, M.; Deschacht, N.; Vincke, C.; Conrath, K.; Muyldermans, S.; Saerens, D. Dual Beneficial Effect of Interloop Disulfide Bond for Single Domain Antibody Fragments. *J. Biol. Chem.* **2012**, *287* (3), 1970–1979. <https://doi.org/10.1074/jbc.M111.242818>.
- (37) Roberts, C. J. Therapeutic Protein Aggregation: Mechanisms, Design, and Control. *Trends Biotechnol.* **2014**, *32* (7), 372–380. <https://doi.org/10.1016/j.tibtech.2014.05.005>.
- (38) Ahmad, Z. A.; Yeap, S. K.; Ali, A. M.; Ho, W. Y.; Alitheen, N. B. M.; Hamid, M. ScFv Antibody: Principles and Clinical Application. *Clin. Dev. Immunol.* **2012**, *2012*. <https://doi.org/10.1155/2012/980250>.
- (39) Cortez-Retamozo, V.; Backmann, N.; Senter, P. D.; Wernery, U.; De Baetselier, P.; Muyldermans, S.; Revets, H. Efficient Cancer Therapy with a Nanobody-Based Conjugate. *Cancer Res.* **2004**, *64* (8), 2853–2857. <https://doi.org/10.1158/0008-5472.CAN-03-3935>.
- (40) Carter, P. J. Potent Antibody Therapeutics by Design. *Nat. Rev. Immunol.* **2006**, *6* (5), 343–357. <https://doi.org/10.1038/nri1837>.
- (41) Klein, C.; Brinkmann, U.; Reichert, J. M.; Kontermann, R. E. The Present and Future of Bispecific Antibodies for Cancer Therapy. *Nat. Rev. Drug Discov.* **2024**, *23* (April), 301–319. <https://doi.org/10.1038/s41573-024-00896-6>.
- (42) Ridgway, J. B. B.; Presta, L. G.; Carter, P. “Knobs-into-Holes” Engineering of Antibody C H 3 Domains for Heavy Chain Heterodimerization. *Protein Eng.* **1996**, *9* (7), 617–621. [https://doi.org/10.1016/1380-2933\(96\)80685-3](https://doi.org/10.1016/1380-2933(96)80685-3).
- (43) Schaefer, W.; Regula, J. T.; Bähner, M.; Schanzer, J.; Croasdale, R.; Dürr, H.; Gassner, C.; Georges, G.; Kettenberger, H.; Imhof-Jung, S.; et al. Immunoglobulin Domain Crossover as a Generic Approach for the Production of Bispecific IgG Antibodies. *Proc. Natl. Acad. Sci. U. S. A.* **2011**, *108* (27), 11187–11192. <https://doi.org/10.1073/pnas.1019002108>.
- (44) Lindhofer, H.; Mocikat, R.; Steipe, B.; Thierfelder, S. Preferential Species-Restricted Heavy Light-Chain Pairing in Rat Mouse Quadromas - Implications for a Single-Step Purification of Bispecific Antibodies. *J. Immunol.* **1995**, *155* (1), 219–225.
- (45) Kreudenstein, T. S. Von; Escobar-Carbrera, E.; Lario, P. I.; D’Angelo, I.; Brault, K.; Kelly, J.; Durocher, Y.; Baardsnes, J.; Jeremy Woods, R.; Xie, M. H.; et al. Improving Biophysical Properties of a Bispecific Antibody Scaffold to Aid Developability: Quality by Molecular Design. *MAbs* **2013**, *5* (5), 646–654. <https://doi.org/10.4161/mabs.25632>.
- (46) Staerz, U. D.; Kanagawa, O.; Bevan, M. J. Hybrid Antibodies Can Target Sites for Attack by T Cells. *Nature* **1985**, *314* (6012), 628–631. <https://doi.org/10.1038/314628a0>.
- (47) Walker, J. M. *Natural Killer Cells. Methods and Protocols*; 2016; Vol. 36.
- (48) Holliger, P.; Prospero, T.; Winter, G. “Diabodies”: Small Bivalent and Bispecific Antibody Fragments. *Proc. Natl. Acad. Sci. U. S. A.* **1993**, *90* (14), 6444–6448. <https://doi.org/10.1073/pnas.90.14.6444>.
- (49) Strebhardt, K.; Ullrich, A. Paul Ehrlich’s Magic Bullet Concept: 100 Years of Progress. *Nat. Rev. Cancer* **2008**, *8* (6), 473–480. <https://doi.org/10.1038/nrc2394>.
- (50) Tsuchikama, K.; An, Z. Antibody-Drug Conjugates: Recent Advances in Conjugation and Linker Chemistries. *Protein Cell* **2018**, *9* (1), 33–46. <https://doi.org/10.1007/s13238-016-0323-0>.
- (51) Kim, M. T.; Chen, Y.; Marhoul, J.; Jacobson, F. Statistical Modeling of the Drug Load Distribution on Trastuzumab Emtansine (Kadcyla), a Lysine-Linked Antibody Drug Conjugate. *Bioconjug. Chem.* **2014**. <https://doi.org/10.1021/bc5000109>.
- (52) Jackson, D. Y. Processes for Constructing Homogeneous Antibody Drug Conjugates. *Org. Process Res. Dev.* **2016**, *20* (5), 852–866. <https://doi.org/10.1021/acs.oprd.6b00067>.
- (53) Shen, B. Q.; Xu, K.; Liu, L.; Raab, H.; Bhakta, S.; Kenrick, M.; Parsons-Reponte, K. L.; Tien, J.; Yu, S. F.; Mai, E.; et al. Conjugation Site Modulates the in Vivo Stability and Therapeutic Activity of Antibody-Drug Conjugates. *Nat. Biotechnol.* **2012**, *30* (2), 184–189. <https://doi.org/10.1038/nbt.2108>.

- (54) Junutula, J. R.; Raab, H.; Clark, S.; Bhakta, S.; Leipold, D. D.; Weir, S.; Chen, Y.; Simpson, M.; Tsai, S. P.; Dennis, M. S.; et al. Site-Specific Conjugation of a Cytotoxic Drug to an Antibody Improves the Therapeutic Index. *Nat. Biotechnol.* **2008**, *26* (8), 925–932. <https://doi.org/10.1038/nbt.1480>.
- (55) Zimmerman, E. S.; Heibeck, T. H.; Gill, A.; Li, X.; Murray, C. J.; Madlansacay, M. R.; Tran, C.; Uter, N. T.; Yin, G.; Rivers, P. J.; et al. Production of Site-Specific Antibody-Drug Conjugates Using Optimized Non-Natural Amino Acids in a Cell-Free Expression System. *Bioconjug. Chem.* **2014**, *25* (2), 351–361. <https://doi.org/10.1021/bc400490z>.
- (56) Van Geel, R.; Wijdeven, M. A.; Heesbeen, R.; Verkade, J. M. M.; Wasielec, A. A.; Van Berkel, S. S.; Van Delft, F. L. Chemoenzymatic Conjugation of Toxic Payloads to the Globally Conserved N-Glycan of Native MAbs Provides Homogeneous and Highly Efficacious Antibody-Drug Conjugates. *Bioconjug. Chem.* **2015**, *26* (11), 2233–2242. <https://doi.org/10.1021/acs.bioconjchem.5b00224>.
- (57) Kolb, H. C.; Finn, M. G.; Sharpless, K. B. Click Chemistry: Diverse Chemical Function from a Few Good Reactions. *Angew. Chemie - Int. Ed.* **2001**, *40* (11), 2004–2021. [https://doi.org/10.1002/1521-3773\(20010601\)40:11<2004::AID-ANIE2004>3.0.CO;2-5](https://doi.org/10.1002/1521-3773(20010601)40:11<2004::AID-ANIE2004>3.0.CO;2-5).
- (58) Rostovtsev, V. V.; Green, L. G.; Fokin, V. V.; Sharpless, K. B. A Stepwise Huisgen Cycloaddition Process: Copper(I)-Catalyzed Regioselective “Ligation” of Azides and Terminal Alkynes. *Angew. Chemie - Int. Ed.* **2002**, *41* (14), 2596–2599. [https://doi.org/10.1002/1521-3773\(20020715\)41:14<2596::AID-ANIE2596>3.0.CO;2-4](https://doi.org/10.1002/1521-3773(20020715)41:14<2596::AID-ANIE2596>3.0.CO;2-4).
- (59) Worrell, B. T.; Malik, J. A.; Fokin, V. V. Direct Evidence of a Dinuclear Copper Intermediate in Cu(I)-Catalyzed Azide-Alkyne Cycloadditions. *Science (80-.)*. **2013**, *340* (6131), 457–460. <https://doi.org/10.1126/science.1229506>.
- (60) Li, Z.; Seo, T. S.; Ju, J. 1,3-Dipolar Cycloaddition of Azides with Electron-Deficient Alkynes under Mild Condition in Water. *Tetrahedron Lett.* **2004**, *45* (15), 3143–3146. <https://doi.org/10.1016/j.tetlet.2004.02.089>.
- (61) Agard, N. J.; Baskin, J. M.; Prescher, J. A.; Lo, A.; Bertozzi, C. R. A Comparative Study of Bioorthogonal Reactions with Azides. *ACS Chem. Biol.* **2006**, *1* (10), 644–648. <https://doi.org/10.1021/cb6003228>.
- (62) Kim, E.; Koo, H. Biomedical Applications of Copper-Free Click Chemistry: In Vitro, in Vivo, and Ex Vivo. *Chem. Sci.* **2019**, *10* (34), 7835–7851. <https://doi.org/10.1039/c9sc03368h>.
- (63) Davis, D. L.; Price, E. K.; Aderibigbe, S. O.; Larkin, M. X. H.; Barlow, E. D.; Chen, R.; Ford, L. C.; Gray, Z. T.; Gren, S. H.; Jin, Y.; et al. Effect of Buffer Conditions and Organic Cosolvents on the Rate of Strain-Promoted Azide-Alkyne Cycloaddition. *J. Org. Chem.* **2016**, *81* (15), 6816–6819. <https://doi.org/10.1021/acs.joc.6b01112>.
- (64) Gordon, C. G.; MacKey, J. L.; Jewett, J. C.; Sletten, E. M.; Houk, K. N.; Bertozzi, C. R. Reactivity of Biarylazacyclooctynones in Copper-Free Click Chemistry. *J. Am. Chem. Soc.* **2012**, *134* (22), 9199–9208. <https://doi.org/10.1021/ja3000936>.
- (65) Debets, M. F.; Van Berkel, S. S.; Dommerholt, J.; Dirks, A. J.; Rutjes, F. P. J. T.; Van Delft, F. L. Bioconjugation with Strained Alkenes and Alkynes. *Acc. Chem. Res.* **2011**, *44* (9), 805–815. <https://doi.org/10.1021/ar200059z>.
- (66) Zotzel, J.; Pasternack, R.; Pelzer, C.; Ziegert, D.; Mainusch, M.; Fuchsbauer, H. L. Activated Transglutaminase from *Streptomyces Mobaraensis* Is Processed by a Tripeptidyl Aminopeptidase in the Final Step. *Eur. J. Biochem.* **2003**, *270* (20), 4149–4155. <https://doi.org/10.1046/j.1432-1033.2003.03809.x>.
- (67) Juettner, N. E.; Schmelz, S.; Bogen, J. P.; Happel, D.; Fessner, W. D.; Pfeifer, F.; Fuchsbauer, H. L.; Scrima, A. Illuminating Structure and Acyl Donor Sites of a Physiological Transglutaminase Substrate from *Streptomyces Mobaraensis*. *Protein Sci.* **2018**, *27* (5), 910–922. <https://doi.org/10.1002/pro.3388>.
- (68) Kashiwagi, T.; Yokoyama, K. ichi; Ishikawa, K.; Ono, K.; Ejima, D.; Matsui, H.; Suzuki, E. ichiro. Crystal Structure of Microbial Transglutaminase from *Streptoverticillium Mobaraense*. *J. Biol. Chem.* **2002**, *277* (46), 44252–44260. <https://doi.org/10.1074/jbc.M203933200>.
- (69) Ando, H.; Adachi, M.; Umeda, K.; Matsuura, A.; Nonaka, M.; Uchio, R.; Tanaka, H.; Motoki, M.

- Purification and Characteristics of a Novel Transglutaminase Derived from Microorganisms. *Agric. Biol. Chem.* **1989**, *53* (10), 2613–2617. <https://doi.org/10.1080/00021369.1989.10869735>.
- (70) Juettner, N. E.; Schmelz, S.; Kraemer, A.; Knapp, S.; Becker, B.; Kolmar, H.; Scrima, A.; Fuchsbaauer, H. L. Structure of a Glutamine Donor Mimicking Inhibitory Peptide Shaped by the Catalytic Cleft of Microbial Transglutaminase. *FEBS J.* **2018**, *285* (24), 4684–4694. <https://doi.org/10.1111/febs.14678>.
- (71) Sugimura, Y.; Yokoyama, K.; Nio, N.; Maki, M.; Hitomi, K. Identification of Preferred Substrate Sequences of Microbial Transglutaminase from *Streptomyces Mobaraensis* Using a Phage-Displayed Peptide Library. *Arch. Biochem. Biophys.* **2008**, *477* (2), 379–383. <https://doi.org/10.1016/j.abb.2008.06.014>.
- (72) Deweid, L.; Avrutina, O.; Kolmar, H. Microbial Transglutaminase for Biotechnological and Biomedical Engineering. *Biol. Chem.* **2018**. <https://doi.org/10.1515/hsz-2018-0335>.
- (73) Strop, P. Versatility of Microbial Transglutaminase. *Bioconjug. Chem.* **2014**, *25* (5), 855–862. <https://doi.org/10.1021/bc500099v>.
- (74) Siegmund, V.; Schmelz, S.; Dickgiesser, S.; Beck, J.; Ebenig, A.; Fittler, H.; Frauendorf, H.; Piater, B.; Betz, U. A. K.; Avrutina, O.; et al. Locked by Design: A Conformationally Constrained Transglutaminase Tag Enables Efficient Site-Specific Conjugation. *Angew. Chemie - Int. Ed.* **2015**, *54* (45), 13420–13424. <https://doi.org/10.1002/anie.201504851>.
- (75) Strop, P.; Liu, S. H.; Dorywalska, M.; Delaria, K.; Dushin, R. G.; Tran, T. T.; Ho, W. H.; Farias, S.; Casas, M. G.; Abdiche, Y.; et al. Location Matters: Site of Conjugation Modulates Stability and Pharmacokinetics of Antibody Drug Conjugates. *Chem. Biol.* **2013**. <https://doi.org/10.1016/j.chembiol.2013.01.010>.
- (76) Jeger, S.; Zimmermann, K.; Blanc, A.; Grünberg, J.; Honer, M.; Hunziker, P.; Struthers, H.; Schibli, R. Site-Specific and Stoichiometric Modification of Antibodies by Bacterial Transglutaminase. *Angew. Chemie - Int. Ed.* **2010**, *49* (51), 9995–9997. <https://doi.org/10.1002/anie.201004243>.
- (77) Benjamin, S. R.; Jackson, C. P.; Fang, S.; Carlson, D. P.; Guo, Z.; Tumey, L. N. Thiolation of Q295: Site-Specific Conjugation of Hydrophobic Payloads without the Need for Genetic Engineering. *Mol. Pharm.* **2019**, *16* (6), 2795–2807. <https://doi.org/10.1021/acs.molpharmaceut.9b00323>.
- (78) Dickgiesser, S.; Rieker, M.; Mueller-Pompalla, D.; Schröter, C.; Tonillo, J.; Warszawski, S.; Raab-Westphal, S.; Kühn, S.; Knehans, T.; Könnig, D.; et al. Site-Specific Conjugation of Native Antibodies Using Engineered Microbial Transglutaminases. *Bioconjug. Chem.* **2020**, *31* (4), 1070–1076. <https://doi.org/10.1021/acs.bioconjchem.0c00061>.
- (79) NISONOFF, A.; RIVERS, M. M. Recombination Antibody of a Mixture of Univalent Fragments of Different Specificity. *Arch. Biochem. Biophys.* **1961**, *2* (93), 460–462. [https://doi.org/10.1016/0003-9861\(61\)90296-x](https://doi.org/10.1016/0003-9861(61)90296-x).
- (80) Langer, H. F.; Von Der Ruhr, J. W.; Daub, K.; Schoenberger, T.; Stellos, K.; May, A. E.; Schnell, H.; Gau, A.; Hafner, R.; Lang, P.; et al. Capture of Endothelial Progenitor Cells by a Bispecific Protein/Monoclonal Antibody Molecule Induces Reendothelialization of Vascular Lesions. *J. Mol. Med.* **2010**, *88* (7), 687–699. <https://doi.org/10.1007/s00109-010-0614-5>.
- (81) Szijj, P.; Chudasama, V. The Renaissance of Chemically Generated Bispecific Antibodies. *Nat. Rev. Chem.* **2021**. <https://doi.org/10.1038/s41570-020-00241-6>.
- (82) Smith, M. E. B.; Schumacher, F. F.; Ryan, C. P.; Tedaldi, L. M.; Papaioannou, D.; Waksman, G.; Caddick, S.; Baker, J. R. Protein Modification, Bioconjugation, and Disulfide Bridging Using Bromomaleimides. *J. Am. Chem. Soc.* **2010**, *132* (6), 1960–1965. <https://doi.org/10.1021/ja908610s>.
- (83) Patterson, J. T.; Gros, E.; Zhou, H.; Atassi, G.; Kerwin, L.; Carmody, L.; Zhu, T.; Jones, B.; Fu, Y.; Kaufmann, G. F. Chemically Generated IgG2 Bispecific Antibodies through Disulfide Bridging. *Bioorganic Med. Chem. Lett.* **2017**, *27* (16), 3647–3652. <https://doi.org/10.1016/j.bmcl.2017.07.021>.
- (84) Kim, C. H.; Axup, J. Y.; Dubrowska, A.; Kazane, S. A.; Hutchins, B. A.; Wold, E. D.; Smider, V. V.;

- Schultz, P. G. Synthesis of Bispecific Antibodies Using Genetically Encoded Unnatural Amino Acids. *J. Am. Chem. Soc.* **2012**, *134* (24), 9918–9921. <https://doi.org/10.1021/ja303904e>.
- (85) Fujii, T.; Ito, K.; Takahashi, K.; Aoki, T.; Takasugi, R.; Seki, T.; Iwai, Y.; Watanabe, T.; Hiramata, R.; Tsumura, R.; et al. Bispecific Antibodies Produced via Chemical Site-Specific Conjugation Technology: AJICAP Second-Generation. *ACS Med. Chem. Lett.* **2023**. <https://doi.org/10.1021/acsmchemlett.3c00414>.
- (86) Wagner, K.; Kwakkenbos, M. J.; Claassena, Y. B.; Maijor, K.; Böhne, M.; Van Der Sluijs, K. F.; Witte, M. D.; Van Zoelen, D. J.; Cornelissen, L. A.; Beaumont, T.; et al. Bispecific Antibody Generated with Sortase and Click Chemistry Has Broad Antiinfluenza Virus Activity. *Proc. Natl. Acad. Sci. U. S. A.* **2014**, *111* (47), 16820–16825. <https://doi.org/10.1073/pnas.1408605111>.
- (87) Baalman, M.; Neises, L.; Bitsch, S.; Schneider, H.; Deweid, L.; Werther, P.; Ilkenhans, N.; Wolfring, M.; Ziegler, M. J.; Wilhelm, J.; et al. A Bioorthogonal Click Chemistry Toolbox for Targeted Synthesis of Branched and Well-Defined Protein–Protein Conjugates. *Angew. Chemie* **2020**, *132* (31), 12985–12993. <https://doi.org/10.1002/ange.201915079>.
- (88) Prenzel, N.; Fischer, O. M.; Streit, S.; Hart, S.; Ullrich, A. The Epidermal Growth Factor Receptor Family as a Central Element for Cellular Signal Transduction and Diversification. *Endocr. Relat. Cancer* **2001**, *8* (1), 11–31. <https://doi.org/10.1677/erc.0.0080011>.
- (89) Pawson, T.; Scott, J. D. Signaling through Scaffold, Anchoring, and Adaptor Proteins. *Science (80-.)*. **1997**, *278* (5346), 2075–2080. <https://doi.org/10.1126/science.278.5346.2075>.
- (90) Yarden, Y.; Sliwkowski, X. M. Untangling the ErbB Signalling Network. *Nat. Rev. Mol. Cell Biol.* **2001**, *2* (February), 127–137. <https://doi.org/10.1038/35052073>.
- (91) Martinelli, E.; De Palma, R.; Orditura, M.; De Vita, F.; Ciardiello, F. Anti-Epidermal Growth Factor Receptor Monoclonal Antibodies in Cancer Therapy. *Clin. Exp. Immunol.* **2009**, *158* (1), 1–9. <https://doi.org/10.1111/j.1365-2249.2009.03992.x>.
- (92) Perrotte, P.; Matsumoto, T.; Inoue, K.; Kuniyasu, H.; Eve, B. Y.; Hicklin, D. J.; Radinsky, R.; Dinney, C. P. N. Anti-Epidermal Growth Factor Receptor Antibody C225 Inhibits Angiogenesis in Human Transitional Cell Carcinoma Growing Orthotopically in Nude Mice. *Clin. Cancer Res.* **1999**, *5* (2), 257–265.
- (93) Thienelt, C. D.; Bunn, P. A.; Hanna, N.; Rosenberg, A.; Needle, M. N.; Long, M. E.; Gustafson, D. L.; Kelly, K. Multicenter Phase I/II Study of Cetuximab with Paclitaxel and Carboplatin in Untreated Patients with Stage IV Non-Small-Cell Lung Cancer. *J. Clin. Oncol.* **2005**, *23* (34), 8786–8793. <https://doi.org/10.1200/JCO.2005.03.1997>.
- (94) Bourhis, J.; Rivera, F.; Mesia, R.; Awada, A.; Geoffrois, L.; Borel, C.; Humblet, Y.; Lopez-Pousa, A.; Hitt, R.; Villegas, M. E. V.; et al. Phase I/II Study of Cetuximab in Combination with Cisplatin or Carboplatin and Fluorouracil in Patients with Recurrent or Metastatic Squamous Cell Carcinoma of the Head and Neck. *J. Clin. Oncol.* **2006**, *24* (18), 2866–2872. <https://doi.org/10.1200/JCO.2005.04.3547>.
- (95) Cunningham, D.; Humblet, Y.; Siena, S.; Khayat, D.; Bleiberg, H.; Santoro, A.; Bets, D.; Mueser, M.; Harstrick, A.; Verslype, C.; et al. Cetuximab Monotherapy and Cetuximab plus Irinotecan in Irinotecan-Refractory Metastatic Colorectal Cancer. *N. Engl. J. Med.* **2004**, *351* (4), 337–345. <https://doi.org/10.1056/nejmoa033025>.
- (96) Burtneß, B.; Harrington, K. J.; Greil, R.; Soulières, D.; Tahara, M.; de Castro, G.; Psyrris, A.; Basté, N.; Neupane, P.; Bratland, Å.; et al. Pembrolizumab Alone or with Chemotherapy versus Cetuximab with Chemotherapy for Recurrent or Metastatic Squamous Cell Carcinoma of the Head and Neck (KEYNOTE-048): A Randomised, Open-Label, Phase 3 Study. *Lancet* **2019**, *394* (10212), 1915–1928. [https://doi.org/10.1016/S0140-6736\(19\)32591-7](https://doi.org/10.1016/S0140-6736(19)32591-7).
- (97) García-Foncillas, J.; Sunakawa, Y.; Aderka, D.; Wainberg, Z.; Ronga, P.; Witzler, P.; Stintzing, S. Distinguishing Features of Cetuximab and Panitumumab in Colorectal Cancer and Other Solid Tumors. *Front. Oncol.* **2019**, *9* (September), 1–16. <https://doi.org/10.3389/fonc.2019.00849>.

- (98) Bourhis, J.; Stein, A.; Paul de Boer, J.; Van Den Eynde, M.; Gold, K. A.; Stintzing, S.; Becker, J. C.; Moran, M.; Schroeder, A.; Pennock, G.; et al. Avelumab and Cetuximab as a Therapeutic Combination: An Overview of Scientific Rationale and Current Clinical Trials in Cancer. *Cancer Treat. Rev.* **2021**, *97*, 102172. <https://doi.org/10.1016/j.ctrv.2021.102172>.
- (99) Oh, D. Y.; Bang, Y. J. HER2-Targeted Therapies — a Role beyond Breast Cancer. *Nat. Rev. Clin. Oncol.* **2020**, *17* (1), 33–48. <https://doi.org/10.1038/s41571-019-0268-3>.
- (100) Clynes, R. A.; Towers, T. L.; Presta, L. G.; Ravetch, J. V. Inhibitory Fc Receptors Modulate in Vivo Cytotoxicity against Tumor Targets. *Nat. Med.* **2000**, *6* (4), 443–446. <https://doi.org/10.1038/74704>.
- (101) Franklin, M.; KD, C.; FF, V.; DJ, L.; de Vos AM; MX, S. Insights into ErbB Signaling from the Structure of the ErbB2-Pertuzumab Complex. *Cancer Cell* **2004**, *5* (April), 317–328. [https://doi.org/doi.org/10.1016/s1535-6108\(04\)00083-2](https://doi.org/doi.org/10.1016/s1535-6108(04)00083-2).
- (102) Baselga, J.; Cortés, J.; Kim, S.-B.; Im, S.-A.; Hegg, R.; Im, Y.-H.; Roman, L.; Pedrini, J. L.; Pienkowski, T.; Knott, A.; et al. Pertuzumab plus Trastuzumab plus Docetaxel for Metastatic Breast Cancer. *N Engl J Med* **2012**, *366* (2), 165–167. <https://doi.org/10.1056/NEJMoa1113216>.
- (103) Keam, S. J. Trastuzumab Deruxtecan: First Approval. *Drugs* **2020**, *80* (5), 501–508. <https://doi.org/10.1007/s40265-020-01281-4>.
- (104) Cortés, J.; Kim, S.-B.; Chung, W.-P.; Im, S.-A.; Park, Y. H.; Hegg, R.; Kim, M. H.; Tseng, L.-M.; Petry, V.; Chung, C.-F.; et al. Trastuzumab Deruxtecan versus Trastuzumab Emtansine for Breast Cancer. *N. Engl. J. Med.* **2022**, *386* (12), 1143–1154. <https://doi.org/10.1056/nejmoa2115022>.
- (105) Jiang, Y.; Chen, M.; Nie, H.; Yuan, Y. PD-1 and PD-L1 in Cancer Immunotherapy: Clinical Implications and Future Considerations. *Hum. Vaccines Immunother.* **2019**, *15* (5), 1111–1122. <https://doi.org/10.1080/21645515.2019.1571892>.
- (106) Sarvaria, A.; Madrigal, J. A.; Saudemont, A. B Cell Regulation in Cancer and Anti-Tumor Immunity. *Cell. Mol. Immunol.* **2017**, *14* (8), 662–674. <https://doi.org/10.1038/cmi.2017.35>.
- (107) Labani-Motlagh, A.; Ashja-Mahdavi, M.; Loskog, A. The Tumor Microenvironment: A Milieu Hindering and Obstructing Antitumor Immune Responses. *Front. Immunol.* **2020**, *11* (May), 1–22. <https://doi.org/10.3389/fimmu.2020.00940>.
- (108) Benicky, J.; Sanda, M.; Kennedy, Z. B.; Grant, O. C.; Woods, R. J.; Zwart, A.; Goldman, R.; Kulikov, A.; Shipaeva, E.; Dmitrieva, A.; et al. Preclinical Characterization of a Novel Anti-Cancer PD-L1 Inhibitor RPH-120. *Front. Pharmacol.* **2021**, *12* (August), 1–10. <https://doi.org/10.3389/fphar.2021.723038>.
- (109) Benicky, J.; Sanda, M.; Kennedy, Z. B.; Grant, O. C.; Woods, R. J.; Zwart, A.; Goldman, R. PD-L1 Glycosylation and Its Impact on Binding to Clinical Antibodies. *J. Proteome Res.* **2021**, *20* (1), 485–497. <https://doi.org/10.1021/acs.jproteome.0c00521>.
- (110) Xiao, D.; Luo, L.; Li, J.; Wang, Z.; Liu, L.; Xie, F.; Feng, J.; Zhou, X. Development of Bifunctional Anti-PD-L1 Antibody MMAE Conjugate with Cytotoxicity and Immunostimulation. *Bioorg. Chem.* **2021**, *116* (September), 105366. <https://doi.org/10.1016/j.bioorg.2021.105366>.
- (111) McDermott, D. F.; Sosman, J. A.; Sznol, M.; Massard, C.; Gordon, M. S.; Hamid, O.; Powderly, J. D.; Infante, J. R.; Fassò, M.; Wang, Y. V.; et al. Atezolizumab, an Anti-Programmed Death-Ligand 1 Antibody, in Metastatic Renal Cell Carcinoma: Long-Term Safety, Clinical Activity, and Immune Correlates from a Phase Ia Study. *J. Clin. Oncol.* **2016**, *34* (8), 833–842. <https://doi.org/10.1200/JCO.2015.63.7421>.
- (112) Chen, Y.; Pei, Y.; Luo, J.; Huang, Z.; Yu, J.; Meng, X. Looking for the Optimal PD-1/PD-L1 Inhibitor in Cancer Treatment: A Comparison in Basic Structure, Function, and Clinical Practice. *Front. Immunol.* **2020**, *11* (May). <https://doi.org/10.3389/fimmu.2020.01088>.
- (113) Hao, H. X.; Xie, Y.; Zhang, Y.; Zhang, O.; Oster, E.; Avello, M.; Lei, H.; Mickanin, C.; Liu, D.; Ruffner, H.; et al. ZNRF3 Promotes Wnt Receptor Turnover in an R-Spondin-Sensitive Manner. *Nature* **2012**, *485* (7397), 195–202. <https://doi.org/10.1038/nature11019>.
- (114) Tsukiyama, T.; Fukui, A.; Terai, S.; Fujioka, Y.; Shinada, K.; Takahashi, H.; Yamaguchi, T. P.;

- Ohba, Y.; Hatakeyama, S. Molecular Role of RNF43 in Canonical and Noncanonical Wnt Signaling. *Mol. Cell. Biol.* **2015**, *35* (11), 2007–2023. <https://doi.org/10.1128/mcb.00159-15>.
- (115) Koo, B. K.; Spit, M.; Jordens, I.; Low, T. Y.; Stange, D. E.; Van De Wetering, M.; Van Es, J. H.; Mohammed, S.; Heck, A. J. R.; Maurice, M. M.; et al. Tumour Suppressor RNF43 Is a Stem-Cell E3 Ligase That Induces Endocytosis of Wnt Receptors. *Nature* **2012**, *488* (7413), 665–669. <https://doi.org/10.1038/nature11308>.
- (116) Zebisch, M.; Jones, E. Y. ZNRF3/RNF43 - A Direct Linkage of Extracellular Recognition and E3 Ligase Activity to Modulate Cell Surface Signalling. *Prog. Biophys. Mol. Biol.* **2015**, *118* (3), 112–118. <https://doi.org/10.1016/j.pbiomolbio.2015.04.006>.
- (117) Luca, V. C.; Miao, Y.; Li, X.; Hollander, M. J.; Kuo, C. J.; Christopher Garcia, K. Surrogate R-Spondins for Tissue-Specific Potentiation of Wnt Signaling. *PLoS One* **2020**, *15* (1), 1–14. <https://doi.org/10.1371/journal.pone.0226928>.
- (118) Mukai, A.; Yamamoto-Hino, M.; Awano, W.; Watanabe, W.; Komada, M.; Goto, S. Balanced Ubiquitylation and Deubiquitylation of Frizzled Regulate Cellular Responsiveness to Wg/Wnt. *EMBO J.* **2010**, *29* (13), 2114–2125. <https://doi.org/10.1038/emboj.2010.100>.
- (119) Giannakis, M.; Hodis, E.; Jasmine Mu, X.; Yamauchi, M.; Rosenbluh, J.; Cibulskis, K.; Saksena, G.; Lawrence, M. S.; Qian, Z. R.; Nishihara, R.; et al. RNF43 Is Frequently Mutated in Colorectal and Endometrial Cancers. *Nat. Genet.* **2014**, *46* (12), 1264–1266. <https://doi.org/10.1038/ng.3127>.
- (120) Hao, H. X.; Jiang, X.; Cong, F. Control of Wnt Receptor Turnover by R-Spondin-ZNRF3/RNF43 Signaling Module and Its Dysregulation in Cancer. *Cancers (Basel)*. **2016**, *8* (6), 1–12. <https://doi.org/10.3390/cancers8060054>.
- (121) Glinka, A.; Dolde, C.; Kirsch, N.; Huang, Y. L.; Kazanskaya, O.; Ingelfinger, D.; Boutros, M.; Cruciat, C. M.; Niehrs, C. LGR4 and LGR5 Are R-Spondin Receptors Mediating Wnt/ β -Catenin and Wnt/PCP Signalling. *EMBO Rep.* **2011**, *12* (10), 1055–1061. <https://doi.org/10.1038/embor.2011.175>.
- (122) Zebisch, M.; Xu, Y.; Krastev, C.; Macdonald, B. T.; Chen, M.; Gilbert, R. J. C.; He, X.; Jones, E. Y. Structural and Molecular Basis of ZNRF3/RNF43 Transmembrane Ubiquitin Ligase Inhibition by the Wnt Agonist R-Spondin. *Nat. Commun.* **2013**, *4*. <https://doi.org/10.1038/ncomms3787>.
- (123) MacDonald, B. T.; Tamai, K.; He, X. Wnt/ β -Catenin Signaling: Components, Mechanisms, and Diseases. *Dev. Cell* **2009**, *17* (1), 9–26. <https://doi.org/10.1016/j.devcel.2009.06.016>.
- (124) Li, S.; Zhang, R.; Lavrijsen, M.; Van Den Bosch, T. P. P.; Peppelenbosch, M. P.; Smits, R. Issues with RNF43 Antibodies to Reliably Detect Intracellular Location. *PLoS One* **2023**, *18* (4 April), 1–16. <https://doi.org/10.1371/journal.pone.0283894>.
- (125) Pedersen, K. S.; Johanna, A. M.; Cercek, A.; Ulahannan, S.; Rossi, M.; Fong, A.; Brickman, D.; Bendell, J. Abstract CT167: First-in-Human Clinical Trial of SC-006, a RNF43 Targeted Antibody-Drug Conjugate, as a Monotherapy and in Combination with Budigalimab in Patients with Advanced Colorectal Cancer. *Cancer Res.* **2020**, *80* (CT167). <https://doi.org/10.1158/1538-7445.AM2020-CT167>.
- (126) Boontanart, M.; Rokkam, D.; Dylla, S. J.; Aujay, M. Novel Anti-Rnf43 Antibodies and Methods of Use. WO2015164392, 2015.
- (127) Cotton, A. D.; Nguyen, D. P.; Gramespacher, J. A.; Seiple, I. B.; Wells, J. A. Development of Antibody-Based PROTACs for the Degradation of the Cell-Surface Immune Checkpoint Protein PD-L1. *J. Am. Chem. Soc.* **2021**, *143* (2), 593–598. <https://doi.org/10.1021/jacs.0c10008>.
- (128) Marei, H.; Tsai, W.-T. K.; Kee, Y.-S.; Ruiz, K.; He, J.; Cox, C.; Sun, T.; Penikalapati, S.; Dwivedi, P.; Choi, M.; et al. Antibody Targeting of E3 Ubiquitin Ligases for Receptor Degradation. *Nature* **2022**, No. November 2021. <https://doi.org/10.1038/s41586-022-05235-6>.
- (129) Siepe, D. H.; Picton, L. K.; Garcia, K. C. Receptor Elimination by E3 Ubiquitin Ligase Recruitment (REULR): A Targeted Protein Degradation Toolbox. *ACS Synth. Biol.* **2023**, *12* (4), 1081–1093. <https://doi.org/10.1021/acssynbio.2c00587>.

- (130) Ciechanover, A.; Orian, A.; Schwartz, A. L. Ubiquitin-Mediated Proteolysis: Biological Regulation via Destruction. *BioEssays* **2000**, *22* (5), 442–451. [https://doi.org/10.1002/\(SICI\)1521-1878\(200005\)22:5<442::AID-BIES6>3.0.CO;2-Q](https://doi.org/10.1002/(SICI)1521-1878(200005)22:5<442::AID-BIES6>3.0.CO;2-Q).
- (131) Plemper, R. K.; Wolf, D. H. Retrograde Protein Translocation: ERADication of Secretory Proteins in Health and Disease. *Trends Biochem. Sci.* **1999**, *24* (7), 266–270. [https://doi.org/10.1016/S0968-0004\(99\)01420-6](https://doi.org/10.1016/S0968-0004(99)01420-6).
- (132) Huibregtse, J. M.; Scheffner, M.; Beaudenon, S.; Howley, P. M. A Family of Proteins Structurally and Functionally Related to the E6-AP Ubiquitin-Protein Ligase. *Proc. Natl. Acad. Sci. U. S. A.* **1995**, *92* (7), 2563–2567. <https://doi.org/10.1073/pnas.92.7.2563>.
- (133) Heller, H.; Hershko, A. A Ubiquitin-Protein Ligase Specific for Type III Protein Substrates. *J. Biol. Chem.* **1990**, *265* (12), 6532–6535. [https://doi.org/10.1016/s0021-9258\(19\)39177-x](https://doi.org/10.1016/s0021-9258(19)39177-x).
- (134) King, R. W.; Peters, J. M.; Tugendreich, S.; Rolfe, M.; Hieter, P.; Kirschner, M. W. A 20s Complex Containing CDC27 and CDC16 Catalyzes the Mitosis-Specific Conjugation of Ubiquitin to Cyclin B. *Cell* **1995**, *81* (2), 279–288. [https://doi.org/10.1016/0092-8674\(95\)90338-0](https://doi.org/10.1016/0092-8674(95)90338-0).
- (135) Lorick, K. L.; Jensen, J. P.; Fang, S.; Ong, A. M.; Hatakeyama, S.; Weissman, A. M. RING Fingers Mediate Ubiquitin-Conjugating Enzyme (E2)-Dependent Ubiquitination. *Proc. Natl. Acad. Sci. U. S. A.* **1999**, *96* (20), 11364–11369. <https://doi.org/10.1073/pnas.96.20.11364>.
- (136) Lisztwan, J.; Imbert, G.; Wirbelauer, C.; Gstaiger, M.; Krek, W. The von Hippel-Lindau Tumor Suppressor Protein Is a Component of an E3 Ubiquitin-Protein Ligase Activity. *Genes Dev.* **1999**, *13* (14), 1822–1833. <https://doi.org/10.1101/gad.13.14.1822>.
- (137) Maxwell, Patrick H. Wiesener, M. S.; Chang, G.-W.; Clifford, S. C.; Vaux, E. C.; Cockman, Matthew E. Wykoff, C. C.; Pugh, Christopher W. Maher, E. R.; Ratcliffe, P. J. The Tumour Suppressor Protein VHL Targets Hypoxia-Inducible Factors for Oxygen-Dependent Proteolysis. *Nature* **1999**, *399* (1997), 271–275.
- (138) Rosenbluh, J.; Nijhawan, D.; Cox, A. G.; Li, X.; Neal, J. T.; Schafer, E. J.; Zack, T. I.; Wang, X.; Tsherniak, A.; Schinzler, A. C.; et al. β -Catenin-Driven Cancers Require a YAP1 Transcriptional Complex for Survival and Tumorigenesis. *Cell* **2012**, *151* (7), 1457–1473. <https://doi.org/10.1016/j.cell.2012.11.026>.
- (139) Verma, R.; Mohl, D.; Deshaies, R. J. Harnessing the Power of Proteolysis for Targeted Protein Inactivation. *Mol. Cell* **2020**, *77* (3), 446–460. <https://doi.org/10.1016/j.molcel.2020.01.010>.
- (140) Sakamoto, K. M.; Kim, K. B.; Kumagai, A.; Mercurio, F.; Crews, C. M.; Deshaies, R. J. Protacs: Chimeric Molecules That Target Proteins to the Skp1-Cullin-F Box Complex for Ubiquitination and Degradation. *Proc. Natl. Acad. Sci. U. S. A.* **2001**, *98* (15), 8554–8559. <https://doi.org/10.1073/pnas.141230798>.
- (141) Ciulli, A.; Trainor, N. A Beginner's Guide to PROTACs and Targeted Protein Degradation. *Biochem. (Lond)*. **2021**, *43* (5), 74–79. https://doi.org/10.1042/bio_2021_148.
- (142) Miles, L. E. M.; Lipschitz, D. A.; Bieber, C. P.; Cook, J. D. Measurement of Serum Ferritin by a 2-Site Immunoradiometric Assay. *Anal. Biochem.* **1974**, *61* (1), 209–224. [https://doi.org/10.1016/0003-2697\(74\)90347-9](https://doi.org/10.1016/0003-2697(74)90347-9).
- (143) Pillow, T. H.; Adhikari, P.; Blake, R. A.; Chen, J.; Del Rosario, G.; Deshmukh, G.; Figueroa, I.; Gascoigne, K. E.; Kamath, A. V.; Kaufman, S.; et al. Antibody Conjugation of a Chimeric BET Degradator Enables in Vivo Activity. *ChemMedChem* **2020**, *15* (1), 17–25. <https://doi.org/10.1002/cmdc.201900497>.
- (144) Rodriguez-Gonzalez, A.; Cyrus, K.; Salcius, M.; Kim, K.; Crews, C. M.; Deshaies, R. J.; Sakamoto, K. M. Targeting Steroid Hormone Receptors for Ubiquitination and Degradation in Breast and Prostate Cancer. *Oncogene* **2008**, *27* (57), 7201–7211. <https://doi.org/10.1038/onc.2008.320>.
- (145) Lu, J.; Qian, Y.; Altieri, M.; Dong, H.; Wang, J.; Raina, K.; Hines, J.; Winkler, J. D.; Crew, A. P.; Coleman, K.; et al. Hijacking the E3 Ubiquitin Ligase Cereblon to Efficiently Target BRD4. *Chem. Biol.* **2015**, *22* (6), 755–763. <https://doi.org/10.1016/j.chembiol.2015.05.009>.

- (146) Gao, X.; Burris III, H. A.; Vuky, J.; Dreicer, R.; Sartor, A. O.; Sternberg, C. N.; Percent, I. J.; Hussain, M. H. A.; Rezazadeh Kalebasty, A.; Shen, J.; et al. Phase 1/2 Study of ARV-110, an Androgen Receptor (AR) PROTAC Degradator, in Metastatic Castration-Resistant Prostate Cancer (MCRPC). *J. Clin. Oncol.* **2022**, *40* (6), 17. https://doi.org/10.1200/JCO.2022.40.6_suppl.017.
- (147) Stevens, D. A.; Ewesuedo, R.; McDonald, A.; Agarwal, S.; Henrick, P.; Perea, R.; Gollerkeri, A.; Gollob, J. Phase 1 Study of KT-413, a Targeted Protein Degradator, in Adult Patients with Relapsed or Refractory B-Cell Non-Hodgkin Lymphoma. *J. Clin. Oncol.* **2022**, *40* (16_suppl), TPS3170–TPS3170. https://doi.org/10.1200/JCO.2022.40.16_suppl.TPS3170.
- (148) Chirnomas, D.; Hornberger, K. R.; Crews, C. M. Protein Degradators Enter the Clinic — a New Approach to Cancer Therapy. *Nat. Rev. Clin. Oncol.* **2023**, *20* (4), 265–278. <https://doi.org/10.1038/s41571-023-00736-3>.
- (149) Zengerle, M.; Chan, K. H.; Ciulli, A. Selective Small Molecule Induced Degradation of the BET Bromodomain Protein BRD4. *ACS Chem. Biol.* **2015**, *10* (8), 1770–1777. <https://doi.org/10.1021/acschembio.5b00216>.
- (150) Hu, J.; Hu, B.; Wang, M.; Xu, F.; Miao, B.; Yang, C. Y.; Wang, M.; Liu, Z.; Hayes, D. F.; Chinnaswamy, K.; et al. Discovery of ERD-308 as a Highly Potent Proteolysis Targeting Chimera (PROTAC) Degradator of Estrogen Receptor (ER). *J. Med. Chem.* **2019**, *62* (3), 1420–1442. <https://doi.org/10.1021/acs.jmedchem.8b01572>.
- (151) Han, X.; Wang, C.; Qin, C.; Xiang, W.; Fernandez-Salas, E.; Yang, C. Y.; Wang, M.; Zhao, L.; Xu, T.; Chinnaswamy, K.; et al. Discovery of ARD-69 as a Highly Potent Proteolysis Targeting Chimera (PROTAC) Degradator of Androgen Receptor (AR) for the Treatment of Prostate Cancer. *J. Med. Chem.* **2019**, *62* (2), 941–964. <https://doi.org/10.1021/acs.jmedchem.8b01631>.
- (152) Zhao, B.; Burgess, K. PROTACs Suppression of CDK4/6, Crucial Kinases for Cell Cycle Regulation in Cancer. *Chem. Commun.* **2019**, *55* (18), 2704–2707. <https://doi.org/10.1039/c9cc00163h>.
- (153) Goracci, L.; Desantis, J.; Valeri, A.; Castellani, B.; Eleuteri, M.; Cruciani, G. Understanding the Metabolism of Proteolysis Targeting Chimeras (PROTACs): The Next Step toward Pharmaceutical Applications. *J. Med. Chem.* **2020**, *63* (20), 11615–11638. <https://doi.org/10.1021/acs.jmedchem.0c00793>.
- (154) Poongavanam, V.; Atilaw, Y.; Siegel, S.; Giese, A.; Lehmann, L.; Meibom, D.; Erdelyi, M.; Kihlberg, J. Linker-Dependent Folding Rationalizes PROTAC Cell Permeability. *J. Med. Chem.* **2022**, *65* (19), 13029–13040. <https://doi.org/10.1021/acs.jmedchem.2c00877>.
- (155) Moon, Y.; Jeon, S. I.; Shim, M. K.; Kim, K. Cancer-Specific Delivery of Proteolysis-Targeting Chimeras (PROTACs) and Their Application to Cancer Immunotherapy. *Pharmaceutics* **2023**, *15* (2), 1–24. <https://doi.org/10.3390/pharmaceutics15020411>.
- (156) Dragovich, P. S.; Adhikari, P.; Blake, R. A.; Blaquiere, N.; Chen, J.; Cheng, Y. X.; den Besten, W.; Han, J.; Hartman, S. J.; He, J.; et al. Antibody-Mediated Delivery of Chimeric Protein Degradators Which Target Estrogen Receptor Alpha (ER α). *Bioorganic Med. Chem. Lett.* **2020**, *30* (4), 126907. <https://doi.org/10.1016/j.bmcl.2019.126907>.
- (157) Maneiro, M.; Forte, N.; Shchepinova, M. M.; Kounde, C. S.; Chudasama, V.; Baker, J. R.; Tate, E. W. Antibody-PROTAC Conjugates Enable HER2-Dependent Targeted Protein Degradation of BRD4. *ACS Chem. Biol.* **2020**, *15* (6), 1306–1312. <https://doi.org/10.1021/acschembio.0c00285>.
- (158) Chan, K.; Soundarya, P.; Queisser, M. A.; Mullin, M.; Shrivs, H. Antibody-Proteolysis Targeting Chimera Conjugate Enables Selective Degradation of Receptor-Interacting Serine/Threonine-Protein Kinase 2 in HER2+ Cell Lines. *Bioconjugate Chem.* **2023**, *31* (11), 2049–2054. <https://doi.org/https://doi.org/10.1021/acs.bioconjchem.3c00366>.
- (159) Dragovich, P. S. Degradator-Antibody Conjugates. *Chem. Soc. Rev.* **2022**, *51* (10), 3886–3897. <https://doi.org/10.1039/d2cs00141a>.
- (160) Schneider, H.; Jäger, S.; Könnig, D.; Rasche, N.; Schröter, C.; Elter, D. PROxAb Shuttle : A Non-Covalent Plug-and-Play Platform for the Rapid Generation of Tumor-Targeting

- Antibody-PROTAC Conjugates. *bioRxiv* **2023**, 2023.09.29.558399. <https://doi.org/10.1101/2023.09.29.558399>.
- (161) Gonzalez-Sapienza, G.; Rossotti, M. A.; Tabares-da Rosa, S. Single-Domain Antibodies as Versatile Affinity Reagents for Analytical and Diagnostic Applications. *Front. Immunol.* **2017**, *8* (AUG), 1–12. <https://doi.org/10.3389/fimmu.2017.00977>.
- (162) Hoey, R. J.; Eom, H.; Horn, J. R. Structure and Development of Single Domain Antibodies as Modules for Therapeutics and Diagnostics. *Exp. Biol. Med.* **2019**, *244* (17), 1568–1576. <https://doi.org/10.1177/1535370219881129>.
- (163) Buckley, D. L.; Gustafson, J. L.; Van-Molle, I.; Roth, A. G.; Tae, H. S.; Gareiss, P. C.; Jorgensen, W. L.; Ciulli, A.; Crews, C. M. Small-Molecule Inhibitors of the Interaction between the E3 Ligase VHL and HIF1 α . *Angew. Chemie - Int. Ed.* **2012**, *51* (46), 11463–11467. <https://doi.org/10.1002/anie.201206231>.
- (164) Raina, K.; Lu, J.; Qian, Y.; Altieri, M.; Gordon, D.; Rossi, A. M. K.; Wang, J.; Chen, X.; Dong, H.; Siu, K.; et al. PROTAC-Induced BET Protein Degradation as a Therapy for Castration-Resistant Prostate Cancer. *Proc. Natl. Acad. Sci. U. S. A.* **2016**, *113* (26), 7124–7129. <https://doi.org/10.1073/pnas.1521738113>.
- (165) Dragovich, P. S.; Pillow, T. H.; Blake, R. A.; Sadowsky, J. D.; Adaligil, E.; Adhikari, P.; Chen, J.; Corr, N.; Dela Cruz-Chuh, J.; Del Rosario, G.; et al. Antibody-Mediated Delivery of Chimeric BRD4 Degraders. Part 2: Improvement of in Vitro Antiproliferation Activity and in Vivo Antitumor Efficacy. *J. Med. Chem.* **2021**, *64* (5), 2576–2607. <https://doi.org/10.1021/acs.jmedchem.0c01846>.
- (166) Uhlén, M.; Fagerberg, L.; Hallström, B. M.; Lindskog, C.; Oksvold, P.; Mardinoglu, A.; Sivertsson, Å.; Kampf, C.; Sjöstedt, E.; Asplund, A.; et al. Tissue-Based Map of the Human Proteome. *Science (80-)*. **2015**, *347* (6220). <https://doi.org/10.1126/science.1260419>.
- (167) Zhang, Z.; Yue, P.; Lu, T.; Wang, Y.; Wei, Y.; Wei, X. Role of Lysosomes in Physiological Activities, Diseases, and Therapy. *J. Hematol. Oncol.* **2021**, *14* (1), 1–39. <https://doi.org/10.1186/s13045-021-01087-1>.
- (168) Riching, K. M.; Mahan, S.; Corona, C. R.; McDougall, M.; Vasta, J. D.; Robers, M. B.; Urh, M.; Daniels, D. L. Quantitative Live-Cell Kinetic Degradation and Mechanistic Profiling of PROTAC Mode of Action. *ACS Chem. Biol.* **2018**, *13* (9), 2758–2770. <https://doi.org/10.1021/acschembio.8b00692>.
- (169) Igawa, T.; Ishii, S.; Tachibana, T.; Maeda, A.; Higuchi, Y.; Shimaoka, S.; Moriyama, C.; Watanabe, T.; Takubo, R.; Doi, Y.; et al. Antibody Recycling by Engineered PH-Dependent Antigen Binding Improves the Duration of Antigen Neutralization. *Nat. Biotechnol.* **2010**, *28* (11), 1203–1207. <https://doi.org/10.1038/nbt.1691>.
- (170) Deng, R.; Loyet, K. M.; Lien, S.; Iyer, S.; DeForge, L. E.; Theil, F. P.; Lowman, H. B.; Fielder, P. J.; Prabhu, S. Pharmacokinetics of Humanized Monoclonal Anti-Tumor Necrosis Factor- α Antibody and Its Neonatal Fc Receptor Variants in Mice and Cynomolgus Monkeys. *Drug Metab. Dispos.* **2010**, *38* (4), 600–605. <https://doi.org/10.1124/dmd.109.031310>.
- (171) Wang, C.; Zhao, T.; Li, Y.; Huang, G.; White, M. A.; Gao, J. Investigation of Endosome and Lysosome Biology by Ultra PH-Sensitive Nanoprobes. *Adv. Drug Deliv. Rev.* **2017**, *113*, 87–96. <https://doi.org/10.1016/j.addr.2016.08.014>.
- (172) Igawa, T.; Maeda, A.; Haraya, K.; Tachibana, T.; Iwayanagi, Y.; Mimoto, F.; Higuchi, Y.; Ishii, S.; Tamba, S.; Hironiwa, N.; et al. Engineered Monoclonal Antibody with Novel Antigen-Sweeping Activity In Vivo. *PLoS One* **2013**, *8* (5). <https://doi.org/10.1371/journal.pone.0063236>.
- (173) Banik, S. M.; Pedram, K.; Wisnovsky, S.; Ahn, G.; Riley, N. M.; Bertozzi, C. R. Lysosome-Targeting Chimaeras for Degradation of Extracellular Proteins. *Nature* **2020**, *584* (7820), 291–297. <https://doi.org/10.1038/s41586-020-2545-9>.
- (174) Ahn, G.; Riley, N. M.; Kamber, R. A.; Wisnovsky, S.; von Hase, S. M.; Bassik, M. C.; Banik, S. M.; Bertozzi, C. R. Elucidating the Cellular Determinants of Targeted Membrane Protein Degradation by Lysosome-Targeting Chimeras. *Science (80-)*. **2023**, *382* (6668). <https://doi.org/10.1126/science.adf6249>.

- (175) Green Ahn, Steven M. Banik, Caitlyn L. Miller, Nicholas M. Riley, Jennifer R. Cochran, C. R. B. LYTACs That Engage the Asialoglycoprotein Receptor for Targeted Protein Degradation. *Nat. Chem. Biol.* **2021**, *17*, 937–946. <https://doi.org/https://doi.org/10.1038/s41589-021-00770-1>.
- (176) Wu, Y.; Lin, B.; Lu, Y.; Li, L.; Deng, K.; Zhang, S.; Zhang, H.; Yang, C.; Zhu, Z. Aptamer-LYTACs for Targeted Degradation of Extracellular and Membrane Proteins. *Angew. Chemie - Int. Ed.* **2023**, *202218106*. <https://doi.org/10.1002/anie.202218106>.
- (177) Nakamura, N. The Role of the Transmembrane RING Finger Proteins in Cellular and Organelle Function. *Membranes (Basel)*. **2011**, *1* (4), 354–393. <https://doi.org/10.3390/membranes1040354>.
- (178) Gramespacher, J. A.; Cotton, A. D.; Burroughs, P. W. W.; Seiple, I. B.; Wells, J. A. Roadmap for Optimizing and Broadening Antibody-Based PROTACs for Degradation of Cell Surface Proteins. **2022**. <https://doi.org/10.1021/acscchembio.2c00185>.
- (179) Pance, K.; Gramespacher, J. A.; Byrnes, J. R.; Salangsang, F.; Serrano, J. A. C.; Cotton, A. D.; Steri, V.; Wells, J. A. Modular Cytokine Receptor-Targeting Chimeras for Targeted Degradation of Cell Surface and Extracellular Proteins. *Nat. Biotechnol.* **2022**. <https://doi.org/10.1038/s41587-022-01456-2>.
- (180) Janssens, R.; Struyf, S.; Proost, P. The Unique Structural and Functional Features of CXCL12. *Cell. Mol. Immunol.* **2018**, *15* (4), 299–311. <https://doi.org/10.1038/cmi.2017.107>.
- (181) Lehmann, T.; Schneider, H.; Tonillo, J.; Jennifer, S.; Schwarz, D.; Kolmar, H.; Hecht, S.; Anderl, J.; Rasche, N.; Rieker, M.; et al. Welding PROxAb Shuttles: A Modular Approach for Generating Bispecific Antibodies via Site-Specific Protein-Protein Conjugation. *bioRxiv* **2024**. <https://doi.org/https://doi.org/10.1101/2024.03.15.585232>.
- (182) Lim, S. M.; Pyo, K. H.; Soo, R. A.; Cho, B. C. The Promise of Bispecific Antibodies: Clinical Applications and Challenges. *Cancer Treat. Rev.* **2021**, *99* (May), 102240. <https://doi.org/10.1016/j.ctrv.2021.102240>.
- (183) Gall, V. A.; Philips, A. V.; Qiao, N.; Clise-Dwyer, K.; Perakis, A. A.; Zhang, M.; Clifton, G. T.; Sukhumalchandra, P.; Ma, Q.; Reddy, S. M.; et al. Trastuzumab Increases HER2 Uptake and Cross-Presentation by Dendritic Cells. *Cancer Res.* **2017**, *77* (19), 5374–5383. <https://doi.org/10.1158/0008-5472.CAN-16-2774>.
- (184) Koteekar, A.; Singh, A. K.; Devaiah, B. N. BRD4 and MYC: Power Couple in Transcription and Disease. *FEBS J.* **2023**, *290* (20), 4820–4842. <https://doi.org/10.1111/febs.16580>.
- (185) Rieker, M.; Jaeger, S.; Rasche, N.; Koenning, D.; Schroeter, C.; Schneider, H. ANTI-PROTAC ANTIBODIES AND COMPLEXES. WO2023275394, 2023.
- (186) Zimmermann, J.; Giersberg, M.; Riehl, M. Antigen Binding Polypeptides against F4 (K88) Fimbriae. WO2007010040, 2006.
- (187) Kamiya, N.; Takazawa, T.; Tanaka, T.; Ueda, H.; Nagamune, T. Site-Specific Cross-Linking of Functional Proteins by Transglutamination. *Enzyme Microb. Technol.* **2003**, *33* (4), 492–496. [https://doi.org/10.1016/S0141-0229\(03\)00154-6](https://doi.org/10.1016/S0141-0229(03)00154-6).
- (188) Strop, P.; Dorywalska, M. G.; Rajpal, A.; Shelton, D.; Liu, S. H.; Pons, J.; Dushin, R. Engineered Polypeptide Conjugates and Methods for Making Thereof Using Transglutaminase. WO2012059882, 2012.
- (189) *Broad Institute, depmap portal*. <https://depmap.org/portal/> (accessed 2024-04-24).
- (190) Parrish, N.; Hormozdiari, F.; Eskin, E. Assembly of Non-Unique Insertion Content Using next-Generation Sequencing. *Bioinforma. Impact Accurate Quantif. Proteomic Genet. Anal. Res.* **2014**, 21–40. <https://doi.org/10.1201/b16589>.
- (191) SJÖSTEDT, E.; ZHONG, W.; FAGERBERG, L.; KARLSSON, M.; MITSIOS, N.; CSABA ADORI, P. O.; EDFORS, F.; LIMISZEWSKA, A.; HIKMET, F.; HUANG, J.; et al. An Atlas of the Protein-Coding Genes in the Human, Pig, and Mouse Brain. *Science (80-.)*. **2020**, *367* (6482). <https://doi.org/10.1126/science.aay5947>.
- (192) Li, C. W.; Lim, S. O.; Xia, W.; Lee, H. H.; Chan, L. C.; Kuo, C. W.; Khoo, K. H.; Chang, S. S.; Cha, J. H.; Kim, T.; et al. Glycosylation and Stabilization of Programmed Death Ligand-1 Suppresses T-Cell Activity. *Nat. Commun.* **2016**, *7*. <https://doi.org/10.1038/ncomms12632>.

- (193) Wang, Q.; Chen, Y.; Park, J.; Liu, X.; Hu, Y.; Wang, T.; McFarland, K.; Betenbaugh, M. J. Design and Production of Bispecific Antibodies. *Antibodies* **2019**, *8* (3), 43. <https://doi.org/https://doi.org/10.3390/antib8030043>.
- (194) Luo, D.; Mah, N.; Krantz, M.; Wilde, K.; Wishart, D.; Zhang, Y.; Jacobs, F.; Martin, L. VI-Linker-vh Orientation-Dependent Expression of Single Chain Fv Containing an Engineered Disulfide-Stabilized Bond in the Framework Regions. *J. Biochem.* **1995**, *118* (4), 825–831. <https://doi.org/10.1093/oxfordjournals.jbchem.a124986>.
- (195) Brinkmann, U.; Kontermann, R. E. The Making of Bispecific Antibodies. *MAbs* **2017**, *9* (2), 182–212. <https://doi.org/10.1080/19420862.2016.1268307>.
- (196) Tanaka, T.; Kamiya, N.; Nagamune, T. N-Terminal Glycine-Specific Protein Conjugation Catalyzed by Microbial Transglutaminase. *FEBS Lett.* **2005**, *579* (10), 2092–2096. <https://doi.org/10.1016/j.febslet.2005.02.064>.
- (197) Boumans, J. W. L. 1191 R. O. aan de A. (NL); Wijbenga, D.-J. 9301 W. R. (NL); Bos, H. T. P. 9781 B. B. (NL); Wijngaards, G.; (NL), 3972 GS Driebergen-Rijsenburg; Heeres, A.; (NL), 9715 AE Groningen. Method for Modification of Proteins by Transglutaminase. WO2001079474, 2001.
- (198) Mindt, T. L.; Jungi, V.; Wyss, S.; Friedli, A.; Pla, G.; Novak-Hofer, I.; Grünberg, J.; Schibli, R. Modification of Different IgG1 Antibodies via Glutamine and Lysine Using Bacterial and Human Tissue Transglutaminase. *Bioconjug. Chem.* **2008**, *19* (1), 271–278. <https://doi.org/10.1021/bc700306n>.
- (199) Zheng, K.; Bantog, C.; Bayer, R. The Impact of Glycosylation on Monoclonal Antibody Conformation and Stability. *MAbs* **2011**, *3* (6). <https://doi.org/10.4161/mabs.3.6.17922>.
- (200) Wang, Z.; Li, H.; Gou, L.; Li, W.; Wang, Y. Antibody–Drug Conjugates: Recent Advances in Payloads. *Acta Pharm. Sin. B* **2023**, *13* (10), 4025–4059. <https://doi.org/10.1016/j.apsb.2023.06.015>.
- (201) Hofmann, T.; Schmidt, J.; Ciesielski, E.; Becker, S.; Rysiok, T.; Schütte, M.; Toleikis, L.; Kolmar, H.; Doerner, A. Intein Mediated High Throughput Screening for Bispecific Antibodies. *MAbs* **2020**, *12* (1). <https://doi.org/10.1080/19420862.2020.1731938>.
- (202) Yumura, K.; Akiba, H.; Nagatoishi, S.; Kusano-Arai, O.; Iwanari, H.; Hamakubo, T.; Tsumoto, K. Use of SpyTag/SpyCatcher to Construct Bispecific Antibodies That Target Two Epitopes of a Single Antigen. *J. Biochem.* **2017**, *162* (3), 203–210. <https://doi.org/10.1093/jb/mvx023>.
- (203) Barron, N.; Dickgiesser, S.; Fleischer, M.; Bachmann, A.; Klewinghaus, D.; Hannewald, J.; Ciesielski, E.; Kusters, I.; Hammann, T.; Krause, V.; et al. A Generic Approach for Miniaturized Unbiased High-Throughput Screens of Bispecific Antibodies and Biparatopic Antibody – Drug Conjugates. *Int. J. Mol. Sci.* **2024**, *25* (4), 2097. <https://doi.org/10.3390/ijms25042097>.
- (204) Trevino, S. R.; Scholtz, J. M.; Pace, C. N. Measuring and Increasing Protein Solubility. *J. Pharm. Sci.* **2008**, *97* (10), 4155–4166. <https://doi.org/10.1002/jps.21327>.
- (205) Gundersen, M. T.; Keillor, J. W.; Pelletier, J. N. Microbial Transglutaminase Displays Broad Acyl-Acceptor Substrate Specificity. *Appl. Microbiol. Biotechnol.* **2014**, *98* (1), 219–230. <https://doi.org/10.1007/s00253-013-4886-x>.
- (206) Ohtsuka, T.; Sawa, A.; Kawabata, R.; Nio, N.; Motoki, M. Substrate Specificities of Microbial Transglutaminase for Primary Amines. *J. Agric. Food Chem.* **2000**, *48* (12), 6230–6233. <https://doi.org/10.1021/jf000302k>.
- (207) Park, J.; Lee, S.; Kim, Y.; Yoo, T. H. Methods to Generate Site-Specific Conjugates of Antibody and Protein. *Bioorg. Med. Chem.* **2021**, *30* (December 2020), 115946. <https://doi.org/10.1016/j.bmc.2020.115946>.
- (208) Strop, P.; Delaria, K.; Foletti, D.; Witt, J. M.; Hasa-Moreno, A.; Poulsen, K.; Casas, M. G.; Dorywalska, M.; Farias, S.; Pios, A.; et al. Site-Specific Conjugation Improves Therapeutic Index of Antibody Drug Conjugates with High Drug Loading. *Nat. Biotechnol.* **2015**, *33* (7), 694–696. <https://doi.org/10.1038/nbt.3274>.
- (209) Greineder, C. F.; Villa, C. H.; Walsh, L. R.; Kiseleva, R. Y.; Hood, E. D.; Khoshnejad, M.; Warden-

- Rothman, R.; Tsourkas, A.; Muzykantov, V. R. Site-Specific Modification of Single-Chain Antibody Fragments for Bioconjugation and Vascular Immunotargeting. *Bioconjug. Chem.* **2018**, *29* (1), 56–66. <https://doi.org/10.1021/acs.bioconjchem.7b00592>.
- (210) Hadjabdelhafid-Parisien, A.; Bitsch, S.; Macarrón Palacios, A.; Deweid, L.; Kolmar, H.; Pelletier, J. N. Tag-Free, Specific Conjugation of Glycosylated IgG1 Antibodies Using Microbial Transglutaminase. *RSC Adv.* **2022**, *12* (52), 33510–33515. <https://doi.org/10.1039/d2ra05630e>.
- (211) Alsenaidy, M. A.; Kim, J. H.; Majumdar, R.; Weis, D. D.; Joshi, S. B.; Tolbert, T. J.; Middaugh, C. R.; Volkin, D. B. High-Throughput Biophysical Analysis and Data Visualization of Conformational Stability of an Igg1 Monoclonal Antibody after Deglycosylation. *J. Pharm. Sci.* **2013**, *102* (11), 3942–3956. <https://doi.org/10.1002/jps.23730>.
- (212) Reslan, M.; Sifniotis, V.; Cruz, E.; Sumer-Bayraktar, Z.; Cordwell, S.; Kayser, V. Enhancing the Stability of Adalimumab by Engineering Additional Glycosylation Motifs. *Int. J. Biol. Macromol.* **2020**, *158*, 189–196. <https://doi.org/10.1016/j.ijbiomac.2020.04.147>.
- (213) Pike, A.; Williamson, B.; Harlfinger, S.; Martin, S.; McGinnity, D. F. Optimising Proteolysis-Targeting Chimeras (PROTACs) for Oral Drug Delivery: A Drug Metabolism and Pharmacokinetics Perspective. *Drug Discov. Today* **2020**, *25* (10), 1793–1800. <https://doi.org/10.1016/j.drudis.2020.07.013>.
- (214) Maple, H. J.; Clayden, N.; Baron, A.; Stacey, C.; Felix, R. Developing Degradable: Principles and Perspectives on Design and Chemical Space. *Medchemcomm* **2019**, *10* (10), 1755–1764. <https://doi.org/10.1039/c9md00272c>.
- (215) Edmondson, S. D.; Yang, B.; Fallan, C. Proteolysis Targeting Chimeras (PROTACs) in 'beyond Rule-of-Five' Chemical Space: Recent Progress and Future Challenges. *Bioorganic Med. Chem. Lett.* **2019**, *29* (13), 1555–1564. <https://doi.org/10.1016/j.bmcl.2019.04.030>.
- (216) O'Brien Laramy, M. N.; Luthra, S.; Brown, M. F.; Bartlett, D. W. Delivering on the Promise of Protein Degradable. *Nat. Rev. Drug Discov.* **2023**, *22* (5), 410–427. <https://doi.org/10.1038/s41573-023-00652-2>.
- (217) Shah, R.; Saleem, Z.; Schwalm, M. P.; Knapp, S. Expanding the Ligand Spaces for E3 Ligases for the Design of Protein Degradable. *Bioorg. Med. Chem.* **2024**, *105* (April), 117718. <https://doi.org/10.1016/j.bmc.2024.117718>.
- (218) Lee, J.; Zhou, P. DCAFs, the Missing Link of the CUL4-DDB1 Ubiquitin Ligase. *Mol. Cell* **2007**, *26* (6), 775–780. <https://doi.org/10.1016/j.molcel.2007.06.001>.
- (219) Schneekloth, A. R.; Pucheault, M.; Tae, H. S.; Crews, C. M. Targeted Intracellular Protein Degradation Induced by a Small Molecule: En Route to Chemical Proteomics. *Bioorganic Med. Chem. Lett.* **2008**, *18* (22), 5904–5908. <https://doi.org/10.1016/j.bmcl.2008.07.114>.
- (220) Ding, Q.; Zhang, Z.; Liu, J. J.; Jiang, N.; Zhang, J.; Ross, T. M.; Chu, X. J.; Bartkovitz, D.; Podlaski, F.; Janson, C.; et al. Discovery of RG7388, a Potent and Selective P53-MDM2 Inhibitor in Clinical Development. *J. Med. Chem.* **2013**, *56* (14), 5979–5983. <https://doi.org/10.1021/jm400487c>.
- (221) Hines, J.; Lartigue, S.; Dong, H.; Qian, Y.; Crews, C. M. MDM2-Recruiting PROTAC Offers Superior, Synergistic Antiproliferative Activity via Simultaneous Degradation of BRD4 and Stabilization of P53. *Cancer Res.* **2019**, *79* (1), 251–262. <https://doi.org/10.1158/0008-5472.CAN-18-2918>.
- (222) Schröder, M.; Renatus, M.; Liang, X.; Meili, F.; Zoller, T.; Ferrand, S.; Gauter, F.; Li, X.; Sigoillot, F.; Gleim, S.; et al. DCAF1-Based PROTACs with Activity against Clinically Validated Targets Overcoming Intrinsic- and Acquired-Degrader Resistance. *Nat. Commun.* **2024**, *15* (1), 1–19. <https://doi.org/10.1038/s41467-023-44237-4>.
- (223) Zhu, H.; Gao, H.; Ji, Y.; Zhou, Q.; Du, Z.; Tian, L.; Jiang, Y.; Yao, K.; Zhou, Z. Targeting P53-MDM2 Interaction by Small-Molecule Inhibitors: Learning from MDM2 Inhibitors in Clinical Trials. *J. Hematol. Oncol.* **2022**, *15* (1), 1–23. <https://doi.org/10.1186/s13045-022-01314-3>.
- (224) Zhang, C.; Pu, K. Molecular and Nanoengineering Approaches towards Activatable Cancer Immunotherapy. *Chem. Soc. Rev.* **2020**, *49* (13), 4234–4253.

- <https://doi.org/10.1039/c9cs00773c>.
- (225) Xie, H.; Zhang, C. Potential of the Nanoplatfom and PROTAC Interface to Achieve Targeted Protein Degradation through the Ubiquitin–Proteasome System. *Eur. J. Med. Chem.* **2024**, *267* (November 2023), 116168. <https://doi.org/10.1016/j.ejmech.2024.116168>.
- (226) Patel, T. K.; Adhikari, N.; Amin, S. A.; Biswas, S.; Jha, T.; Ghosh, B. Small Molecule Drug Conjugates (SMDCs): An Emerging Strategy for Anticancer Drug Design and Discovery. *New J. Chem.* **2021**, *45* (12), 5291–5321. <https://doi.org/10.1039/d0nj04134c>.
- (227) Hong, K. B.; An, H. Degradable – Antibody Conjugates: Emerging New Modality. **2023**. <https://doi.org/10.1021/acs.jmedchem.2c01791>.
- (228) He, S.; Fang, Y.; Wu, M.; Zhang, P.; Gao, F.; Hu, H.; Sheng, C.; Dong, G. Enhanced Tumor Targeting and Penetration of Proteolysis-Targeting Chimeras through IRGD Peptide Conjugation: A Strategy for Precise Protein Degradation in Breast Cancer. *J. Med. Chem.* **2023**, *66* (24), 16828–16842. <https://doi.org/10.1021/acs.jmedchem.3c01539>.
- (229) Nakazawa, Y.; Miyano, M.; Tsukamoto, S.; Kogai, H.; Yamamoto, A.; Iso, K.; Inoue, S.; Yamane, Y.; Yabe, Y.; Umihara, H.; et al. Delivery of a BET Protein Degradable via a CEACAM6-Targeted Antibody–Drug Conjugate Inhibits Tumour Growth in Pancreatic Cancer Models. *Nat. Commun.* **2024**, *15* (1), 1–17. <https://doi.org/10.1038/s41467-024-46167-1>.
- (230) Zhang, A.; Seiss, K.; Laborde, L.; Palacio-Ramirez, S.; Guthy, D.; Lanter, M.; Lorber, J.; Vulpetti, A.; Arista, L.; Zoller, T.; et al. Design, Synthesis, and In Vitro and In Vivo Evaluation of Cereblon Binding Bruton’s Tyrosine Kinase (BTK) Degradable CD79b Targeted Antibody–Drug Conjugates. *Bioconjug. Chem.* **2024**, *35* (2), 140–146. <https://doi.org/10.1021/acs.bioconjchem.3c00535>.
- (231) Peter Armstrong Thompson; Edris, B.; Coburn, C. A.; Baum, P. R. Antibody Construct Conjugates. WO2018227023, 2018.
- (232) Fishkin, N.; Park, P. U. Conjugates. WO2021198966, 2021.
- (233) Lua, W. H.; Ling, W. L.; Yeo, J. Y.; Poh, J. J.; Lane, D. P.; Gan, S. K. E. The Effects of Antibody Engineering CH and CL in Trastuzumab and Pertuzumab Recombinant Models: Impact on Antibody Production and Antigen-Binding. *Sci. Rep.* **2018**, *8* (1), 1–9. <https://doi.org/10.1038/s41598-017-18892-9>.
- (234) Mayor, S.; Pagano, R. E. Pathways of Clathrin-Independent Endocytosis. *Nat. Rev. Mol. Cell Biol.* **2007**, *8* (8), 603–612. <https://doi.org/10.1038/nrm2216>.
- (235) Nath, N.; Godat, B.; Zimprich, C.; Dwight, S. J.; Corona, C.; McDougall, M.; Urh, M. Homogeneous Plate Based Antibody Internalization Assay Using PH Sensor Fluorescent Dye. *J. Immunol. Methods* **2016**, *431*, 11–21. <https://doi.org/10.1016/j.jim.2016.02.001>.
- (236) Jäger, S.; Wagner, T. R.; Rasche, N.; Kolmar, H.; Hecht, S.; Schröter, C. Generation and Biological Evaluation of Fc Antigen Binding Fragment–Drug Conjugates as a Novel Antibody-Based Format for Targeted Drug Delivery. *Bioconjug. Chem.* **2021**, *32* (8), 1699–1710. <https://doi.org/10.1021/acs.bioconjchem.1c00240>.
- (237) Ram, S.; Kim, D.; Ober, R. J.; Ward, E. S. The Level of HER2 Expression Is a Predictor of Antibody–HER2 Trafficking Behavior in Cancer Cells. *MAbs* **2014**, *6* (5), 1211–1219. <https://doi.org/10.4161/mabs.29865>.
- (238) Jedema, I.; Barge, R. M. Y.; van der Velden, V. H. J.; Nijmeijer, B. A.; van Dongen, J. J. M.; Willemze, R.; Falkenburg, J. H. F. Internalization and Cell Cycle-Dependent Killing of Leukemic Cells by Gemtuzumab Ozogamicin: Rationale for Efficacy in CD33-Negative Malignancies with Endocytic Capacity. *Leukemia* **2004**, *18* (2), 316–325. <https://doi.org/10.1038/sj.leu.2403205>.
- (239) Browning, A. P.; Ansari, N.; Drovandi, C.; Johnston, A. P. R.; Simpson, M. J.; Jenner, A. L. Identifying Cell-to-Cell Variability in Internalization Using Flow Cytometry. *J. R. Soc. Interface* **2022**, *19* (190), 151–171. <https://doi.org/10.1098/rsif.2022.0019>.
- (240) Fielding, A. B.; Willox, A. K.; Okeke, E.; Royle, S. J. Clathrin-Mediated Endocytosis Is Inhibited during Mitosis. *Proc. Natl. Acad. Sci. U. S. A.* **2012**, *109* (17), 6572–6577. <https://doi.org/10.1073/pnas.1117401109>.
- (241) Schneider, B.; Grote, M.; John, M.; Haas, A.; Bramlage, B.; Lckenstein, L. M.; Jahn-Hofmann,

- K.; Bauss, F.; Cheng, W.; Croasdale, R.; et al. Targeted SiRNA Delivery and mRNA Knockdown Mediated by Bispecific Digoxigenin-Binding Antibodies. *Mol. Ther. - Nucleic Acids* **2012**, *1* (9), e46. <https://doi.org/10.1038/mtna.2012.39>.
- (242) Devaiah, B. N.; Mu, J.; Akman, B.; Uppal, S.; Weissman, J. D.; Cheng, D.; Baranello, L.; Nie, Z.; Levens, D.; Singer, D. S. MYC Protein Stability Is Negatively Regulated by BRD4. *Proc. Natl. Acad. Sci. U. S. A.* **2020**, *117* (24), 13457–13467. <https://doi.org/10.1073/pnas.1919507117>.
- (243) Chen, Y.; Tandon, I.; Heelan, W.; Wang, Y.; Tang, W.; Hu, Q. Proteolysis-Targeting Chimera (PROTAC) Delivery System: Advancing Protein Degradation towards Clinical Translation. *Chem. Soc. Rev.* **2022**, *51* (13), 5330–5350. <https://doi.org/10.1039/d1cs00762a>.
- (244) Liang, D.; Yu, Y.; Ma, Z. Novel Strategies Targeting Bromodomain-Containing Protein 4 (BRD4) for Cancer Drug Discovery. *Eur. J. Med. Chem.* **2020**, *200*, 112426. <https://doi.org/10.1016/j.ejmech.2020.112426>.
- (245) Muddassir, M.; Soni, K.; Sangani, C. B.; Alarifi, A.; Afzal, M.; Abduh, N. A. Y.; Duan, Y.; Bhadja, P. Bromodomain and BET Family Proteins as Epigenetic Targets in Cancer Therapy: Their Degradation, Present Drugs, and Possible PROTACs. *RSC Adv.* **2020**, *11* (2), 612–636. <https://doi.org/10.1039/d0ra07971e>.
- (246) Petrylak, D. P.; Stewart, T. F.; Gao, X.; Berghorn, E.; Lu, H.; Chan, E.; Gedrich, R.; Lang, J. M.; McKean, M. A Phase 2 Expansion Study of ARV-766, a PROTACandrogen Receptor (AR) Degradation, in Metastatic Castration-Resistant Prostate Cancer (MCRPC). *J. Clin. Oncol.* **2023**, *41* (6_suppl), TPS290–TPS290. https://doi.org/10.1200/jco.2023.41.6_suppl.tps290.
- (247) Zhou, X. L.; Zhao, F.; Xu, Y. T.; Guan, Y. Y.; Yu, T.; Zhang, Y. Z.; Duan, Y. C.; Zhao, Y. A Comprehensive Review of BET-Targeting PROTACs for Cancer Therapy. *Bioorganic Med. Chem.* **2022**, *73* (July), 117033. <https://doi.org/10.1016/j.bmc.2022.117033>.
- (248) Zeng, S.; Huang, W.; Zheng, X.; Liyan cheng; Zhang, Z.; Wang, J.; Shen, Z. Proteolysis Targeting Chimera (PROTAC) in Drug Discovery Paradigm: Recent Progress and Future Challenges. *Eur. J. Med. Chem.* **2021**, *210*, 112981. <https://doi.org/10.1016/j.ejmech.2020.112981>.
- (249) Ocean, A. J.; Starodub, A. N.; Bardia, A.; Vahdat, L. T.; Isakoff, S. J.; Guarino, M.; Messersmith, W. A.; Picozzi, V. J.; Mayer, I. A.; Wegener, W. A.; et al. Sacituzumab Govitecan (IMMU-132), an Anti-Trop-2-SN-38 Antibody-Drug Conjugate for the Treatment of Diverse Epithelial Cancers: Safety and Pharmacokinetics. *Cancer* **2017**, *123* (19), 3843–3854. <https://doi.org/10.1002/cncr.30789>.
- (250) Schmid, D.; Buntz, A.; Hanh Phan, T. N.; Mayer, K.; Hoffmann, E.; Thorey, I.; Niewöhner, J.; Vasters, K.; Sircar, R.; Mundigl, O.; et al. Transcytosis of Payloads That Are Non-Covalently Complexed to Bispecific Antibodies across the HCMEC/D3 Blood-Brain Barrier Model. *Biol. Chem.* **2018**, *399* (7), 711–721. <https://doi.org/10.1515/hsz-2017-0311>.
- (251) Chen, W.; Yang, F.; Wang, C.; Narula, J.; Pascua, E.; Ni, I.; Ding, S.; Deng, X.; Chu, M. L. H.; Pham, A.; et al. One Size Does Not Fit All: Navigating the Multi-Dimensional Space to Optimize T-Cell Engaging Protein Therapeutics. *MAbs* **2021**, *13* (1). <https://doi.org/10.1080/19420862.2020.1871171>.
- (252) Shaw, A.; Hoffecker, I. T.; Smyrlaki, I.; Rosa, J.; Grevys, A.; Bratlie, D.; Sandlie, I.; Michaelsen, T. E.; Andersen, J. T.; Högberg, B. Binding to Nanopatterned Antigens Is Dominated by the Spatial Tolerance of Antibodies. *Nat. Nanotechnol.* **2019**, *14* (2), 184–190. <https://doi.org/10.1038/s41565-018-0336-3>.
- (253) Sengers, B. G.; McGinty, S.; Nouri, F. Z.; Argungu, M.; Hawkins, E.; Hadji, A.; Weber, A.; Taylor, A.; Sepp, A. Modeling Bispecific Monoclonal Antibody Interaction with Two Cell Membrane Targets Indicates the Importance of Surface Diffusion. *MAbs* **2016**, *8* (5), 905–915. <https://doi.org/10.1080/19420862.2016.1178437>.
- (254) Sakata, J.; Tatsumi, T.; Sugiyama, A.; Shimizu, A.; Inagaki, Y.; Katoh, H.; Yamashita, T.; Takahashi, K.; Aki, S.; Kaneko, Y.; et al. Antibody-Mimetic Drug Conjugate with Efficient Internalization Activity Using Anti-HER2 VHH and Duocarmycin. *Protein Expr. Purif.* **2024**, *214* (September 2023), 106375. <https://doi.org/10.1016/j.pep.2023.106375>.

-
- (255) Maso, K.; Montagner, I. M.; Grigoletto, A.; Schiavon, O.; Rosato, A.; Pasut, G. A Non-Covalent Antibody Complex for the Delivery of Anti-Cancer Drugs. *Eur. J. Pharm. Biopharm.* **2019**, *142* (April), 49–60. <https://doi.org/10.1016/j.ejpb.2019.06.012>.

Appendix

A Supporting information

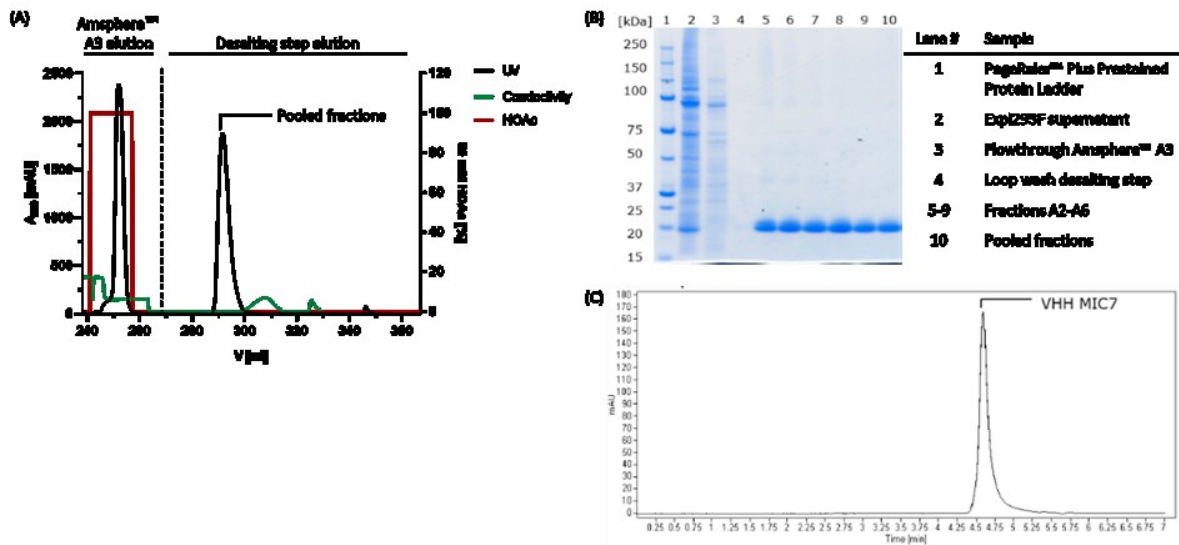


Figure S 1 Purification and characterization of mammalian expressed G₃-MIC7. (A) Affinity chromatography of purification and desalting of HEK293F supernatant using ÄKTA Xpress with Amsphere™ A3 and HiPrep™26/10 desalting column. (B) Semi-quantitative SDS-PAGE analysis of fractions revealed of purification steps using 4-12 % Bis-Tris gel and non-reduced sample preparation. Final pooled fraction of G₃-MIC7 is in lane 10. (C) Analytical SE-HPLC chromatogram of final G₃-MIC7 shows high monomeric purity. Figure adapted from Lehmann *et al.*¹⁸¹.

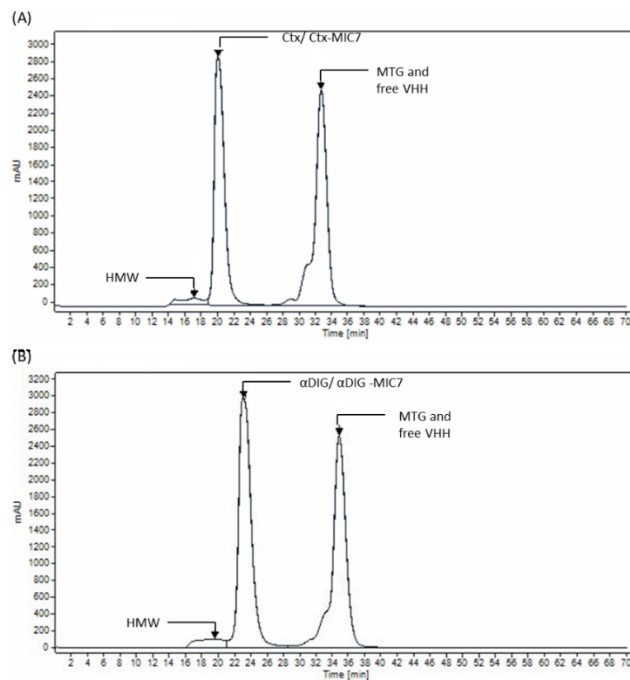


Figure S 2 Chromatograms of preparative SEC of antibody-VHH conjugates. (A) Purification MTG-mediated conjugation reaction of Ctx-MIC7. High molecular weight (HMW) species are 3.5% and eluted at 17.1 min, while the target Ctx-MIC7 eluted at 19.8 min. The free VHH and MIC7 eluted at 32.7 min. (B) Purification after MTG-mediated conjugation reaction of αDIG-MIC7. HMW are approximately 4% and eluted at 19.5 min, while the target Ctx-MIC7 eluted at 23.1 min. The free VHH and MIC7 eluted at 34.8 min. HPLC 1260 system with Superdex 200 10/300 GL increase column was used. Figure adapted from Lehmann *et al.*¹⁸¹.

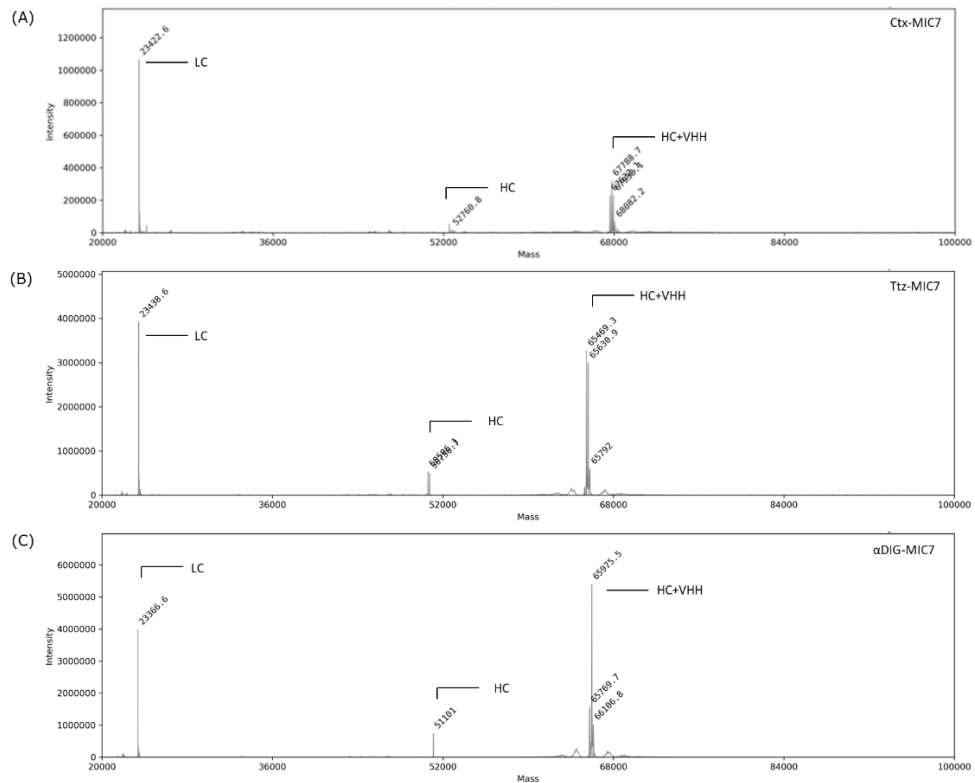


Figure S 3 VHH-to-antibody ratio (VAR) determination after purification of antibody-VHH conjugates. Deconvoluted MS spectra for assigging RP peaks to individual LC or HC species conjugated with VHH 'MIC7' via MTG-mediated conjugation to (A) Cetuximab, (B) Trastuzumab or (C) α DIG antibody. LC corresponds to the antibody light chain, HC to the heavy chain and HC+VHH represents the heavy chain conjugated with VHH. Figure adapted from Lehmann *et al.*¹⁸¹.

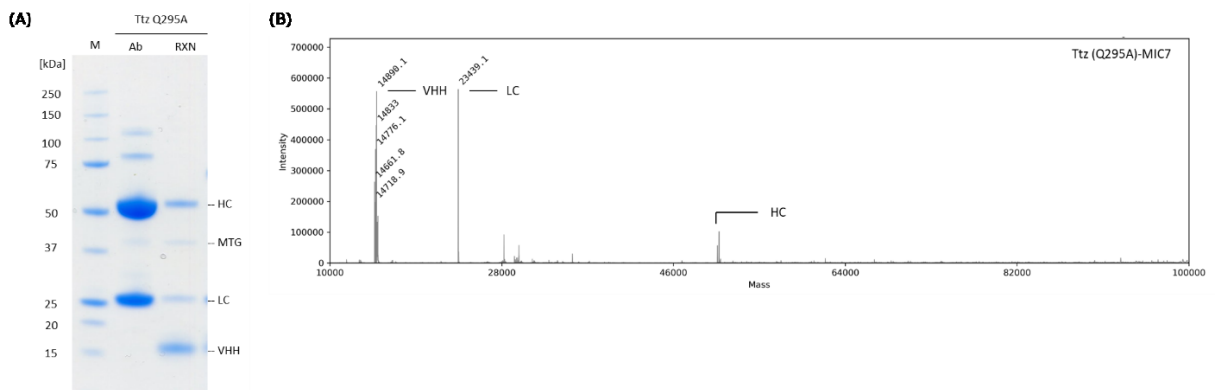


Figure S 4 Determination of VAR after conjugation reaction of Ttz (Q295A) and G₃-MIC7. (A) Reduced SDS-PAGE after MTG-mediated conjugation of Ttz Q295A. Ttz Q295A showed expected bands at 25 kDa (LC) and 50 kDa (HC). The reaction mix (RXN) shows the same bands plus unconjugated VHH G₃-MIC7 (approx. 15 kDa) and MTG (approx. 38 kDa) but no additional bands that would indicate VHH-mAb conjugation. (B) Deconvoluted MS spectra used to assign RP peaks to individual LC or HC species and VHH 'MIC7'.

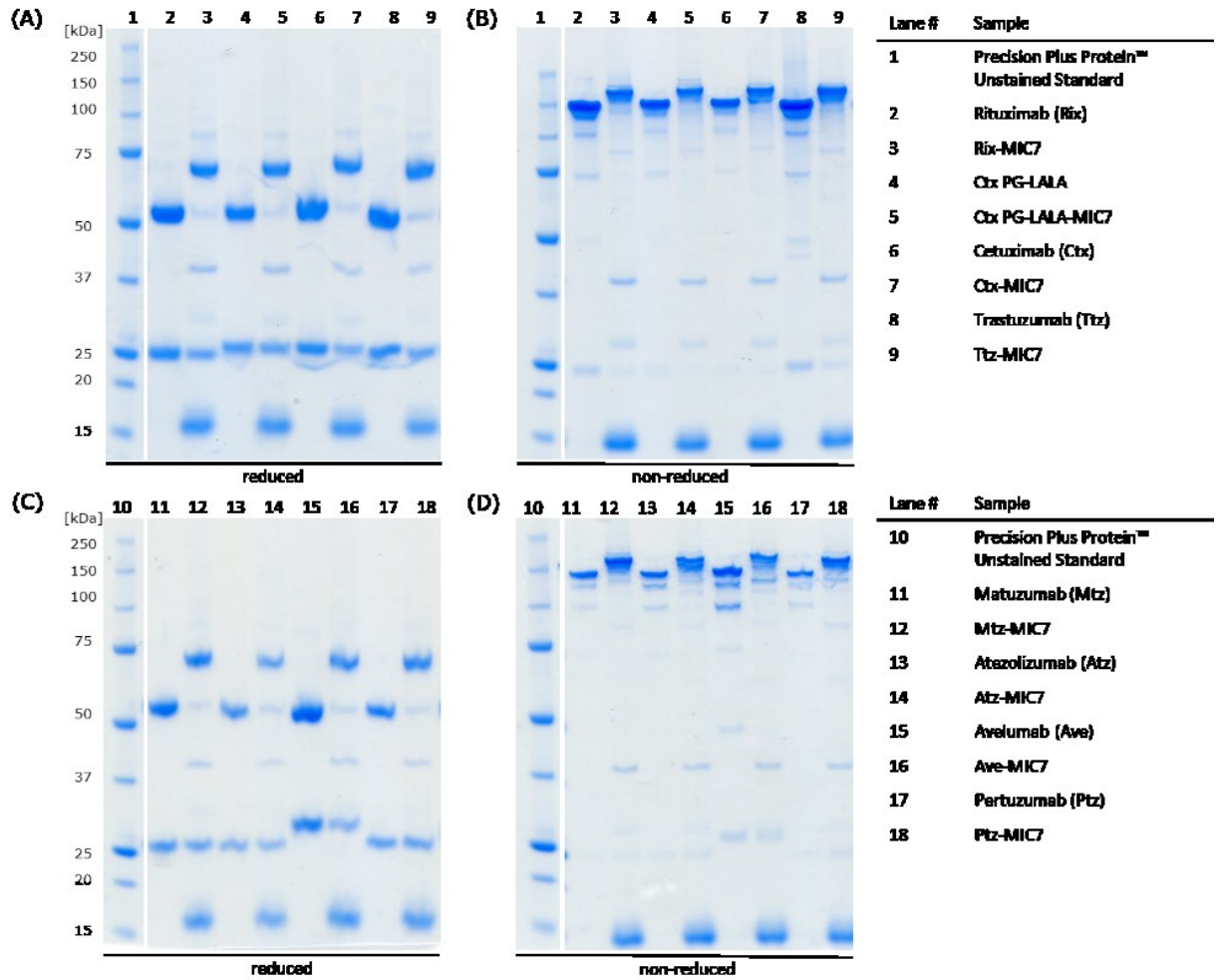


Figure S 5 Antibody-VHH conjugates of MTG-mediated coupling reaction. (A) Semi-quantitative analysis by gel electrophoresis of reduced reaction mixes and controls. In lanes of parental antibodies, bands at 25 kDa and 50 kDa were detected. A shift to 65 kDa is visible in the reaction mixture and represents the conjugation of VHH to the HC. (B) Non-reduced sample preparation of reaction mix containing Rituximab (Rix), Cetuximab (Ctx) and Trastuzumab (Ttz) antibody variants, G₃-MIC7 and MTG and parental antibodies. Bands of 150 kDa (VAR 0), 165 kDa (VAR 1) and 180 kDa (VAR 2) in non-reduced SDS-PAGE were visible in reaction mixtures. Reduced (C) and non-reduced (D) reaction mixes and references of Matuzumab (Mtz), Atezolizumab (Atz), Avelumab (Ave) and Pertuzumab (Ptz) analyzed by gel electrophoresis. MTG at 38 kDa and excess VHH at 15 kDa were detected in both reduced and non-reduced SDS-PAGEs. Figure adapted from Lehmann *et al.*¹⁸¹.

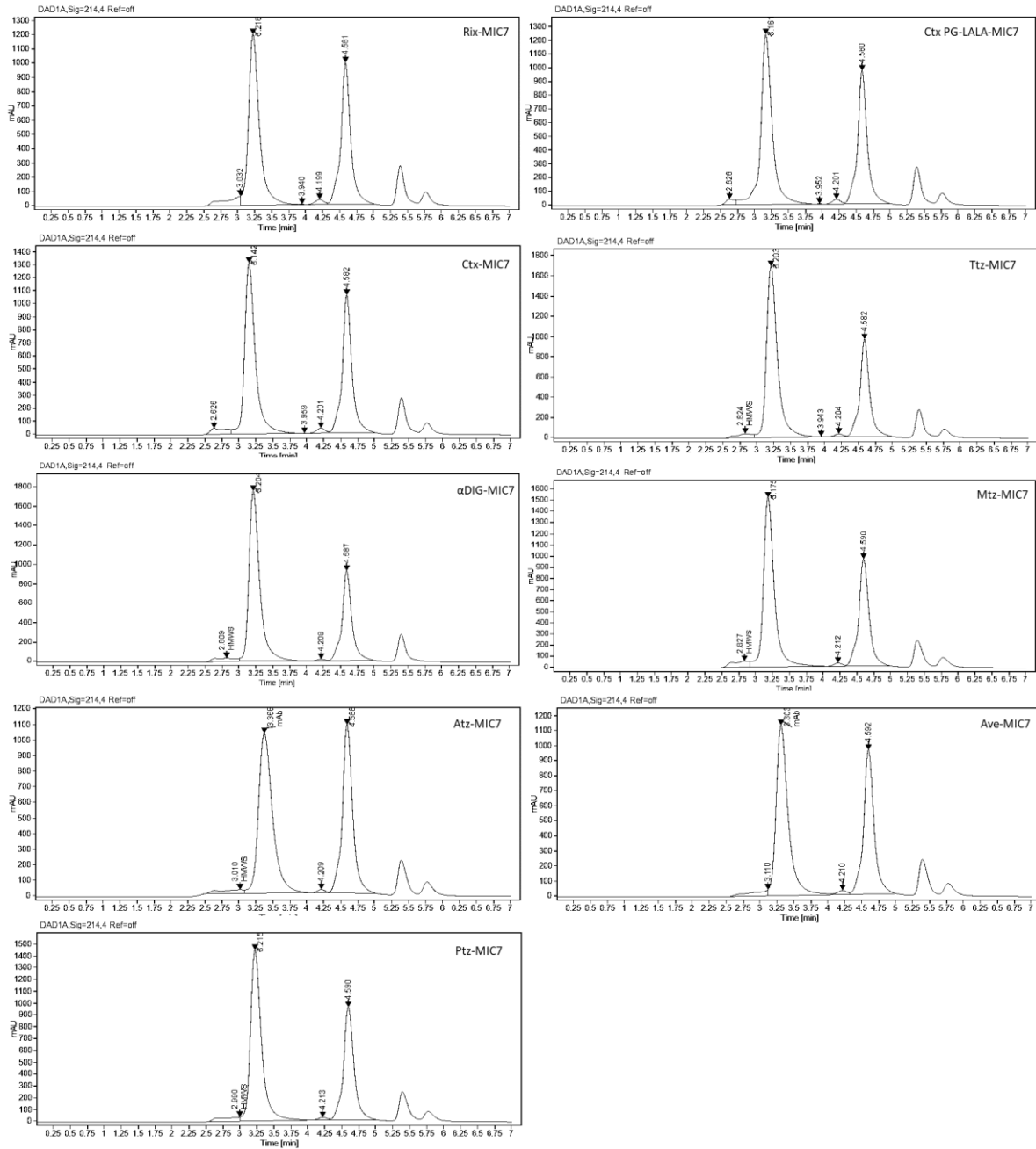


Figure S 6 A₂₁₄ signal of analytical SE-HPLC chromatogram of MTG-mediated conjugation reaction mixes. Antibody-VHH conjugate elute between 3.17 min and 3.36 min, MTG at 4.25 and free excess VHH at 4.59 min. High molecular weight (HMW) species eluted about 2.82 min. and were less than 3.96%.

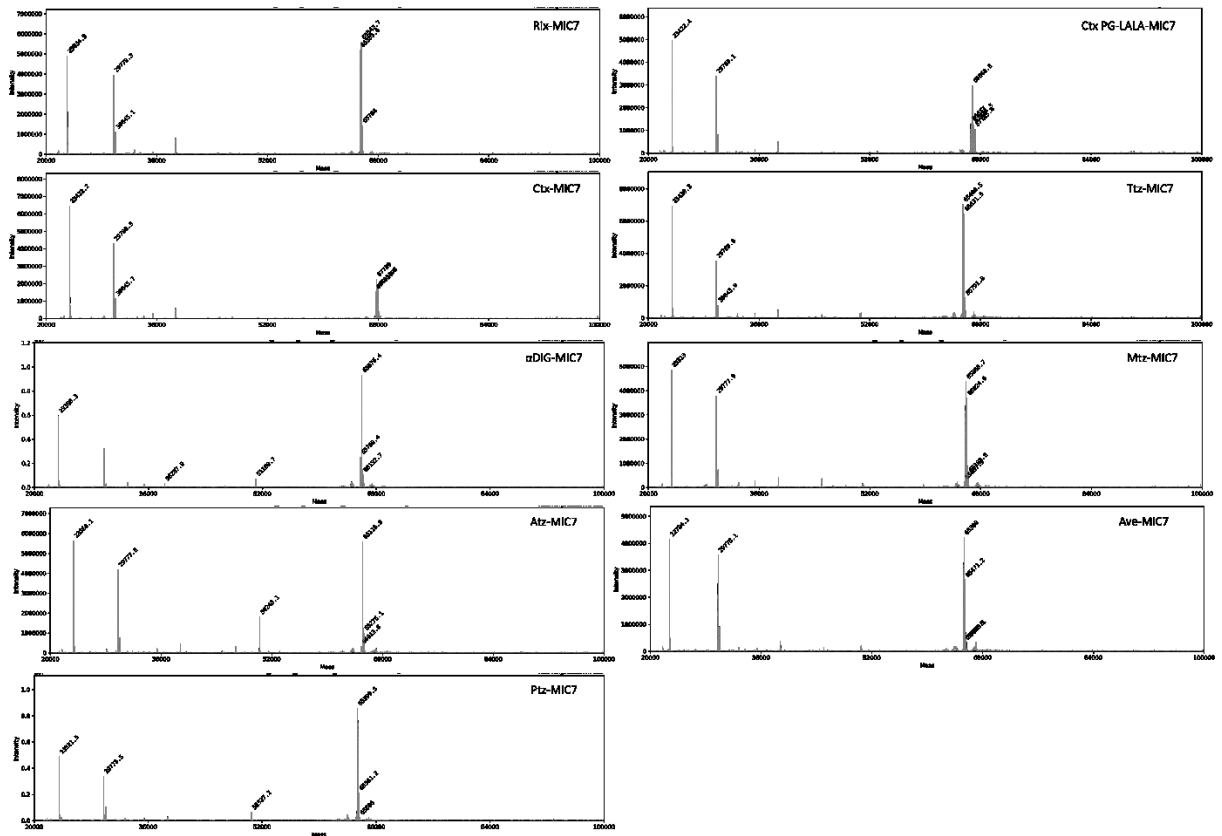


Figure S 7 Deconvoluted MS spectra of antibody-VHH conjugates for VAR determination. Peaks represent components of reaction mix including LC, MTG, HC and HC+VHH. Data set was acquired by the Lab of Roland Kellner, Merck KGaA.

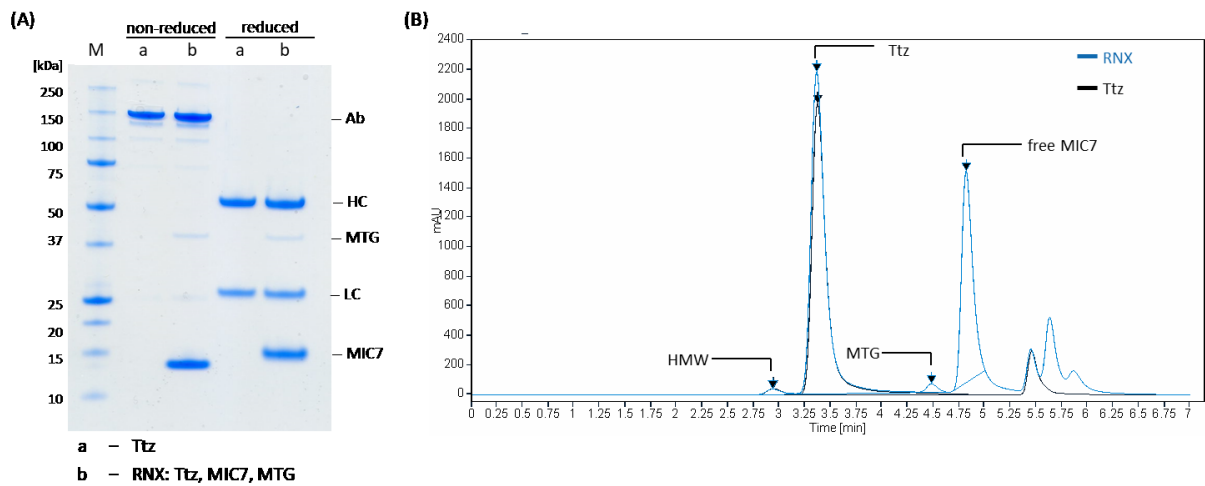


Figure S 8 Analysis of conjugation reaction mix of MIC7 missing G_3 -tag. **(A)** Semi-quantitative analysis of conjugation reaction and parental antibody. MTG-mediated conjugation was performed using G_3 -tag free MIC7 to verify MTG recognition motif and to exclude additional MTG recognition site. **(B)** Overlay of analytical SE-HPLC chromatograms of Ttz (black) and conjugation reaction (RNX, blue). 2% HMW were observed in Ttz and RNX at 2.94 min. Peak retention of Ttz at 3.37 min in RNX and reference confirms absence of conjugation. MTG elutes at 4.48 min and free MIC7 at 4.81 min.

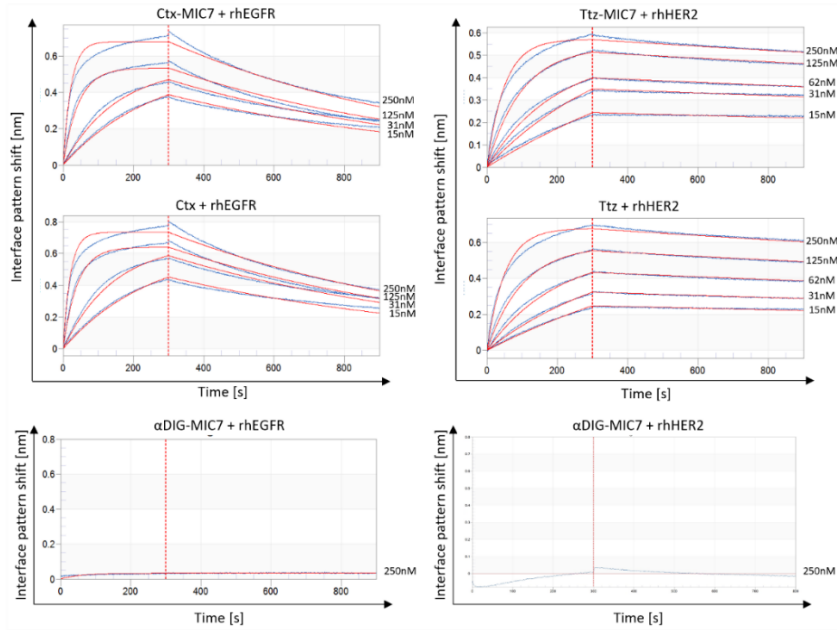


Figure S 9 Antigen binding analysis of antibody-VHH conjugate via BLI. The data were fitted using a 1:1 global full-fit binding model. The wavelength interference shift in nm is plotted on the x-axis of the sensorgrams, and the y-axis represents the time in seconds (s), with the fittings displayed in red. Figure adapted from Lehmann *et al.*¹⁸¹.

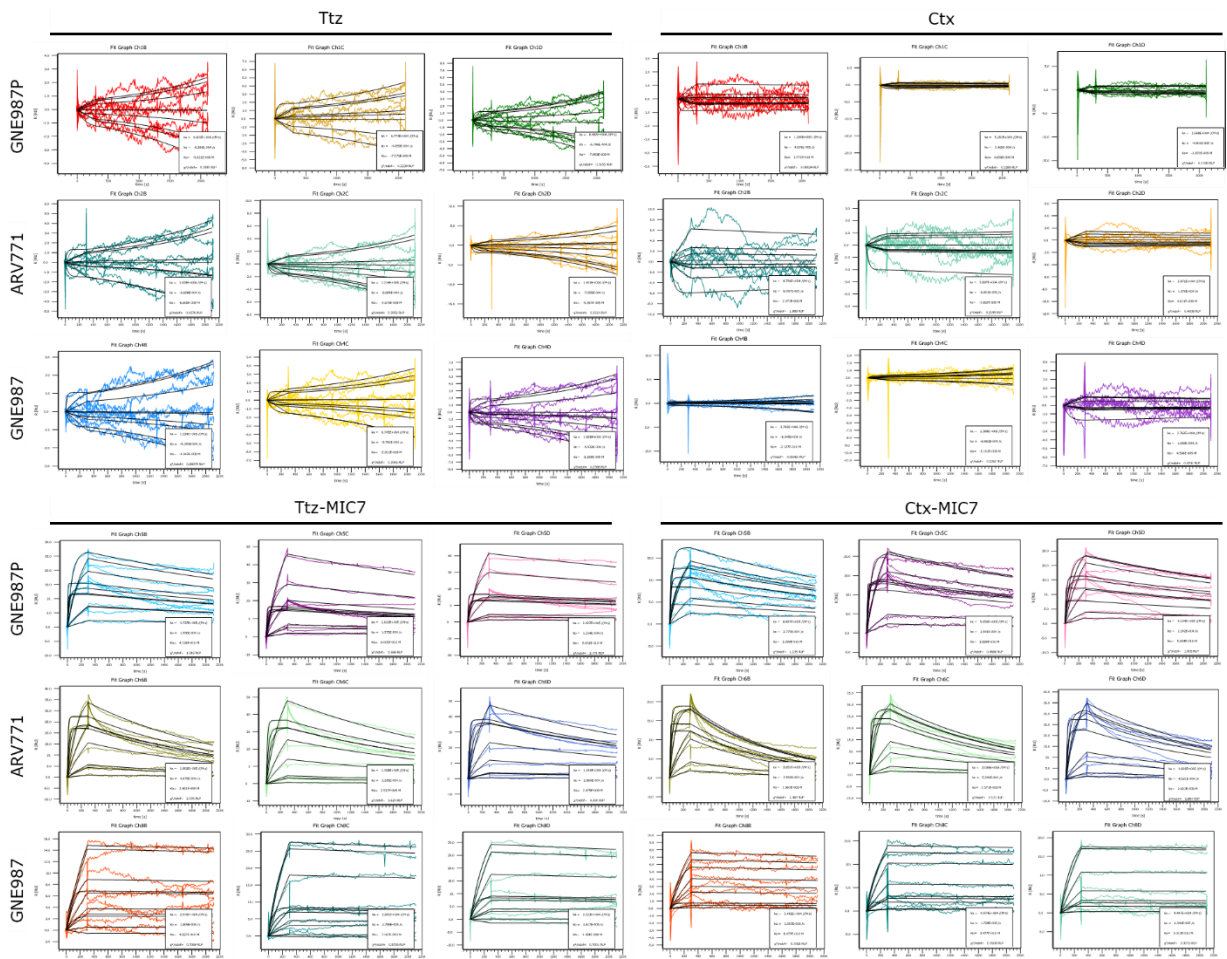


Figure S 10 PROTAC binding analysis of Ttz-MIC7 and Ctx-MIC7 and controls Ttz and Ctx via SPR analysis. All datasets were fit to a 1:1 Langmuir binding model. The fit is represented by a black line, and the data were obtained in triplicates. Data set was acquired by the laboratory of Dr. Daniel Schwarz, Merck KGaA.

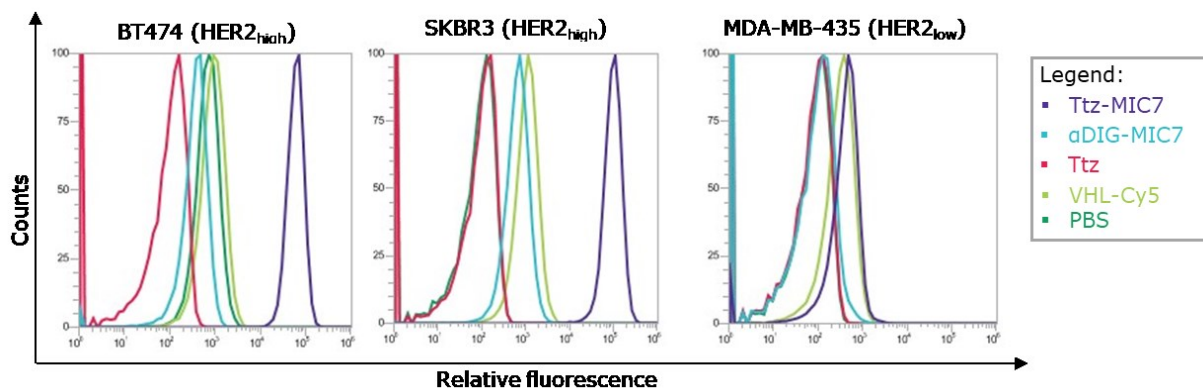


Figure S 11 Cellular binding of Ttz-MIC7, Ttz and reference molecules to different HER2-expressing cell lines. Ttz-MIC7 complexed with VHL-Cy5 shows binding to HER2_{pos} cell lines. No significant binding to HER2_{low} was observed. In addition, a reduced fluorescence signal was observed in VHL-Cy5-treated cells, indicating non-specific interaction induced by VHL-Cy5. No fluorescence signal was detected for Ttz, as VHL-Cy5 was not complexed.

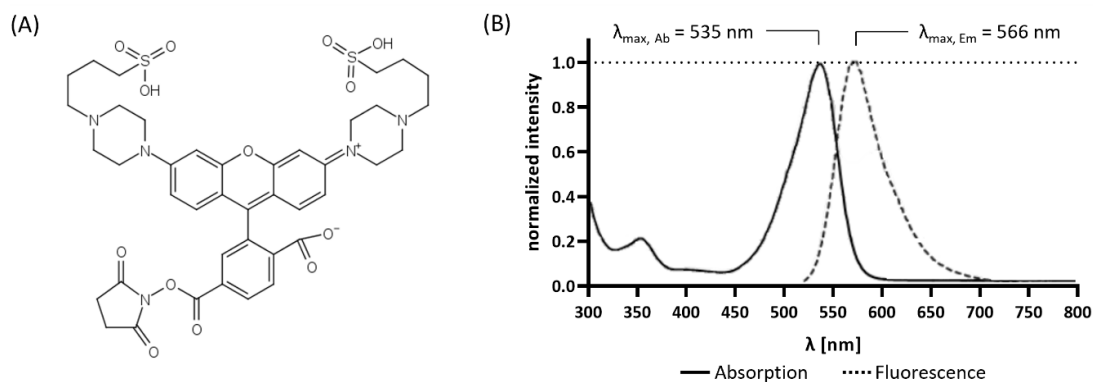


Figure S 12 (A) Structure of pHAb-amine reactive dye with NHS-active ester reacting with amino groups of e.g., lysine side chains. **(B)** Absorption spectra at 535 nm and fluorescence spectra at 566 nm of pHAb dye.

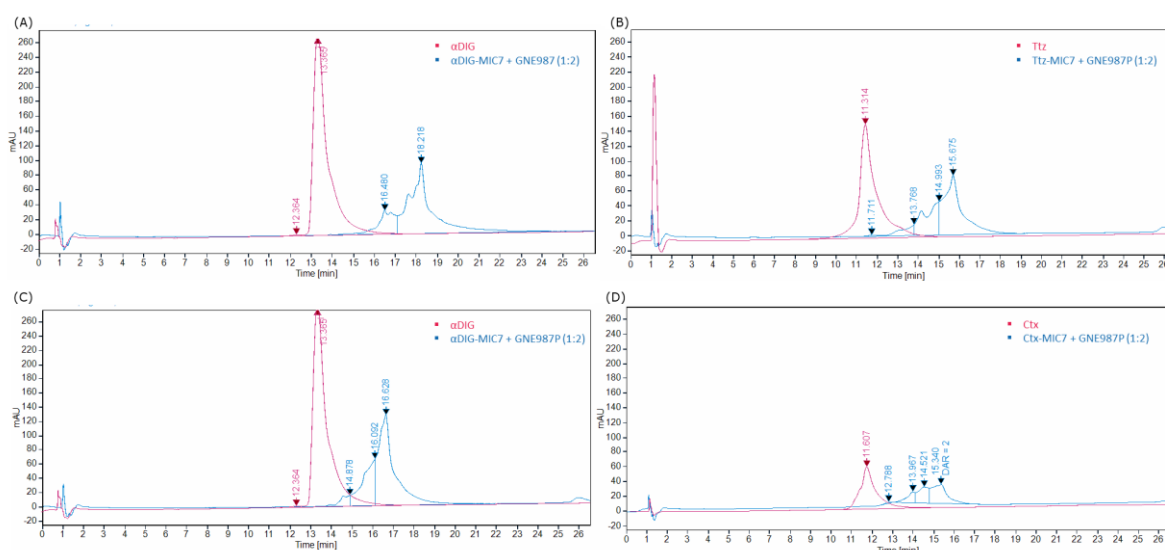


Figure S 13 HI-HPLC chromatograms of successful complexation between PROTACs and respective antibody-VHH conjugates. **(A)** An overlay of αDIG-MIC7 with GNE987 at a molar ratio of 1:2 (blue), along with the chromatogram of the αDIG parental antibody (pink). **(B)** Ttz-MIC7 complexed with GNE987P at a molar ratio of 1:2 (blue), with the chromatographic overlay showcasing Ttz (pink). **(C)** The complexation of αDIG-MIC7 with GNE987P at a molar ratio of 1:2 (blue), compared with the chromatogram of the parental antibody (pink). **(D)** The complex formation of Ctx-MIC7 with GNE987P at a molar ratio of 1:2 (blue), alongside the chromatogram of Ctx only (pink).

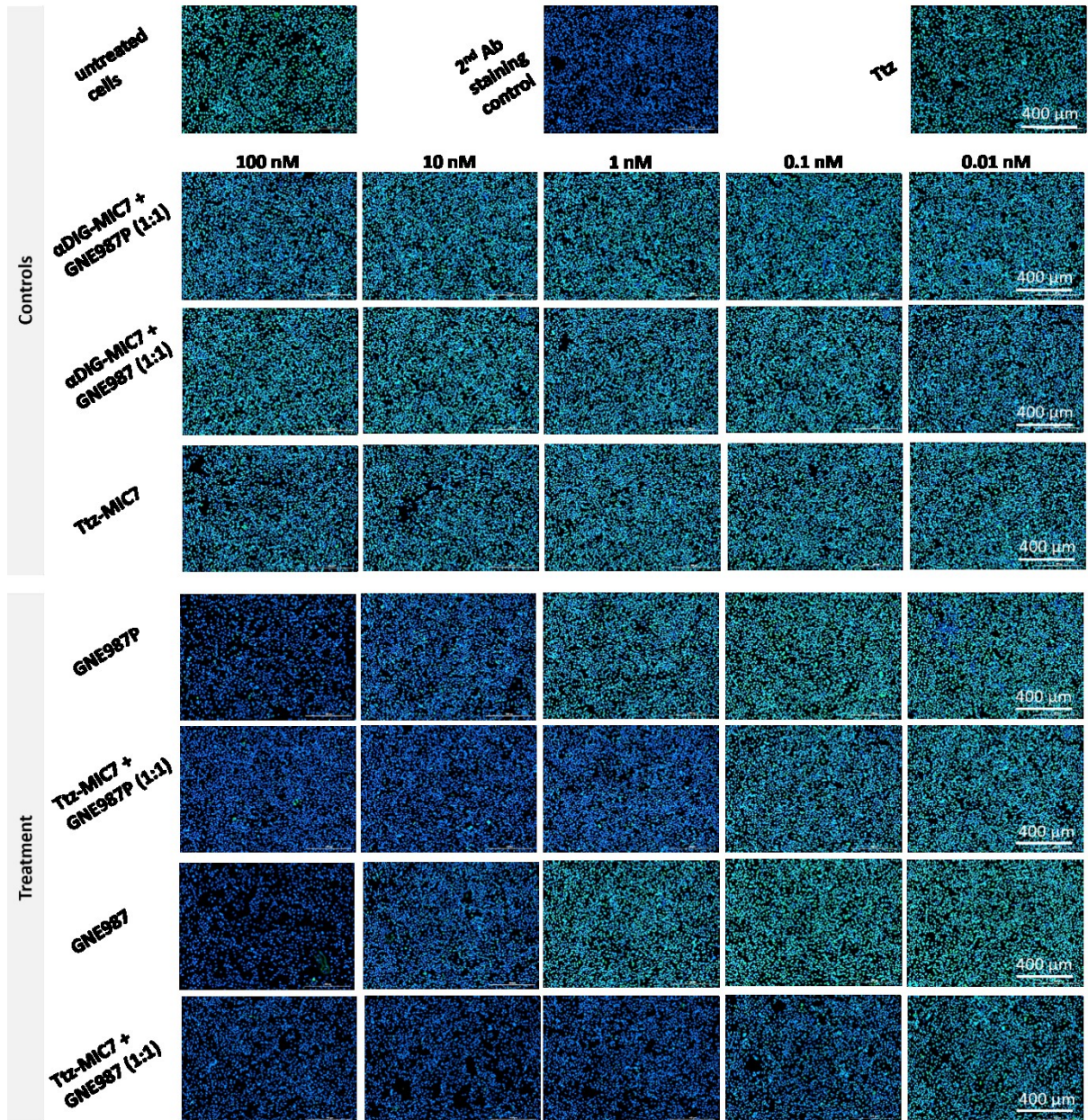


Figure S 14 Immunofluorescence microscopy of SKBR3 cancer cells. The cells underwent treatment with a 10-fold serial dilution of GNE987 and GNE987P, Ttz-MIC7 or α DIG-MIC7 loaded with GNE987 and GNE987P, and unloaded Ttz-MIC7, while untreated cells were utilized as a reference. Staining with only the secondary detection antibody was conducted to eliminate false-positive signals. Images were taken with Cell Imaging Multimode Reader Cytation 5 (BioTek/Agilent) including 10x objective and LED intensity 10. GFP channel: ex.: 469 nm, em: 525 nm and DAPI channel: ex.: 377 nm, em.: 447 nm were used. Integration time of 48 ms with a camera gain of 24 were applied for the GFP channel. For the DAPI channel 5 ms integration time and camera gain of 17 were used.

Table S 1 Inhibitory activity of complexed and free PROTACs. IC₅₀ values are given as mean for N=3 technical replicates. nd: not determined, -: low or no impact on cell viability. Table adapted from Lehmann *et al.*¹⁸¹.

IC ₅₀ [M]	SKBR3			BT474		
	GENE987	GENE987P	Non-complexed	GENE987	GENE987P	Non-complexed
Ttz-MIC7	4.2 x 10 ⁻¹⁰	5.5 x 10 ⁻¹⁰	1.5 x 10 ⁻⁹	6.7 x 10 ⁻¹⁰	7.3 x 10 ⁻¹⁰	1.1 x 10 ⁻⁹
αDIG-	2.2 x 10 ⁻⁷	>1.0 x 10 ⁻⁷	>1.0 x 10 ⁻⁷	>1.0 x 10 ⁻⁷	2.9 x 10 ⁻⁷	>1.0 x 10 ⁻⁷
Ttz	-	-	8.5 x 10 ⁻¹⁰	-	-	8.0 x 10 ⁻¹⁰
free PROTAC	5.5 x 10 ⁻¹⁰	2.5 x 10 ⁻⁸	-	3.5 x 10 ⁻¹⁰	1.3 x 10 ⁻⁸	-

	A431			MDA-MB-468		
	GENE987	GENE987P	Non-complexed	GENE987	GENE987P	Non-complexed
Ctx-MIC7	1.8 x 10 ⁻¹⁰	4.3 x 10 ⁻¹⁰	3.2 x 10 ⁻⁹	1.8 x 10 ⁻¹⁰	2.4 x 10 ⁻¹⁰	>1.0 x 10 ⁻⁷
αDIG-	nd	3.0 x 10 ⁻⁸	>1.0 x 10 ⁻⁷	nd	>1.0 x 10 ⁻⁷	>1.0 x 10 ⁻⁷
Ctx	-	-	3.1 x 10 ⁻⁹	-	-	>1.0 x 10 ⁻⁷
free PROTAC	1.8 x 10 ⁻¹⁰	3.7 x 10 ⁻⁸	-	9.3 x 10 ⁻¹¹	2.8 x 10 ⁻⁸	-

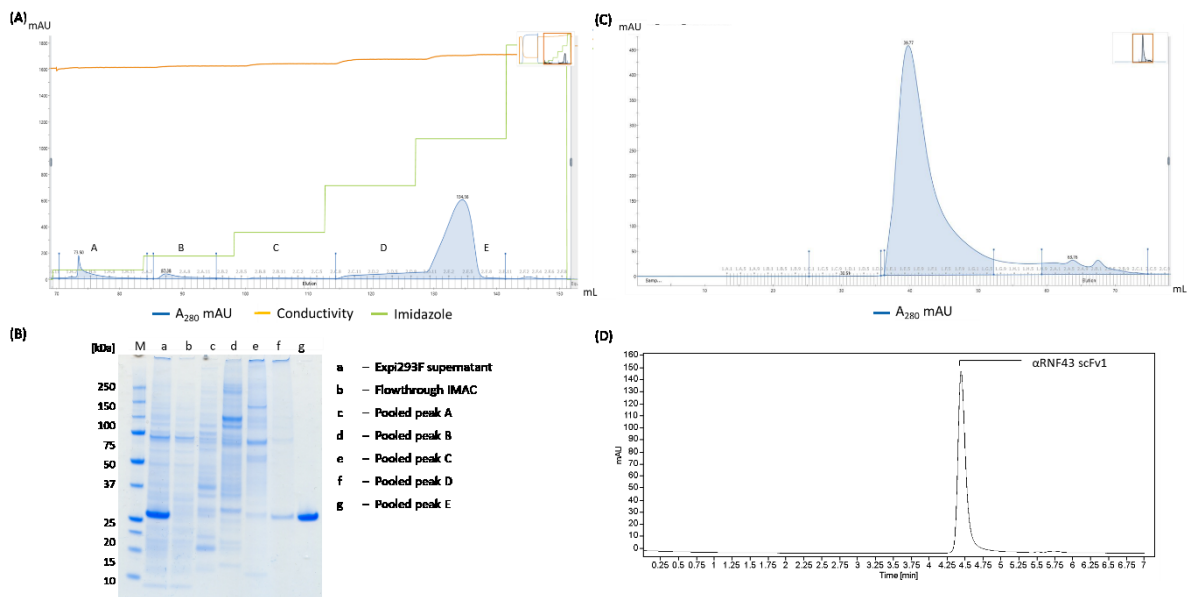


Figure S 15 IMAC purification process exemplarily shown for scFv1 variant targeting RNF43. (A) ÄKTA pure chromatogram showing the elution of protein in IMAC affinity chromatography with 50 mM sodium phosphate, 0.5 M NaCl, pH 7.4 and stepwise gradient of 500 mM imidazole final. (B) SDS-PAGE analysis using 4-12% Bis-Tris gel of the following samples: non-reduced Expi293F supernatant, IMAC flowthrough, pools of peak A-E. (C) ÄKTA pure chromatogram showing the elution of purified protein (peak E) in the desalting step. (D) A₂₈₀ signal of analytical SE-HPLC chromatogram of purified scFv1 shows high purity and no high molecular weight species.

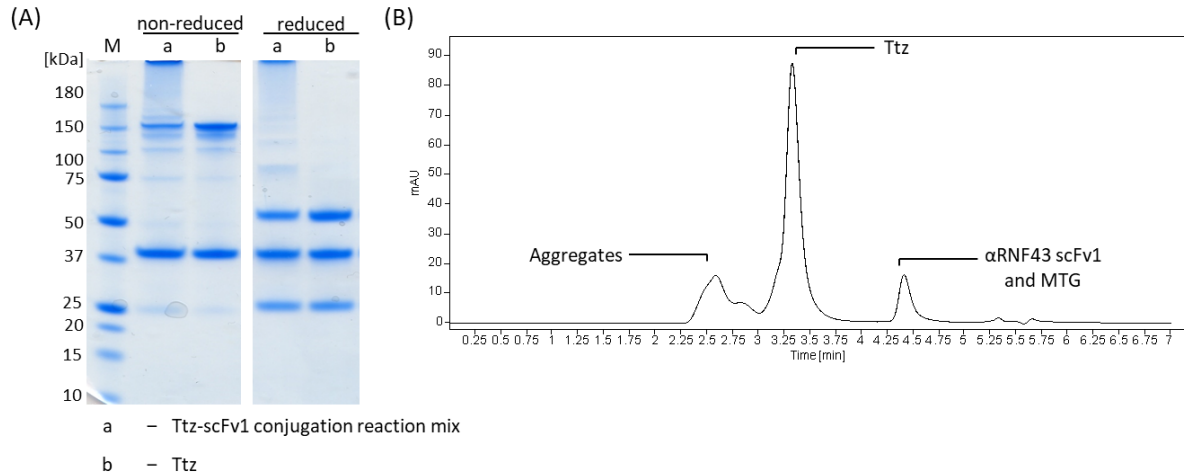


Figure S 16 (A) SDS-PAGE analysis using 4-12% Bis-Tris gel of the following samples: conjugation reaction mix of Ttz, scFv1 and MTG and Ttz only. Samples were prepared as non-reduced and reduced set. **(B)** A_{280} signal of analytical SE-HPLC chromatogram of purified scFv1 shows the Ttz peak and 25% high molecular weight species. Unconjugated scFv1 and MTG eluted at approximately 4.41 min.

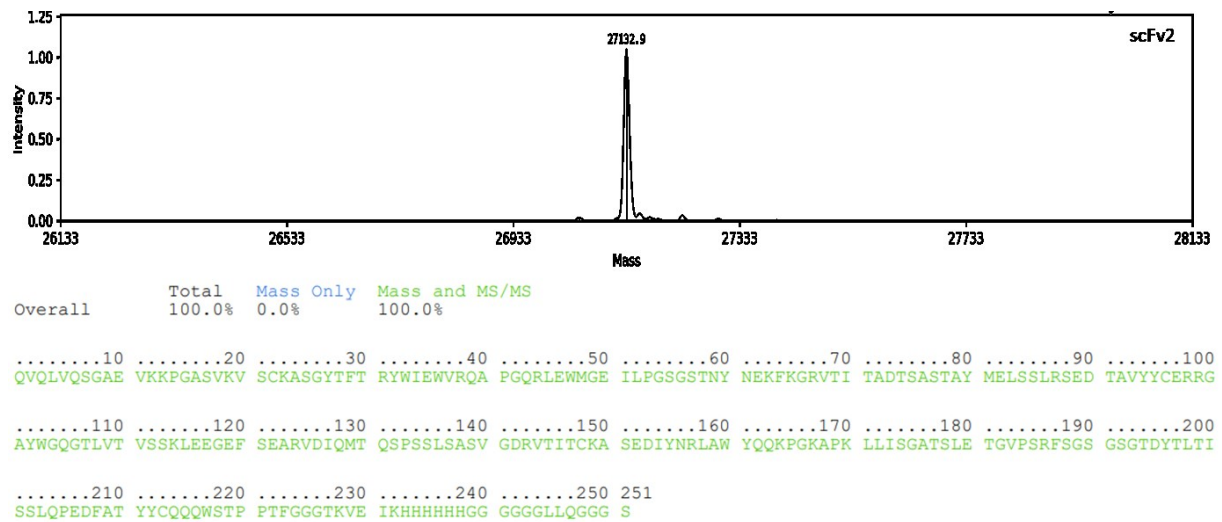
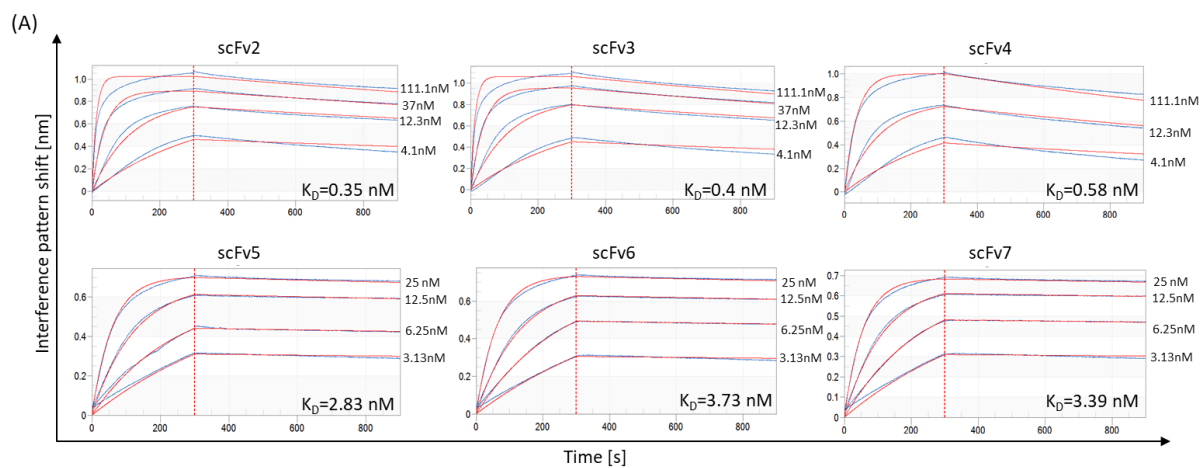


Figure S 17 Determination of identity of scFv variant 2. The MS spectra shows the MW of 27132.9 Da for scFv2, which is within the expected range. The sequence was confirmed by peptide mapping and LC-MS. This data set is shown as an example for scFv2 and can be transferred to the other variants. Data set was acquired by the laboratory of Roland Kellner, Merck KGaA.



SeqID	Antigen	K_D [M]	K_{on} [$M^{-1}s^{-1}$]	K_{dis} [s^{-1}]
scFv 2	rhRNF43	3.5×10^{-10}	6.93×10^5	2.42×10^{-4}
scFv 3	rhRNF43	4.0×10^{-10}	6.92×10^5	2.80×10^{-4}
scFv 4	rhRNF43	5.8×10^{-10}	7.32×10^5	4.24×10^{-4}
scFv 5	rhRNF43	2.83×10^{-9}	9.37×10^5	2.65×10^{-3}
scFv 6	rhRNF43	3.73×10^{-9}	8.71×10^5	3.25×10^{-3}
scFv 7	rhRNF43	3.39×10^{-9}	1.29×10^6	4.38×10^{-3}

Figure S 18 Binding analysis of scFv variants with rhRNF43 antigen via BLI. (A) Association and dissociation were fitted by a 1:1 global full-fit binding model. The x-axis of the sensorgrams represents the wavelength interference shift in nm and the y-axis the time in seconds (s). Fittings are shown in red. **(B)** Respective dissociation constants (K_D) were calculated from fitting using FortéBio data analysis software.

Table S 2 Test conjugation for activated scFv variants. For scFv variants DAR is given as a mean from RP-HPLC and LC-MS analysis. SE-HPLC purity refers to the final monomer click derivate conjugate.

	1		3		4		5		6	
	DAR	Purity [%]	DAR	Purity [%]	DAR	Purity [%]	DAR	Purity [%]	DAR	Purity [%]
scFv 2	0.79	100	0.91	100						
scFv 3	0.78	100	0.68	100						
scFv 4	0.89	100								
scFv 5	0.86	100	0.95	99.2	0.9	99.2	0.81	98	0.57	100
scFv 6	0.84	100	0.95	99.3	0.9	99.3	0.74	97.4	0.53	100
scFv 7	0.86	100	0.95	99.3	0.9	99.3	0.83	100	0.62	100

Table S 3 Test conjugation for activated scFv variants. For Ttz DAR is given as a mean from RP-HPLC and LC-MS analysis. SE-HPLC purity refers to the final monomer click derivate conjugate.

[U/mL]	1		2	
	DAR	Purity [%]	DAR	Purity [%]
10	1.90	99.1	1.84	99.2
15	2.00	99.4	1.92	99.4
25	1.96	99.1	1.92	99.3
50	1.98	98.8	1.88	99.0
75	1.96	98.8	1.98	99.0

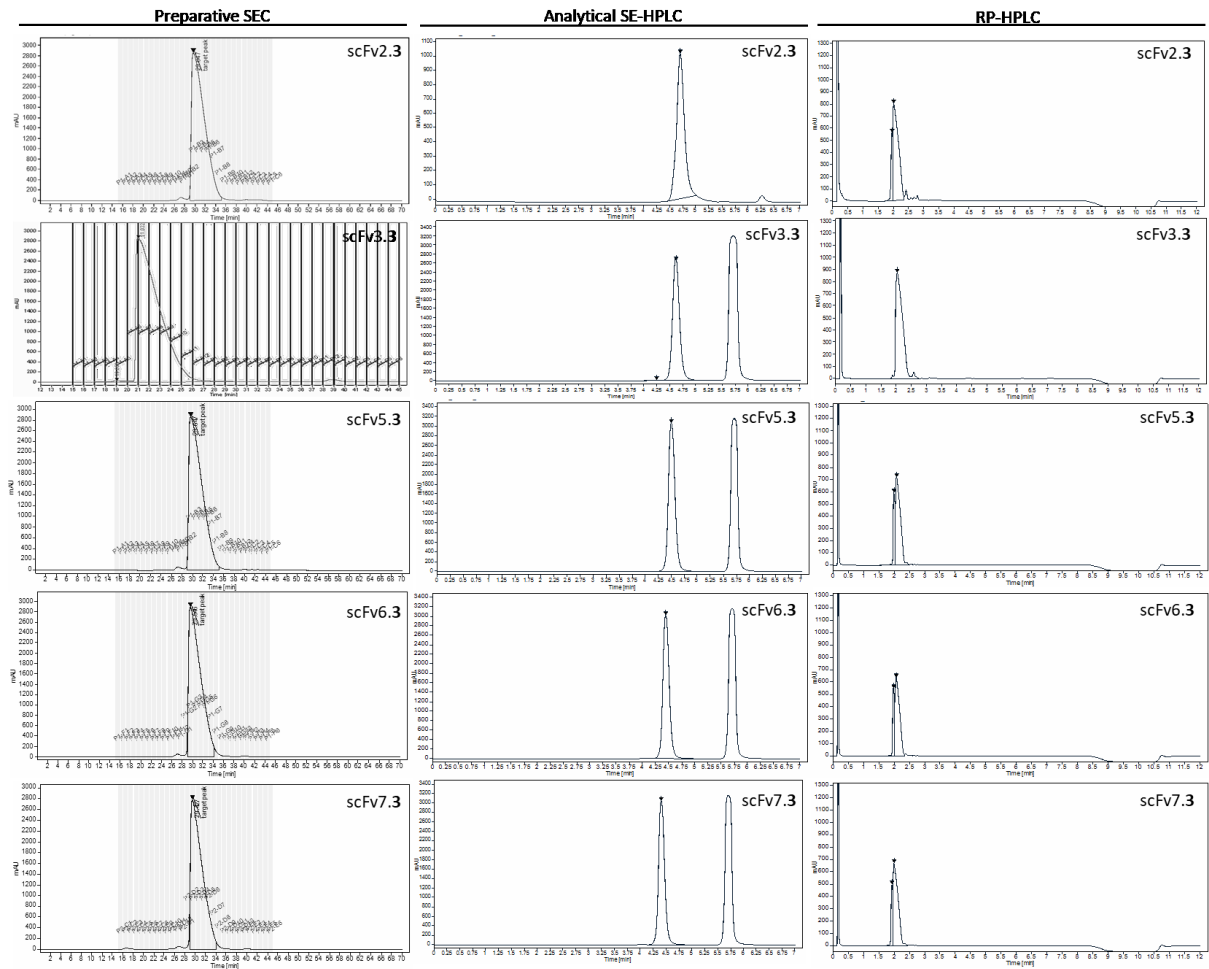


Figure S 19 Chromatographical purification and characterization of MTG-mediated click derivate conjugation of scFv variants. A₂₈₀ chromatogram of preparative SEC was used to separate the product peak from HMW. A₂₁₄ chromatogram of analytical SEC reveals the monomeric purity of the final conjugates and RP-HPLC was used to determine the final DAR.

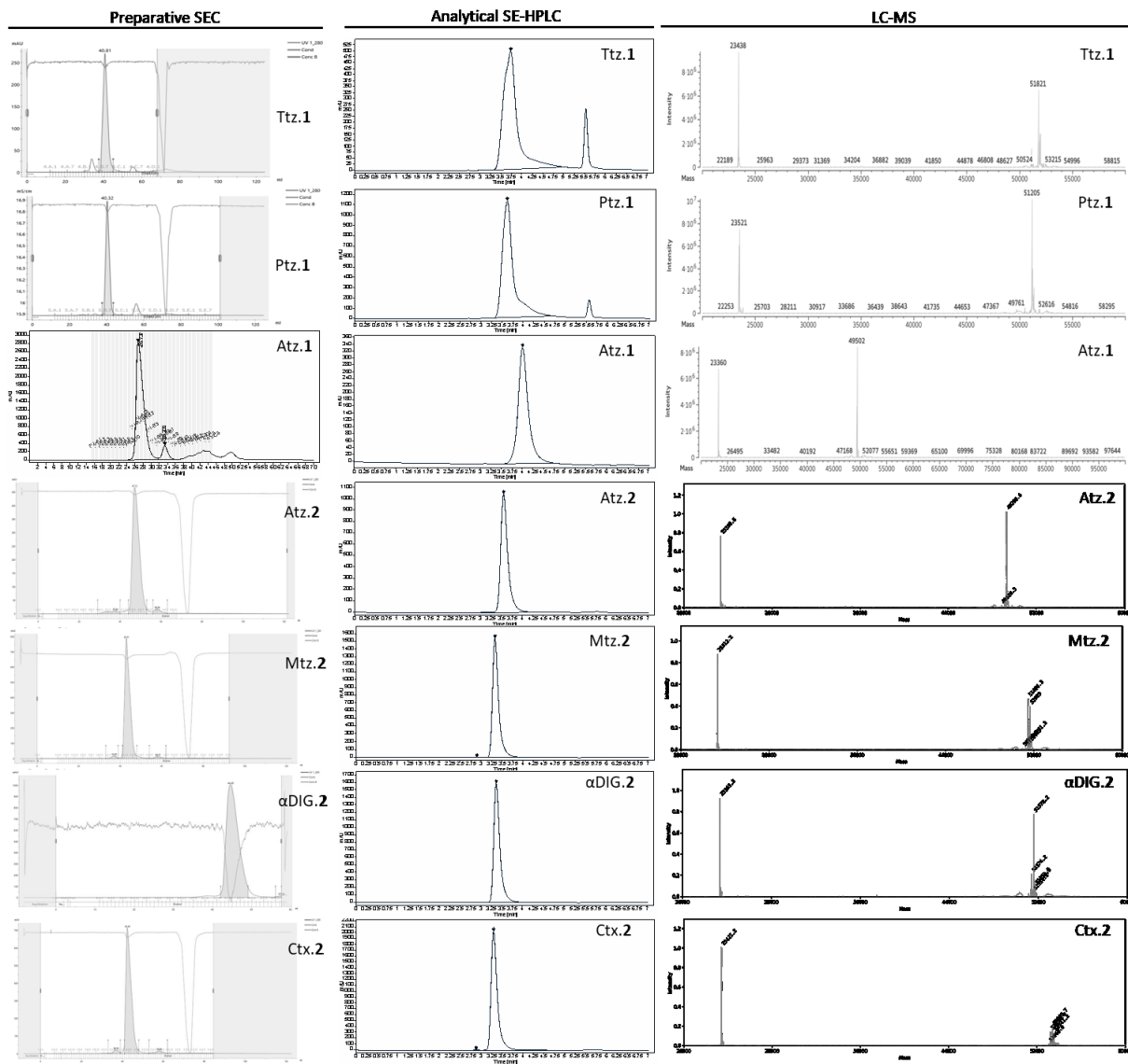


Figure S 20 Chromatographical purification and characterization of MTG-mediated click derivate conjugation of antibodies. A₂₈₀ chromatogram of preparative SEC was used to separate the product peak from HMW. A₂₁₄ chromatogram of analytical SE-HPLC reveals the monomeric purity of the final conjugates and reduced LC-MS was used to determine the final DAR. LC-MS data set was acquired by the Lab of Roland Kellner, Merck KGaA.

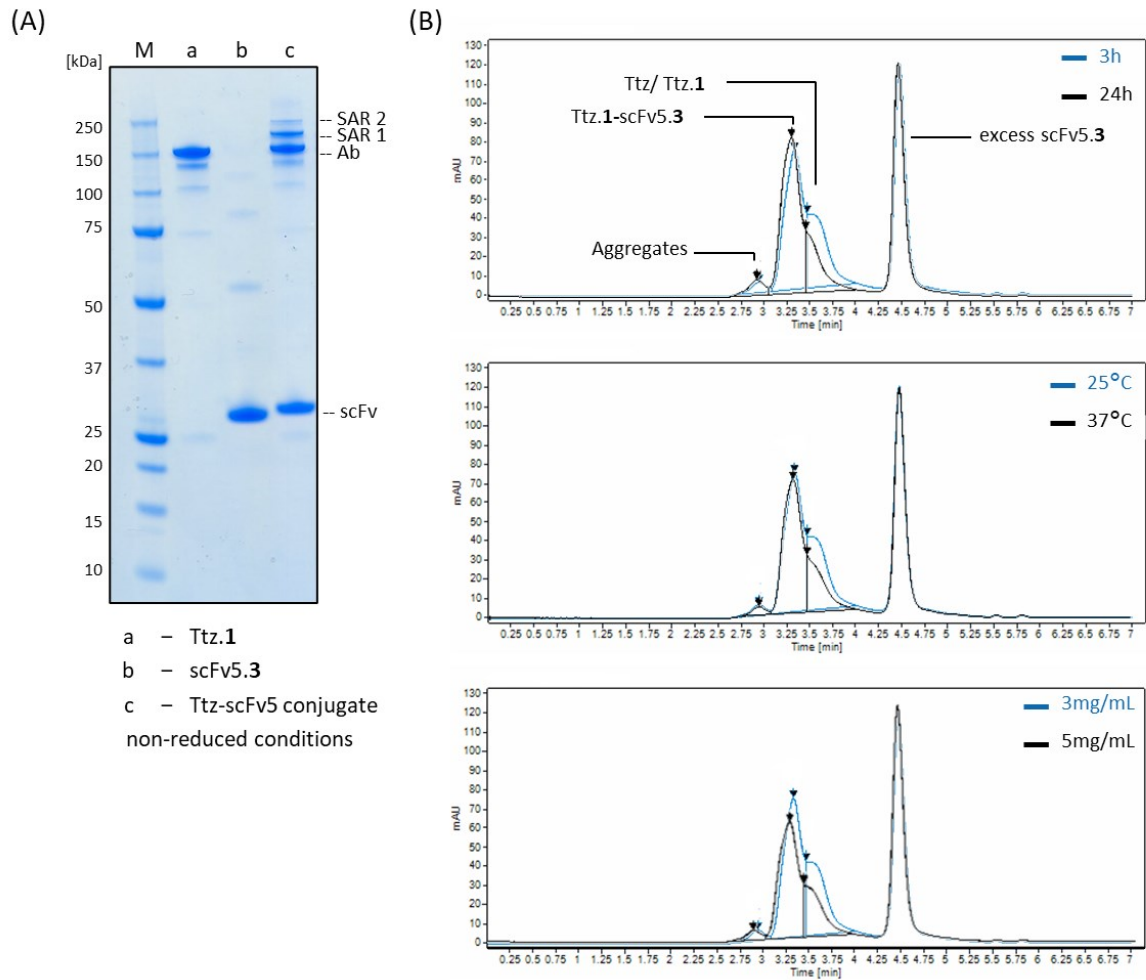
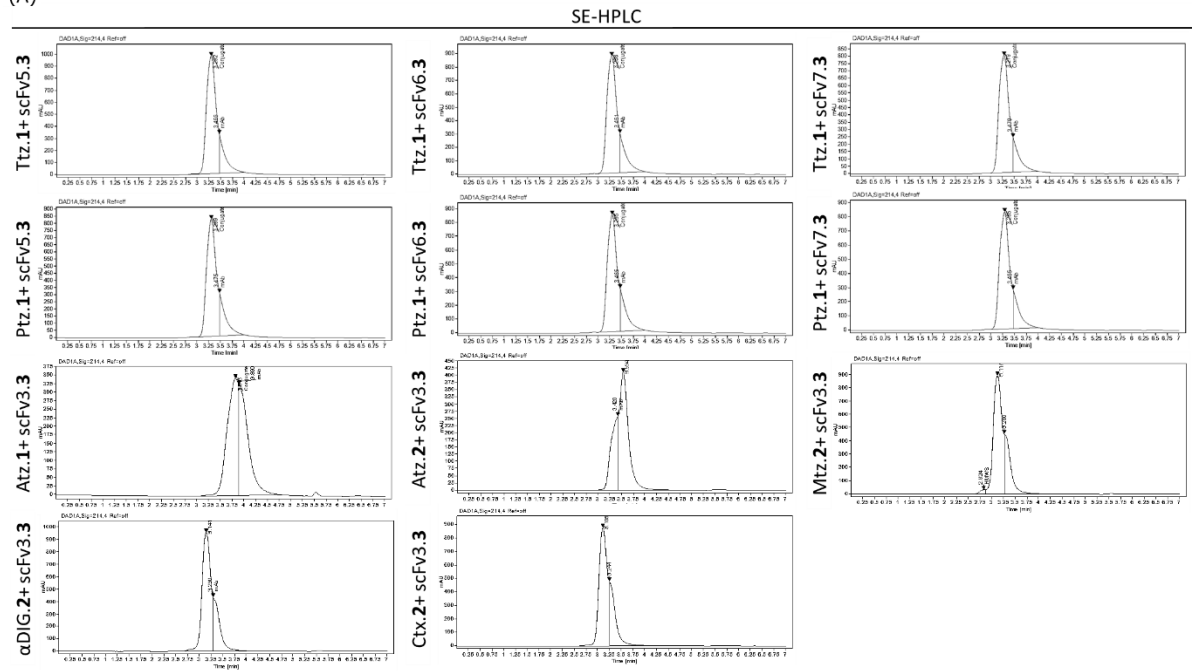


Figure S 21 (A) SDS-PAGE analysis using 4-12% Bis-Tris gel of the following samples: Ttz.1 (lane a), scFv5.3 (lane b) and reaction mix after 3 hours and 30 °C SPAAC click reaction (lane c). Samples were prepared under non-reducing conditions. **(B)** Overlay of analytical SE-HPLC chromatogram with A_{280} signal of SPAAC reaction mixes including Ttz.1 and scFv5.3 at different reaction conditions. The clicked bispecific Ttz.1-scFv5.3 elutes after 3.29 min, while the Ttz.1 elutes at 3.60 min. HMW species of approximately 4% were detected at 2.92 min and non-clicked scFv5.3 eluted after around 4.46 min.

(A)



(B)

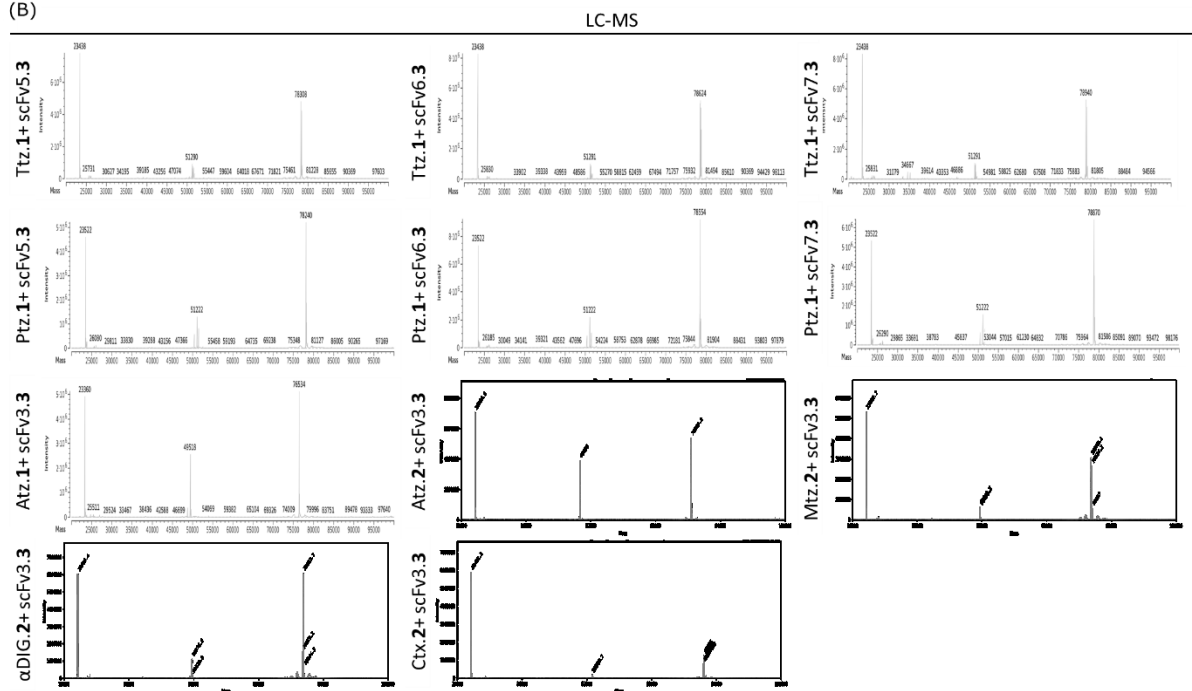
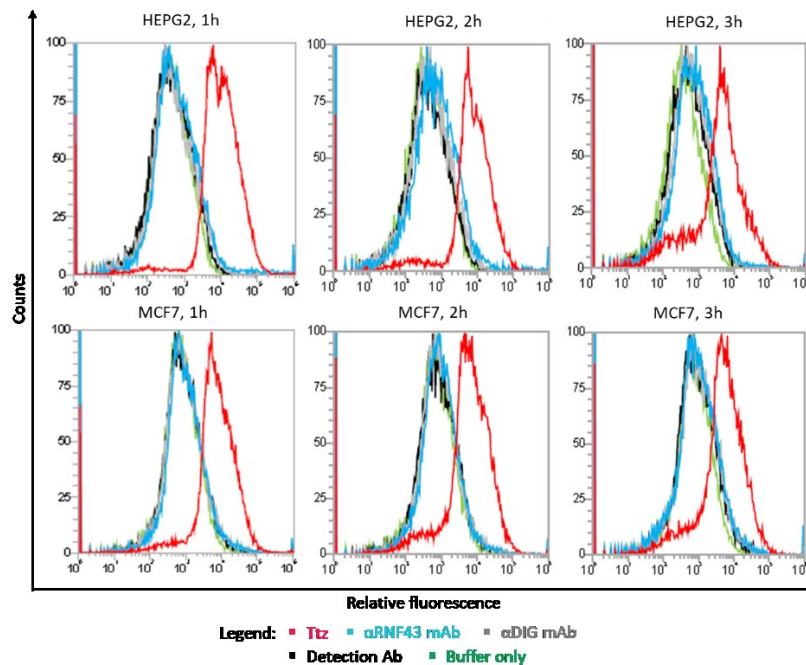
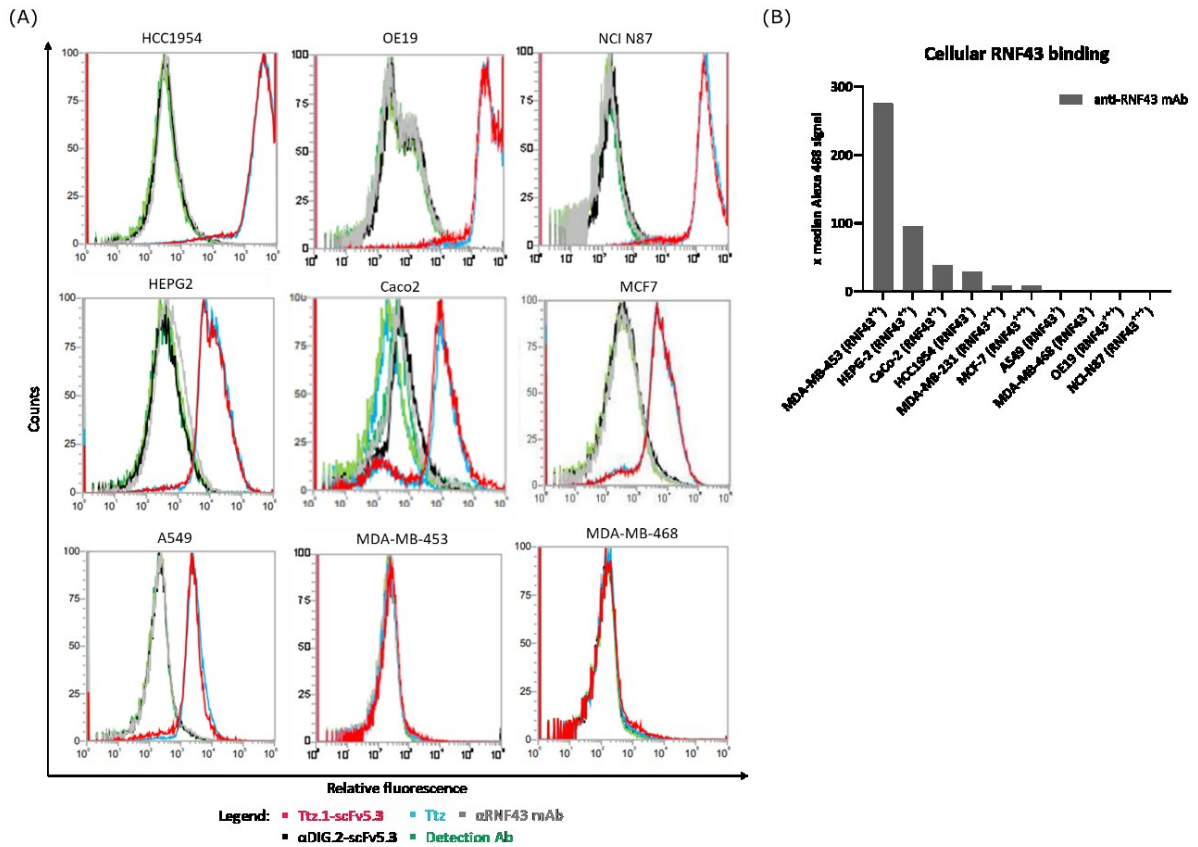


Figure S 22 Determination of scFv- to-Antibody ratio (SAR) of IgG-scFv conjugates. (A) SE-HPLC chromatograms (A_{214nm}) of purified IgG-scFv conjugates. **(B)** Deconvoluted MS spectra were employed to assign RP peaks to light chain and heavy chain species conjugates with scFv variants. Data set was acquired by the Lab of Roland Kellner, Merck KGaA.



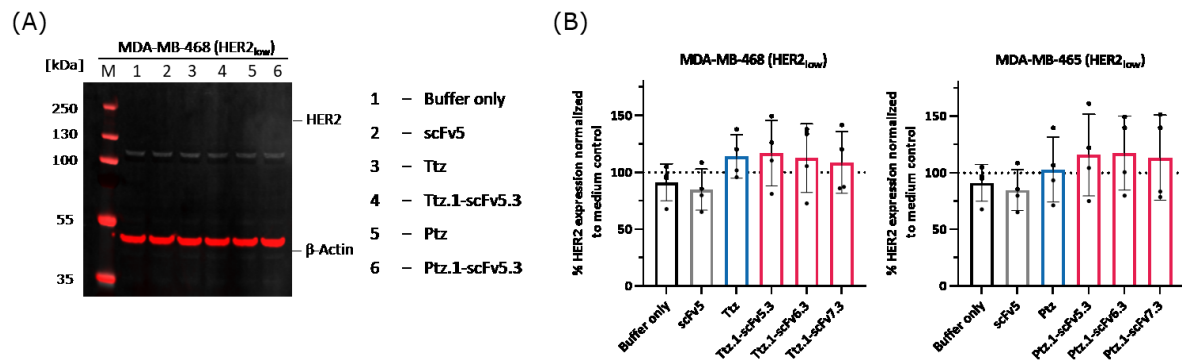


Figure S 25 Target degradation on HER2_{low} cell line MDA-MB-468. (A) Western Blot analysis of HER2 levels after 24 hours treatment with 10 nM Ttz.1-scFv5.3 and Ptz.1-scFv5.3. Monospecific molecules, including scFv5, Ttz and Ptz were used as a reference along with buffer treatment. After treatment, cells were lysed and 150 μM protein was used for Western Blot analysis. β-actin served as a housekeeping control and was detected with fluorophore-labeled secondary antibody. **(B)** Flow cytometric analysis of HER2 level on MDA-MB-468 cell surface. Cells were treated with 10 nM Ttz.1-scFv5.3 and Ptz.1-scFv5.3 for 24 hours and after harvest and staining FACS analysis was performed. Treatment results are normalized to buffer only treatment. The values represent the mean of technical triplicates with SD as error bar.

B List of figures

Figure 1 Structure of antibody and fragments. (A) The IgG-based antibody is depicted in a schematic representation, featuring two identical heavy (HC) and light chains (LC). The fragment crystalline (Fc) region is composed of C_H2 and C_H3 domains, while the fragment antigen binding (Fab) unit is formed by V_H and C_H1 of the HC and V_L and C_L of the LC. The antigen binding sites are formed by the Fragment variable (Fv) form with the CDR 1-3 regions. The glycosylation site is in the Fc fragment at position N297. **(B)** Schematic representation of antibody fragments. The monovalent Fab, capable of binding the antigen with the variable region, lacks the Fc part and does not exhibit effector functions. The scFv, comprising the V_H and V_L along with a linker unit, weighs approx. 25 kDa and can bind its antigen through the CDR regions. The smallest antigen-binding unit, the camelid heavy-chain variable domain (VHH), weighs around 15 kDa and binds the antigen with one prolonged CDR region..... 7

Figure 2 Bispecific antibody formats categorized by non-IgG-like formats without Fc-fragment and Fc-fragment based formats. The Fc-fragment based fragments are further classified in asymmetric and symmetric architecture. Each color represents a variable domain (variable heavy chain specificity 1 - green, variable light chain specificity 1 - light green, variable heavy chain specificity 2 - blue, variable light chain specificity 2 - light blue), the connecting peptide linkers are shown as black line. The dark grey colored C_L shows the light chain switch for. The “knob-into-hole” amino acid exchange for correct heavy chain pairing is shown as black circle within the C_H3 domain of the antibody..... 10

Figure 3 Schematic conjugation strategies for generation of different antibody-drug conjugates (ADC). FDA-approved ADCs are typically conjugated via chemical methods, such as the reaction of cysteines with maleimides in a Michael addition. Newer approaches of chemoenzymatic and enzymatic strategies show promising results in pre-clinical studies. For simplicity, the conjugation to the antibody is only shown on one chain of the protein.	13
Figure 4 Strain-promoted azide-alkyne cycloaddition (SPAAC). The bicyclononyne- (BCN) or dibenzocyclooctyne- (DBCO) derivate reacts with organic azide and forms a stable 1,2,3-triazol. The R groups represent the rest of the molecule.	14
Figure 5 Mechanism of transglutaminase-mediated transamidation. MTG catalyzes the transfer of primary amines to the γ -carboxamide group of the glutamine. The nucleophilic attack of Cys64 on the γ -carboxamide group of the acyl-donor results in the formation of a thioester, accompanied by the release of ammonia. Subsequently, the ϵ -amino group of the acyl-acceptor (in this case, lysine) interacts with the side chain, leading to the formation of an iso-peptide bond between the donor and acceptor, while regenerating Cys64. Figure based on Deweid <i>et al.</i> ⁷²	15
Figure 6 Canonical Wnt-signaling of RNF43 regulating the surface level of Fzd receptor in presence and absence of RSPO. (A) RNF43 inhibits the interaction through intrinsic ubiquitination and subsequent degradation of Fzd, leading to the downregulation of the Wnt signaling pathway. (B) Rsondin binds RNF43 and LGR4/5/6 and induces autoubiquitination of RNF43 and following lysosomal degradation of RNF43. Wnt/ β -catenin signaling pathway is activated. Fzd – Frizzled receptor, LRP5/6 - lipoprotein receptor-related proteins 5 and 6, Ub - Ubiquitin, RSPO - Rspodin, LGR4/5/6 - G-protein-coupled receptor 4,5,6. Figure based on Hao <i>et al.</i> ¹²⁰	20
Figure 7 The ubiquitin-proteasome system. Ubiquitin activation by ubiquitin-activating enzyme (E1), then the transmission of activated ubiquitin (Ub) moiety to ubiquitin-conjugating enzymes (E2) and transfer of activated Ub from E2 to a cysteine residue on ubiquitin-protein ligases (E3) or directly to the substrate. The polyubiquitinated substrate is then degraded by the 26S proteasome complex that causes release and reusable Ub and E3 ligase.	22
Figure 8 Target protein degradation mediated by PROTACs through the UPS. (A) The PROTAC consists of a ligand for the POI (turquoise) and a E3 ligase ligand (rose) linked by a spacer, enabling the target to be brought into proximity to an E3 ligase complex (gray). Subsequently, the target protein is ubiquitinated (yellow) and degradation is enabled by recognition of the 26S proteasome. Following degradation, the PROTAC can be recycled and bind again. (B) VH032-based PROTAC GNE987P targeting BRD4. ¹⁴³	24

- Figure 9 Schematic representation of the mechanisms of NBE-based targeted protein degradation.** Glycan-based recycling receptors are addressed by 1st and 2nd generation of LYTAC, which share the same mechanism of action. AbTAC and PROTAB are bispecific antibodies targeting an E3-ligase and the target of interest and cause receptor-mediated uptake and degradation through the endosome-lysosome pathway. KineTACs comprising a target binding arm and a cytokine arm for binding the cytokine receptor. 28
- Figure 10 Vector map of pTT5 plasmid.** This was used for mammalian expression and contains essential elements, shown using the example of α RNF43 scFv2. It includes an origin of replication (EBV oriP), an ampicillin resistance, a bacterial origin of replication (pUC ori), a cytomegalovirus immediate early promoter (CMV) and the adenovirus tripartite leader (TPL). The TPL is a synthetic intron that includes an enhancer element from the adenovirus major late promoter, which enhances protein expression. Downstream of the protein sequence is the rabbit β -globulin polyadenylation signal, while upstream is the leader sequence. The pTT5 vector was developed by the National Research Council of Canada..... 32
- Figure 11 Modular approach to generate bispecific PROTAC-binding antibodies using bioconjugation. (A)** Process for generating an antibody-MIC7 conjugate loaded with PROTAC to enable **(B)** target receptor-mediated binding and internalization of complexed PROTACs. Figure adapted from Lehmann *et al.*¹⁸¹..... 60
- Figure 12 Chromatogram of analytical HI-HPLC.** Overlay of the UV-absorption signals of G₃-MIC7 (black) and PROTAC-loaded G₃-MIC7 (blue). 10.9% unloaded G₃-MIC7 at retention time 8.89 min and 89.1% of G₃-MIC7+GNE987 at retention time 11.21 min were detected. 61
- Figure 13 Semi-quantitative analysis of MTG-mediated conjugation.** 4-12% Bis-Tris SDS-PAGE gel showing reduced reaction mixes and respective controls. As expected, bands of parental antibody appear at 25 kDa (LC) and 50 kDa (HC) and free excess of G₃-MIC7 appears at approx. 15 kDa and MTG at 38 kDa. No cross-linking was observed between Ttz and MTG or G₃-MIC7 and MTG. Within the reaction mixture (lane 7), a shift of the heavy chain band towards 65 kDa is visible. The Precision Plus Protein™ Unstained Standard was used as the marker for size estimation. Figure adapted from Lehmann *et al.*¹⁸¹..... 62
- Figure 14 Chromatograms of Ttz-MIC7 preparation and analysis. (A)** Chromatogram of preparative SEC. The probe was injected onto a SEC column. Sample was separated by an isocratic gradient in target peak (Ttz/ Ttz-MIC7), HMW, excess G₃-MIC7 and MTG. **(B)** Chromatogram of analytical SE-HPLC. Overlay of the UV-absorption signals of blue, the Ttz and black, the purified Ttz-MIC7. The shift towards higher molecular weight is in the expected range but does not indicate formation of further multimeric species. **(C)** RP-

HPLC chromatogram of purified Ttz-MIC7. Overlay of the UV-absorption signals of the Ttz and the purified Ttz-MIC7. No unconjugated mAb at retention time 3.85 min, 16.1% of VAR 1 species at retention time 4.10 min and VAR 2 species at retention time 4.19 min were detected. This reaction had an overall VAR of 1.80 **(D)** Chromatogram of HI-HPLC analysis. Overlay of the UV-absorption signals of Ttz and the purified Ttz-MIC7. Purified Ttz-MIC7 analysis revealed final VAR of 1.72. Figure adapted from Lehmann *et al.*¹⁸¹..... 63

Figure 15 Cellular binding of Ttz-MIC7, Ttz and reference molecules to different HER2 expressing cell lines. The HER2-targeting antibodies and references selectively bind to HER2 overexpressing cell lines, SKBR3 and BT474. A slight binding was observed to HER2_{low} cells MDA-MB-435. The experimental procedure included incubation of cells at a concentration of 100 nM for each treatment condition for 60 min at 4 °C. After incubation, cells were washed twice with DPBS + 1% (w/v) BSA and then incubated for 30 min in the dark at 4 °C with 500 nM AF488-labeled detection antibody. After two further washes with DPBS + 1% (w/v) BSA, the fluorescence intensity was measured by flow cytometry. Figure adapted from Lehmann *et al.*¹⁸¹..... 67

Figure 16 Receptor-mediated internalization of pHAb-dye labeled constructs in HER2 expressing cell lines. (A) Intracellular accumulation of Ttz-MIC7 in BT474, SKBR3 and MDA-MB-435 cancer cells were presented as an example for selected time points. The cells were incubated at 37 °C, 80% humidity and 5% CO₂ with 100 nM pHAb-dye labeled Ttz-MIC7. Images of the cells in the RFP channel (Exc. 531 nm, Em. 593 nm) were recorded every 30 min for 24 h using a cell imaging reader. **(B)** The time series images demonstrated an increase in cellular uptake for HER2-binding constructs. The fluorescence intensity was normalized based on both the cell number and the pHAb-dye DOL value of each construct. 69

Figure 17 Generation of Ttz-MIC7 PROTAC complexes. Incubation of Ttz-MIC7 with GNE987 at molar ratios of 1:0.5, 1:1 to 1:2 followed by monitoring of complex formation via HI-HPLC. R0, R1 and R2 indicate the ratio elution range corresponding to conjugates loaded with 0, 1, or 2 PROTACs, respectively. Figure adapted from Lehmann *et al.*¹⁸¹ 70

Figure 18 Targeted BRD4 degradation mediated by antibody delivery of PROTAC. (A) Degradation of BRD4 evaluated in SKBR3 (HER2_{pos}) cancer cells using immunofluorescence microscopy analysis. Cells were treated with 10 nM Ttz-MIC7 or α Dig-MIC7 complexed with GNE987P at molar ratio 1:1, along with respective controls, for 24 h. Following the treatment, cells were fixated, permeabilized and stained using primary anti-BRD4 antibody. For staining with secondary antibody an Alexa Fluor™ 488-labeled antibody was used (green). Cell nuclei are counterstained with Hoechst 33342 dye (blue). **(B)** Relation between normalized BRD4 level and different treatment

concentrations. The BRD4 level was normalized to cell count and untreated cells. Serial dilution of treatment concentrations between 0.01 and 100 nM treatment were selected and plotted, which were performed in technical triplicates. The solid line connects the data points for the BRD4 level at respective concentration for the antibody-based treatment, while the dotted line connects free GNE987 and GNE987P data points 72

Figure 19 Dose-response curves of PROTAC-loaded Ttz-MIC7 and respective controls. HER2_{high} and HER2_{low} cells were treated with Ttz-MIC7 and α Dig-MIC7 complexed with **(A)** GNE987P (molar ratio 1:1) and **(B)** GNE987 and control molecules. Cells were treated for six days with serial dilution. Each curve represents the mean of technical duplicates, standard deviation shown as error bars. Figure adapted from Lehmann *et al.*¹⁸¹..... 74

Figure 20 Dose-response curves of GNE987P-loaded Ctx-MIC7 and respective controls. EGFR_{high} and EGFR_{low} cells were treated with Ctx-MIC7 and α Dig-MIC7 complexed with GNE987P (molar ratio 1:1) and control molecules. Cells were treated for three days with serial dilution. Each curve represents the mean of biological triplicates, standard deviation shown as error bars. 75

Figure 21 Dose-response curves of GNE987P-loaded G₃-MIC7 and respective controls. Cells were treated for three days with G₃-MIC7 complexed with GNE987P (molar ratio 1:1) and control molecules in serial dilution. Each curve represents the mean of biological triplicates, standard deviation shown as error bars..... 75

Figure 22 Schematic representation of chemoenzymatic conjugation steps to generate an antibody-based degrader and the mediated target receptor degradation mode. (A) MTG-mediated direct conjugation strategy for generation of bispecific anti-body-scFv conjugates was not successful. **(B)** Native IgG1-based antibodies are site-selectively coupled with click derivate using microbial transglutaminase (MTG). A SPAAC reaction was performed to covalently bind scFv and antibody. **(C)** Mode of action of transmembrane E3 ligase mediated internalization and lysosomal degradation. 76

Figure 23 (A) Protein yields after purification. **(B)** Confirmed sequence identity by peptide mapping and determination of molecular weight. The binding affinity is expressed as K_D value and were derived by a 1:1 global full-fit binding model..... 81

Figure 24 Results of click derivate conjugation to scFv variants. (A) Conjugation efficiency of different click derivatives to scFv variants shown as DAR. **(B)** Mean and \pm SD of protein stabilities based on the monomeric content upon conjugation with different click derivatives (1, 3-6). Data set obtained by SE-HPLC analysis..... 82

Figure 25 Results of click derivate conjugation to Ttz. (A) Conjugation efficiency of click derivatives 1 and 2 to Ttz shown as DAR. **(B)** Mean and \pm SD of protein stabilities based

on the monomeric content upon conjugation with different click derivatives. Data set obtained by SE-HPLC analysis. 83

Figure 26 Optimization of SPAAC reaction. (A) Semi-quantitative gel electrophoresis of Ttz.1-scFv5.3 after 3 hours and 30°C SPAAC click reaction and controls. Samples were prepared under non-reduced conditions. **(B)** Ttz.1 was clicked with scFv5.3 using different reaction conditions. Reaction time (h), temperature (°C) and Ttz.1 protein concentration (mg/mL) was studied. Reactivity was evaluated using SE-HPLC with respective chromatograms in Figure S 21 (B) and gel electrophoresis. The percentage reactivity is determined by the proportion of 100% free, non-clicked antibody in the reaction mixture..... 85

Figure 27 Antibody-based degrader production and analysis. (A) Chromatogram of preparative SEC analysis. The probe was injected to a PBS pH 7.4 equilibrated column. Linear gradient was used for elution and fractions were collected and pooled. The UV-signal is shown in black. **(B)** Chromatographical analysis of analytical SE-HPLC. The blue signal is the UV absorption of Ttz and the black signal corresponds to Ttz.1-scFv5.3. **(C)** Semi-quantitative analysis of final purified Ttz.1-scFv5.3 and Ttz. Non-reduced and reduced sample preparation was performed..... 86

Figure 28 Simultaneous binding analysis of RNF43 and HER2 by IgG-scFv conjugate via BLI. The conjugates were immobilized on AHC biosensors. Then, association of rhRNF43 followed by HER2 was monitored. For both association steps a shift could be observed indicating simultaneous binding of both antigens. Buffer controls indicated no unspecific binding to AHC biosensors. 88

Figure 29 Theoretical RNA expression levels of HER2 and RNF43 in different cancer cell lines. (A) Expression level is stated as \log_2 of transcripts per million (TPM) stated in DepMap portal from Broad Institute.¹⁸⁹ The \log_2 TPM represents the expression level of the gene at one million transcripts in one sample. **(B)** The cell lines were grouped into low (light grey), medium (grey) and high (black) HER2 expressing cell lines depending on their TPM value..... 89

Figure 30 Cellular binding of IgG-scFv conjugates and references to several cell lines. Cell lines were incubated with 100 nM antibody and binding was revealed with AF488-labeled detection antibody. **(A)** HER2 expressing cells incubated with Ttz.1-scFv5.3 (red) and Ttz (blue) and a fluorescent detection antibody show equal MFI compared to controls (α DIG.2-scFv5.3 (black), α RNF43 mAb (grey), and AF488-labeled anti-human detection antibody (green) in flow cytometry analysis. **(B)** MFI values obtained for Ttz.1-scFv5.3 and Ttz on HER2 cell lines expressing different levels of HER2..... 90

Figure 31 Target cell receptor degradation. (A) Western Blot analysis of HER2 level in HEPG2 cells after treatment with 10 nM Ttz.1-scFv5.3 and Ptz.1-scFv5.3 for 24 hours. For

reference monospecific molecules, including scFv5, Ttz and Ptz along with buffer treatment were used. After treatment cells were lysed and 150 μ M protein was used for analysis. β -actin served as housekeeping control and was detected with fluorophore-labeled secondary antibody. **(B)** Flow cytometric analysis of HER2 level on HEPG2 cell surface. Cells were treated with 10 nM Ttz.1-scFv5.3 and Ptz.1-scFv5.3 for 24 hours and after harvest and staining FACS analysis was performed. Treatment results are normalized to buffer only treatment. The values represent the mean of technical triplicates with SD as error bar. **(C)** Western Blot analysis of PD-L1 level in different cancer cell lines (MDA-MB-231, T24, HCC827) after treatment with 10 nM Atz.1-scFv3.3 for 24 hours. GAPDH was used as housekeeping protein. **(D)** Flow cytometric analysis of PD-L1 level on surface of different cell lines (MDA-MB-231, T24, HCC827) after treatment with Atz.1-scFv3.3 and controls. Treatment results are normalized to buffer only treatment. The values represent the mean of technical triplicates with SD as error bar. 92

C List of tables

Table 1 Evaluation of different reaction conditions for increasing conjugation efficiency.	
Studies were performed by keeping two concentrations of the reaction components constant and varying one. The VHH-to-antibody ratio (VAR) represents the conjugation efficiency determined by LC-MS.	62
Table 2 Upscaling conjugation of G₃-MIC7 to different antibodies using MTG.	
Chromatographic analysis, including SE-HPLC, allowed determination of the highest final purity and VAR determination was performed using RP-HPLC, HI-HPLC and LC-MS. Percent yield was calculated by $m(\text{conjugate})/m(\text{parental mAb}) \times 100$	64
Table 3 Conjugation MIC7 VHH to several native mAbs to verify modular approach and confirm of conjugation site.	
G ₃ -MIC7 was conjugated using MTG and reaction mixes were analyzed using LC-MS and SE-HPLC. Efficient conjugation with VHH-to-antibody ratios (VAR) close to 2 and high purity was revealed. The glutamine to alanine substitution at position 295 showed no conjugation, confirming Q295 position as selective antibody conjugation site.	64
Table 4 Binding kinetics of conjugates and parental antibodies against respective soluble antigen.	
.....	65
Table 5 Binding affinities of conjugated VHH G₃-MIC7 to PROTACs GNE987, GNE987P and ARV771.	
*no binding detected up to a tested concentration of 0.5 μ M. #determined off-rates are outside of instrument specifications and were therefore reported as $k_{\text{off}} < 0.0001$	

1/s; reported KD values are estimated by an assumption of $k_{on} > 1.0 \times 10^5$ [1/(M*s)]. \$n.d. – not determined as k_{off} is not measured unambiguously.....	66
Table 6 pHAb-dye labeled constructs generated for internalization studies. The labeling of the constructs was achieved through random lysine conjugation. The DOL values, determined via LC-MS, correspond to the quantity of pHAb-dyes conjugated to each antibody.	68
Table 7 Complexation results of different PROTACs with Ttz-MIC7, Ctx-MIC7 and αDIG-MIC7. Loading efficiency was determined for molar complexation ratios of 1:2 Ttz-MIC7 to PROTAC. n.d.: not determined.	71
Table 8 Modified scFv variant used in this study. SeqID refers to each scFv variant. Protein orientation shows the V_H to V_L sequence alignment in N- to C-terminal direction, connected by either YOL (sequence: KLEEGEFSEARV) or glycine-serine linker. A His ₆ -tag for purification and the terminal tag for MTG-mediated conjugation were installed. The N- and C-terminal tag represent the terminal attachment site of the scFv. N/A: not available. ...	77
Table 9 Chemical structure of click derivatives used in this study. Derivate number and structure of each peptide are listed and related to the click reactive side (R2).	80
Table 10 Azide-based scFv conjugates. All scFv variants were conjugated with click derivate 3 by MTG-mediated transamination. DAR values are given as mean of RP-HPLC and LC-MS analysis. Monomer content of conjugates was derived from SE-HPLC analysis.....	83
Table 11 Ring-strained alkyne-based antibody conjugates. Click derivate 1 was conjugated to Ttz, Ptz and Atz while 2 was installed at Atz, Mtz, α DIG and Ctx. DAR is given by LC-MS analysis. Monomeric content was derived from SE-HPLC analysis.....	84
Table 12 Overview of generated antibody-based degraders using two-step chemoenzymatic conjugation.	87
Table 13 Binding of rhHER2 an rhRNF43 by conjugates and controls. Both affinities (K_D) and rates of association and dissociates (K_{on} and K_{dis}) were determined.....	88

D Abbreviations

AA	Amino acid
Ab	Antibody
Abs (or λ)	Absorbance
AbTAC	Antibody-based PROTAC
ADC	Antibody-drug conjugate
ADCC	Antibody-dependent cellular cytotoxicity

AHC	anti-human IgG Fc capture biosensors
APC	Antigen-presenting cells
Ar	Peak area [mAU*sec]
ASGPR	Asialoglycoprotein receptor
Atz	Atezolizumab
AUC	Area under the curve
Ave	Avelumab
BCA	Bicinchoninic acid
BCN	Bicyclononyne
BD	Bromodomain
BET	Bromo- and extra-terminal family
BiTE	Bispecific T-cell Engager
BLI	Bio-layer-Interferometry
BRD4	Bromodomain-containing protein 4
BSA	Bovine serum albumin
c	Concentration [M]
CDC	Complement-dependent cytotoxicity
CDR	Complementary Determining Regions
CI-M6PR	Cation-independent mannose 6-phosphate receptor
CK1 α	Casein kinase 1 α
CRBN	Cereblon
CRC	Colorectal cancer
Ctx	Cetuximab
CuAAC	copper(I)-catalyzed Huisgen azide-alkyne cycloadditions
CV	Column volume
CV	Column volumes
DAR	Drug-to-antibody ratio
DBCO	dibenzocyclooctyne
DIG	Digoxigenin
DOL	Degree of labeling
E1	Ubiquitin-activating enzyme 1
E2	Ubiquitin-conjugating enzyme 2
E3	Ubiquitin-protein ligase 3
ECD4	Extracellular domain 4
EGFR	Epidermal Growth Factor Receptor

ESI-MS	Electrospray ionization mass spectrometry
F	Flow rate [$\mu\text{L}/\text{sec}$]
Fab	Antigen-Binding Region
Fc	Fragment Crystallizable
FcRs	Fc receptors
FDA	Food and Drug Administration
Fzd	Frizzled receptor
G ₃	Triple glycine sequence
GalNAc	N-acetylgalactosamine
GCO	Global Cancer Observatory
HC	Heavy chain
HER2	Human epidermal growth factor receptor 2
HI-HPLC	Hydrophobic interaction chromatography
IF	Immunofluorescence Assay
IGF1R	Insulin-like growth factor 1 receptor
IMAC	Immobilized Metal Affinity Chromatography
K _D	Equilibrium dissociation constant
KIH	"knob-into-hole"-technology
KineTAC	Cytokine receptor-targeting chimeras
l	Flow cell path length [cm]
L	Liter
LC	Light chain
LGR4/5/6	G-protein-coupled receptor 4,5,6
LplA	Lipoic acid protein ligase A
LRP5/6	Lipoprotein receptor-related proteins 5 and 6
LYTAC	Lysosome-Targeting Chimeras
M6Pn	Mannose 6-phosphonates
mAb	Monospecific antibody
MAPK	Mitogen-activated protein kinase
MED	Minimum efficacious dose
MFI	Mean fluorescence intensity
MTD	Maximum tolerated dose
MTG	Microbial transglutaminase
Mtz	Matuzumab
MW	Molecular Weight

MWCO	Molecular weight cut off
N ₃	Azide
NBE	New Biological Entities
PD-L1	Programmed cell death ligand-1
PEG	Polyethylene glycol
PI3K	Phosphatidylinositol-3 kinase
PI3K	Phospholipid inositol-3-kinase
PK	Pharmacokinetic
POI	Protein of interest
PROTAB	Proteolysis-targeting antibody
PROTAC	Proteolysis Targeting Chimeras
Ptz	Pertuzumab
PVDF	polyvinylidene difluoride
REULR	Receptor Elimination by E3 Ubiquitin Ligase Recruitment
Rix	Rituximab
RNF43	Ring finger protein 43
RP-HPLC	Reversed phase chromatography
RP-HPLC	Reversed Phase-HPLC
RSPO	Rspondin
RT	Room temperature
RTK	receptor tyrosine kinases
RU	Response units
<i>S. Lad</i>	<i>Streptomyces Ladakanum</i>
SAR	scFv-to-antibody ratio
scFv	Single-Chain Variable Domain
SDS-PAGE	Sodium dodecyl sulfate polyacrylamide gel electrophoresis
SEC	Size exclusion chromatography
SEC	Size-Exclusion Chromatography
SHP-2	Src homology 2 domain-containing protein tyrosine phosphatase-2
SPAAC	Strain-promoted azide-alkyne cycloaddition
SPR	Surface plasmon resonance spectroscopy
SrtA	Sortase A
TC	Tissue culture
TFA	Trifluoroacetic acid
TPD	Targeted Protein Degradation

Ttz	Trastuzumab
Ub	Ubiquitin
VAR	VHH-antibody ratio
VHH	Camelid Heavy-Chain Variable Domains
VHL	Von Hippel-Lindau
WHO	World Health Organization

E Acknowledgements

Zu Beginn möchte ich Prof. Dr. Harald Kolmar für die akademische Betreuung meiner Dissertation an der TU Darmstadt und die unkomplizierte Kooperation herzlich danken. Besonders auch beim Kleinwalsertal-Retreat schätze ich den Kontakt und wissenschaftlichen Austausch zwischen den DoktorandInnen und Alumni des Arbeitskreises.

Prof. Dr. Dr. Siegfried Neumann danke ich für die bereitwillige Übernahme des Korreferats. Mein Dank gilt Prof. Dr. Beatrix Süß und Prof. Dr. Katja Schmitz für ihre Bereitschaft, als Fachprüferinnen zu fungieren. Dank gilt auch Dr. Jan Anderl und Dr. Stefan Hecht, die mir die Promotion im aktuellen Forschungsfeld von Merck ermöglicht haben.

Insbesondere möchte ich mich herzlich bei Dr. Marcel Rieker und Dr. Stephan Dickgießer für die Übernahme der wissenschaftlichen Betreuung, dem fachlichen Rat, der kontinuierliche Unterstützung und Ermutigung nach Rückschlägen und dem Mitfiebern bei neuern Ergebnissen bedanken. Danke auch für die motivierende Arbeitsatmosphäre sowie eure Ausdauer und inspirierende Arbeitsweise. Euer prüfender Blick und Ideenreichtum haben mir das ein oder andere Mal viel Leid erspart.

Gleichermaßen möchte ich Dr. Nicolas Rasche für seine wertvolle Kritik und seinem tollen Biokonjugations-Team danken. Dem ganzen ADC-Fabrik Team, Jens Hannewald, Ingrid Schmidt und Patrick Steiner gilt mein besonderer Dank für die großartige Zusammenarbeit und Unterstützung, es war eine unvergessliche Zeit besonders die gemeinsamen Wanderungen durch den Darmstadt Stadtwald mit dem ein oder anderen Heißgetränk.

Ganz besonders möchte ich M.Sc. Laura Basset und M.Sc. Saran Aswathaman Sivashanmugam für ihre wertvolle Mitarbeit und den fachlichen Austausch im Rahmen ihrer Masterarbeiten danken. Die zahlreichen gemeinsamen Mittagspausen und die Weihnachtsfrühstücke bleiben mir in guter Erinnerung, und ich habe es sehr genossen, dich als Schreibtisch-Nachbarin zu haben.

Dr. Hendrik Schneider und Dr. Sebastian Jäger möchte ich für Unterstützung im PROxAb Shuttle Projekt danken. Einen großen Dank gilt Stefan Keller, Markus Fleischer und Julius Finkernagel, welche mir mit großem Engagement immer zur Seite standen und neben Bereitstellung von Anlagen auch immer ein offenes Ohr hatten. Dem MS-Team um Jennifer Schanz, Dr. Jason Tonillo und Johanna Meder danke ich für die stets zügige Durchführung der Probenmessungen und die Analyse ungewöhnlicher Anfragen. Dr. Birgit Piater und ihrem Team, Konstanze Waurisch und Kirsten Leidinger danke ich für die Bereitstellung der Laborflächen und Geräte, sowie für die Unterstützung am Cytation 5. Konstanze danke ich besonders für die Füllung meiner Wissenslücke um den König der Andalen und der Ersten Menschen.

Des Weiteren danke ich Dr. Daniel Schwarz und Dr. Christian Schröter für ihren fachlichen Input und Unterstützung im Rahmen von experimentellen Datenerhebung für die Publikation. Für die

Hilfe beim Design der Plasmide und dem Interesse an meiner Arbeit möchte ich außerdem Dr. Simon Krahn danken.

Danken möchte ich auch Iris Willenbücher, Deniz Demir, Kerstin Hallstein, Christina Bauer, Daniela Noack, Marion Wetter, Ramona Gaa, Sonja Dreher, Vanessa Lautenbach und Dominik Reitz für die angenehme jahrelange Arbeitsatmosphäre und die netten. Ein Dank gilt ebenso vielen Mitarbeitern bei Merck, die auf unterschiedliche Weise meine Arbeit unterstützt haben, sei es durch die Bereitstellung von Zellen oder Materialien, die Durchführung von Analysen oder fachliche Beratung: Dr. Stefan Zielonka, Dr. Desislava Elter, Dr. Lukas Pekar, Dr. Stefan Becker, Hannah Mayer, Dr. Steffen Wöll, Alexander Müller, Dr. Carolin Sellmann, Nils Bahl, Dr. Achim Dörner, Claudia Kubis, Anja Lamack, Pia Stroh, Andreas Schönemann, Dr. Stanley Sweeney-Lasch, Dr. Judith Stein, Dr. Jean Wakim, Gernot Musch, Oliver Edler, Dr. Vanessa Siegmund, Sigrid Auth, Teresa Gorgol, Selma Bozkurt, Dr. Anita Seshire, Julia Rolf, Maria Heim, Ana Cristina Silva Castro und Vanessa Waschk.

Für eine tolle gemeinsame Zeit möchte ich allen aktuellen und ehemaligen Merck-Doktoranden danken, M.Sc. Britta Lipinski und M.Sc. Lexane Fournier, M.Sc. Laura Unmuth und M.Sc. Jan-Phillip Kahl für den Austausch auf Level 6. Dir Britta, danke ich vor allem für die großartige Woche im KWT mit vielen angenehmen Gesprächen, erfolgreichen Schneeballschlachten und coolen Abfahrten und Aufstiegen. Dr. Anita Jäger, Dr. Sandra Müller, Dr. Anna Kaempffe, Dr. Tim Hofmann, und Dr. Martina Grabner gilt mein Dank für die Komlarschule-Mittagspausen.

Dank gilt auch Barbara Diestelmann für die organisatorische Hilfe.

Meinen Freunden Sarah, Janina, Kim, Zora, Judith, Uli und den Zeller-Mädels möchte ich für die Unterstützung, Nachsicht und stetiges Interesse an meiner Arbeit in den letzten Jahren herzlich danken. Besonderen Dank gilt auch Justus für das Korrekturlesen der Einleitung gelesen und den gemeinsamen Dienstags-skype-Abenden. Vor allem Julia und ihrer Familie möchte ich für die langjährige Freundschaft, Unterstützung und stetigen Glauben an mich danken. In so vielen Lebensphasen hast du meine Hochs und Tiefs mitbekommen, mir zugehört und Mut zugesprochen.

Ganz besonders möchte ich meiner Familie danken, für den Rückhalt während des Studiums und meiner Promotionszeit. Mein Dank gilt meiner Mutter Rita und meinem Vater Andreas, die mir alles ermöglichten und mich immer in meinen Vorhaben unterstützen. Meinem Bruder Lukas und seiner Familie für das stetig Interesse an meiner Arbeit und das Verständnis in stressigen Phasen. Zu guter Letzt danke ich Yannic, für den Rückhalt und das Verständnis, für deine Geduld mit meinen Launen in den letzten Monaten, die stetige Unterstützung bei verschiedenen Projekten, deine ehrlichen Einschätzungen und auch deinen unermüdlichen Zuspruch. Du hast einen enormen Anteil an der Fertigstellung dieser Arbeit!

Affirmation

Erklärungen

§8 Abs. 1 lit. c der Promotionsordnung der TU Darmstadt

Ich versichere hiermit, dass die elektronische Version meiner Dissertation mit der schriftlichen Version übereinstimmt und für die Durchführung des Promotionsverfahrens vorliegt.

§8 Abs. 1 lit. d der Promotionsordnung der TU Darmstadt

Ich versichere hiermit, dass zu einem vorherigen Zeitpunkt noch keine Promotion versucht wurde und zu keinem früheren Zeitpunkt an einer in- oder ausländischen Hochschule eingereicht wurde. In diesem Fall sind nähere Angaben über Zeitpunkt, Hochschule, Dissertationsthema und Ergebnis dieses Versuchs mitzuteilen.

§9 Abs. 1 der Promotionsordnung der TU Darmstadt

Ich versichere hiermit, dass die vorliegende Dissertation selbstständig und nur unter Verwendung der angegebenen Quellen verfasst wurde.

§9 Abs. 2 der Promotionsordnung der TU Darmstadt

Die Arbeit hat bisher noch nicht zu Prüfungszwecken gedient.

Ort, Datum:

Darmstadt, 15.05.2024

Name und Unterschrift:

Tanja Lehmann

